Chapter 2: Observations: Atmosphere and Surface

Coordinating Lead Authors: Dennis Hartmann (USA), Albert Klein Tank (Netherlands), Matilde Rusticucci (Argentina)

Lead Authors: Lisa Alexander (Australia), Stefan Broennimann (Switzerland), Yassine Abdul-Rahman Charabi (Oman), Frank Dentener (EU / Netherlands), Ed Dlugokencky (USA), David Easterling (USA), Alexey Kaplan (USA), Nzioka John Muthama (Kenya), Brian Soden (USA), Peter Thorne (USA / UK), Martin Wild (Switzerland), Panmao Zhai (China)

Contributing Authors: Robert Adler (USA), Richard Allan (UK), Robert Allan (UK), Aiguo Dai (USA), Robert Davis (USA), Sean Davis (USA), Markus Donat (Australia), Vitali Filotev (Canada), Erich Fischer (Switzerland), Leopold Haimberger (Austria), Ben Ho (USA), John Kennedy (UK), Stefan Kinne (Germany), James Kossin (USA), Norman Loeb (USA), Carl Mears (USA), Christopher Merchant (UK), Steve Montzka (USA), Colin Morice (UK), Joel Norris (USA), David Parker (UK), Bill Randel (USA), Andreas Richter (Germany), Ben Santer (USA), Dian Seidel (USA), Tom Smith (USA), David Stephenson (UK), Ryan Teuling (Netherlands), Junhong Wang (USA), Ray Weiss (USA), Kate Willett (UK), Simon Wood (UK), Tingjun Zhang (China)

Review Editors: Jim Hurrell (USA), Jose Marengo (Brazil), Fredolin Tangang (Malaysia), Pedro Viterbo (Portugal)

Date of Draft: 16 December 2011

Notes: TSU Compiled Version

Table of Contents

Executive Summary

The observations of the atmosphere and surface indicate that:

- Globally averaged land surface air temperatures have increased since the late 19th Century and this warming has been particularly marked since the 1970s. This is *virtually certain*. Several independently analyzed global and regional land surface temperature data products of substantial heritage support this conclusion.

  It is *likely* that urban heat-island effects and land use change effects have not raised the centennial global land surface air temperature trends by more than 10% of the observed trend.

  Confidence in diurnal temperature range changes *is medium-to-low* as recent analyses of the raw data, on which previous analyses were based, point to the potential for pervasive biases that differently affect maximum and minimum temperatures.

  With *very high confidence* the global average sea surface temperatures have increased since the beginning of the Twentieth Century. Intercomparisons of new data products obtained by different measurement methods, including satellite data, have resulted in better understanding of errors and biases in the record.

  The global combined land and ocean temperature data show an increase of about 0.8°C over the period 1901–2010 and about 0.5 °C over the period 1979–2010 when estimated by a linear trend (note that comparable values for the period until 2005 reported in the AR4 are about 0.7°C and 0.5°C).

  Based upon multiple independent analyses from weather balloons and satellites it can be concluded with *very high confidence* that globally the troposphere has warmed since the mid-twentieth Century. There is *medium confidence* in the rate of change and its vertical structure in the Northern Hemisphere extra-tropics, but elsewhere *confidence is low*, particularly in the tropical upper troposphere. Estimates of tropospheric warming rates include the potential for less warming or greater warming than that reported at the surface (which has much less uncertainty).

  While it can be concluded with *very high confidence* based on four independent observing technologies that globally the stratosphere has cooled since the mid-twentieth Century there is only *low confidence* in the cooling rate and vertical structure.

- Global precipitation averaged over land areas has increased, with most of the increase occurring in the early to mid 20th Century as reported in the AR4. However, *confidence* in these global precipitation estimates *is low* because of data incompleteness. When virtually all the land area is filled in using a reconstruction method, the resulting time series shows little change in land-based precipitation since 1900.

  Precipitation in the tropics has *likely* increased over the last decade reversing the drying trend that occurred from the mid-1970s to mid-1990s reported in the AR4. The mid-latitudes and higher latititudes of the Northern Hemisphere do show an overall increase in precipitation from 1900–2010, however *confidence is low* because there is much uncertainty in the results for the early 20th Century. Insufficient evidence exists to define long-term temporal change of precipitation in the mid-latitudes of the Southern Hemisphere.

  In most regions analyzed, it is *likely* that decreasing numbers of snowfall events are occurring where increased winter temperatures have been observed. Antarctica is the exception where increased snowfall is occurring with increased temperatures.

  The most recent and most comprehensive analyses of river runoff do not support the AR4 conclusion that global runoff has increased during the 20th Century.

  As reported in the AR4, absolute moistening of the atmosphere has been widespread across the globe since the 1970s, with *very high confidence*. However, during recent years this has abated over land,

coincident with greater warming over land relative to the oceans. This has resulted in fairly widespread decreases in relative humidity over land. Observations from radiosonde, GPS, and satellite measurements indicate increases in tropospheric water vapour at large spatial scales, which are consistent with the observed increase in atmospheric temperature. It is *very likely* that tropospheric specific humidity has increased since the 1970s. Significant trends in tropospheric relative humidity at large spatial scales have not been observed.

While trends of cloud cover are consistent between independent data sets in certain regions, substantial ambiguity and therefore *low confidence* remains in the observations of global-scale cloud variability and trends. What trends do exist are *likely* to be within the range of uncertainties for both satellite and observational cloud data sets.

- It is *virtually certain* that increasing atmospheric burdens of most long-lived greenhouse gases (LLGHG), especially CO_2, resulted in a further increase in their radiative forcing from 2005 to 2010.

  The short-lived greenhouse gas tropospheric ozone has *likely* been increasing at many undisturbed (background) locations in the 1990s. These increases have continued mainly over Asia and flattened over Europe during the last decade.

  Satellite datasets indicate a continuing decrease of Aerosol Optical Depth in the US, Europe, and Japan, and a continuing increase of AOD over Eastern and Southern Asia since the 1980s, which is consistent with long-term surface aerosol observations over North America and Europe.

  Changes in ozone and aerosol have *likely* contributed to geographical changes in patterns of radiative forcing.

- The quantification of the global mean energy balance as presented in earlier IPCC assessment reports requires substantial revision. This revision includes updates in the magnitudes of a number of components, particularly higher downward thermal radiation and latent heat flux at the surface, as well as the provision of uncertainty estimates, which were lacking in prior assessments.

  Since the AR4, the satellite records of top of the atmosphere (TOA) radiation fluxes have been substantially expanded, and indicate a continuation of the decadal variations in the tropical radiation budget. Globally, no significant changes in the global planetary albedo are apparent since 2000. The variability in the Earth's energy imbalance at the TOA, related to El Niño-Southern Oscillation (ENSO), is consistent with ocean heat content records.

  At the surface, the evidence for widespread decadal changes in surface solar radiation (dimming until the 1980s and subsequent brightening) has been substantiated. *Confidence is high* because these changes are in line with observed changes in a variety of other related variables, such as sunshine duration and hydrological quantities. There are also *medium confidence* indications for increasing downward thermal and surface net radiation in recent decades.

- Large variability on interannual to decadal time scales and remaining differences between data sets precludes robust conclusions on long-term changes in large-scale atmospheric circulation. *Confidence is high* that some trend features that appeared from the 1950s or earlier to the 1990s reported in the AR4 (e.g., an increase in the mid-latitude westerly winds and the NAO index or a weakening of the Pacific Walker circulation) have reversed in more recent decades.

  Nevertheless, it is *likely* that, in a zonal mean sense, circulation features have moved poleward (widening of the tropical belt, poleward shift of storm tracks and jet streams, contraction of the polar vortex) since the 1970s.

- Recent analyses of extreme events generally support the AR4 conclusions. It is *very likely* that the overall number of cold days and nights has decreased and the overall number of warm days and nights on the global scale has increased since 1950. Globally, there is *medium confidence* that the length or number of warm spells, including heat waves, has increased since the middle of the 20th Century although there is

high confidence that this is the case for large parts of Europe.

Consistent with AR4 conclusions, it is *likely* that the number of heavy precipitation events (e.g., 95th percentile) has increased significantly in more regions than it has decreased. Confidence is highest for North America where the most consistent trends towards heavier precipitation events are found.

There continues to be a lack of evidence and thus *low confidence* regarding the sign of trend in the magnitude and/or frequency of floods on a global scale.

New results indicate that the AR4 conclusions regarding global increasing trends in droughts since the 1970s are no longer supported. Not enough evidence exists at present to suggest medium or high confidence in observed trends in dryness, due to lack of direct observations, geographical inconsistencies in the trends, and dependencies of inferred trends on the index choice.

Recent re-assessments of tropical cyclone data confirm the AR4 conclusion that there is evidence of an increase in the most intense tropical cyclones since the 1970s. However, the new evidence does not support the AR4 conclusion that globally, estimates of the potential destructiveness of all hurricanes show a significant upward trend since the mid-1970s.

There is still *insufficient evidence* to determine whether robust global trends exist in small-scale severe weather events.

2.1 Introduction

This chapter assesses the scientific literature on atmospheric and surface observations since the AR4 (IPCC, 2007a). The most likely changes in physical climate variables and climate forcing agents are indentified based on current knowledge, following the IPCC AR5 uncertainty guidance.

As described in the AR4 (Trenberth et al., 2007), the climate varies over all spatial and temporal scales: from the diurnal cycle to interannual variability such as El Niño to multi-decadal and millennial variations. In this chapter, the changes are examined for the period with instrumental observations, since about 1800. Observed changes prior to this date are assessed in Chapter 5. Trends have been assessed for the periods starting in 1850, 1901, 1951, 1979 and ending in 2010 provided that data are available. For many variables derived from satellite data, information becomes available in 1979.

In recent decades, advances in the global climate observing system have contributed to improved monitoring capabilities. The results of new observation techniques, in particular satellites, provide additional measures for climate change, which have been assessed in this and subsequent chapters together with more traditional measures. Dynamical reanalyses datasets of the global atmosphere are also used (see Box 2.3).

The longest observational series arise from land surface air temperatures and sea surface temperatures (Section 2.2). Like all physical climate system measurements they suffer from non-climatic artifacts that must be removed (Box 2.1). Even though largely based on traditional observation techniques and associated with some unresolved uncertainties, the global mean surface temperature remains an important climate change measure for several reasons. Climate sensitivity is typically assessed in the context of global surface temperature responses to a doubling of CO_2 (Chapter 8) and global mean surface temperature is thus a key metric in the climate change policy framework. Also, because it extends back in time farther than any other observational series it is key to understanding both the causes of change (Chapter 10) and the patterns, role and magnitude of natural variability. Starting at various points in the 20th Century, additional observations, including balloon-borne measurements, satellite measurements and reanalysis products, allow analyses of indicators such as hydrological cycle changes (Section 2.3), atmospheric composition, radiation budget, circulation indices and extreme event characterizations, all covered in this chapter. A full understanding of the climate system characteristics and changes requires analyses of all such variables as well as ocean (Chapter 3) and cryospheric (Chapter 4) indicators. Through such a holistic analysis a clearer and more robust assessment of the changing climate system emerges (FAQ 2.1).

Observations of the abundances of greenhouse gases (GHG) and of aerosols are also included in this chapter (Section 2.4). Trends in GHG are indicative of the imbalance between sources and sinks in GHG budgets, and play an important role in emissions verification. The radiative forcing effects of GHG and aerosols are assessed in Chapter 8. Observed changes in radiative fluxes with time are discussed in Section 2.5.

Besides global averages of climate variables, this chapter also focuses on the changes over large regions (typically latitudinal bands or continents) and on a limited number of preferred patterns (or modes) of variability, which determine the main seasonal and longer-term climate anomalies at the regional scale. Trends in these patterns are discussed in Section 2.6. The regional changes associated with global warming can be complex and perhaps even counter-intuitive, such as changes in planetary waves in the atmosphere that result in regional cooling (Trenberth et al., 2007).

Changes in variability and extremes are also assessed (Section 2.7). Extremes of weather and climate, such as droughts and wet spells, are important because of their large impacts on society and the environment. The nature of variability at different spatial and temporal scales is vital to our understanding of extremes.

The chapter uses the word ‘trend’ to designate a generally monotonic change in the level of a variable (IPCC, 2007a). Where numerical values are given, they are equivalent linear changes (see Box 2.2), though more complex non-linear changes in the variable will often be clear from the description and plots of the time series. The chapter also assesses the physical consistency across different observations, which helps to provide additional confidence in the reported changes.

As described in the AR4, many different drivers for the observed changes may exist. It is important to note that the question whether the observed changes are outside the possible range of natural internal climate variability is not addressed in this Chapter, but rather in Chapter 10 (detection and attribution). No attempt to further interpret the observed changes in terms of multidecadal oscillatory variations and/or secular trends (e.g., as in Wu et al., 2011) has been attempted either, because the results of such analyses depend entirely on the null hypothesis one formulates (Cohn and Lins, 2005). In this chapter, the robustness of the observed changes is assessed in relation to various sources of observational uncertainty (see Box 2.1).

Each of the following Sections 2.2 to 2.7 starts with a brief review of the main conclusions of the AR4 relevant to the section. This is followed by a summary of the major conclusions of the current assessment for the relevant section, and their relationship to AR4 conclusions. Then the new science that supports these conclusions is summarized. Section 2.8 discusses the consistency across the observations described in this chapter.

[START BOX 2.1 HERE]

Box 2.1: Uncertainty in Observational Records

The vast majority of historical and present weather observations were taken for weather forecasting purposes and never intended for climate research. Measurements have changed in nature over time as data demands, observing practices and technologies have changed. These changes almost always alter the characteristics of the measurements, changing their mean, their variability or both such that it is necessary to process the raw measurements before they can be considered useful for assessing the true evolution of the climate. This is true of all observing techniques that measure physical atmospheric characteristics. The uncertainty in observational records encompasses instrumental errors, errors of representivity (e.g., related to exposure, observing frequency, local time of observation, measurement geometry, and instrument environment) as well as errors due to physical changes in the instrumentation (such as station relocations or new satellites). All further processing steps (gridding, interpolating, averaging) have their own particular uncertainties. For instance, changes in the in-situ observing network or irregular spacing of stations may cause errors in a spatially averaged series.

There is no unique, unambiguous, solution to identify and account for non-climatic artefacts in the vast majority of records, which leads to a degree of uncertainty as to how the climate system changed. The only exception is certain atmospheric composition and flux measurements that are directly traceable through an unbroken, well-characterized measurement chain to internationally recognized absolute measurement standards. Such records, including the CO_2 record (Keeling, 1976), can be considered an accurate record of the true changes in the measured quantity as sensed by the instrument, although this obviously does not preclude non-instrumental effects. This is very much the exception to the norm.

Uncertainty in dataset production for all remaining variables falls into two distinct classes – parametric uncertainty and structural uncertainty. Parametric uncertainty is the range of estimates that arises solely through varying a restricted subset of methodological choices for which no rigorous basis exists, e.g., when adjusting for an apparent break in a time series whether to use 2, 3 or 5 years of data either side to estimate this adjustment. But the overall methodological framework is not substantially questioned or varied in assessing parametric uncertainty. In contrast, structural uncertainty involves questioning fundamental assumptions about the choice of methodological framework. This uncertainty is most easily ascertained from having multiple independent groups assess the same data as they will have distinct approaches. It follows that structural uncertainty is almost always larger than parametric uncertainty and arguably more useful in assessing knowledge of the true changes in climate. Therefore whenever multiple published estimates exist for a given parameter they are included wherever possible to ensure a holistic assessment.

Many of the analyses assessed include a published estimate of parametric or structural uncertainty and this is far more the case now than it was at the time of AR4 (Trenberth et al., 2007). It is important to note that the literature now includes a very broad range of approaches. Great care has been taken in comparing the published uncertainty ranges as they almost always do not constitute a like-for-like comparison. In general, studies that have been formulated and assessed against a comprehensive error model and account for

multiple potential error sources in a rigorous manner yield larger uncertainty ranges than those that consider a more restricted subset of error sources. This yields an apparent paradox in interpretation as one might think that lower uncertainty should be associated with a better product. However, in many cases this would be an incorrect inference as the smaller uncertainty range may instead reflect that the published estimate considered only a subset of the plausible sources of uncertainty. Where this is likely to cause confusion, it is clarified which approach was used to calculate published estimates of uncertainty, and how comprehensive the error consideration was.

To conclude, the vast majority of the raw observations used to monitor the state of the climate contain residual non-climatic influences. Removal of these influences cannot be done definitively and neither can the uncertainties or errors be unambiguously defined. Therefore care is required in interpreting both data products and their stated uncertainty estimates. Confidence can be built from one or more of redundancy in efforts to create products, from product heritage, and from cross-comparisons of indicators that would be expected to co-vary such as land surface temperatures and sea surface temperatures around coastlines. Finally, trends are often quoted as a way to synthesize the data into a single number. Uncertainties that arise from such a process and the choice of technique used within this chapter are described in more detail in Box 2.2.

[END BOX 2.1 HERE]

[START BOX 2.2 HERE]

Box 2.2: Quantifying Changes in the Mean: Trend Models and Estimation

Many different statistical methods are available for estimating trends in environmental time series (Chandler and Scott, 2011). The assessment of long-term changes in historical climate data requires trend models that are transparent and reproducible, and that can provide credible uncertainty estimates. Various trend approaches are briefly assessed here, and a simple linear trend estimation procedure is proposed for analysis of the data sets in this Chapter.

Linear trends

Historical climate trends are almost always quantified in climate science by assuming that the mean has changed linearly over time (e.g., AR4). Such linear trend modelling is simple and easy to communicate: it has broad acceptance and understanding based on its frequent and widespread use.

Many options remain regarding the method of fitting a straight line to the time series data and estimating the associated uncertainty in the trend, however. Linear trends are generally fitted by minimizing the sum of squared residuals about the trend i.e., Least Squares (LS) estimation. This method is widely employed, and its strength and weakness are well known (von Storch and Zwiers, 1999; Wilks, 2006). The most difficulty arises in assessing the uncertainty in the trend and its dependence on the assumptions about the sampling distribution and the serial correlation of the residuals about the trend. Serial correlation has been dealt with by assuming that the residuals are an AR(1) process and then reducing the number of degrees of freedom (e.g., Santer et al., 2008) or by prewhitening the data and recomputing the regression (Von Storch, 1999). A more consistent approach is to use Generalized Least Squares (GLS) or Restricted Maximum Likelihood regression (REML) to estimate trends with serially correlated residuals, as was done for AR4 where the residuals were assumed to be an AR(1) process. Zhang and Zwiers (2004) found that the maximum likelihood approach works well for long time series and that for shorter time series iterative methods such as that proposed by (Wang and Swail, 2001) are very effective. For estimating linear trends in this chapter the simpler explicit method proposed by (Santer et al., 2008) will be used, which produces results that are similar to the more complex methods of (Wang and Swail, 2001) or REML of AR4 (see Appendix 2.A).

Non-linear trends

There are no a priori physical reasons why the long-term trend in climate should be linear-in-time. Historical climatic time series often have trends for which a straight line is not a good approximation (e.g., Seidel and

Lanzante, 2004) In particular, the residuals from a linear fit in time are often non-stationary and do not follow a simple autoregressive or moving average process. Furthermore, linear trend estimates can easily change when estimates are recalculated using data covering shorter or longer time periods e.g., when new data is added.

An alternative approach is to estimate local trends using non-parametric trend models obtained by penalized smoothing of time series (e.g., Wahba, 1990; Wood, 2006, Section 6.7.2). Shown in Box 2.2, Figure 1 is an example analysis of the global annual surface temperature values from the HadCRUT4 data set, in which the value in any year is considered to be the sum of a non-parametric smooth trend and a low-order autoregressive noise term. The trend is represented locally by cubic spline polynomials (Scinocca et al., 2010) and the smoothing parameter is estimated using REML allowing for AR(1) serial correlation in the residuals. This smoothed time series (Wood, 2006) is arguably a more justifiable alternative to a linear trend fit.

[INSERT BOX 2.2, FIGURE 1 HERE]

Box 2.2, Figure 1: (Top): HadCRUT4 global annual mean data from 1850 to 2010 (dots), grey line is a trend line for 1901–2010, black line is trend line for 1979–2010, both assuming AR1 errors. (Bottom): Same data as top, with spline smooth (solid curve) and the 95% confidence limits on the smooth curve, also assuming AR1 errors.

In this example, the differences between the two methods in the estimates of mean change in this data set (including 95% uncertainty limits) for the periods 1901–2010 and 1979–2010 are small (Box 2.2, Table 1). Both the linear method and the smoothing spline method suggest that the change in means between the early 20th Century and recent decades is statistically significant at the 1% level (using a two-sided t-test) with a stronger rate of warming over the last 30 years, consistent with prior assessments.

Box 2.2, Table 1: Estimates of the mean change per decade in global mean temperature between 1901 and 2010, and 1979 and 2010, obtained from the linear (OLS) and non-linear (Splines) trend models. Approximate 95% confidence intervals (± 2 standard errors in the mean change) in the estimates are also given for each trend model and are required in order to test if the changes are statistically significant. From the spline fit the 95% confidence interval for the difference in change rates between the two periods can be computed directly, and is 0.086 ± 0.038 (i.e., the change is significant at $p<0.0001$). Note that the ranges quoted in the table are solely that arising from the statistical trend model. Structural uncertainties and parametric (and other remaining) uncertainties are not considered (see Box 2.1).

	Change estimates (°C per decade) and two SE range for selected periods	
Method	1901–2010	1979–2010
OLS	0.074 ± 0.016	0.168 ± 0.040
Splines	0.084 ± 0.013	0.170 ± 0.046

[END BOX 2.2 HERE]

[START BOX 2.3 HERE]

Box 2.3: Global Dynamical Reanalyses

Dynamical reanalyses constitute an increasingly valuable and utilized resource for assessing weather and climate phenomena. Applications span a very broad range of disciplines. Although used in previous assessments, their characteristics have not been clearly outlined. Given their more abundant use in this assessment their characteristics are outlined here.

Reanalyses are distinct from and complement more ‘traditional’ statistical approaches to assessing the raw data. They do not provide gridded fields of observations. At the most basic level they use a modern day data assimilation scheme and weather forecasting model to integrate all historically available observations from multiple disparate sources and create a dynamically consistent estimate of the past atmospheric states. Unlike real-world observations, reanalyses are complete in space and time, which makes them intuitively appealing

for climate applications, particularly for some aspects of climate model validation where traditional observations simply are not available.

Several groups are actively pursuing reanalysis development and many of these have several generations of reanalyses products available (Box 2.3, Table 1). Since the first generation of reanalyses produced in the 1990s, substantial development has taken place. The reanalyses MERRA and ERA-Interim show improved tropical precipitation and hence better represent the global hydrological cycle. The NCEP/CFSR reanalysis uses a coupled ocean-atmosphere assimilation system (Saha et al., 2010). The 20th Century Reanalyses (20CR, Compo et al., 2011) is a 56 member ensemble (thus providing some information on uncertainty) and covers 140 years by assimilating only sea surface temperature, sea-ice and sea-level pressure (SLP) information. This variety of groups and approaches provides better estimates of uncertainties for any given application.

Box 2.3, Table 1: Overview of global dynamical reanalysis data sets. In addition to the global reanalyses listed here, several regional reanalyses exist or are currently being produced. A further description of reanalyses and their technical derivation is given in pp.S33-35 of Arndt et al. (2011).

Institution	Reanalysis	Period	Resolution at equator	Reference
Cooperative Institute for Research in Environmental Sciences (CIRES), USA	20th Century Reanalysis, Vers. 2 (20CR)	1871–2008	320 km	Compo et al. (2011)
National Centers for Environmental Prediction (NCEP) and National Center for Atmospheric Research (NCAR), USA	NCEP/NCAR R1 (NNR)	1948–	320 km	Kistler et al. (2001)
European Centre for Medium Range Weather Forecasts (ECMWF)	ERA-40	1957–2002	125 km	Uppala et al. (2005)
NCEP, US Department of Energy, USA	NCEP/DOE R2	1979–	320 km	Kanamitsu et al. (2002)
Japanese Meteorological Agency (JMA)	JRA-25	1979–	190 km	Onogi et al. (2007)
National Aeronautics and Space Administration (NASA), USA	MERRA	1979–	75 km	Rienecker et al. (2011)
European Centre for Medium Range Weather Forecasts (ECMWF)	ERA-Interim	1989–	80 km	Dee et al. (2011)
National Centers for Environmental Prediction (NCEP), USA	CFSR	1979–	50 km	Saha et al. (2010)

Reanalyses products provide invaluable information on process understanding and interannual variability. Their ability to characterize long-term trends remains an active question within the climate research community. Although reanalyses projects by definition use a “frozen” assimilation system, there are many other sources of potential errors. Changes in the observational systems (e.g., the introduction of satellite data) and errors in the underlying observations or in the boundary conditions can lead to inhomogeneities, even in latest generation reanalyses (Bosilovich, 2011). Reanalysis projects are complex and processing errors cannot be avoided completely.

Early generation reanalyses contained ubiquitous step changes in time that rendered them of limited value for trend characterization (Thorne and Vose, 2010). As subsequent products have learned from these pioneering efforts the ability to determine trends and quantify the uncertainties has improved. This has led to a more nuanced position whereby trend adequacy depends upon the variable under consideration, the time period and the region of interest. For example, the ERA-40 reanalyses from ECMWF have been shown to perform well for surface air temperature over land and humidity - variables not directly assimilated and therefore quasi-independent (Simmons et al., 2010) but caused controversy when applied to polar tropospheric temperature trends (Bitz and Fu, 2008; Grant et al., 2008; Graversen et al., 2008; Thorne, 2008).

[END BOX 2.3 HERE]

2.2 Changes in Temperature

2.2.1 Land-Surface Air Temperature

2.2.1.1 Large-Scale Records and their Uncertainties

AR4 concluded global land-surface air temperatures had increased, with the rate of change in the most recent 50 years being almost double that in the past Century. Since AR4, substantial developments have occurred including the production of revised datasets, an increase in available digital data density, and new dataset efforts. These innovations have improved understanding of data issues and uncertainties and allowed better understanding of regional changes. Long-term variations and trends of available global land surface estimates are in broad agreement despite the broader range of approaches and the greater difference in station counts, and the key findings in AR4 remain essentially unaffected. It is concluded with *very high confidence* that it is *virtually certain* that global land-surface air temperatures have experienced multi-decadal warming.

Observations are available for much of the global land surface since the mid-1800s to early 1900s. Availability historically is reduced in the most recent years due in large part to international data exchange latencies. Non-digital temperature records continue to be found in various country archives and are being digitized (Allan et al., 2011; Brunet and Jones, 2011). Efforts to create a single comprehensive raw digital data holding with provenance tracking and version control have advanced (Thorne et al., 2011b).

Improvements have been made to the historical global data sets of land-based station observations used in AR4. In addition, a new dataset has been produced from a group based at Berkeley (Rhode et al., submitted). Gross methodological details of the current versions of these datasets are given in Table 2.1. GHCN V3 improvements (Lawrimore et al., 2011) included elimination of "duplicate" time series for many stations, updating more station data with the most recent data, the application of enhanced quality assurance procedures (Durre et al., 2010) and a new pairwise homogenization approach for individual station time series (Menne and Williams, 2009). At the largest global scales version 3 was found to be virtually indistinguishable from version 2. GISS continues to provide an estimate based upon primarily GHCN but with different station inclusion criteria, additional night light based urban adjustments and a distinct gridding and infilling method (Hansen et al., 2010). CRUTEM4 (Jones et al., submitted) incorporates additional series and also newly homogenized versions of the records for a number of previously existing stations. It continues the model of incorporating the best available estimates for each station arising from research papers or individual national meteorological services on the assumption that such efforts have had most attention paid to them and access to the best metadata. In contrast the remaining products undertake a globally consistent homogenization processing of a given set of input data, although that data may itself not be truly raw observations. A new data product from a group at Berkeley (Rhode et al., submitted) use a kriging technique, commonly used in geostatistics, to create a global mean timeseries accounting for time-varying station biases by treating each apparently homogeneous segment as a unique record. This is substantially methodologically distinct from earlier efforts so helps to better span structural uncertainty in LSAT estimates.

Table 2.1: Summary of methods used by producers of global Land-Surface Air Temperature products. Only gross methodological details are included to give a flavour of the methodological diversity, further details can be found in the papers describing the dataset construction processes cited in the text.

Dataset	Start of Record	Number of Stations	Quality Control and Homogeneity Adjustments	Infilling	Averaging Procedure
CRUTEM4	1850	5583 (4842 used in gridding)	Source specific QC and homogeneity applied generally to source data prior to collation	none	Average of the two hemispheric averages weighted 2/3 NH and 1/3 SH.
GHCNv3	1880	7280	Outlier and neighbour QC and pairwise comparison based adjustments	Limited infilling by eigenvectors (for global mean calculations only)	Average of gridboxes area weighted

GISS	1880	c.6300	Night lights based adjustments for urban influences	Averages to 40 large scale bins	Average of the bins
Berkeley	1800	39028 / 7280[1]	Individual outliers are implicitly down-weighted. Neighbour-based test to identify breaks and each apparently homogeneous segment treated independently.	No gridding, but kriging produces field estimate based upon the station constraint at each timestep.	Kriged field estimate limited to maximum 1500Km distance from any station

The long-term variations and trends of available global land surface estimates are in broad agreement (Figure 2.1, Table 2.2) despite the broad range of approaches and the difference in station counts (Table 2.1). Land surface air temperature evolution exhibits inter-annual, decadal and inter-decadal variability that is grossly similar across all datasets, particularly since the mid-twentieth Century when available record sampling density is higher. In the early period of record sampling is far from global so differences are larger and different groups have made different decisions as to when meaningful global coverage ceases, reflected in the range of dataset start dates and in large part explaining the increase in the variance of the multi-dataset mean estimate. Uncertainties arising from choice of dataset do not impact the conclusion that global land surface air temperatures have increased and that the linear trend component of the change has been increasing (Table 2.2). Linear trend estimates for all the multi-decadal periods considered are highly significant.

[INSERT FIGURE 2.1 HERE]

Figure 2.1: Global land surface temperature timeseries evolution estimates from 1800 to present. Lower panel shows the mean of all available datasets available at each timestep (which varies prior to 1880). The top panel shows offsets from this multi-dataset mean series behavior (datasets in this panel are denoted in the key). Note the top plot range is much reduced compared to the lower plot and that inter-dataset differences are much smaller than the long-term series changes. All timeseries have been smoothed with a digital filter (Lynch and Huang, 1992) to emphasize variations on interannual timescales. GISS land data series have had a land mask applied to avoid interpolation over oceans undertaken in their public dataset release, which provides a more like-for-like comparison.

Table 2.2: Trend estimates and two standard error ranges corrected for AR1 autocorrelation impacts (see Box 2.2) for land surface dataset global average values over four common periods all ending in December 2010. GHCN and GISS do not extend prior to 1880 and so no values are given for these over 1850–2010. The range quoted is solely that arising from trend fitting uncertainty. Structural uncertainties, to the extent sampled, are apparent from the range of dataset estimates. Parametric (and other remaining) uncertainties, which many groups include (and calculate in distinct ways), are not considered. See Box 2.1 for further discussion of uncertainties. GISS data series have had a land mask applied to avoid interpolation over oceans undertaken in their public dataset release, which provides a more like-for-like comparison.

	OLS trend estimates (°C per decade) and two SE range (adjusted for AR1 autocorrelation effects) for selected periods			
Dataset	1850–2010	1901–2010	1951–2010	1979–2010
CRUTEM4	0.061 ± 0.006	0.094 ± 0.010	0.180 ± 0.024	0.274 ± 0.050
GHCNv3.0.0		0.091 ± 0.010	0.192 ± 0.024	0.282 ± 0.056
GISS		0.075 ± 0.010	0.168 ± 0.024	0.271± 0.050
Berkeley	0.086 ± 0.006	0.100 ± 0.010	0.193 ± 0.024	0.285 ± 0.056

Various theoretical challenges have been raised over the veracity of global land surface air temperature records since AR4 (Pielke et al., 2007) and some studies for sub-regions using a greater number of stations have yielded somewhat different regional characteristics (Christy et al., 2009). Subsequent research concludes these concerns to be largely unimportant in characterizing global-mean scale changes and serves to reinforce confidence in the reality of the reported time series behaviour. Station siting has been best documented for the USA, through a citizen science effort (Fall et al., 2011), for the USHCN network (Menne

[1]There are two versions of the Berkeley product and the version in Figures and Tables in the FOD comes from the methods paper that uses the NCDC GHCNv3 raw data holdings.

et al., 2009). Many sites exhibit far from optimal modern siting and may be expected to suffer large siting-induced biases (Fall et al., 2011). Within the USA modern siting quality is very highly correlated with instrument type and the biases for the network as a whole have been documented to be largely dominated by instrument type, rather than siting, biases (Menne et al., 2010; Williams et al., submitted). Regardless, homogenization procedures (Menne and Williams, 2009; Rhode et al., submitted) remove most, if not all, of the impacts (Fall et al., 2011; Menne et al., 2010; Muller et al., submitted; Williams et al., Submitted). Sampling and methodological independence has been assessed through sub-sampling, which shows very little sensitivity to use of entirely independent samples (Jones et al., Submitted; Parker et al., 2009), and creation of an entirely new and structurally distinct product (Rhode et al., submitted) and a complete reprocessing of the GHCN product (Lawrimore et al., 2011). None of these yielded more than minor perturbations to the records. Willett et al. (2008) and Peterson et al. (2011) explicitly showed that changes in humidity helped to confirm reported temperature trends, a result replicated in the ERA reanalyses (Simmons et al., 2010). Various investigators (Parker, 2011; Simmons et al., 2010; Vose et al., Submitted-a) showed that temperature trends and time series from modern reanalyses were in very good agreement with observed products. By removing entire countries and recalculating averages Jones et al. (Submitted) showed how, even for very large countries such as the USA or former USSR, there is very little impact on time series behaviour or trends of global means. Large summertime warm bias adjustments for very early records were revisited and grossly confirmed by a range of approaches including replication of non-standard exposures in long-term field studies (Bohm et al., 2010; Brunet et al., 2011).

McKitrick and Michaels (2004) and de Laat and Maurellis (2006) analysed surface air temperature trend fields and assessed potential for biases in terms of national socioeconomic and geographical indicators. Both studies concluded that urbanisation and related land surface changes have caused much of the observed warming. According to the AR4, the correlation of warming with industrial and socioeconomic development ceases to be statistically significant if one takes into account the fact that the locations of greatest socioeconomic development are also those that have been most warmed by atmospheric circulation changes. AR4 provided no explicit evidence for this overall assessment result. In subsequent analysis McKitrick and Michaels (2007) claimed to corroborate their earlier finding and concluded that about half the reported warming trend in global-average land surface air temperature in 1980–2002 resulted from local land-surface changes and faults in the observations. In contrast, Schmidt (2009), showed that much of the reported correlation between warming and socio-economic indicators likely arose due to naturally occurring climate variability and model over-fitting and was not robust. Further, it is impossible to reconcile such gross biases with the very good agreement seen between the methodologically diverse set of modern reanalysis products, none of which directly assimilate land-surface air temperatures, and the land-surface air temperature records at global and regional levels (Parker, 2011; Simmons et al., 2010; Vose et al., Submitted-a). These reanalysis products on average imply slightly more, rather than significantly less, warming than the observed datasets.

Particular attention since AR4 has been paid to the LSAT record over the United States. The US national dataset, USHCN, has evolved substantially, and issues beyond siting (above) have been addressed. A new homogeneity assessment approach has been employed (Menne and Williams, 2009), which was found to perform as well or better than many manually intensive approaches in a comprehensive European-data based suite of tests of candidate homogenization methods (Venema et al., 2011). Vose et al. (Submitted-a) showed the homogenised product to be both in substantially better agreement than the raw data and within the range of modern reanalyses products since 1979 for average, maximum, and minimum temperature. Fall et al. (2010) found that the North American Regional Reanalysis generated overall surface air temperature trends for 1979–2003 similar to the USHCN; the geographical pattern of observations-minus-reanalysis trends was in good qualitative agreement with Hansen et al. (2001)'s nightlights-based adjustments. (Williams et al., Submitted) produced an ensemble of USHCN and benchmarked against a suite of analogs. Benchmarking unveiled a propensity to under-estimate adjustments in the presence of network-wide systematic biases; with the extent being dependent upon the error structure. At least two such system-wide biases exist in the USHCN record relating to time of observation changes and a pervasive sensor-type change. When applied to the observations both minimum and maximum temperatures warm. As this is the most densely sampled region in the world, and given the breadth of analyses undertaken, that the lower 48 states as a whole have been warming on multi-decadal timescales is unequivocal.

A number of additional national or regional assessments have been undertaken, e.g., for Europe (Bohm et al., 2010) and East Africa (Christy et al., 2009). These analyses have used a range of methodologies and, in

many cases, more data and metadata than available to the global analyses. Despite the range of analysis techniques these more regional analyses are generally in broad agreement with the global analysis products at least in terms of the sign of the long-term changes in mean temperatures. This further enhances confidence in the reality of global and regional land surface air temperature increases on multi-decadal timescales.

2.2.1.2 Urban Heat Island Effects

In AR4 Urban Heat Island effects were concluded to be real local phenomena with negligible impact on changes in the global average. Substantial additional analysis has accrued, including evidence that in localized rapidly developing regions urban warming may account for upwards of 20% of the signal in the last 30 years. Equally, in some mature urban areas where the UHI has been stable over time multi-decadal trends may be unaffected. It is concluded with high confidence that urban heat island effects are real and have real impacts on urban populations but that their impact on the current global Land Surface Air Temperature analyses trends is small compared to the multi-decadal warming signal (less than 10%).

Urban Heat Islands (UHI) form because the modified surface affects the storage and transfer of heat. For the characterization of the true global mean, perhaps with the exception of very large metropolis areas where they represent regional-scale land use change, the impacts of UHI are considered a contaminating effect as sites are disproportionately located in urban or semi-urban locations. Many of these sites have potentially experienced increasing UHI effects not representative of broader regions.

Regionally, most attention since AR4 has focussed upon China where in some regions that have rapidly developed, UHI and land use changes impacts on regional trends have been substantial. A variety of investigations using methods as diverse as sea surface temperature comparisons (e.g., Jones et al., 2008), urban minus rural (e.g., Ren et al., 2008; Yang et al., 2011b) and observations minus reanalysis (e.g., Yang et al., 2011b; Hu et al., 2010) agree that the effect could be upwards of 20% in Eastern China and of the order 0.1°C/decade nationally (see Table 1 in Yang et al., 2011b) over the last 30 years. Observations-minus-reanalysis trends were most positive for barren and urban areas and negative in agricultural areas (Lim et al., 2008). Land-use changes to urban or barren (agriculture) caused observations-minus-reanalysis warming (cooling) respectively as expected from changes in surface heat fluxes. Hu et al. (2010) compared 4 reanalyses with surface air temperatures in eastern China, ascribing nearly a third of the overall warming in 1979–2008 to land-use changes. The influence of land-use change was greater at night, explaining nearly half of the observed decrease in frequency of nights colder than the 10th percentile. Given that China has seen the greatest pace of development globally in this period this likely places an upper-limit on the UHI impact for any region over this period. Fujibe (2009) implicitly ascribes about 25% of warming trends in Japan in 1979–2006 to urban development. Das et al. (2011) confirmed that many sites have experienced urban heat island warming and that for some individual stations this is double the background warming, but that apparently rural stations show plausibly unaffected behaviour given regional sea surface temperature evolution. Conversely, Jones and Lister (2009) and Wilby et al. (2011) using data from London (UK) concluded that some urban sites which have always been urban and where the heat island has not grown in magnitude will exhibit regionally indicative trends and that UHI effects may exhibit multi-decadal trends driven primarily by synoptic variations.

Estimates of large-scale temperature change have tended either to avoid urban observing sites, or adjusted their data to match regional rural trends (Hansen et al., 2010; Menne and Williams, 2009; Parker, 2010). Globally, (Hansen et al., 2010) used satellite-based nightlight radiances to estimate the worldwide influence on land surface air temperature of local urban development down to 1 km granularity. Adjusting trends in lit areas to match neighbouring dark areas only reduced the global 1900–2009 temperature change (averaged over land and ocean) from 0.71°C to 0.70°C. (Wickham et al., submitted) similarly used satellite data (from MODIS which classifies land types at finer granuality) and a much larger network of stations and found that urban locations exhibited less warming than rural stations, although not statistically significantly so, over 1950 to 2010.Efthymiadis and Jones (2010) estimated an absolute upper limit on urban influence of 0.02°C per decade, or ~15% of the total trends, in 1951–2009 from trends of coastal land and sea surface temperature but argued on physical theoretical grounds that the true value was likely to be lower than this.

2.2.1.3 Diurnal Temperature Range

In AR4 Diurnal Temperature Range (DTR) was found, globally, to have narrowed with minimum increasing faster than maximum; but significant multi-decadal variability was highlighted including a recent period of no change. New insights regarding the likelihood of differential bias impacts between minimum and maximum temperatures lead to an assessment of medium-to-low confidence in reported DTR changes at the global and regional levels, as to date these almost exclusively rely upon analysing the raw, bias impacted, data.

No global analysis has been undertaken subsequent to (Vose et al., 2005a), reported in AR4 for the period 1950–2004. Regional analyses since this time have reported some differences. (Makowski et al., 2009) find that the long-term trend of annual DTR in Europe over 1950 to 2005 changed from a decrease to an increase in the 1970s in Western Europe and 1980s in Eastern Europe. Roy and Balling (2005) found significant increases in both maximum and minimum temperatures for India, but little change in DTR over 1931–2002. Christy et al. (2009) reported that for East Africa there has been no pause in the narrowing of DTR in recent decades.

AR4 discussed a so-called "weekend" effect in DTR for a number of regions including the USA, China, Japan, and Mexico (Forster and Solomon, 2003). Since then similar effects have been found for Germany (Baumer and Vogel, 2007), China (Gong et al., 2007; Ho et al., 2009a), southern Europe (Sanchez-Lorenzo et al., 2008b), and all Europe (Laux and Kunstmann, 2008). In each case the DTR for weekdays and weekend days is significantly different, in most cases greater on the weekend.

Various investigators (e.g., Christy et al., 2009; Pielke et al., 2007) have raised on theoretical grounds and for specific areas doubts over the interpretation of minimum temperature trends. Essentially it has been argued that microclimate and local atmospheric composition impacts are most apparent in minimum temperatures because the dynamical mixing is much reduced and therefore minimum temperatures should not be considered when analysing global trends. Parker (2006) used the difference between calm and windy nights to address issues with minimum temperature trends and found no difference between trends for calm and windy nights on a global average basis. If the data were fundamentally affected, as posited, then a difference would be expected. However, recent analyses (Vautard et al., 2010), imply modest reductions in mean wind-speeds in recent decades which may have an impact on night-time minima. Regardless, global average temperatures are averages over space and time and should include the full characteristics of the data, which requires understanding changes in the long-term mean and therefore the diurnal characteristics, so minimum temperatures are necessary to include.

However, there certainly are real non-climatic data artefacts that affect maximum and minimum differently in the raw records for both recent (Fall et al., 2011; Williams et al., submitted) and older (Bohm et al., 2010; Brunet et al., 2011) records. Hence there could be issues over interpretation of apparent DTR trends and variability in many regions (Christy et al., 2009; Christy et al., 2006; Fall et al., 2011; Williams et al., Submitted), particularly when accompanied by regional-scale Land Use / Land Cover changes (Christy et al., 2006). As most studies looking at diurnal temperature ranges to date have considered raw data, including those in AR4 (e.g., Vose et al., 2005a), it is unclear to what extent the conclusions from such studies are afflicted by diurnally differentiated biases in the data yielding spurious time series behaviour in DTR.

2.2.2 Sea Surface Temperature and Marine Air Temperature

AR4 concluded that "recent" warming (since the 1950s) was strongly evident at all latitudes in sea surface temperatures (SST) over each ocean. Prominent spatio-temporal structures including the El Nino and Pacific Decadal variability patterns in the Pacific Ocean and a hemispheric asymmetry in the Atlantic Ocean were highlighted as contributors to the regional differences in surface warming rates, which in turn affect atmospheric circulation. Since AR4 there has been a step change in availability of metadata, improvements in data completeness and a number of new SST products. Intercomparisons of data obtained by different measurement methods, including satellite data, have resulted in better understanding of errors and biases in the record. While these new products and information have helped highlight and quantify uncertainties, they do not alter the conclusion with very high confidence that global SSTs have increased both since 1950s and since the late 19th Century.

2.2.2.1 Advances in Assembling Data Sets and in Understanding Data Error

2.2.2.1.1 In situ data records

Most historical SST observations arise from ships, with buoy measurements and satellite data becoming a significant contribution in the 1980s. Digital archives such as the International Comprehensive Ocean-Atmosphere Data Set (ICOADS, currently version 2.5, Woodruff et al., 2011) are constantly augmented as paper archives are imaged and digitised (Brohan et al., 2009). Because of the irregular nature of sampling in space and time when observations are made from the moving platforms (ships and floating buoys), it is customary to use statistical summaries of "binned" (most commonly grid box) observations rather than individual observed values (Table 2.3). Means or medians of all SST values in a given bin that pass quality control procedures represent reported SST values. Standard deviations and numbers of observations in individual bins are useful for estimating uncertainties. These procedures usually serve as an initial step for producing more sophisticated gridded SST products, which involve bias correction and, possibly, interpolation and smoothing. Despite substantial efforts in data assembly, the total number of available SST observations and the percentage of the Earth surface area that they cover remain very low before 1850 and drop drastically during the two World Wars.

Improvements in the understanding of uncertainty have been expedited by the use of metadata such as WMO Publication 47 International List of Selected and Supplementary Ships (Kent et al., 2007) and the recovery of observer instructions and other related documents. Early data were systematically biased cold because they were made using canvas or wooden buckets that, on average, lost a great deal of heat to the air before the measurements were taken. This effect has long been recognized, and various "bucket correction" schemes developed, which use simplified physical modelling of a bucket's heat exchange with the air (Folland and Parker, 1995; Rayner et al., 2006) or statistical modelling based on the difference between measured SST and Night Marine Air Temperature (NMAT) observations (Smith and Reynolds, 2002). Prior to AR4 this was the only artefact adjusted in SST products, and these adjustments were applied only before 1941, since more advanced measurement methods as well as buckets of improved design became popular in the later period; these exhibited smaller systematic biases (Figure 2.2, top). Beginning in the 1930s some ships began taking measurements of engine room intake (ERI) water. It is hypothesized that proximity to the hot engine often biases these measurements warm (Kent et al., 2010). Because of the prevalence of the ERI measurements among SST data from ships, the ship SSTs are biased warm by 0.12-0.18K on average compared to the buoy data (Kennedy et al., 2011a; Kennedy et al., 2011c; Reynolds et al., 2010). Since the 1980s, drifting and moored buoys have been producing an increasingly large fraction of global SST observations. As fractions of data obtained by each method in the global data set are changing in time, so does the overall bias in the global SST time series (Figure 2.2, bottom), if no adjustment is made.

[INSERT FIGURE 2.2 HERE]

Figure 2.2: Temporal changes in the prevalence of different measurement methods in the ICOADS. (top) Fractional contributions of observations made by different measurement methods: bucket observations (blue), ERI and hull contact sensor observations (green), moored and drifting buoys (red), and unknown (yellow). (bottom) Global annual average SST anomaly based on different kinds of co-located data: ERI and hull contact sensor (green), bucket (blue), buoy (red), and all (black). Adapted from Kennedy et al., (2011b).

A traditional approach to estimating random error in binned averages of in situ SST data has been assuming the independence of individual measurements, so that the error variance in the average decreases inversely proportionally to the number of averaged observations. Kent and Berry (2008) proposed, in addition to the random error of individual observations, to allow for platform-dependent biases, which can be assumed constant within the same platform (an individual ship or buoy) but may change from a platform to a platform in a random fashion.When a bin includes many observations from the same platform, this new error model results in a larger, more realistic error estimates for the bin average. Kennedy et al. (2011a; 2011c) further substantiated and verified this model.

Although noisier than SSTs, MATs are likely to be physically constrained to track SST variability (although not at all times / locations e.g., Christy et al., 2001; Smith and Reynolds, 2002), because of the continuous air-sea heat exchange. Thus they provide an independent measure of marine temperature change. Adjustments have been applied to account for the change in deck heights and for the use of non-standard practices during World War II (Rayner et al., 2003) and the nineteenth Century (Bottomley et al., 1990) Because of biases due to solar heating, only NMATs have so far been widely used in climate analyses. The

progress on the analytical correction of solar heating biases in recent day-time MAT data allowed their use in a recent analysis (Berry and Kent, 2009; Berry et al., 2004).

2.2.2.1.2 Satellite SST data records

SSTs are observed from space by sensors measuring the radiation leaving Earth in both infra-red (IR) and microwave (MW) parts of the electromagnetic spectrum. IR-based estimates are available at spatial resolutions of 1 to 10 km, when clouds do not intervene between the surface and sensor. The MW sensors give observations of SST with spatial resolutions of 25 to 50 km for most of the global ocean in the absence of precipitation and at distances more than 50 km from coasts, islands and sea ice. With both IR and MW, the spatio-temporal coverage is generally far denser than with *in situ* SST measurements. On the other hand, satellite measurements are indirect, it being necessary to eliminate the atmospheric influence on the radiation observed from space in order to infer SST, usually through reference to in-situ measurements. Satellite data adds spatial and temporal fidelity compared to in-situ measures.

The majority of satellite SST data arise from operational meteorological sensors. The principal IR sensor is the Advanced Very High Resolution Radiometer (AVHRR) series. AVHRR SSTs are tied to the calibration of the drifting buoy network by empirical regression of the satellite observations to matched drifting buoy SSTs. Since AR4, the AVHRR time series has been reprocessed consistently back to March 1981 (Casey et al., 2010) to create the AVHRR Pathfinder v5.2 (PFV52) data set. Passive MW data sets of SST are available since 1997 for lower latitudes (<40 degrees of latitude) and since 2002 near-globally. MW SSTs are also tuned to *in situ* observations. They are generally less accurate than IR-based SST data sets, although the superior sampling coverage in areas of persistent cloudiness can help address sparseness in the IR record (Reynolds et al., 2010).

The Along Track Scanning Radiometer (ATSR) series of three sensors was designed for climate monitoring of SST, and now has a record exceeding two decades (since August 1991). The ATSRs are “dual-view” IR radiometers intended to support atmospheric effects removals without use of *in situ* observations. Kennedy et al. (2011a) used ATSR SST observations to estimate biases in *in situ* observations. Since AR4, ATSR observations have been reprocessed with new estimation techniques (Embury and Merchant, 2011). The new ATSR SSTs seem to be more accurate than many *in situ* observations (Embury et al., 2011). Despite the independent technique of estimating SST, and only marginal dependence on *in situ* observations (through other aspects of the reprocessing), the ATSR SST time series of global monthly mean SST anomaly is highly coherent with that obtained using only *in situ* observations (represented in Figure 2.3 by the HadSST3 ensemble).

[INSERT FIGURE 2.3 HERE]

Figure 2.3: Global monthly mean SST anomalies measured from satellites (ATSRs) and *in situ* (HadSST3). Black lines: HadSST3 ensemble of 100. Red line: ATSR night-time SST timeseries from the ATSR Reprocessing for Climate (ARC) project. One month is missing in 1996 due to non-complete overlap of successive satellite missions.

2.2.2.1.3 Comparing different types of data and their error

Comparisons are complicated as different technologies measure somewhat different physical characteristics of the surface ocean. IR and MW radiometers sense water temperature of the 10–20 μm and 1–2 mm respectively, whereas in situ SST measurements are made in the depth range between 10 cm and several meters and are often called “bulk” SST, with an implicit assumption that that the ocean surface layer is well-mixed. This assumption is valid only for night-time conditions or when surface winds are strong. Otherwise, the surface layer is stratified and its temperature exhibits diurnal variability (Kawai and Wada, 2007; Kennedy et al., 2007), such that a measured temperature value typically depends on the depth and time of day at which the measurement is made (Donlon et al., 2007). Aside from the diurnal variability, an independent phenomenon of a thermal skin layer takes place in the top 1 mm or so of the ocean surface and results in a strong temperature gradient across this layer (usually, cooling towards the surface), especially enhanced in the top 100 μm. While all in situ and satellite measurements might be affected by diurnal variability, only IR satellite data are subject to the thermal skin effect. IR radiometers are said to measure “skin” temperature. Temperature at the bottom of the thermal skin layer is called “subskin temperature.” MW radiometer measurements are close to this variable. To estimate error variance or to verify error estimates for SST observations by comparison of different kinds of SST data, data values have to be adjusted

for time and depth differences by modelling the skin effect and diurnal variability or by constraining the comparison to the night-time data only, to minimize the diurnal variability effects.

Comparisons between in situ measurements and different satellite instruments have been used to assess the uncertainties in the individual measurements. Random errors on ATSR measurements have been estimated (Embury et al., 2011; Kennedy et al., 2011a; O'Carroll et al., 2008) to lie between 0.1 and 0.2 K. The uncertainties associated with random errors for AATSR are therefore much lower than for ships (around 1–1.5 K: Kent and Challenor, 2006; Kent et al., 1999; Kent and Berry, 2005; Reynolds et al., 2002; Kennedy et al., 2011a) or drifting buoys (0.15–0.65 K: Kennedy et al., 2011a; Reynolds et al., 2002; Emery et al., 2001; O'Carroll et al., 2008).

Characterizing relative mean biases between different systems informs the procedures for homogenizing data sets that combine different kinds of measurements. Embury et al. (2011) found average biases of less than 0.1 K between reprocessed AATSR retrievals and drifting buoy observations and of around 0.1 K between ATSR2 retrievals and buoys. Kennedy et al. (2011a) found that ships were warmer than AATSR retrievals by 0.08 K and drifting buoys colder by 0.10K on average and hypothesized that HadSST2 contained an increasing cool bias because of a decrease in the relative proportion of warm-biased ship observations. They applied a time-varying adjustment to the HadSST2 global means in the form of 0.18 K times the fraction of drifting buoys compared to the 1991–1995 period. This correction improved the consistency between trends in global average anomalies from the in situ and ATSR data sets. However, Kennedy et al. (2011b) found a smaller relative bias between ships and drifting buoys and found that changes in the biases associated with ship measurements might have been as large, or larger than, this effect.

2.2.2.2 Gridded SST Products and Trends

Gridded dataset development involves binning, quality control, conversion to anomalies, and if deemed necessary bias adjustment. Globally complete objective analyses of historical SST apply to such datasets spatial and temporal analysis: usually, some form of kriging (optimal interpolation) procedure with a goal of producing a data set with a complete coverage over the global ocean without any temporal gaps. Many such operational (systematically updated) data sets blend in satellite data starting from the autumn 1981.

"Historical" gridded SST data sets span periods longer than a century and usually have monthly temporal resolution and a nominal spatial resolution of 1° or coarser. For the satellite data period higher resolution globally complete interpolated data sets are possible (Reynolds et al., 2007; Stark et al., 2008). Table 2.3 gives a brief description of well-known historical SST products, organized by their type. Figure 2.4 intercompares global averages of anomalies from these data sets. Linear trend estimates for these timeseries in different subperiods are presented in Table 2.4.

Table 2.3: Data Sets of SST and NMAT Observations Used in Subsection 2.2.2. These data sets belong to the following categories: a database of individual in situ observations; gridded data sets of climate anomalies (with bucket and potentially additional bias corrections applied); and globally complete interpolated data sets based on the latter products.

Data Set	Period	Space-Time Grid Resolution	Bucket/ Bias Corrections Applied
Historical Database of In Situ Observations			
International Comprehensive Ocean – Atmosphere Data Set, ICOADS, v2.5	1662 – present; 1800 – present, 1960 – present	Individual reports; 2° x 2° mon summ; 1° x 1° mon summ	No
Gridded Data Sets of Observed Climate Anomalies			
U.K.M.O. Hadley Centre SST, v.2, HadSST2	1850 – present	5° x 5° monthly	Yes, 1850–1941
U.K.M.O. Hadley Centre SST, v.3, HadSST3	1850–2006	5° x 5° monthly	Yes, 1850–2006
U.K.M.O. Hadley Centre NMAT, v.4.3 MOHMAT4.3N	1856–2007	5° x 5° monthly	Yes, 19th Century and WWII
Globally Complete Objective Analyses (Interpolated Products) of Historical SST Records			

U.K.M.O. Hadley Centre Interpolated SST, v.1, HadISST	1870 – present	1° x 1° monthly	Yes, 1870–1941
JMA Centennial in-situ Observation Based Estimates of variability of SST, COBE SST	1891 – present	1° x 1° monthly	Yes, 1891–1941
NOAA Extended Reconstruction of SST, ERSSTv3b	1854 – present	2° x 2° monthly	Yes, 1854–1941

[INSERT FIGURE 2.4 HERE]

Figure 2.4: Global means of SST timeseries since 1854. Lower panel shows the mean on the three interpolated products (COBE, ERRSTv3b and HadISST). The top panel shows offsets from this average for two uninterpolated products (HadSST2 and HadSST3), the raw SST measurement archive (ICOADS) and night marine air temperatures (MOHMAT43N). The mean timeseries and the offset series have had a digital filter applied as described in Figure 2.1.

Table 2.4: Temporal linear trend slopes (in ^{o}C per decade) for annual averages of global mean anomalies and their 5% to 95% confidence intervals (results for incomplete time periods are italicized). Trend slopes were estimated using ordinary least squares regression with the lag-1 autocorrelation taken into account for the uncertainty calculation (Santer et al., 2008).

Data Set	1850–2010	1901–2010	1951–2010	1979–2010
HadSST2	0.041 ± 0.012	0.070±0.015	0.096 ± 0.023	0.135 ± 0.038
HadSST3	*0.038 ± 0.012 (1850–2006)*	*0.065 ± 0.015 (1901–2006)*	*0.070 ± 0.036 (1951–2006)*	*0.152 ± 0.035 (1979–2006)*
MOHMAT43N	*0.033 ± 0.016 (1856–2005)*	*0.072 ± 0.014 (1901–2005)*	*0.099 ± 0.030 (1951–2005)*	*0.107 ± 0.037 (1979–2005)*
HadISST1	*0.038 ± 0.007 (1870–2010)*	0.053 ± 0.007	0.066 ± 0.016	0.080 ± 0.025
ERSSTv3b	*0.032 ± 0.019 (1854–2010)*	0.066 ± 0.009	0.082 ± 0.015	0.102 ± 0.028
COBE	*0.051 ± 0.009 (1891–2010)*	0.058 ± 0.008	0.073 ± 0.015	0.080 ± 0.022

Data coverage prior to the second half of the nineteenth Century is extremely poor (with little or no data available prior to 1800). Hence global analyses start in 1850 or later. Temporal and spatial variations in relative contributions of different measurement methods to the total database of historical observations create a time-varying bias in the SST values (Figure 2.2). The largest component of this bias, the effect of uninsulated buckets before 1940s has been corrected in all data sets intended for studies of the long-term SST variability. The size of these corrections roughly matches the difference between NMAT and ICOADS anomalies seen in the top panel of Figure 2.4.

In the HadSST3 product biases and their uncertainties are estimated throughout the whole record (Kennedy et al., 2011b). Adjustments for these biases are responsible for differences between the estimates of global-average SST calculated from HadSST2 and HadSST3 (Figure 2.4), significant differences due to the ERI-to-bucket transition at the end of World War II (Thompson et al., 2008) are confined to the period 1945 to 1960. Their effect on linear trend estimates for periods of the order of a century is quite small relative to the trend uncertainty and smaller than or similar to between dataset structural uncertainties (Table 2.4). As a result of the new approach to error modelling (described above), the error estimates for grid boxes where most observations came from the same ship or buoy have increased substantially compared to HadSST2. Since the new error model introduces a correlation between different grid boxes as well, estimated errors in regional averages increased: error estimates in global and hemispheric monthly means are more than double the estimates from HadSST2 (Kennedy et al., 2011a).

Globally complete objective analyses of historical SST depend on their "analysis" method (e.g., how missing data are imputed and how existing data are smoothed) as well as on the underlying set of observations, their uncertainty estimates, quality control (QC), and bias correction procedures. SST analyses such as HadISST1 (Rayner et al., 2003), ERSSTv3b (Smith et al., 2008) and COBE (Ishii et al., 2005), use statistical methods to

fill areas of missing data. At the time of writing HadISST1 remains unchanged from AR4.The low-frequency component calculation has been optimised in version 3 of ERSST (Smith et al., 2008); the most current ERSST version, 3b, restricted the procedure to the use of the in situ data only.

Local linear trend estimates for three interpolated globally complete gridded SST analyses are shown in Figure 2.5. Trend magnitudes and spatial patterns exhibit a great deal of similarity across different products. Since the 110-year trends (1901–2010) are less affected by decadal variability than trends computed for shorter periods, they display a more spatially uniform pattern of general warming. By contrast, shorter period trend patterns are affected by natural climate variability in various ways: the overall trend patterns for 1979-2010 in the Atlantic and Pacific Ocean reflect contributions from changes in the Atlantic Multidecadal Oscillation (AMO) pattern and the Pacific Decadal Oscillation (PDO) pattern (see Box 2.4), in agreement with the 1979–2010 trends in indices of these oscillations: AMO, 0.802 ± 0.305 s.d./decade and PDO, –0.386 ± 0.308 s.d./decade. Areas in the 1979–2010 trend patterns where the trend slopes do not reach even 10% significance are areas of large interannual variability due to ENSO and its teleconnections. Large swings of the PDO index during this time period might have contributed to the loss of trend significance too.

[INSERT FIGURE 2.5 HERE]

Figure 2.5: Linear trend slope estimates for 1901–2010 and 1979–2010 periods in the annual means of interpolated globally complete SST data sets. See Table 2.3 for data set details. Color patches show trends with higher than 90% confidence. In the areas where the 5% to 95% confidence interval for the slope contains zero, the field of slope estimates is shown by dotted color contours. Trend slopes were estimated using ordinary least squares regression with the lag-1 autocorrelation taken into account for the uncertainty calculation (Santer et al., 2000).

2.2.3 Global Combined Surface Temperature

AR4 concluded that the global average surface temperature had increased, especially since 1950. The three available independently produced datasets were concluded to be consistent with each other. Subsequent developments have led to better understanding of the data and their uncertainties. In particular instrumental artefacts have cast doubt on aspects of the reported decadal variability in the mid-twentieth Century and the magnitude of the local maxima in the 1940s. It is concluded with very high confidence that the world is warming on multi-decadal (greater than 30 years) timescales and that this warming has been particularly marked since the mid-twentieth Century.

Innovations have occurred for all three data products that were utilized in AR4. Table 2.5 summarizes current methodological approaches. For HadCRUT4 both the land and the ocean data sources have been updated (preceding sections), and the product now consists of 100 equi-probable solutions (Morice et al., Submitted). Changes to the SST data and inclusion of more high latitude land stations lead to: i) significant changes in the period 1940–1970 with much less of a 1940s local maxima in global mean temperatures and ii) greater warming in the most recent decade than in the previous dataset version relegating 1998 to third warmest. This change in the most recent decade is consistent with the remaining products and with a comparison with reanalyses (Simmons et al., 2010) that implied the previous version had under-estimated most recent decade warming. NOAA's MLOST product has incorporated GHCNv3 and ERSST3b (a variant on version 3 (Smith et al., 2008) which removes the satellite data which was discovered to have a relative bias to in-situ measures) and reinstated high-latitude land data (Vose et al., Submitted-b). Since AR4 NASA GISS have undertaken updates and a published sensitivity analysis focussed primarily around their urban heat island adjustments approach (previous section) and choice of product and method for merging pre-satellite era and satellite era SSTs (Hansen et al., 2010). For SST several alternative datasets or combinations of datasets were considered and these choices had an impact of the order 0.04 K for the net change over the period of record. An improved concatenation of pre-satellite era and satellite era SST products removed a small apparent cooling bias in recent times. Following the release of their code the GISS method has been independently replicated in a completely different programming language (Barnes and Jones, 2011).

Table 2.5: Methodological details for the current global merged surface temperature products. Only gross methodological details are included to give a flavour of the methodological diversity, further details can be found in the papers describing the dataset construction processes.

Dataset	Start Date	Land Dataset	Marine Dataset	Merging of Land and Marine	Infilling	Averaging Technique

HadCRUT4 (100 versions)	1850	CRUTEM4 (100 versions)	HadSST3 (100 versions)	Weighted average based upon the percentage coverage	None, spatial coverage incompleteness accounted for in error model	Average of area weighted Northern and Southern Hemisphere averages
MLOST	1880	GHCNv3	ERSST3b	Weighted average based upon the percentage coverage	Low frequency component filtered. Anomaly spatial covariance patterns for high frequency component. Land and ocean interpolated separately.	Area weighted average of available gridbox values
NASA GISS	1880	GHCNv3, USHCNv2 plus Antarctic SCAR data	HadISST1 (1870–1981), OISSTv2 (1981–)	Priority given to land data	Radius of influence up to 1200 km for land data	After gridding, non-missing values are averaged over the zones 90°S–23.6S, 23.6°S–0°, 0°–23.6°N, 23.6°N–90°N; and the four means are averaged with 3:2:2:3 weighting to represent their area.

Global mean surface temperatures have increased since the late nineteenth Century. Warming has not been linear; most warming occurred in two periods – 1900–1940 and 1970 onwards. Starting in the 1980s each decade has been warmer than all preceding decades in the record by a larger amount than can be accounted for by recognized uncertainties in the data products (Figure 2.6). Furthermore, each year in these decades has been warmer than the average of the preceding decade. All ten of the warmest years in the global records have occurred since 1997 with 2010 and 2005 effectively tied for the warmest year on record in all three products.

[INSERT FIGURE 2.6 HERE]

Figure 2.6: Decadal mean anomalies and associated uncertainties (2.5–97.5 percentile ranges) based upon the HadCRUT4 ensemble(Morice et al., Submitted). Anomalies are relative to a 1961–1990 climatology period. NCDC MLOSTand GISS dataset estimates are also shown and their uncertainties would yield grossly similar results and a similar conclusion that each of the last three decades in turn has been significantly warmer than all preceding decades in the record.

Differences between datasets are much smaller than both inter-annual variability and the long-term trend (Figure 2.7). However, there are some decadal timescale differences. Much interest has focussed on differences in the period since 1998 and the popularly posed question ‘has global warming stopped?’ based upon HadCRUT3 trends. Various investigators have pointed out the futility of such short-term trend analysis in the presence of auto-correlated series variability and that there exist several other similar length phases of no warming in all the observational records and in climate model simulations (Easterling and Wehner, 2009; Peterson et al., 2009; Santer et al., 2011). None of these earlier decadal-timescale cessations in warming portended a cessation of the longer-term warming trend. This issue is discussed in more detail in the context of model behaviour and natural variability in Chapter 10. Regardless, changes to HadCRUT4, primarily as a result of incorporation of more high-latitude Northern Hemisphere land data mean that all products now show a warming trend since 1998 (Morice et al., Submitted). Differences between datasets are larger in earlier periods that have received less focus. They are particularly large prior to c.1945 when observational sampling is much more incomplete (and many of the well the sampled areas may have been globally unrepresentative (Bronnimann, 2009), the data errors and subsequent methodological impacts are larger (Thompson et al., 2008), and the different ways of accounting for data void regions become more important (Vose et al., 2005b).

[INSERT FIGURE 2.7 HERE]

Figure 2.7: Global mean temperature series at annual resolution from a straight average of the three data products, plus differences between each product and this mean. For details of the smoothing applied refer to Figure 2.1.

Since 1901 almost the whole globe has experienced warming (Figure 2.8). This warming is greater over land than ocean in general although the SE contiguous United States, Central Africa, SE Asia, Australia and Patagonia have exhibited little or no net warming. The only ocean region not to have exhibited warming is the North Atlantic south of Greenland. Warming is generally greater in mid- to high-latitude regions. Over the satellite era again most of the globe has exhibited warming at the surface. Exceptions are parts of Australia and S. America, much of the Southern Ocean and the Eastern Pacific. The global mean warming rate has been much greater in this recent period than for the record as a whole (Table 2.6).

[INSERT FIGURE 2.8 HERE]

Figure 2.8: Global trend maps from NCDC MLOST surface record for 1901 to 2010 (left hand panel) and 1979 to 2010 (right hand panel). Trends have been calculated only for those gridboxes with greater than 70% complete records using OLS regression with standard errors adjusted for AR1 autocorrelation effects (Box 2.2). Gridboxes where the absolute trend is greater than 2 standard errors from zero are highlighted with a black cross.

Table 2.6: Trend estimates and two standard error ranges (see Box 2.2) for combined surface dataset global average values over four common periods all ending in December 2010. GHCN and GISS do not extend prior to 1880 and so no values are given for these over 1850–2010. The range quoted is solely that arising from trend fitting uncertainty. Structural uncertainties, to the extent sampled, are apparent from the range of dataset estimates. Parametric and other uncertainties, which many groups include, are not considered. See Box 2.1 for further discussion of uncertainties.

	OLS trend estimates (°C per decade) and two SE range (adjusted for AR1 autocorrelation effects) for selected periods			
Dataset	1850–2010	1901–2010	1951–2010	1979–2010
HadCRUT4	0.045 ± 0.004	0.075 ± 0.008	0.109 ± 0.020	0.171 ± 0.032
NCDC MLOST		0.077 ± 0.008	0.118 ± 0.016	0.163 ± 0.030
GISS		0.070 ± 0.006	0.113 ± 0.016	0.167 ± 0.034

2.2.4 Upper Air Temperature

Understanding of free atmosphere temperature trends has evolved substantially since inception of the IPCC process. All previous reports highlighted the presence of significant uncertainty and possibility of hitherto unidentified issues (Thorne, 2011b). Despite this AR4 concluded that globally the troposphere was warming at a rate indistinguishable from reported surface trends over the common period of record. Trends in the tropics were concluded to be more uncertain although even this region was concluded to be warming. Globally, the stratosphere was concluded to be cooling over the satellite era starting in 1979. New advances since AR4 have highlighted the substantial degree of uncertainty in both satellite and weather balloon records that were never intended primarily to serve climate-monitoring needs. It is concluded with very high confidence that the troposphere has been warming and the stratosphere cooling since the mid-twentieth Century. There is medium to low confidence in the rate and vertical structure of tropospheric temperature changes globally, and low confidence in the tropics. Estimates of tropospheric warming rates encompass surface temperature rate estimates. There is low confidence in the rate and in particular the vertical structure of stratospheric cooling trends.

The major global radiosonde records extend back to 1958 with temperatures, measured as the balloon ascends, reported on distinct levels. Satellites have monitored tropospheric and lower stratospheric temperature trends since late 1978 through the Microwave Sounding Unit (MSU) and its follow-on Advanced Microwave Sounding Unit (AMSU) since 1998. These measures of upwelling radiation represent bulk atmospheric temperature (Figure 2.9). The ‘Mid-Tropospheric’ (MT) MSU channel that most directly corresponds to the troposphere has 10–15% of its signal from both the skin temperature of the Earth’s surface and the stratosphere. Two alternative approaches have been suggested for removing the stratospheric component based upon differencing of view angles and statistical recombination with the ‘Lower Stratosphere’ (LS) channel (Fu et al., 2004; Spencer and Christy, 1992). On the MSU satellite series in addition there was a Stratospheric Sounding Unit (SSU) that measured at higher altitudes (Seidel, 2011).

[INSERT FIGURE 2.9 HERE]

Figure 2.9: Vertical weighting functions for those satellite temperature retrievals discussed in this chapter. The dashed line indicates the typical maximum altitude achieved in the historical radiosonde record.

2.2.4.1 Advances in Radiosonde Records

For AR4 only two published radiosonde temperature estimates that had assessed homogeneity issues existed – RATPAC (Free et al., 2005) and HadAT (Thorne et al., 2005b). Three additional estimates now exist using novel and distinct approaches (Table 2.7) in addition to a systematic effort to understand uncertainty in the HadAT product. These advances significantly modify understanding of the structural uncertainty (Thorne et al., 2005a). A group at University of Vienna have produced RAOBCORE and RICH (Haimberger, 2007) using ERA reanalysis products (Box 2.3) to ascertain breakpoints. Uncertainties in adjustments arising from reanalyses for RAOBCORE have been addressed by several variants and sensitivity studies (Haimberger, 2004, 2007; Haimberger et al., 2008). The RICH product has only an indirect dependency on this field as the adjustments are neighbour based. Sherwood and colleagues developed an iterative universal kriging approach for radiosonde data (Sherwood, 2007) and applied this to a global network (Sherwood et al., 2008) to create IUK. They concluded that issues likely remained in the deep tropics even after homogenisation. Recourse to metadata and the analog cases used in the HadAT work (Titchner et al., 2009) increased confidence in the product (Sherwood et al., 2008). The original HadAT algorithm (Thorne et al., 2005b) included substantial human input which has distinct drawbacks regarding reproducibility and the ability to assess fundamental uncertainties. The group created an automated version of HadAT, identifying a large number of non-rigorously based methodological steps as tunable parameters (McCarthy et al., 2008). They then created four distinct analog worlds that shared the spatio-temporal sampling of the real world and, crucially, had known error structures. Running the ensemble against these analogs enabled a degree of benchmarking and a reassessment of likely real-world trends and their uncertainties (Titchner et al., 2009). In a final analysis step more wide ranging methodological choices were examined against the analogs (Thorne et al., 2011a). The largest impact was varying the input data temporal resolution. Subsets of results were combined using conditional probabilities to yield a final estimate. This includes all other radiosonde datasets for global mean trends over the common period of record (Figure 2.10). A similar ensemble approach has also been applied to the RICH product although limited in its scope solely to the adjustment choices (Haimberger et al., Submitted) and without recourse to similar benchmarks. This ensemble spread was of a similar magnitude to the conditional probability estimates of Thorne et al. (2011a) and generally showed more warming / less cooling that existing products at all levels. Globally the radiosonde records all imply the troposphere has warmed and the stratosphere cooled since 1958 but with substantial uncertainty in the rate of change that grows with height. This uncertainty is much greater at sub-global scales, particularly outside the well sampled Northern Hemisphere extra-tropics (Haimberger et al., Submitted; Thorne, 2011a) c.f. Figures 2.14 and 2.15.

[INSERT FIGURE 2.10 HERE]

Figure 2.10: Radiosonde product global temperature trend estimates from four datasets (symbols) and the estimated structural uncertainty in the HadAT product from (Thorne et al., 2011a) (Box whiskers denote median estimator, 25–75th percentile and range) over the common period of record 1958–2003. All trend estimates are from median of pairwise slopes technique (Lanzante, 1996). Global averages were created by calculating zonal means and then weighting zonal anomalies by cos(lat). The four best estimates used are HadAT2 (Δ), IUK (□), RICH (+) and RAOBCORE (◊). [Note that new versions of RICH / RAOBCORE will be used in the SOD].

Table 2.7: Summary of methodologies used to create the radiosonde products considered in this report. Except IUK (1960) all timeseries begin in 1958. Only gross methodological details are included to give a flavor of the methodological diversity, further details can be found in the papers describing the dataset construction processes.

Dataset	Temporal Resolution	Number of Stations	Breakpoint Test	Adjustments Method
HadAT2	Seasonal / monthly	676	KS-test on difference series from neighbour averages together with metadata, manually interpreted	Target minus neighbour difference series based.
RATPAC	monthly	87	Multiple indicators and metadata assessed manually by three investigators until 1993, first difference method with t-test and metadata after 1994	Manually based adjustments prior to 1993, first difference derived breaks after 1994.

IUK	Individual launch	527	Derived hierarchically looking 1. for breaks in 00Z-12Z series, 2. breaks in the series with twice daily measures, and 3. once daily ascents. Breakpoint detection was undertaken at the monthly timescale with no recourse to metadata	Relaxation to an iterative solution minimum given breaks and set of spatial and temporal basis functions.
RICH-obs (64 member ensemble)	Individual launch	2881	SNHT test on the difference between the observed data and ERA reanalysis product background expectation field modified by metadata information.	Difference between station and number of apparently homogeneous neighbours
RICH-tau (64 member ensemble)	Individual launch	2881	As above	Difference between station innovation (candidate station and reanalysis background expectation field) and innovation estimates for apparently homogeneous neighbors.
RAOBCORE	Individual launch	2881	As above	Difference between candidate station and reanalysis background expectation field

2.2.4.2 Advances in MSU Satellite Records

AR4 considered estimates produced from three groups: UAH (University of Alabama in Huntsville); RSS (Remote Sensing Systems) and VG2 (Vinnikov and Grody, since not updated and so not discussed further). A new product has been created by NOAA labelled STAR. Gross methodological details of these products are summarized in Table 2.8. The UAH fundamental method remains essentially unaltered having removed an apparent seasonal cycle artefact in the latter part of their record related to the introduction of AMSU in version 5.3 and changed the climatological baseline to 1981–2010 to produce version 5.4. Both changes had negligible impact on trend estimates. Version 3.2 of the RSS product (Mears and Wentz, 2009a, 2009b) for the first time incorporated a subset of AMSU instruments. It was concluded that an instantaneous correction is required to merge MSU and AMSU as they sense slightly different layers and that there will also be a systematic long-term impact unless real-world trends are vertically isothermal (Mears, 2011). Using HadAT data this impact was estimated to be no more than 5% of the trend. Two more significant changes were accounting for latitudinal error structure dependencies, and a more physical handling of instrument body temperature effect issues in response to (Grody et al., 2004). In early 2011 version 3.3 was released which incorporated all the AMSU instruments and led to a de-emphasising of the last MSU instrument which still remained operational after 15 years, a trend reduction over the post-1998 period, and a reduction in apparent noise. RSS also produced a comprehensive model of their parametric uncertainty (Box 2.1) (Mears, 2011) employing a Monte-Carlo approach allowing methodological inter-dependencies to be fully expressed. For large-scale trends dominant effects were inter-satellite offset determinations and, for tropospheric channels, diurnal drift. Uncertainties in resulting trend estimates were concluded to be of the order 0.1°C per decade at the global mean for both tropospheric channels and the stratospheric channel.

The new STAR analysis used a fundamentally distinct approach for the critical inter-satellite warm target calibration step (Zou et al., 2006a). Satellites orbit in a pole-to-pole configuration with typically two satellites in operation at any time. Over most of the globe they never intersect. The exception is the polar regions where they quasi-regularly (typically once every 24 to 48 hours but this is orbital geometry dependent) sample in close proximity in space (<111 km) and time (<100s). The STAR technique uses these Simultaneous Nadir Overpass (SNO) measures to characterize inter-satellite biases and the impact of instrument body temperature effects before accounting for diurnal drift. SNO estimates remain two point comparisons between uncertain measures over a geographically limited domain so cannot guarantee absolute accuracy. Initially they produced MT near-nadir measures since 1987 over the oceans (Zou et al., 2006a); then included more view angles and additional channels including LS and multi-channel recombinations (Zou et al., 2009); then extended back to 1979 and included land and residual instrument body temperature effects building upon the UAH methodology and diurnal corrections based upon RSS (Zou and Wang, 2010). In the latest version 2.0, STAR incorporated the AMSU observations inter-calibrated by the SNO method to extend to the present (Zou and Wang, 2011). STAR exhibits more warming / less cooling at all

levels than UAH and RSS. For MT and LS (Zou and Wang, 2010) concluded that this does not primarily relate to use of the SNO technique but rather differences in remaining processing steps.

Table 2.8: Summary of methodologies used to create the MSU products considered in this report. All timeseries begin in 1978–1979. Only gross methodological details are included to give a flavour of the methodological diversity, further details can be found in the papers describing the dataset construction processes.

Dataset	Inter-Satellite Calibration	Diurnal Drift Adjustments	Calibration Target Temperature Effect	MSU / AMSU Weighting Function Offsets
UAH	Backbone method – adjusting all other satellites to a subset of long-lived satellites	Cross-scan differences used to infer adjustments. Measurements are adjusted to refer to the measurement time at the beginning of each satellite's mission.	Calibration target coefficients are determined as solution to system of daily equations to explain the difference between co-orbiting satellites	No accounting for differences beyond inter-satellite calibration.
RSS	Stepwise pairwise adjustments of all satellites based upon difference in means. Adjustments are a function of latitude and constant in time.	Climate model output used to infer diurnal cycle. All measurements adjusted to refer to local midnight.	Values of the target temperature factors and scene temperature factors are obtained from a regression using all satellites of the same type together.	Stepwise adjustment to account for the change in weighting functions.
STAR	Simultaneous nadir overpass measures	RSS adjustments are multiplied by a constant factor to minimize inter-satellite differences.	Largely captured in the SNO satellite intercomparison but residual artefacts are removed using the UAH method.	Channel frequency shifts on each satellite estimated and adjusted for.

2.2.4.3 Intercomparisons Between Various Long-Term Products

Since AR4 there have been a large number of intercomparisons between upper-air datasets. Because none of the raw data is directly and continuously traceable to measurement standards such comparisons cannot definitively determine whether residual biases exist in any single product. They can highlight areas of disagreement between products and such information can potentially be used in combination with physical understanding to elucidate issues. Interpretation is complicated as most studies considered dataset versions that have since been superseded and it is unclear whether documented issues any longer pertain. These studies have highlighted the large degree of uncertainty in the vertical structure and time evolution of tropospheric temperature changes. They have also highlighted that the two most critical satellite dataset uncertainties arise from diurnal drift effects and inter-satellite offsets.

Several studies compared UAH and RSS products to raw / homogenized radiosonde station level data locally or regionally. Christy and Norris (2006) concluded that UAH was more reasonable than RSS when compared to VIZ manufactured radiosondes operated by the United States. Christy et al. (2007) drew similar conclusions for LT using tropical radiosonde stations operated by a mixture of countries and with a mix of instrumentation. Christy and Norris (2009) confirmed these general findings for Australian radiosonde data. The transition from NOAA-11 to NOAA-12 (early 1990s) was identified as the primary period when the different comparisons consistently pointed towards an issue in RSS. Christy et al. (2007) noted that this coincided with Pinatubo and that RSS was the only product, either surface or tropospheric, that exhibited tropical warming immediately after the eruption when physically cooling would be expected. (Randall and Herman, 2008) came to similar findings independently. Using reanalyses data Bengtsson and Hodges (2011) also found evidence of a potential jump in RSS in 1993 over the tropical oceans. Christy et al. (2010) later expanded this analysis incorporating additional new data products, again concluding that RSS exhibited spurious warming. But these various studies also revealed other potential issues in the datasets. All MSU records were most uncertain when satellite orbits are drifting rapidly (Christy and Norris, 2006, 2009) and it was cautioned that there were potential common residual biases (of varying magnitudes) in the MSU records.

Drifts could not be explained as residual radiosonde artefacts by the comprehensive metadata gained for the VIZ and Australian networks (Christy and Norris, 2009; Christy et al., 2007).

Mears and Wentz (2009b) compared global, tropical and hemispheric RSS LT to UAH and the various radiosonde datasets. Mears et al. (2011) generalized this approach to other levels and incorporated both STAR and the RSS internal uncertainty estimates. RSS parametric uncertainties overlapped with other datasets only in approximately half of cases. Mears et al. (2011) noted that there are potentially many intercomparison performance metrics and that although UAH exhibited better trend agreement on average with the radiosonde records globally it exhibited much greater equator to pole trend gradients than any other dataset. Several additional dataset papers or data-model comparisons have compared regional / global trends of suites of estimates with one another e.g., (Christy, 2010; Douglass et al., 2008b; Santer et al., 2008; Sherwood et al., 2008; Thorne et al., 2011a; Titchner et al., 2009). Most have treated each observational estimate equally. Some analyses, however, have used deductive reasoning to discard or downplay certain datasets, often based upon published intercomparisons (Christy, 2010; Christy, 2011). This yields trend estimates that have one or more existing dataset outside the quoted range (in those approaches published precluding solutions which exhibit greatest warming rates). Whilst these products may well be implausible estimates of the single, unknown, real-world climate trajectory it is not scientifically possible to conclude so definitively.

2.2.4.4 GPS-RO Data and Intercomparisons with Datasets

Global Positioning System (GPS) radio occultation (RO) now represents a mature remote sensing technique (Anthes et al., 2008; Hajj et al., 2004; Ho et al., 2009c). The highly stable observations can be used as global references in orbit (Baringer et al., 2010). Currently, it represents the only self-calibrated SI traceable raw satellite measurements (Baringer et al., 2010). The fundamental observation is time delay of the occulted signal's phase traversing the atmosphere. With a GPS receiver on board a low-Earth orbiting (LEO) satellite, the occulted signal's phase transmitted from GPS satellites, which are delayed and bent due to atmospheric refraction, can be detected. Traceability is established by subsequently correcting and resolving the clocks of the GPS satellites and LEO satellites with a network of GPS ground receivers, tied to atomic clocks. Subsequent analysis converts the time delay to temperature and other parameters, which inevitably adds some degree of uncertainty to the temperature data, which is not the directly measured quantity.

GPS RO measurements have several attributes that make them suited for climate studies: (i) they exhibit no satellite-to-satellite bias (Hajj et al., 2004; Ho et al., 2009c), (ii) they are of very high precision (Anthes et al., 2008; Foelsche et al., 2009; Ho et al., 2009c), (iii) they are not affected by clouds and precipitation, and (iv) they are insensitive to retrieval error when used to estimate inter-annual trends in the climate system (Ho et al., 2009d). GPS-RO observations can be used to derive atmospheric temperature profiles in the upper troposphere and lower stratosphere (UT/LS) ((Hajj et al., 2004; Ho et al., 2009c; Kuo et al., 2004). With their quality unaffected by the surrounding environment (e.g., geo-location, day and night, etc.), these data have been used to identify systematic temperature biases for different radiosonde sensors (Baringer et al., 2010; He et al., 2009; Kuo et al., 2005; Sun et al., 2010). Recently, Ho et al., (2009b; 2007; 2009c) used the high-resolution CHAMP and COSMIC temperature profiles (from ~60 m near the surface to ~1.5 km at 40 km) from 2001 to 2010 to simulate the AMSU LS temperature and used these data to calibrate LS from various AMSU missions. The calibrated series agree well with all long-term MSU datasets (Figure 2.11). Such redundant verification serves to build confidence in the records of stratospheric temperature changes. In contrast, Ladstadter et al. (2011) find relatively large differences between their GPS RO reconstruction and the same MSU records implying that there are still uncertainties in GPS RO derived temperatures and / or how to undertake such intercomparisons.

[INSERT FIGURE 2.11 HERE]

Figure 2.11: LS anomalies of RSS, UAH, STAR, and RO_AMSU for (a) the entire globe (82.5ºN–82.5ºS), b) 82.5ºN–60ºN, (c) 60ºN–20ºN, (d) 20ºN–20ºS, (e) 20ºS–60ºS, and (f) 60ºS–82.5ºS. The orange line indicates the mean trend for RO_AMSU.

2.2.4.5 Stratospheric Sounding Unit Data

The SSU instrument, carried upon the same satellites as MSU, senses temperatures at higher altitudes (Figure 2.9). They provide the only long-term near-global temperature data above the lower stratosphere, extending from the upper troposphere to the lower mesosphere (Randel et al., 2009; Seidel, 2011), with the series terminating in 2006. In theory five channels of AMSU should be able to continue this series (Kobayashi et al., 2009) but despite incipient efforts at an AMSU only record (Mo, 2009) and plans to merge, the current long-term series ends in 2006. The raw record has three unique additional issues to those encountered in MSU dataset construction. The satellite carries a cell of CO_2 which tends to leak causing a spurious increase in observed temperatures. Compounding this the CO_2 content varies among SSU instruments (Kobayashi et al., 2009). At the higher altitudes sensed, large diurnal and semi-diurnal tides (due to absorption of solar radiation) require substantial corrections (Brownscombe et al., 1985). Finally, long-term temperature trends derived from SSU need adjustment for increasing atmospheric CO_2 (Shine et al., 2008) as this affects radiation transmission in this band.

Until recently solely one SSU dataset existed (Brownscombe et al., 1985; Scaife et al., 2000), recently updated by Randel et al. (2009). Liu and Weng (2009) have now produced an alternative analysis for Channels 25 and 26 (but not channel 27) and (Wang et al., Submitted) for all three channels, permitting cursory evaluation of structural uncertainty. Differences between the independent estimates, documented in Seidel et al. (2011) and Wang et al. (Submitted) are much larger than differences between MSU records or radiosonde records at lower levels, with substantial inter-decadal timeseries behavior departures and trend differences of the order 0.5°C per decade. Although all SSU datasets agree that the stratosphere is cooling beyond that very substantial uncertainty currently remains.

2.2.4.6 Indirect Estimates from Changes in Atmospheric Winds

Atmospheric circulation is driven by thermal gradients. Any change in horizontal temperature gradients should be accompanied by a shift in winds. Radiosonde wind records are far less obviously afflicted by time varying biases than their temperature records (Gruber and Haimberger, 2008; Sherwood et al., 2008). Allen and Sherwood (2007) first investigated applicability of using these winds to infer relative temperature gradients to the Tropical West Pacific warm pool region. They then extended to a global analysis (Allen and Sherwood, 2008) which implied a distinct tropical upper tropospheric maximum, but with large uncertainty. This uncertainty largely arose because winds can only tell about relative change based upon changes in atmospheric thickness and require an anchor point such as the HadAT trends at 62.5°N utilized (Allen and Sherwood, 2008). The large uncertainty range was predominantly driven by uncertainty that arises through this choice of anchor point, a finding later confirmed by (Christy, 2010), who in addition questioned the stability of such an approach given the sparse geographical sampling, particularly in the tropics, and possible systematic wind speed bias sampling effects amongst other potential issues. Anchoring the analysis closer to the tropics tended to reduce or remove the appearance of a tropical upper tropospheric maximum.

2.2.4.7 Synthesis of Free Atmosphere Temperature Estimates

Global-mean lower tropospheric temperatures have increased since the mid-twentieth Century with each decade warmer than all preceding decades in the record (Figure 2.12, bottom), as is the case for the surface (Figure 2.7). Structural uncertainties are larger than for surface datasets over the common period of record but it can still be concluded that globally the troposphere has warmed. Uncertainty relates to the rate rather than sign of long-term changes, at least at the global mean (Table 2.9). On top of this long-term trend is super-imposed short-term variations that are highly correlated with those at the surface but of slightly greater amplitude. Global mean lower stratospheric temperatures have decreased since the mid-twentieth Century punctuated by short-lived warming events associated with explosive volcanic activity (Figure 2.12, top). Each decade has been cooler than all preceding decades. Uncertainties are larger still than for the troposphere but these uncertainties again impact understanding of rate but not sign of long-term changes. Cooling rates are on average greater from radiosonde datasets than MSU products. This likely relates to widely recognized cooling biases in radiosondes (Mears et al., 2006) which several dataset producers explicitly caveat are likely to remain to some extent in their final products (Haimberger et al., 2008; Sherwood et al., 2008; Thorne et al., 2011a). Since the mid-1990s little net change has occurred.

[INSERT FIGURE 2.12 HERE]

Figure 2.12: Global average lower stratospheric (top) and lower tropospheric (bottom) temperature anomaly timeseries for the mean of all included radiosonde datasets (HadAT, RICH and RAOBCORE(v1.4)) and offset therefrom the differences from this composite for each dataset. Note the difference in y-axis resolution between the various panels. All timeseries have been anomalized to a common 1981–2010 reference period.STAR do not produce a lower tropospheric temperature product. For details of the smoothing applied refer to Figure 2.1.

Table 2.9: Trend estimates and two standard error ranges (see Box 2.2) for radiosonde and MSU dataset global average values over the radiosonde and satellite periods. Satellite records only start in 1979 and STAR do not produce an LT product. The range quoted is solely that arising from trend fitting uncertainty. Structural uncertainties, to the extent sampled, are apparent from the range of dataset estimates. Parametric uncertainties, which many groups include (and calculate in distinct ways), are not considered. See Box 2.1 for further discussion of uncertainties.

	OLS trend estimates (°C per decade) and two SE range (adjusted for AR1 autocorrelation effects) for selected periods					
Dataset	1958–2010			1979–2010		
	LT	MT	LS	LT	MT	LS
HadAT2	0.163 ± 0.028	0.100 ± 0.032	–0.341 ± 0.056	0.176 ± 0.048	0.086 ± 0.056	–0.454 ± 0.146
RAOBCORE 1.5	0.151 ± 0.026	0.097 ± 0.026	–0.250 ± 0.066	0.141 ± 0.050	0.090 ± 0.050	–0.349 ± 0.184
RICH-obs	0.165 ± 0.024	0.098 ± 0.028	–0.354 ± 0.068	0.174 ± 0.048	0.104 ± 0.050	–0.456 ± 0.188
RICH-tau	0.171 ± 0.026	0.108 ± 0.028	–0.318 ± 0.068	0.162 ± 0.048	0.088 ± 0.048	–0.430 ± 0.184
UAH				0.141 ± 0.056	0.053 ± 0.056	–0.393 ± 0.274
RSS				0.149 ± 0.050	0.092 ± 0.056	–0.309 ± 0.250
STAR					0.165 ± 0.046	–0.330 ± 0.248

Global-average analyses hide interesting geographical trend variability (Figure 2.13). Over the satellite era the surface exhibits greater warming over land than oceans globally with substantial geographic trend structure and some areas exhibit a cooling trend. In comparison tropospheric channels exhibit much smoother geographic trends with warming dominating cooling north of approximately 45°S and greatest warming in high Northern latitudes. The lower stratosphere is cooling almost everywhere but this cooling also exhibits substantial structure. Cooling is greatest in the highest southern latitudes and smallest in high northern latitudes, with some slight warming over the Northern Pacific Arctic sector. There is also some slight warming apparent in the Southern Ocean at similar longitudes.

[INSERT FIGURE 2.13 HERE]

Figure 2.13: Linear trend estimates for the surface, lower troposphere and lower stratosphere estimated from the ERA-Interim reanalysis product over 1979–2010. Trends have been estimated as described in Box 2.2.

Available global and regional trends from radiosondes since 1958 (Figure 2.14) show agreement that the troposphere has warmed and the stratosphere cooled over this period. While there is little ambiguity in the sign of the changes, the rate and details of the vertical structure are distinctly dataset dependent. Differences are greatest in the tropics and Southern Hemisphere extra-tropics where the historical radiosonde data coverage is poorest. Within the tropics possible vertical structural changes range from slight damping of near-surface trends aloft within the upper-troposphere to a distinct amplification. Not shown in the figure are estimates of parametric dataset uncertainties (Figure 2.10) or trend-fit uncertainties – both of which are of the order at least 0.1°C per decade (although being independent would combine in quadature to an estimate of the same order of magnitude rather than linearly; see also Box 2.1 and 2.2).

[INSERT FIGURE 2.14 HERE]

Figure 2.14: Linear trend estimates for all available data products that contain records for 1958–2010 for the globe (top) and tropics and extra-tropics (bottom). The bottom panel trace in each case is for trends on distinct pressure levels. Note that the pressure axis is not linear. The top panel points show MSU layer equivalent measure trends over the same period. MSU layer equivalents have been processed using the method of Thorne et al. (2005b). No attempts have been made to sub-sample to a common data mask.

Since 1979 in addition satellite estimates from MSU exist (Figure 2.15). Over this period differences between available radiosonde datasets are greater than the full radiosonde period of record in all regions and at most levels. The RAOBCORE product exhibits greater vertical trend gradients than remaining datasets

and this has been posited to relate to its dependency upon reanalysis fields in the adjustment (Christy, 2010; Sakamoto and Christy, 2009). Even if RAOBCORE is discounted, remaining estimates again include possible behaviour in the tropics from slight damping of trends aloft to substantial amplification. Over a slightly shorter period the parametric uncertainty in the HadAT product (Thorne et al., 2011a) also implies that such a range of solutions are possible. MSU estimates within the troposphere are generally bracketed by the radiosonde range. In the stratosphere MSU deep layer estimates tend to show slightly less cooling (as discussed previously).

[INSERT FIGURE 2.15 HERE]
Figure 2.15: As Figure 2.14 except for the satellite era 1979–2010 period.

2.2.5 Summary of Temperature Trends

Globally averaged near-surface temperatures, as estimated by several independent analyses since the late nineteenth Century, are consistent in exhibiting warming of 0.075 ± 0.008°C per decade since 1901. Much of this warming has occurred since 1979 (0.167 ± 0.034°C per decade). Super-imposed upon the long-term changes are high frequency variations so the warming is not monotonic and trend estimates at decadal or shorter timescales tend to be dominated by such effects. Quantifying long-term temperature trends has improved with redundancy in measurement and analysis techniques and multiple published sensitivity and uncertainty studies. While there is an inevitable degree of uncertainty regarding the precise magnitude, long-term global-mean near-surface temperatures have unequivocally warmed since the late 19th Century, and much of this has occurred in recent decades.

It can be concluded with very high confidence that globally averaged land surface air temperatures have warmed since the late 19th Century and that this warming has been particularly marked since the 1970s. There is low confidence in changes prior to 1880 owing to the reduced number of estimates, the greater spread, and the much reduced observational sampling density. Several independently analyzed global and regional land surface temperature data products of substantial heritage support this conclusion. Since AR4 significant efforts have been undertaken to identify and adjust for data issues and new estimates have been produced. These innovations have strengthened confidence in the land temperature records.

Several studies undertaken since AR4 show that it is *likely* that urban heat-island effects have not raised the centennial global near-surface temperature trends by more than 10% of the observed trend and many studies imply negligible or no impact. Contributions are not globally uniform. They are *likely* to underlie about a quarter of the observed warming trends in recent decades in limited regions experiencing rapid development such as China, but have little overall impact elsewhere or on the global mean.

New insights regarding the likelihood of differential bias impacts between minimum and maximum temperatures in many station records have reduced confidence in reported Diurnal Temperature Range (DTR) changes at the global and regional levels to medium-to-low. To date these DTR changes almost exclusively rely upon analysing the raw, bias impacted, data. Available DTR estimates suggest a narrowing with minimum temperatures increasing faster than maximum temperatures.

It can be concluded with very high confidence that global average sea surface temperatures have increased since the beginning of the twentieth Century. Since AR4 there has been a step change in availability of metadata, improvements in data completeness and a number of new estimates of SSTs produced. Intercomparisons of data obtained by different measurement methods, including satellite data, have resulted in better understanding of errors and biases in the record. While these new products and information have helped highlight and quantify uncertainties, they do not alter the conclusion with very high confidence that global SSTs have increased both since 1950s and since the late 19th Century.

Based upon multiple independent analyses from weather balloons and satellites it can be concluded with very high confidence that globally the troposphere has warmed since the mid-twentieth Century. There is medium confidence in the rate of change and its vertical structure in the Northern Hemisphere extra-tropics, but elsewhere confidence is low, particularly in the tropical upper troposphere. Through construction of several additional datasets, detailed intercomparisons, and a greater elucidation of uncertainties in a subset of

pre-existing datasets the large uncertainty has become much more apparent since AR4. Estimates of tropospheric warming rates encompass surface temperature rate estimates.

While it can be concluded with very high confidence based on four independent observing technologies that globally the stratosphere has cooled since the mid-twentieth Century there is only low confidence in the cooling rate and vertical structure. Cooling of the lower stratosphere is consistently estimated to have levelled off in the past decade. Confidence is low in temperature changes in the mid- and upper stratosphere where only one observing technology exists and datasets are both substantially less mature and poorly documented.

[START FAQ 2.1 HERE]

FAQ 2.1: How do We Know the World is Warming?

That the world has warmed is unequivocal. Evidence for warming arises from multiple indicators from the top of the atmosphere to the depths of the oceans studied by multiple independent groups of scientists from many different countries. These include changes in surface, atmospheric, and oceanic temperatures; glaciers, snow cover, and sea ice; sea level; and atmospheric water vapour. All published data products agree that the world has warmed. Evidence of a warming world does not depend upon a single group or a single indicator – it is broad and deep and has been verified entirely independently many times over. Further details for each indicator are discussed in Chapters 2 through 4.

The best-known indicator that global climate is changing is the rise in global average surface temperatures. The world warmed between 1900 and 1940, there followed a period of some thirty years during which temperatures changed little; then from around the mid-1970s a second period of warming ensued. The IPCC AR4 concluded that this "warming of the climate system is unequivocal".

Although popular discussion tends to centre on temperature records made at weather stations over the land, these represent only one single, albeit important, line of evidence. The different elements of the climate system are strongly interlinked and though they have been considered separately, the broader evidence for a warming world comes from bringing together a wide range of physically consistent measurements (FAQ 2.1, Figure 1).

[INSERT FAQ 2.1, FIGURE 1 HERE]
FAQ 2.1, Figure 1: Schematic of those climate elements that have been measured quasi-globally and on multi-decadal timescales that would be expected to change if the world were indeed warming; and the direction in which they would be expected to change.

The global average temperature data sets are based on air temperatures measured by weather stations over the land and on measurements of sea-surface temperature over the oceans. The underlying archives of land and ocean temperatures are completely independent, but the several independently estimated changes in temperature recorded in them follow one another closely. The rise in sea-surface temperature is slower in part because it requires more energy to heat the sea than it does the land. Although sea-surface temperature is most often used to measure temperature change over the oceans, air temperatures taken by ships are also available. Physically, one would expect that marine air temperatures would be closely linked to the changes in the sea-surface temperatures and this is borne out by a number of independent analyses.

Both the atmosphere and ocean are well-mixed fluid bodies, so warming at the surface would be expected to be transmitted both up into the lower atmosphere and down into the upper oceans. The observed warming is not confined to the surface. Several analyses of measurements made by weather balloons and satellites consistently show that the temperature of the troposphere – the active weather layer of the atmosphere – has increased. The warming also penetrates into the upper ocean. More than 80% of the energy absorbed by the climate system since the 1960s has been stored in the oceans. This can be seen in numerous estimates of ocean heat content, for which global records exist going back to the 1950s. As the oceans warm, the water itself expands, making the largest contribution along with changes in glaciers, ice sheets and freshwater

storage to sea level changes. Several independently assessed records of rising sea-levels extend back more than a century.

A warmer world is also a wetter one as warmer air will, on average, contain a greater quantity of water. Globally, analyses show that specific humidity, which measures the amount of moisture in the atmosphere, has also increased over both the land and the oceans.

The icy parts of the planet – known collectively as the cryosphere – affect, and are affected by, local changes in temperature. The mass of water stored in mountain glaciers globally has been falling every year for 20 years. The lost mass contributes to the observed rise in sea-level. Snow cover is sensitive to changes in temperature particularly during the spring when the snow starts to melt. Spring snow cover has fallen across the northern hemisphere since the 1950s. There have been substantial losses in sea-ice in the Arctic Ocean particularly at the time of the summer minimum in extent. There has been little change in Antarctic sea-ice.

Individually, any single analysis might be unconvincing, but for all of these different indicators and independent data sets many research groups have come to the same conclusion. From the deep oceans to the edge of the atmosphere, the evidence of warmer airs and oceans, of melting ice and rising seas, of increasing humidity, all points unequivocally to one thing: the world has warmed (FAQ 2.1, Figure 2).

[INSERT FAQ 2.1, FIGURE 2 HERE]

FAQ 2.1, Figure 2: Multiple redundant indicators of a changing global climate. Each line represents an independently derived estimate of change in the climate element. All publically available, documented, datasets known to the authors have been used in their latest version with no further screening criteria applied. Further details are given in (Baringer et al., 2010).

[END FAQ 2.1 HERE]

2.3 Changes in Hydrological Cycle

Changes in the hydrological cycle are less easily measured than changes in temperature, however they potentially have large and long-lasting effects on the climate system as well as society. Changes in atmospheric water vapour impact both the energy balance, as water vapour is one of the most abundant greenhouse gases, and the hydrologic cycle. Long-term measurements of precipitation are available only for land areas and thus do not provide true global coverage. Satellite estimates of precipitation do provide global coverage since they include both ocean and land areas, but are only available since about 1979. This section covers the main aspects of the hydrologic cycle including large-scale average precipitation, stream flow and runoff, soil moisture, atmospheric water vapour, and clouds. Meteorological drought is assessed in Section 2.7, Changes in Extreme Events. A more detailed discussion of issues with measurements of precipitation, and climate impacts of the hydrological cycle including aerosols and the energy balance and other impacts are contained in Section 3.3 of the AR4 (Trenberth et al., 2007) and are not repeated here.

2.3.1 Large Scale Changes in Precipitation

2.3.1.1 Global Land and Combined Land-Ocean Areas

The AR4 included analysis of both the GHCN and CRU precipitation data sets for the globally averaged annual precipitation over land and concluded that the overall linear trend from 1900–2005 (1901–2002 for CRU) for both data sets was increasing but not statistically significant (Table 3.4 from AR4). The changes in the time series were not linear and show an increase in the early part of the 20th Century, slight declines to the 1990s and increases thereafter. Futher, the period 1951–2005 was also analyzed for precipitation trends over land using five different data sets with all but one showing a decreasing trend. Last, trends over the period 1979–2005 from six data sets showed a mix of negative (4) and positive (2) trends. Analyses since AR4 indicate that confidence in precipitation estimates is low, because of data incompleteness. Most data sets indicate that global precipitation averaged over land areas has increased, but when virtually all the land area is filled in using a reconstruction method, the resulting time series shows little change in land-based precipitation since 1900.

Figure 2.16 shows the century-scale variations and trends on globally and zonally averaged annual precipitation using the GHCN data set updated through 2010 (Vose et al., 1992). Also plotted are the smoothed time series from a number of other data sets including the Global Precipitation Climatology Project (GPCP, (Adler et al., 2003); and the Global Precipitation Climatology Centre data set (Rudolf et al., 2011). One new global data set for monthly total precipitation that is included is a reconstructed data set by (Smith et al., 2010). This is a statistical reconstruction using Empirical Orthogonal Functions, similar to the NOAA global temperature product (Smith et al., 2008); (Vose et al., Submitted-b) that does provide coverage for most of the global surface area from 1900–2008. The reconstruction merges several analyses. Monthly reconstructions that interpolate using large-scale spatial covariance information and gauge data were found to be representative of most interannual variations. Over land such reconstructions are also representative of multi-decadal variations. However, because there are no gauges over the oceans to anchor those analyses, their oceanic multi-decadal signal was found to be less stable. An annual reconstruction using correlations between precipitation and combined sea-level pressure and sea-surface temperature was found to be more stable for analysis of multi-decadal variations. The merged reconstruction combines these two by combining the oceanic multi-decadal signal from the correlation-based analysis with the gauge-based analysis.

[INSERT FIGURE 2.16 HERE]

Figure 2.16: Annual precipitation averaged over land areas for four latitudinal bands and the globe from GHCN (green bars) with respect to the 1981–2000 base period. Smoothed curves (see Appendix 3.A from Trenberth et al., 2007) for GHCN and other global precipitation data sets as listed. [PLACEHOLDER FOR SECOND ORDER DRAFT: Figure to be updated with latest data.]

As discussed above, the land based GHCN, GPCC, CRU and Smith data sets provide the longer term perspective, and the satellite-based data sets provide true global coverage, including over the oceans. However, for Figure 2.16, only land areas are included. The GHCN, CRU and GPCC data sets show a century-scale increase in global precipitation averaged over land areas, with most of the increase occurring in the early to mid 20th Century. The land-only time series from the Smith data set suggests that when virtually all the land area is filled in using this reconstruction method, the resulting time series shows little change in land-based precipitation since 1900.

Examining the latitude band plots in Figure 2.16 precipitation in the tropics appears to have increased over the last decade reversing the drying trend that occurred from the mid-1970s to mid-1990s. Elsewhere, the mid-latitudes of the Northern Hemisphere does show an overall increase in precipitation from 1900–2010 and the high latitudes (60–90^{o}N) also shows an increase, however there is much uncertainty in the results for the early 20th Century. In the mid-latitudes of the Southern Hemisphere there is much decadal variability but little evidence of long-term change.

When analyzed as a function of climate zones, global satellite observations (Allan et al., 2010) and land-based gauge measurements (Zhang et al., 2007a) both indicate that precipitation has increased over wet regions of the tropics and northern hemisphere mid-latitudes, and decreased over dry regions of the subtropics. These patterns of precipitation change are consistent with that expected in response to the observed increase in tropospheric humidity (Section 2.3.6).

2.3.1.2 Spatial Variability of Observed Trends

Spatial patterns of observed trends of annual precipitation in the AR4 were calculated using GHCN only, interpolated to a 5° x 5° latitude/longitude grid. Trends were calculated for each grid box and showed quite a number of statistically significant changes, particularly increases in eastern and northwestern North America, and parts of Europe and Russia, and southern South America, and Australia, and declines in the Sahel region of Africa, and a few scattered declines elsewhere. The general pattern was increases in the mid- and high-latitudes, declines in the tropical regions.

Figure 2.17 shows the spatial variability of long-term trends (%/century, 1901–2010) and more recent trends (1979–2010) in annual precipitation. The trends, only over land, are computed using the GHCN data set and interpolated to a 5° x 5° latitude/longitude grid. Increases for the longer period are seen in the mid- and

higher-latitudes of both the Northern and Southern hemispheres, although compared to the same figures in the AR4 (Trenberth et al., 2007) there are many fewer statistically significant trends at the grid box level. The decrease in annual precipitation in the Sahel region of Africa continues to be a significant decline, however, over North America there are now no statistically significant grid box values. Explanations for fewer significant trends is probably due to areas that are getting wetter over the long-term, experiencing drought in recent years, and vice versa. Comparing the two maps in Figure 2.17, many of the areas that showed statistically significant long term trends in the AR4 show opposite trends between the 1901–2010 period and 1979–2010 period (e.g., parts of North America, Russia, Africa).

The same holds true for the shorter period map (1979–2010) with many fewer statistically significant trends. The Sahel region for this period continues to show a shorter term increase, although not as strong as in the AR4. Other regions that show a shift in sign between the longer term trends and shorter term include the western US, parts of southern South America, southern Africa, northeastern Africa and Spain, and Iceland.

[INSERT FIGURE 2.17 HERE]

Figure 2.17: Linear trend, in % per century for annual precipitation from the GHCN data set for 1901–2010 (top) and 1979–2010 (bottom). Grid boxes with statistically significant trends at the 5% level are indicated by +. [Note that a slightly different trend calculation method than described in Appendix 2.A has been used; PLACEHOLDER FOR SECOND ORDER DRAFT: updated results will be included.]

2.3.1.3 Changes in Snowfall

The AR4 discussed changes in snowfall on a region by region basis, but mainly focussed on North America and Eurasia. Conclusions were there was a general increase in winter precipitation in high latitudes, although subject to uncertainties as discussed in the AR4, which still hold. Statistically significant increases were found in most of Canada, parts of northern Europe and Russia. A number of areas showed a decline in number of snowfall events, especially those where climatological averaged temperatures were close to 0°C owing to the earlier onset of spring. Further, an increase in lake-effect snowfall was found for areas near the North American Great Lakes. Studies since AR4 indicate that, in most regions analyzed, decreasing numbers of snowfall events are occurring where increased winter temperatures have been observed.

Since the AR4, studies have confirmed that more winter-time precipitation is falling as rain rather than snow in the Western United States (Knowles et al., 2006), the Pacific Northwest and Central United States (Feng and Hu, 2007). Kunkel et al. (2007) discuss many of the issues with detecting trends in snowfall citing, for example, a decline in daily observations of 10:1 snowfall-to-liquid equivalent ratio that was due, mainly to a change in observing practices. Kunkel et al. (2009) analyzed trends in U.S. snowfall using a specially quality-controlled data set of snowfall observations over the contiguous U.S. and found that snowfall has been declining in the Western U.S., Northeastern U.S. and southern margins of the seasonal snow region, but increasing in the western Great Plains and Great Lakes regions.

Other regions that have been analyzed include Japan (Takeuchi et al., 2008), where warmer winters in the heavy snowfall areas on Honshu are associated with decreases in snowfall and precipitation in general. Shekar et al. (2010) found declines in total seasonal snowfall along with increases in maximum and minimum temperatures in the western Himalaya. Serquet et al. (2011) analyzed snowfall and rainfall days since 1961 and found the proportion of snowfall days to rainfall days in Switzerland was declining in association with increasing temperatures.

Over Antarctica recent satellite measures analyzed by Shepherd and Wingham (2007) have shown a link between global temperatures and increased rates of snowfall over the past decade. Further, van Ommen and Morgan (2010) draw a link between increased snowfall in coastal East Antarctica and increased southwest Western Australia drought.

In summary, in most regions analyzed, decreasing numbers of snowfall events are occurring where increased winter temperatures have been observed. Antarctica is the exception where increased snowfall is occurring with increased temperatures.

2.3.2 Streamflow and Runoff

The AR4 found that streamflow records for the world's major rivers show large decadal variability with small secular changes. Increased streamflow occurred in regions that had increased precipitation since about 1950. These regions included many parts of the United States and southeastern South America. However, decreased streamflow was reported over many Canadian river basins during the last 30–50 years in areas where precipitation decreased during the same period. Decreases in river-flow into the Arctic and North Atlantic from high-latitude Canadian rivers was also discussed. Other changes included significant trends of more extreme flood events from 29 large river-basins in one study, but others found increases, decreases, or no change in annual extreme flow from examining 195 river basins around the world. In summary, the AR4 concludes that runoff and river discharge generally increased at high latitudes, with some exceptions. Based on newer evidence, this conclusion no longer holds.

River discharge is unique among water cycle components in that it both spatially and temporally integrates surplus waters upstream within a catchment (Shiklomanov et al., 2010), which makes it well suited for in-situ monitoring (Arndt et al., 2011). Due to its integrated nature, relatively few discharge gauges placed near the mouth of large watersheds can capture a large portion of the continental river fluxes to oceans (Fekete et al., 2002). However, it must also be noted that many if not most large rivers have been impacted by human influences, such as dam construction, so results must be interpreted with caution. Dai et al. (2009) assembled a data set of 925 most downstream stations on the largest rivers monitoring 80 % of the global ocean draining land areas and capturing 73 % of the continental runoff. Dai et al. (2009) found that only about one-third of the top 200 rivers (including the Congo, Mississippi, Yenisey, Paraná, Ganges, Columbia, Uruguay, and Niger) shows statistically significant trends during 1948–2004, with the rivers having downward trends (45) outnumbering those with upward trends (19). The interannual variations are correlated with the El Niño–Southern Oscillation (ENSO) events for discharge into the Atlantic, Pacific, Indian, and global ocean as a whole. For ocean basins other than the Arctic, and for the global ocean as a whole, the discharge data show small or downward trends, which are statistically significant for the Pacific (-9.4 km^3 yr^{-1}). Precipitation is a major driver for the discharge trends and large interannual-to-decadal variations. For the Arctic drainage areas, upward trends in streamflow are not accompanied by increasing precipitation, especially over Siberia, based on available data, although recent surface warming and associated downward trends in snow cover and soil ice content, as well as changes in evaporation, over the northern high latitudes may have contributed to increased runoff in these regions (Adam and Lettenmaier, 2008). The most recent and most comprehensive analyses (Milliman et al., 2008; Dai et al., 2009) do not support earlier work (Labat et al., 2004) concluding that there has been an increasing trend in global runoff associated with global warming during the 20th Century.

2.3.3 Soil Moisture

The AR4 concluded that since historical records from in-situ measurements of soil moisture content are available only for limited regions in Eurasia and the U.S., and they are short in length (10–30 years) little can be said about long-term changes in direct soil moisture measurements. A rare, 45-year record of soil moisture over Ukraine agricultural lands shows little change over the last three decades. Because of this, most studies have relied on simulations from land-surface models (LSMs), and owing to differences in the forcings (radiation, clouds, precipitation, etc.) estimates differ widely. Nevertheless, since the AR4 these LSM soil moisture data, which often cover a whole continent or the global land and extend back to 1950 or 1900, have been increasingly used to document spatial and temporal variations and long-term changes in soil moisture in relation to drought (e.g., Andreadis and Lettenmaier, 2006; Sheffield and Wood, 2007, 2008), see Section 2.7.

2.3.4 Evapotranspiration Including Pan Evaporation

The AR4 concluded that decreasing trends have been found in sparse records of pan evaporation over recent decades over the USA, India, Australia, New Zealand, China and Thailand and speculated on the causes including decreased surface solar radiation, sunshine duration, increased humidity, and increased clouds. However, the AR4 also reported that direct measurements of evapotranspiration over global land areas are scarce, and concluded that reanalysis evaporation fields from are not reliable because they are not well constrained by precipitation and radiation. Since then gridded datasets have been developed that estimate

actual evapotranspiration from either atmospheric forcing and thermal remote sensing, sometimes in combination with direct measurements (e.g., from FLUXNET, a global network of flux towers), or interpolation of FLUXNET data using regression techniques, providing an unprecedented look at global evapotranspiration (Mueller et al., 2011).

Since the AR4 some new material has been published on pan evaporation. Zhang et al. (2007c) found decreasing pan evaporation at stations across the Tibetian Plateau, even with increasing air temperature. Similarly decreases in pan evaporation were also found for northeastern India (Jhajharia et al., 2009) and the Candian Praries (Burn and Hesch, 2007). A continuous decrease in reference and pan evaporation for the period 1960–2000 was reported by Xu et al. (2006a) for a humid region in China, consistent with reported continuous increase in aerosol levels over China (Qian et al., 2006). Roderick et al. (2007) examine the relationship between pan evaporation changes and many of the possible causes listed above using a physical model and conclude that many of the decreases (USA, China, Tibetian Plateau, Australia) cited above are related to declining wind speeds and to a lesser extent decreasing solar radiation. Last, Fu et al. (2009a) provide a overview of pan evaporation trends and conclude the major possible causes (wind speed, humidity, and solar radiation) have been changing, but the importance of each is regionally dependent.

Different processes can control regional evapotranspiration trends depending on whether evapotranspiration is limited by water or energy. Measurements of actual evapotranspiration from FLUXNET reveal a large North-South gradient over Europe in their response to interannual variations in available energy and precipitation (Teuling et al., 2009). Thus, the recent increase in incoming shortwave radiation in regions with decreasing aerosol concentrations (Wild et al., 2005) can explain positive evapotranspiration trends only in the humid part of Europe. In (semi-)arid regions, trends in evapotranspiration largely follow trends in precipitation (Jung et al., 2010). Trends in surface winds (Vautard et al., 2010) and CO_2 also alter the partitioning of available energy into evapotranspiration and sensible heat. While surface wind trends may explain pan evaporation trends over Australia (Rayner, 2007; Roderick et al., 2007), their impact on actual evapotranspiration is limited due to the compensating effect of boundary-layer feedbacks (van Heerwaarden et al., 2010). In vegetated regions where a large part of evapotranspiration comes from transpiration through plants' stomata, rising CO_2 concentrations lead to reduced stomatal opening and evapotranspiration (Idso and Brazel, 1984; Leakey et al., 2006). Additional regional effects that impact evapotranspiration trends are lengthening of the growing season and land use change.

In summary, pan evaporation continues to decline in most regions studied since the AR4 and is related to changes in wind speed, solar radiation and humidity. On a global scale, evapotranspiration increased from the early 1980s up to the late 1990s (Jung et al., 2010; Wang et al., 2010; Wild et al., 2008) at a rate of 0.6 W m^{-2} per decade for the period 1982–2002 (Wang et al., 2010). After 1998, an increase in moisture limitation in the Southern Hemisphere has acted as a constraint to further increase of global evapotranspiration (Jung et al., 2010).

2.3.5 Surface Humidity

AR4 reported widespread increases in surface air moisture content, alongside near-constant relative humidity over large scales though with some significant changes specific to region, time of day or season. However, this was mostly based on regional studies mainly without homogeneity testing or adjustment: identification and removal/adjustment of biases is essential for any surface air moisture dataset to be considered robust. Most of the conclusions of AR4 still stand, but since AR4 there have been advances in our knowledge and understanding of surface humidity through observations, reanalyses and models.

Surface water vapour is routinely measured synoptically both over land and ocean with some records dating back to the 1800s. However, it has received far less attention than temperature and precipitation. This is largely because additional complexities associated with its monitoring have made quality assurance difficult and partly because it has been considered of lesser importance to society. Water vapour is the most prolific and therefore one of the most significant of the greenhouse gases thereby affecting the radiation budget. Its properties of evaporation, condensation and consequent latent heating make it fundamental to the Earth energy budget and hydrological cycle. Absolute humidity governs precipitation amounts in intense rainfall events, when most of the water may be rained out of an air parcel. Furthermore, it has significant

implications for both human, livestock and crop health where high humidity restricts the cooling mechanisms of the body and may also promote some pests and diseases.

In good agreement with previous analyses from Dai (2006), Willett et al. (2008) show widespread increasing specific humidity across the globe from the homogenised gridded monthly mean anomaly product HadCRUH. There are some small isolated but coherent areas of drying over the more arid regions (Figure 2.18a). The globally averaged moistening trend from 1973–2003 is 0.07 g kg^{-1} $decade^{-1}$, with very high confidence and comparable with Dai's (2006) 0.06 g kg^{-1} $decade^{-1}$ for 1976–2004. Moistening is largest in the Tropics (Table 2.10) and summer hemisphere over both land and ocean. There remains large uncertainty over the southern hemisphere where data are sparse. Global specific humidity is sensitive to large scale phenomena such as ENSO (Figure 2.18b-e) and strongly correlated with surface temperature – land only averages over the 23 (Giorgi and Francisco, 2000) regions for the period 1973–2003 show mostly increases at or above Clausius-Clapeyron scaling (about 7% K^{-1}) with very high confidence (Willett et al., 2010).

[INSERT FIGURE 2.18 HERE]

Figure 2.18: Trends and variability in surface humidity. a) Decadal trends in surface specific humidity in g kg^{-1} per decade from HadCRUH over 1973–2003. b) Globally averaged monthly mean anomaly time series of land surface specific humidity. c) Globally averaged monthly mean anomaly time series of land surface relative humidity. d) Globally averaged monthly mean anomaly time series of marine surface specific humidity. e) Globally averaged monthly mean anomaly time series of marine surface relative humidity. Time series show data from HadCRUH (solid thick black) and HadCRUHext (solid thick grey). [PLACEHOLDER FOR SECOND ORDER DRAFT: additional datasets will be included.]

Table 2.10: Summary of global surface humidity datasets and large scale trends as reported in the literature.

Dataset, Reference, source data, period of record and regional delimitations	Specific Humidity (g kg^{-1} $decade^{-1}$)				Relative Humidity (% $decade^{-1}$)			
	Global	Northern Hemisphere	Tropics	Southern Hemisphere	Global	Northern Hemisphere	Tropics	Southern Hemisphere
LAND								
(Dai, 2006) NCAR DS464.0 GTS weather station reports December 1975 to April 2005 Globe (60°S–75°N), N. Hem (0–75°N), S. Hem (60–0°S)	---	---	---	---	0.05	0.12	---	–0.12
HadCRUH, (Willett et al., 2008) NCDC ISD weather station reports January 1973 to December 2003 Globe (60°S–60°N), N. Hem (20–60°N), Tropics (20°S–20°N), S. Hem (60–20°S)	0.11	0.12	0.16	0.01	–0.03	0.07	–0.10	–0.34
OCEAN								
(Dai, 2006) NCAR DS464.0 GTS marine ship reports and ICOADS data December 1975 to May 2005 (boundaries – as above)	---	---	---	---	–0.16	–0.11	---	–0.22
HadCRUH, (Willett et al., 2008) ICOADS v2.1 marine ship, buoy and platform data January 1973 to December 1997, NCEP GTS marine data January 1998 to December 2003 (boundaries - as above)	0.07	0.08	0.10	0.01	–0.10	–0.10	–0.11	–0.11
(Berry and Kent, 2009) ICOADS v2.4 marine ship data 1970 to 2006	0.13	---	---	---	---	---	---	---

Atlantic Trends only 40°S–70°N								
LAND & OCEAN COMBINED								
(Dai, 2006) (as above combined) December 1975 to May 2005 (boundaries - as above)	0.06	0.08	---	0.02	–0.09	–0.02	---	–0.20
HadCRUH, (Willett et al., 2008) (as above combined) January 1973 to December 2003 (boundaries - as above)	0.07	0.08	0.10	0.02	–0.06	0.00	–0.10	–0.10

There is good agreement with ERA reanalyses over land, where ERA-interim shows improvement over ERA-40 as a surface humidity monitoring product for large scale averages (Simmons et al., 2010) (Figure 2.18b, c). Notably, the extended series from ERA-interim shows a flattening of the global land specific humidity series since 2000. While HadCRUH concluded negligible change in surface RH over land in 1973–2003, the more up to date 1989–2008 record from ERA-interim reveals a reduction in RH since 2000, compatible with the plateau in specific humidity. A 'quick-look' extension of HadCRUH to 2007 supports this (Simmons et al., 2010) (Figure 2.18c). This may be linked to the differential warming between land and oceans (Joshi et al., 2008).

There have been advances in marine humidity analysis since AR4. The specific humidity series of Berry and Kent (2009) include uncertainty estimates and adjustments for ship height and data from screens, which are often poorly ventilated, as opposed to handheld psychrometers. The specific humidity and relative humidity dataset HadCRUH (Willett et al., 2008) excludes data failing neighbour consistency checks. Both show good agreement with (Dai, 2006) (Figure 2.18d, e, Table 2.10). All originate from various releases of the ICOADS database. However, whereas Berry and Kent and Dai use only data from Voluntary Observing Ships, Willett et al. use all data from ships, buoys and marine platforms and shift to operationally telecommunicated data made available by NOAA NCEP from 1998–2003. The marine specific humidity, like that over land, shows widespread increases, that correlate strongly with sea surface temperature. However, there is a marked decline in marine relative humidity around 1982 (Figure 2.18e). This is reported in Willett et al. (2008) where its origin is concluded to be a non-climatic data issue.

To conclude, absolute moistening has been widespread across the globe since the 1970s, with very high confidence. However, over recent years this has abated over land, coincident with greater warming over land relative to the oceans (see Section 2.2.3). This has resulted in fairly widespread decreases in relative humidity over land. Whether this is part of a longer term trend or merely a short lived feature remains to be seen.

2.3.6 Tropospheric Humidity

Tropospheric water vapour plays an important role in regulating the energy balance of the surface and top-of-atmosphere, provides a key feedback mechanism and is essential to the formation of clouds and precipitation. Observations from radiosonde, GPS, and satellite measurements indicate increases in tropospheric water vapour at large spatial scales which are consistent with the observed increase in atmospheric temperature.

2.3.6.1 Radiosonde

Radiosonde humidity data for the troposphere were used sparingly in AR4, noting a renewed appreciation for biases with the operational radiosonde data that had been highlighted by several major field campaigns and intercomparisons. Since the AR4 there have been three distinct efforts to homogenize the tropospheric humidity records from operational radiosonde measurements (Dai et al., 2011; Durre et al., 2009; McCarthy et al., 2009) (Table 2.11). All agree that there are significant issues with the raw data that preclude its use for climate analysis. Each study takes a unique methodological approach to data selection and homogenization. Over the common period of record from 1973 onwards, the resulting estimates are in substantive agreement regarding specific humidity trends at the largest geographical scales. All remove an artificial temporal trend

towards drying in the raw data and indicate a positive trend in free tropospheric specific humidity over the period of record. In each analysis, the rate of increase is concluded to be grossly consistent with the increase in equilibrium vapour pressure from the Clausius-Clapeyron relation (about 7% per degree Celsius increase in temperature). There is no evidence for a significant change in tropospheric relative humidity. McCarthy et al. (2009) show close agreement between their radiosonde product at the lowest levels and independent surface relative humidity data (Willett et al., 2008) both in low frequency and high frequency behavior.

Table 2.11: Methodologically distinct aspects of the three approaches to homogenizing tropospheric humidity records from radiosondes.

Dataset	Region Considered	Time Resolution and Reporting Levels	Neighbours	First Guess	Statistical Test	Automated	Variables Homogenized
Durre et al.	Northern Hemisphere	Monthly, mandatory and significant levels to 500hPa	Pair-wise homogenization	No	SNHT	Yes	PW (inferred from T, P and DPD)
McCarthy et al.	Northern Hemisphere	Monthly, mandatory levels to 300hPa	All neighbour average, iterative	Yes	KS-test	Yes	T, q, RH
Dai et al.	Globe	Observation resolution, mandatory levels to 100hPa	None	Yes	KS-test and PMF test	Yes	DPD

2.3.6.2 GPS

Since the early 1990s, estimates of column integrated water vapour have been obtained from ground-based Global Position System (GPS) receivers. An international network started with about 100 stations in 1997 and has currently been expanded to over 400 (primarily land-based) stations. Several studies have compiled long-term GPS water vapour datasets for climate studies (Jin et al., 2007; Wang et al., 2007; Wang and Zhang, 2008; Wang and Zhang, 2009). Using such data, Mears (2011) demonstrated general agreement of the interannual anomalies between ocean-based SSM/I and land-based GPS column integrated water vapor data. The interannual water vapour anomalies are closely tied to the atmospheric temperature changes in a manner consistent with that expected from the Clausius-Clapeyron relation. Jin et al. (2007) found an average column integrated water vapour trend of about 2 mm per decade during 1994–2006 for 150 (primarily land-based) stations over the globe, with positive trends at most of Northern Hemispheric stations and negative trends in the Southern Hemisphere. However, given the short length (about 10 years) of the GPS PW records, the estimated trends are sensitive to the start and end years and the analyzed time period, and thus they should not be interpreted as long-term trends.

2.3.6.3 Satellite

The AR4 reported positive decadal trends in lower and upper tropospheric water vapour based upon satellite observations. Since AR4, there has been continued strong evidence for widespread increases in lower tropospheric water vapour from microwave satellite measurements of column integrated water vapour (Santer et al., 2007; Wentz et al., 2007) and globally from satellite measurements of spectrally-resolved reflected solar radiation (Mieruch et al., 2008). Both the interannual variability and longer term trends in column integrated water vapour are closely tied to changes in SST both at the global and regional scales (Figure 2.19). Consistent with surface and radiosonde measurements, the rate of moistening at large spatial scales is close to that expected from the Clausius Clapeyron relation with invariant relative humidity.

[INSERT FIGURE 2.19 HERE]

Figure 2.19: Top**:** Time series of anomalies in total precipitable water vapour (TPW, blue) and sea surface temperature (SST, green) averaged over ocean surfaces from 60°N–60°S. Bottom: The linear trend in TPW in (kg m^{-2} per decade, shaded) and time-mean TPW (kg m^{-2}, contours) from Special Sensor Microwave Imager (SSM/I, Wentz et al., 2007) for the period 1988–2010.

Upper tropospheric relative humidity (UTH) in the tropics is strongly related to the convective activity and SST of the wet regimes(Chuang et al., 2010). Interannual co-variation in temperature and upper tropospheric water vapour have been diagnosed from spectrally-resolved infrared satellite data (Gettelman and Fu, 2008; Dessler et al., 2008) and inferred from increases in broadband clear-sky outgoing longwave radiation (OLR) satellite data (Chung et al., 2010) and are consistent with invariant RH at large spatial scales. On decadal time-scales, increased greenhouse gas concentrations reduce clear-sky OLR (Allan, 2009; Chung and Soden, 2010), thereby influencing inferred relationships between moisture and temperature. Using Meteosat infrared radiances, (Brogniez et al., 2009) demonstrated that interannual variations in free tropospheric humidity over subtropical dry regions are heavily influenced by lateral mixing between the deep tropics and the extra tropics. Regionally, UTH changes in the tropics were shown to relate strongly to the movement of the ITCZ based upon microwave satellite data (Xavier et al., 2010). While microwave satellite measurements have become increasingly relied upon for studies of UTH, the absence of a homogenized data set across multiple satellite platforms presents some difficulty in documenting coherent trends from these records (John et al., 2011).

Using NCEP reanalyses for the period 1973–2007, (Paltridge et al., 2009) found negative trends in specific humidity above 850 mb over both the tropics and southern midlatitudes, and above 600 mb in the northern midlatitudes. However, as noted in AR4, reanalysis products suffer from time dependent biases and have been shown to simulate unrealistic trends and variability over the ocean (John et al., 2009; Mears et al., 2007); see also Box 2.3). As a result, different reanalysis products yield opposing trends in free tropospheric specific humidity (Chen et al., 2008). Furthermore, the main source of observations, radiosondes (Section 2.3.6.1) and infrared satellite measurements (Soden et al., 2005), indicate positive trends in tropospheric specific humidity. Consequently, reanalysis products are still considered to be unsuitable for the analysis of water vapour trends (Sherwood et al., 2009).

To summarize, while reanalysis products of water vapour remain unreliable for trend detection, radiosonde, GPS, and satellite observations of tropospheric water vapour indicate positive trends at large spatial scales occurring at a rate that is generally consistent with the Clausius-Clapeyron relation and the observed increase in atmospheric temperature. Significant trends in tropospheric relative humidity at large spatial scales have not been observed. It is *very likely* that tropospheric specific humidity has increased since the 1970s.

2.3.7 Clouds

Clouds are important regulators of solar and infrared radiation and can provide potentially important feedbacks on changes in surface temperature.

2.3.7.1 Surface Observations

The AR4 reported that surface-observed total cloud cover may have increased over many land areas since the middle of the 20th Century, including the USA, the former USSR, Western Europe, midlatitude Canada, and Australia. A few regions exhibited decreases, including China and central Europe. Trends were less globally consistent since the early 1970s, and regional reductions in cloud cover were reported for western Asia and Europe but increases over the USA.

Work done since the AR4 has largely confirmed and extended the preceding research. In agreement with prior results, Milewska (2004) reported a significant increase in the frequency of mostly cloudy conditions at most stations in Canada from 1953 to 2002. Wibig (2008) found that total cloud cover over Poland decreased during 1971–2000, with stratiform cloud types becoming less frequent and convective cloud types becoming more frequent. Xia (2010b) reported that total cloud cover declined over most of China since 1954 but then levelled off or slightly increased from the 1990s to 2005. Clear-sky frequency increased over China during the 1971–1996 time period (Endo and Yasunari, 2006). Duan and Wu, (2006) documented a diurnal mean reduction in total cloud cover and a night time enhancement of low-level cloud cover over Tibet during 1961–2003, and they attributed part of the observed local warming to these cloud trends. Warren et al. (2007) noted that the cloud cover decrease previously documented for China extended into neighbouring countries as well and was primarily attributable to a decrease in higher-level clouds.

Some new developments for surface-observed cloud cover over land since the AR4 include the report of a large decrease in total cloud cover between 1971 and 1996 over South America (Warren et al., 2007). Warren et al. also found small decreases in total cloud cover over Eurasia and Africa and no trend for North America during 1971–1996. In general, low- and mid-level convective cloud types increased, stratiform cloud types decreased, and cirrus cloud cover declined over all continents (Warren et al., 2007).

Warren et al. (2007) found no evidence that interannual anomalies in cloud cover were related to anomalies in smoke aerosol in land regions of biomass burning. They did find a positive correlation between cloud base and surface temperature at middle latitudes. This result is consistent with the finding of Sun et al. (2007), who reported that surface temperature and the ceiling height of clouds with bases below 3.6 km increased between the 1950s and 1990s over most of the USA.

The AR4 documented decreasing trends in upper-level cloud cover over mid- and low-latitude oceans between 1952 and 1997. These appeared generally consistent with satellite observations of upper-level cloud during the period of overlap. In contrast, surface observers reported increasing trends in low-level cloud cover and total cloud cover between 1952 and 1997 whereas satellites reported decreasing trends in these quantities since 1983. The reasons for this discrepancy have not yet been resolved. Updates to the surface ocean cloud record since the AR4 indicate that the positive trends in low-level and total cloud cover during the second half of the 20th Century changed sign around 2000, and both quantities decreased until the end of the record in 2008 (Eastman et al., submitted). The cause of the trend reversal is unknown. Further evidence that global decadal variations in surface-observed low-level and total cloud cover are spurious is the finding that interannual anomalies in ship observations of cloud cover agree with nearby island observations of cloud cover only after the removal of biases from the ship data (Eastman et al., submitted).

Regional variability in surface-observed cloudiness over the ocean appeared more credible than zonal and global mean variations in the AR4. Multidecadal changes in upper-level cloud cover and total cloud cover over particular areas of the tropical Indo-Pacific Ocean were consistent with island precipitation records and SST variability. This has been extended more recently by Deser et al. (2010a), who found that an eastward shift in tropical convection and total cloud cover from the western to central equatorial Pacific occurred over the 20th Century and attributed it to a long-term weakening of the Walker circulation. Eastman et al. (submitted) report that, after the removal of apparently spurious globally coherent variability, cloud cover decreased in all subtropical stratocumulus regions from 1954 to 2008.

2.3.7.2 Satellite Observations

Satellite cloud observations offer the advantage of much better spatial and temporal coverage compared to surface observations. However they require careful efforts to identify and correct for temporal discontinuities in the data sets associated with orbital drift, sensor degradation, and inter-satellite calibration differences.

The AR4 noted that there were substantial uncertainties in decadal trends of cloud cover in all data sets available at the time and concluded that there was no clear consensus regarding the decadal changes in total cloud cover. Since AR4 there has been continued effort to assess the quality of and develop improvements to multi-decadal cloud products from operational satellite platforms (Evan et al., 2007; O'Dell et al., 2008; Heidinger and Pavolonis, 2009). New cloud climatologies have also recently become available from improved sensors on the Earth Observation System (EOS) adding to our knowledge of the distribution and characterization of cloud properties (Ackerman et al., 2008).

There are two primary satellite data sets which offer multi-decadal records of cloud cover: the International Satellite Cloud Climatology Project (ISCCP; Rossow and Schiffer, 1999) and the Pathfinder Atmospheres Extended dataset (PATMOS-x; Jacobowitz et al., 2003) both of which begin in the early 1980s. As reported in AR4, there are discrepancies in global cloud cover trends between ISCCP and other data products. Most notable is the large downward trend of global cloudiness in ISCCP since the late 1980s, which is inconsistent with PATMOS-x and surface observations (Baringer et al., 2010). Recent work has confirmed the conclusion of AR4, that much of the downward trend is spurious and an artefact of changes in satellite viewing geometry (Evan et al., 2007). Cermak et al. (2010) has further documented inconsistencies in the spatial patterns of cloud cover trends between PATMOS-x and ISCCP. However, comparisons of PATMOS-x data with new satellite cloud observations from EOS available since 2000 suggest better agreement on interannual

anomalies of global cloud cover (Baringer et al., 2010). Satellite observations of low level marine clouds suggest no long term trends in cloud liquid water path or optical properties (O'Dell et al., 2008; Rausch et al., 2010).

Using surface and satellite data, Clement et al. (2009) documented multidecadal variations in total cloud cover and low-level cloud cover over the northeast subtropical Pacific that were consistent with SST and SLP variations associated with the Pacific Decadal Oscillation. Their analysis applied an adjustment to the ISCCP data to correct for artefacts which result from changes in viewing angle geometry (Evan et al., 2007) and other inhomogeneities (Loeb et al., 2007). They found that reductions in low cloud were associated with an increase in SST and symptomatic of positive cloud shortwave radiative feedback.

The responses of water vapour and cloud inferred from the top of atmosphere radiation were noted to be time-scale dependent (Harries and Futyan, 2006) and highly sensitive to the time-periods and regions chosen for analysis (Murphy, 2010; Lindzen and Choi, 2009; Spencer and Braswell, 2010; Chung et al., 2010; Trenberth et al., 2010). Using recently updated radiation data from the CERES satellite, Dessler (2010) found evidence for a weak interannual global relationship between cloud impacts on net top-of-atmosphere radiation and surface temperature, primarily explained by a positive cloud longwave radiative feedback consistent with theoretical expectations (Zelinka and Hartmann, 2010).

To summarize, while there is consistency in trends of cloud cover between independent data sets in certain regions, substantial ambiguity remains in the observations of global-scale cloud variability and trends. What trends do exist are likely to be within the range of uncertainties for both satellite and observational cloud data sets.

2.3.8 Summary

The conclusions of the AR4, that substantial uncertainty remains in trends of components of the hydrological cycle, remain valid. Large interannual variability, coupled with either short time series, or uneven spatial sampling, particularly early in the record (pre-1950), leads to uncertainty in trends in hydrological variables. Precipitation in the tropics appears to have increased over the last decade reversing the drying trend that occurred from the mid-1970s to mid-1990s. Elsewhere, the mid-latitudes of the Northern Hemisphere does show an overall increase in precipitation from 1900–2010. The high latitudes also shows an increase, however there is much uncertainty in the results for the early 20th Century.

Studies using surface, homogeneity-adjusted radiosonde and satellite data indicate increases in surface and tropospheric water vapour since the 1970s at a rate consistent with that expected with the observed warming and the Clausius-Clapeyron relationship. Thus water vapour at the surface and through the troposphere has *very likely* been increasing since the 1970s. Clouds observed from the surface also continue to show increases over many land areas (e.g., North America, former USSR, parts of Europe and Australia), however other regions show declines (e.g., China and central Europe) and there does not appear to be a globally consistent trend.

2.4 Atmospheric Composition

2.4.1 Long-Lived Greenhouse Gases

AR4 (IPCC, 2007a) concluded that increasing atmospheric burdens of long-lived greenhouse gases (LLGHG) resulted in a 9% increase in their radiative forcing from 1998 to 2005.While the atmospheric abundances of many of the gases increased, there were decreases in the burdens of some of the ozone depleting substances (ODS) whose production and emissions were controlled by the Montreal Protocol on Substances that Deplete the Ozone Layer. Based on updates of these observations, this assessment concludes that these trends continue, resulting in a 6% increase in radiative forcing from 2005 to 2010. Of note is an increase in the growth rate of atmospheric CH_4 from ~0.5 ppb yr^{-1} during 1999 to 2006 to ~6 ppb yr^{-1} from 2007 through 2010. Understanding of the global CH_4 budget is not good enough to determine if this recent period is anomalous or a return to the rates of increase observed prior to 1999. Current observation networks are sufficient to quantify global annual mean burdens used to calculate radiative forcing and to constrain

global emission rates, but they are not sufficient for accurately estimating regional scale emissions and how they are changing with time.

The abundances reported here are used to calculate radiative forcing, which totals 2.79 W m^{-2}, in Chapter 8. These observations are also used to constrain the budgets of LLGHGs. A global GHG budget consists of the total atmospheric burden, total global rate of production or emission (i.e., sources), and the total global rate of destruction or removal (i.e., sinks). Precise, accurate systematic observations from globally distributed measurement networks are used to estimate global means for LLGHGs, and these allow estimates of the global burden. The observed rate of increase (trend) results from the imbalance between emissions and sinks. When the trend is zero, emissions and sinks are equal, the burden is at steady state, and the atmospheric lifetime is equal to the global burden divided by the global rate of emission or of removal. Emissions are predominantly from surface sources, which are described in Chapter 6 for CO_2, CH_4, and N_2O. Direct use of observations of LLGHGs to model their regional budgets can also play an important role in emissions verification (Nisbet and Weiss, 2010).

Methods to estimate GHG emissions are described as "bottom-up" and "top-down" (Montzka et al., 2011a). Bottom-up methods are inventory-based and rely on estimates of emission factors and activities (e.g., CH_4 emissions per cow multiplied by the number of cows). Top-down methods use the observations of atmospheric GHG trends and spatial gradients described here with a chemical transport model to estimate emissions over various spatial scales.

LLGHGs are removed from the atmosphere by physical, chemical and biological processes. The concept of lifetime is relatively straightforward when the sink processes result in the destruction of the LLGHG, but for processes involving exchange between the atmosphere and other reservoirs the concept is more complicated. Atmospheric CO_2 exchanges on comparatively short time scales with the terrestrial biosphere and with the upper layers of the oceans, but more slowly with the deep oceans, which are isolated from atmospheric exchange (see Chapter 6) and play a major role in the long-term uptake of CO_2 emitted by fossil fuel combustion. For most other LLGHGs, the major sinks are photolysis and reaction with hydroxyl radical (OH). OH concentrations depend, in turn, on the abundances of CH_4, VOCs, CO, NOx, H_2O, and flux of solar UV radiation in the troposphere (IPCC, 2001). As a result, the impacts of LLGHGs on climate strongly depend on atmospheric chemistry.

Systematic time series of atmospheric measurements of LLGHGs in ambient air began at various times during the last six decades, with earlier atmospheric histories being reconstructed from measurements of air trapped in polar ice cores or in firn. In contrast to the physical meteorological parameters discussed elsewhere in this chapter, measurements of LLGHGs are reported relative to standards developed from fundamental SI base units (SI = International System of Units) as dry-air mole fractions, a unit that is conserved with changes in temperature and pressure. This eliminates dilution effects from variable amounts of H_2O vapour, which range up to 4% of the total atmospheric composition. Here the following abbreviations are used: ppm = µmol mol^{-1}; ppb = nmol mol^{-1}; and ppt = pmol mol^{-1}.

Table 2.12 summarizes globally, annually averaged abundances for LLGHGs from three independent measurement programs. Sampling strategies and techniques for estimating global means and their uncertainties vary among programs. AGAGE include an estimate of the absolute uncertainity in their standard scales in their annual means, so they are not directly comparable with NOAA and UCI uncertainties. Uncertainties in the increases from 2005 to 2010 are comparable, because absolute uncertainties in the standard scales will cancel when taking the difference between annual means. Agreement among measurement programs is reasonably good from the standpoint of estimating radiative forcing. Time series of the LLGHGs are plotted in Figures 2.20 (CO_2), 2.21 (CH_4), 2.22 (N_2O), and 2.23 (halogen-containing compounds).

Table 2.12: Comparison of globally, annually averaged dry air mole fractions and their change since 2005 for LLGHGs from three measurement networks. Units are ppt (parts per trillion) except where noted (ppm = parts per million; ppb = parts per billion). Uncertainties are 90% confidence limits.[a]

	Lifetime	GWP	UCI	UCI	AGAGE	AGAGE	NOAA	NOAA

Species	(year)	(100 year)	2010	2010–2005	2010	2010–2005	2010	2010–2005
CO_2 (ppm)	---	---	---	---	---	---	388.54 ± 0.16	9.76 ± 0.23
CH_4 (ppb)	~9	25	1792.4 ± 0.7	20.9 ± 1.0	1797.398 ± 14.839	22.728 ± 3.042	1799.06 ± 1.07	24.44 ± 1.47
N_2O (ppb)	120	298	---	---	323.148 ± 2.63	3.838 ± 0.095	323.13 ± 0.12	3.93 ± 0.24
SF_6	3200	22,800	---	---	6.985 ± 0.231	1.356 ± 0.054	7.02 ± 0.02	1.36 ±0.03
CF_4	50000	7,390	---	---	78.263 ± 1.922	3.295 ± 0.099	---	---
C_2F_6	10000	12,200	---	---	4.088 ± 0.199	0.42 ± 0.025	---	---
CHF_2CF_3	29	3,500	---	---	8.239 ± 0.685	4.479 ± 0.372	---	---
CH_2FCF_3	14	1,430	57.8 ± 0.9	22.1 ± 1.4	57.766 ± 1.451	22.836 ± 0.708	57.56 ± 0.56	22.81 ± 0.79
CH_3CHF_2	1.4	124	---	---	6.268 ± 0.328	2.535 ± 0.184	---	---
CHF_3	270	14,800	---	---	23.2 ± 0.966	4.413 ± 0.475	---	---
$CFCl_3$	45	4,750	240.1 ± 0.5	–11 ± 0.8	239.822 ± 4.152	–9.784 ± 0.196	240.52 ± 0.21	–11.18 ± 0.34
CF_2Cl_2	100	10,900	527.9 ± 0.5	–10.2 ± 0.8	532.824 ± 8.956	–10.388 ± 0.243	530.82 ± 0.33	–10.64 ± 0.49
$CF_2ClCFCl_2$	85	6,130	75.6 ± 0.5	–3.9 ± 0.8	75.207 ± 1.946	–3.292 ± 0.104	75.38 ± 0.03	–3.39 ±0.05
CHF_2Cl	12	1,810	203.6 ± 1.0	36.1 ± 1.4	206.601 ± 3.422	36.945 ± 1.16	206.20 ± 1.36	37.28 ± 1.86
CH_3CFCl_2	9.3	725	20.1 ± 0.3	3.0 ± 0.5	20.537 ± 0.674	2.701 ± 0.14	20.46 ± 0.14	2.83 ± 0.20
CH_3CF_2Cl	17.9	2,310	20.0 ± 0.3	4.9 ± 0.5	20.672 ± 0.679	4.859 ± 0.189	20.18 ± 0.12	4.91 ± 0.17
CCl_4	26	1,400	89.1 ± 0.3	–5.1 ± 0.5	86.268 ± 3.018	–5.54 ± 0.209	88.19 ± 0.25	–6.36 ± 0.34
CH_3CCl_3	5	146	8.0 ± 0.3	–13.6 ± 0.5	7.462 ± 0.901	–10.77 ± 0.54	7.61 ± 0.08	–10.83 ± 0.20

Notes:
AGAGE = Advanced Global Atmospheric Gases Experiment; NOAA = National Oceanic and Atmospheric Administration, Earth System Research Laboratory, Global Monitoring Division; UCI = University of California, Irvine, Department of Chemistry.
(a) Each program uses different techniques to estimate uncertainties. AGAGE uncertainties are larger than those for UCI and NOAA because they include absolute uncertainties in standard scales. In calculating uncertainties in the change since 2005, the absolute uncertainty in the standard scales cancels, so comparisons of this uncertainty are appropriate.
Budget lifetimes are shown; for CH_4 and N_2O, perturbation lifetimes (12 year for CH_4 and 114 year for N_2O) are used to estimate global warming potentials.
Pre-indistrial (1750) values are not measureable for all species except CO_2 (278 ± 2 ppm), CH_4 (722 ± 25 ppb), N_2O (270 ± 7 ppb) and CF_4 (34.7 ± 0.2 ppt).

[INSERT FIGURE 2.20 HERE]
Figure 2.20: a) Solid line shows globally averaged CO_2 dry air moles fractions; dashed line is a deseasonalized trend curve fitted to the global averages. b) Instantaneous growth rate for globally averaged atmospheric CO_2. The growth rate is the time-derivative of the dashed line in a).

[INSERT FIGURE 2.21 HERE]

Figure 2.21: a) Solid line shows globally averaged CH_4 dry air moles fractions; dashed line is a deseasonalized trend curve fitted to the global averages. b) Instantaneous growth rate for globally averaged atmospheric CH_4. The growth rate is the time-derivative of the dashed line in a).

[INSERT FIGURE 2.22 HERE]

Figure 2.22: a) Solid line shows globally averaged N_2O dry air moles fractions; dashed line is a deseasonalized trend curve fitted to the global averages. b) Instantaneous growth rate for globally averaged atmospheric N_2O. The growth rate is the time-derivative of the dashed line in a).

[INSERT FIGURE 2.23 HERE]

Figure 2.23: Temporal evolution of the global average dry-air mole fractions (ppt) at Earth's surface of the major halogen-containing LLGHGs. These are derived mainly using monthly mean measurements from the AGAGE and NOAA/GMD networks. For clarity, only the most abundant chemicals are shown in different compound classes and results from different networks have been combined when both are available. While differences exist, different network measurements agree reasonably well (except for CCl_4 (differences of 2–4% between networks) and HCFC-142b (differences of 3–6% between networks)) (see also WMO, 2011, Chapter 1).

2.4.1.1 Kyoto Protocol Gases (CO_2, CH_4, N_2O, HFCs, PFCs, and SF_6)

2.4.1.1.1 Carbon dioxide (CO_2)

Although atmospheric CO_2 contributes only 20% of the total terrestrial greenhouse effect, and non-CO_2 GHGs supply an additional 5%, together they sustain the greenhouse effect, with water vapour (50%) and clouds (25%) providing the remaining 75% of the effect as fast feedbacks (Lacis et al., 2010). An increasing atmospheric burden of CO_2 also affects the ocean food chain through acidification (see Chapter 3).

Precise, accurate systematic measurements of atmospheric CO_2 were begun by C. D. Keeling in 1957 (Keeling, 1976), and estimates of CO_2 atmospheric abundance prior to that date have since been reconstructed from measurements of air extracted from ice cores and from firn. The pre-industrial (1750) globally averaged abundance of atmospheric CO_2 was 278 ± 2 ppm (Etheridge et al., 1996). The following discussion is based on the NOAA CO_2 data. In 2010, globally averaged CO_2 was 388.54 ± 0.16 ppm, and the increase was 2.37 ± 0.15 ppm. Since the AR4, CO_2 has increased by 9.8 ± 0.2 ppm (see Figure 2.20). From 1980 to 2010, the average rate of increase in globally averaged CO_2 was 1.66 ± 0.28 ppm yr^{-1}. For the past decade, CO_2 has increased at ~2.0 ppm yr^{-1}. The CO_2 growth rate varies significantly from year to year; since 1980, the range in annual increase is 0.67 ± 0.14 ppm in 1992 to 2.90 ± 0.14 ppm in 1998. Most of this interannual variability in growth rate is driven by small changes in the balance between photosynthesis and respiration on land, each having global fluxes of about 100 Pg C yr^{-1} (see Chapter 6).

The main contributors to increasing atmospheric CO_2 abundance are fossil fuel combustion and land use change. Multiple lines of observational evidence suggest that during the past few decades, most of the increasing atmospheric burden of CO_2 is from fossil fuel combustion (Tans, 2009).

Comparisons of the observed rate of atmospheric increase with inventories of anthropogenic CO_2 emissions show that approximately half the CO_2 emitted from fossil fuel combustion and cement production from 1751 to 2007 (337 Pg C; ±5 to 10%) (Boden et al., 2010) has been taken up by the ocean and terrestrial biosphere. Several recent studies have suggested that the airborne fraction (AF), that is the fraction of CO_2 emitted from anthropogenic activities (fossil fuel combustion, cement production, and land use change) that remains in the atmosphere, has been increasing (Canadell et al., 2007; Le Quere et al., 2009; Raupach et al., 2008). This would mean the oceans and terrestrial biosphere are becoming less effective as sinks for anthropogenic CO_2. However, Gloor et al. (2010) show that likely omissions in reported emissions from land use change and external forcing events (e.g., volcanic eruptions) are sufficient to explain the observed long-term trend in airborne fraction, while Knorr (2009) found that the trend in the AF since 1850 has been 0.7 ± 1.4% per decade, and not significantly different from zero.

2.4.1.1.2 Methane (CH_4)

Globally averaged CH_4 in 1750 was about 722 ± 25 ppb (Etheridge et al., 1998). Evidence suggests that human influences on the global CH_4 budget began much earlier than the industrial era (Ferretti et al., 2005; Ruddiman, 2003, 2007). By 2010, globally averaged CH_4 at Earth's surface was 1799.06 ± 1.07 ppb based on NOAA measurements (see Figure 2.21). Other programs agree well. This makes methane the second most

abundant LLGHG, and it is the second largest contributor to radiative forcing among LLGHGs. NOAA reported that globally averaged CH_4 has increased by 24.4 ± 1.5 ppb since 2005, in good agreement with AGAGE. This increase began in 2007 (see Figure 2.21) after a period of near constant atmospheric burden from 1999 to 2006 (Dlugokencky et al., 2009; Rigby et al., 2008). This increase was also observed in CH_4 column averages retrieved from irradiances measured by the satellite sensor SCIAMACHY on board ENVISAT, but these observations are not presice enough to aid in understanding the causes (Frankenberg et al., 2011). Causes for the increase in atmospheric CH_4 since 2007 are unclear.

Rigby et al. (2008) concluded that an increase in emissions was necessary to explain the CH_4 observations. The magnitude and distribution of the emissions change depended on assumptions about changes in [OH]. Assuming no inter-annual variability in [OH] required a substantial increase in emissions from both hemispheres in 2007 compared to 2006. If an [OH] decrease of 4 ± 14% determined from the 1,1,1-trichloroethane measurements was used, then a smaller increase in emissions, predominantly in the northern hemisphere, was required. Changes in [OH] of more than a few percent are unlikely based on the observed rate of decay in CH_3CCl_3 (Montzka et al., 2011b).

Dlugokencky et al. (2009) suggested that the most likely drivers of increased atmospheric CH_4 were anomalously high temperatures in the Arctic in 2007 and greater than average precipitation in the tropics during 2007 and 2008. These drivers increased emissions from wetlands in both regions, where CH_4 production is strongly influenced by water table height and temperature. They also suggested that contributions to the increased CH_4 from biomass burning and changes in [OH] were small.

Bousquet et al. (2011) used CH_4 observations and two independent model approaches to assess changes in emissions and sinks during 2006–2008 and found that global CH_4 emissions increased by 19 Tg CH_4 (16 to 21 Tg) in 2007 and 13 Tg CH_4 in 2008 (6 to 20 Tg) relative to the average of emissions for 1999–2006. Changes in tropical wetland emissions were the dominant driver in 2007, with a minor contribution from Arctic wetlands. For 2008, the two independent model approaches were not consistent. Neither suggested a strong increase in emissions from wetlands in the tropics nor the Arctic. They found that changes in [OH] were less than 1%, and had only a small impact on observed CH_4 changes.

Observed increases in CH_4 abundance are the result of small differences (15 to 20 Tg CH_4 yr^{-1} since 2007) between emissions and sinks, both of which are currently on the order of 550 Tg CH_4 yr^{-1}. Small relative changes in emissions from any large source can result in significant changes to methane's rate of increase. Although the major sources of CH_4 have been identified (see Chapter 6), trends in emissions from specific sources cannot be quantified with existing observation networks. Observations of atmospheric CH_4 (Dlugokencky et al., 2009) suggest that it is unlikely that climate feedbacks have measureably increased CH_4 emissions in the Arctic from natural sources.

2.4.1.1.3 Nitrous oxide (N_2O)

Globally averaged N_2O in 2010 reported by NOAA was 323.1 ± 0.1 ppb, an increase of 3.9 ± 0.2 ppb over the value reported for 2005 in AR4 (see Figure 2.22). This is an increase of 19% over the value estimated for 1750 from ice cores of 270 ± 7 ppb. Measurements of N_2O and its isotopic composition in firn air suggest the increase, at least since the early 1950s, is dominated by emissions from soils (Ishijima et al., 2007). Since systematic measurements began in the late 1970s, N_2O has increased at an average rate of about 0.75 ppb yr^{-1} (see Figure 2.22); this, combined with a decreasing atmospheric burden of CFC-12 makes it the third most important LLGHG contributing to radiative forcing. NO produced by reaction of $O(^1D)$ with N_2O also depletes stratospheric O_3. N_2O emissions, weighted by ozone depletion potential (ODP), now dominate emissions of all O_3 depleting substances (Ravishankara et al., 2009).

Approximately 55–70% of N_2O emissions is from natural sources with the remainder, mostly from use of synthetic nitrogen fertilizers and manure (Davidson, 2009; Syakila and Kroeze, 2011) in agriculture, from anthropogenic sources. Emissions may increase if nitrogen fertilizer use increases to produce biofuels (Crutzen et al., 2008). Its main loss process is photochemical destruction in the stratosphere resulting in a lifetime of ~120 year (Hsu and Prather, 2010).

Observations of N_2O show latitudinal gradients in annual mean values, with maxima in the northern subtropics, values about 1.7 ppb lower in the Antarctic, and values about 0.4 ppb lower in the Arctic (Huang

et al., 2008). These persistent gradients contain information about anthropogenic emissions from fertilizer use at northern mid-latitudes and natural ocean emissions in upwelling regions of the tropics. N_2O time series also contain seasonal variations with peak-to-peak amplitudes of about 1 ppb in high latitudes of the Northern Hemisphere and about 0.4 ppb at high southern and tropical latitudes. In the Northern Hemisphere, exchange of air between the stratosphere and troposphere is the dominant contributor to observed seasonal cycles (Jiang et al., 2007), not seasonality in emissions. Nevison et al. (2011) found correlations between the magnitude of detrended N_2O seasonal minima and lower stratospheric temperature providing evidence for a stratospheric influence on the timing and amplitude of the seasonal cycle at surface monitoring sites. In the Southern Hemisphere, observed seasonal cycles are also affected by stratospheric influx, but there are contributions to the seasonal cycle from ventilation and thermal out-gassing of N_2O from the oceans.

Since AR4, Huang et al. (2008) used N_2O measurements from AGAGE, NOAA, and CSIRO and estimated 16.3 [–1.2, +1.5] Tg N (N_2O) yr^{-1} for 1997–2001 and 15.4 [–1.3, +1.7] Tg N (N_2O) yr^{-1} for 2001–2005 (uncertainties are 68% confidence limits). These results are in good agreement with those reported in AR4. They also conclude that uncertainties in air mass exchange between the stratosphere and troposphere (STE) results in a significant portion of the uncertainty in estimated fluxes, particularly on regional scales. Nevison et al. (2007) used complementary stratospheric tracers with strong sinks in the stratosphere (e.g., CFC-12) to assess the contribution of STE to the observed N_2O seasonal cycle. New observations of N_2O from aircraft are also being used to determine the influence of STE as a function of latitude (Ishijima et al., 2010).

2.4.1.1.4 HFCs, PFCs, and SF_6

Current atmospheric abundances of HFCs are low and their contribution to radiative forcing is relatively small. However, as they replace CFCs and HCFCs phased out by the Montreal Protocol in many applications, their contribution to future climate forcing is projected to grow considerably in the absence of controls on global production (Velders et al., 2009). Agreement among measurement programs for this suite of species is good.

HFC-134a is a replacement for CFC-12 in automobile air conditioners and is also used in foam blowing applications. In 2010, it reached 57.6 ± 0.6 ppt, an increase of 22.8 ± 0.8 ppt since 2005. Based on analysis of high-frequency measurements, significant emissions occur in N. America, Europe, and East Asia (Stohl et al., 2009).

HFC-23 is a byproduct of HCFC-22 production. Atmospheric HFC-23 mole fractions increased 4.413 ± 0.475 ppt since 2005 to 23.2 ± 0.97 ppt in 2010. Atmospheric observations agree, within uncertainties, with bottom-up inventories. Based on an inverse model analysis of current atmospheric observations and measurements of a Southern Hemisphere air archive, Miller et al. (2010) show that HFC-23 emissions increased from the late 1970s, peaked in 2006 at 15 (+1.3/–1.2) Gg yr^{-1}, then decreased to 8.6 (+0.9/–1.0) Gg yr^{-1} in 2009. Factors contributing to these changes since the late 1990s are decreased emissions from developed countries because of voluntary destruction followed by increased emissions from developing countries. They find that most of the decrease in HFC-23 emissions since 2006 is consistent with abatement efforts under the Clean Development Mechanism (CDM) of the UNFCCC. Montzka et al. (2010), using measurements of HFC-23 in firn and modern air, infer that HFC-23 emissions from developing countries averaged 11 ± 2 Gg yr^{-1} during 2006–2008 which is about double the ~6 Gg yr^{-1} destroyed under the CDM during 2007 and 2008. The lifetime of HFC-23 has been revised from 270 to 222 years (WMO, 2011) based on new laboratory studies.

HFC-125 increased by 4.479 ± 0.372 ppt since 2005 to 8.239 ± 0.685 ppt in 2010. The relative rate of increase at the beginning of 2008 was 16% yr^{-1}, and global emissions were 21 Gg in 2007, having increased by 15% yr^{-1} since 2000 (O'Doherty et al., 2009). These estimated emissions are within about 20% of emissions reported to the UNFCCC when estimates of emissions from East Asia, which are not reported to the UNFCCC, are included. HFC-152a, which is used as a foam-blowing agent and as an aerosol propellant (Greally et al., 2007), increased by 2.535 ± 0.184 in 2005 to 6.268 ± 0.328 ppt in 2010. New measurements of several HFCs have been reported since AR4: HFC-365mfc (Stemmler et al., 2007), HFC-245fa (Vollmer et al., 2006), and HFC-227ea (Laube et al., 2010). All were ≤2 ppt in recent years, but their abundances are increasing.

CF_4 and C_2F_6 (PFCs), strongly absorb thermal IR radiation and have lifetimes of 50 kyr and 10 kyr, respectively. CF_4 and C_2F_6 are emitted as a byproduct of aluminum production and used in plasma etching of electronics. Because of their physical properties they are difficult to measure, but new instrumental developments that can pre-concentrate trace species from ambient air at –165°C now allow precise measurements of both species (Miller et al., 2008). CF_4 has a natural lithospheric source (Deeds et al., 2008) with a preindustrial level (about 1750) determined from Greenland and Antarctic firn air of 34.7 ± 0.2 ppt (Muhle et al., 2010) in good agreement with Worton et al. (2007). In 2010, atmospheric abundances were 78.263 ± 1.922 ppt for CF_4, increasing by 3.295 ± 0.099 ppt since 2005, and 4.088 ± 0.199 ppt for C_2F_6, increasing by 0.42 ± 0.025. The sum of emissions of CF_4 reported by aluminum producers and for non-aluminum production in EDGAR (Emission Database for Global Atmospheric Research) v4 only accounts for about half of global emissions estimated from atmospheric observations (Muhle et al., 2010). For C_2F_6, emissions reported to the UNFCCC are also substantially lower than those estimated from atmospheric observations (Muhle et al., 2010).

Global annual mean SF_6 in 2010 was 6.985 ± 0.231 ppt, increasing by 1.356 ± 0.054 ppt since 2005. SF_6 has a lifetime of about 3200 years, so its emissions accumulate in the atmosphere and can be estimated directly from its observed rate of increase. Levin et al. (2010) and Rigby et al. (2010) showed that SF_6 emissions decreased after 1995, most likely because of emissions reductions in developed countries, but then increased after 1998. During the past decade, they found that actual SF_6 emissions from developed countries are at least twice the reported values.

Since AR4, atmospheric observations of two new species that are not covered by the Kyoto Protocol were reported. Prather and Hsu (2008) suggested that NF_3 is a missing greenhouse gas with a potential large impact on radiative forcing. It is a substitute for PFCs as a plasma source in the semiconductor industry, has a lifetime of 500 years, and a GWP_{100} = 17,500 (WMO, 2011) (GWPs are described in Chapter 8). Weiss et al. (2008) determined 0.45 ppt for its global annual mean mole fraction in 2008, growing from almost zero 1978. In 2010, NF_3 was 0.583 ± 0.032 ppt, increasing by 0.279 ± 0.025 ppt since 2005. Initial bottom-up inventories underestimated its emissions; based on the atmospheric observations, NF_3 emissions were 0.62 Gg in 2008. SO_2F_2 replaces CH_3Br, an ODS, as a fumigant. Its $GWP_{100} \approx 4740$, is comparable to CFC-11. A new estimate of its lifetime, 36 ± 11 years (Muhle et al., 2009), is significantly longer than previous estimates. Its global annual mean mole fraction in 2010 was 1.636 ± 0.081 ppt and it increased by 0.286 ± 0.019 ppt from 2005 to 2010.

2.4.1.2 Montreal Protocol Gases (CFCs, Chlorocarbons, HCFCs, and Halons)

CFC atmospheric abundances are decreasing because of the successful reduction in emissions resulting from the Montreal Protocol on Substances that Deplete the Ozone Layer. By 2010, the Montreal Protocol had reduced emissions from ODSs by an amount equivalent to about 11 Pg CO_2 yr^{-1} (including offsets); this is 5 to 6 times the reduction target of the first commitment period (2008–2012) of the Kyoto Protocol (2 Pg CO_2 eq yr^{-1}) (Velders et al., 2007). Recent observations in Arctic and Antarctic firn air further confirm that emissions of CFCs are predominantly anthropogenic (Martinerie et al., 2009). CFC-12 has the largest atmospheric abundance and GWP-weighted emissions of the CFCs. Its tropospheric abundance peaked during 2000–2004. Since AR4, its global annual mean mole fraction declined 10.388 ± 0.243 to 532.824 ± 8.956 ppt in 2010. Small differences among reported global annual means are within the uncertainties in standard scales. CFC-11 continued to decrease. AGAGE reported a decrease of 9.784 ± 0.196 since 2005, ~10% smaller than NOAA reported. In 2010, CFC-11 was 239.822 ± 4.152 ppt. CFC-113 decreased by 3.292 ± 0.104 ppt since 2005 to 75.207 ± 1.946 ppt in 2010. A discrepancy exists between top-down and bottom-up methods for calculating CFC-11 emissions. Emissions calculated using top-down methods come into agreement with bottom-up estimates when a lifetime of 64 yr is used for CFC-11 in place of the accepted value of 45 years; this longer lifetime (64 years) is at the upper end of the range estimated by Douglass et al. (2008a) in a study of the CFC-11 lifetime with models that more accurately simulate stratospheric circulation. Future emissions of CFCs will largely come from "banks" (i.e., material residing in existing equipment or stores) rather than current production.

AGAGE reported that the CCl_4 global annual mean decreased by 5.54 ± 0.209 ppt since 2005, which again is smaller than NOAA reports (–6.36 ± 0.34), to 86.268 ± 3.018 ppt in 2010. The observed rate of decrease and interhemispheric difference of CCl_4 suggest that emissions determined from the observations are on average

greater and less variable than bottom-up emission estimates, although large uncertainties in the CCl_4 lifetime result in large uncertainties in the top-down estimates of emissions. CH_3CCl_3 has declined exponentially for about a decade, decreasing by 10.77 ± 0.54 ppt since 2005 to 7.462 ± 0.901 ppt in 2010, with good agreement among reported values. Because its atmospheric loss is dominated by reaction with hydroxyl radical (OH), CH_3CCl_3 has been used extensively to estimate globally averaged OH concentrations (e.g., Prinn et al., (2005)). Montzka et al. (2011b) exploited the exponential decrease and small emissions in CH_3CCl_3 to show that interannual variations in OH concentration from 1998 to 2007 are 2.3 ± 1.5%, which is consistent with the interannual variability in OH estimated from other species including CH_4, C_2Cl_4, CH_2Cl_2, CH_3Cl, and CH_3Br.

HCFCs are classified as "transitional substitutes" by the Montreal Protocol, so their global production and use will ultimately be phased out. But global HCFC production is not currently capped and has increased in recent years. As a result, global levels of the three most abundant HCFCs in the atmosphere continue to increase. HCFC-22 increased by 36.945 ± 1.16 ppt since 2005 to 36.945 ± 1.16 ppt in 2010. HCFC-141b increased by 2.701 ± 0.14 ppt since 2005 to 20.537 ± 0.674 ppt in 2010, and for HCFC-142b, the increase was 4.859 ± 0.189 to 20.672 ± 0.679 ppt in 2010. The rates of increase in these 3 HCFCs increased since 2004, but the change in HCFC-141b growth rate was smaller and less persistent than for the others, which approximately doubled from 2004 to 2007 (Montzka et al., 2009). Based on changes in observed spatial gradients, there has likely been a shift in emissions within the Northern Hemisphere from regions north of about 30°N to regions south of 30°N.

Atmospheric abundances of halons, except for halon-1301, have been decreasing. All have relatively small atmospheric burdens, ≤ 5 ppt, and are unlikely to accumulate to levels that can significantly affect radiative forcing, if current projections are followed (WMO, 2011).

2.4.2 Short-Lived Greenhouse Gases

This section covers observed trends in tropospheric and stratospheric ozone (O_3), nitrogen dioxide (NO_2), stratospheric water vapor, hydroxyl radical (OH), carbon monoxide (CO), and surface and column aerosol. A variety of measurement techniques and the heterogeneity of reported data preclude a standard method of analysing the changes in observations. Instead, the trend estimates are taken directly from the cited literature. Hence, issues such as data records of different length, potential lack of of comparability among measurement methods, and different trend calculation methods, add to the uncertainties in the trend estimates, but could not be quantified.

2.4.2.1 Tropospheric Ozone

Assessment of long-term O_3 trends is challenging, due to a paucity of long-term measurement sites, combined with the relatively short average atmospheric lifetime of O_3 (a few weeks) and its resulting large variability. AR4 reported regional and seasonal long-term O_3 trends varying in magnitude and sign, and concluded that a large uncertainty in the associated O_3 radiative forcing arose from the inability of models to reproduce the semi-quantitative observations during the late 19th Century. This uncertainty is currently unresolved. Since AR4, further analysis of background tropospheric ozone measurements at the coasts of Europe and North America and from aircraft suggest an overall upward trend of tropospheric ozone between 0.3–0.5% yr^{-1} in the last 2–3 decades, but a flattening of this trend between 2000–2010 in many (but not all) locations around the world. The level of scientific understanding of changes in tropospheric ozone remains medium (unchanged from AR4).

There are marked differences between ozone changes at the surface in polluted and remote regions. An overview of various reported trend estimates is given in Table 2.13. Analyses of O_3 data from EMEP (European Monitoring and Evaluation Programme) stations in Europe (Pozzoli et al., 2011; Jonson et al., 2006), which are close to pollution sources, show partly opposing positive winter and negative summer O_3 trends between 1990 and 2005, in response to reductions in O_3 precursor emissions. Wilson et al. (2011) report an average net positive trend of 0.16 ± 0.03 ppb yr^{-1} (2σ) for Europe for the period 1996–2006; the trends were similar for the mean, 5th and 95th percentile ozone values. Most stations with positive trends were positioned in northern Europe, while in southern Europe negative trends were observed. For the eastern US, Chan (2009) reports temperature-adjusted decreasing trends in 8-hour average ozone mixing ratios for

1997–2006 ranging from –0.53 ± 0.2 to –2.7 ± 0.86% yr^{-1} (or –0.2 to –1.3 ppb yr^{-1}), whereas significant increasing trends of 0.44 ± 0.37% yr^{-1} and 0.98 ± 0.76% yr^{-1} (corresponding to 0.16 ppb yr^{-1} to 0.3 ppb yr^{-1}) were found in Atlantic and Pacific Canada, respectively. Reported trends without temperature-adjustments were generally quite different, showing the impact of meteorology on the trend estimates using relatively short time series.

[INSERT TABLE 2.13 HERE]

Table 2.13: Overview of O_3 trends reported in literature, using datasets with more than 8 years of data availability.

In less-polluted regions, there are limited datasets available from surface stations and ozone soundings. For the past 15 years, high quality measurements from the MOZAIC aircraft programme also provide a consistent 3-dimensional insight into ozone changes. There has been particular emphasis on identifying the causes of trends in O_3 in background air masses entering N. America and Europe from the west, since these changes have direct implications for air quality policies. The cause of increasing tropospheric O_3 over the past few decades in the Northern Hemisphere has been connected to increasing emissions of O_3 precursors, especially in Asia (HTAP, 2010), but a model analysis of (Hess and Zbinden, 2011) suggests an important role for interannual variability resulting from stratospheric ozone transport in the troposphere as well.

Measured trends (Table 2.13) at European background stations (Mace Head, Hohenpeissenberg and Zugspitze), with the earliest timeseries starting in the 1970s, are between 0.2 and 0.6 ppb yr^{-1} and are generally somewhat higher in winter and spring than in summer (HTAP, 2010). Trends at the Jungfraujoch high-altitude observatory (3850 m asl) were positive from 1990 to 1999 (ranging from 0.99 ± 0.46 ppb yr^{-1} in winter to 0.69 ± 0.80 ppb yr^{-1} in summer; uncertainties are 95% c.l.). From 1999 to 2008, no significant trends were observed (Cui et al., 2010). These results are in good agreement with the analysis of O_3 trends at 4 European alpine sites (Gilge et al., 2010). An analysis of (Logan et al., 2011) combining surface ozone at four alpine sites, ozone sondes, and MOZAIC aircraft data, all corrected for inconsistencies, suggests seasonal increases from 7–9 ppb (0.6–0.8 ppb yr^{-1}) between 1978 and 1989, 3–7 ppb in the 1990s (0.3–0.7 ppb yr^{-1}), and a decrease of 1–5 ppb in the 2000s (–0.1 to –0.5 ppb yr^{-1}).

In view of the dominating westerly circulation, O_3 trends at North America's West Coast may be indicative of large-scale ozone changes in the Asian Pacific region. The magnitudes and reasons for these trends are somewhat debated. Oltmans et al. (2008) report trends from 19 to 25 years of surface measurements of 0.53 ± 0.13% yr^{-1} (or ca. 0.34 ppb yr^{-1} and 0.82 ± 0.14% yr^{-1} (or 0.17 ppb yr^{-1}), with uncertainties indicating the 95% c.l.) for two remote California sites (Lassen Volcanic National Park and Yreka), however they suggest that local O_3 production rather than long-range transport has contributed to these trends. Oltmans et al. (2008) do not find significant changes in ozone derived from a 10 yr dataset of vertical soundings at Trinidad Head. Parrish et al. (2009) analyse data from 8 Pacific stations with time series between 8 and 25 years, to derive a trend of 0.34 ± 0.09 ppb yr^{-1} (Figure 2.24). These trends are very similar to the trends measured at Mace Head (west coast Ireland), although the North American trends continue after 2000, but flatten in Europe. Trends at the surface of the North American west coast during winter are highest with 0.45 ± 0.13 ppb yr^{-1}. Cooper at al. (2010) derived a trend of 0.63 ± 0.34 ppb yr^{-1} in springtime free tropospheric ozone over western North America between 1984–2008, in approximate accord with the trends derived from the surface measurements by Parrish et al. (2009), and the trends were stronger in air with strong influence from the south and east Asian boundary layer. Jaffe et al. (2007) report that average O_3 mixing ratios generally increased from 1987–2004 at 7 rural sites in the western and northern US, with significant increase rates of 0.19 to 0.51 ppb yr^{-1} at 7 sites, while no significant trends were detected at two others sites. Based on a statistical analysis of measurements at 97 non-urban monitoring sites for 1997 to 2006, (Chan and Vet, 2010) found that baseline O_3 mixing ratios increased on the West Coast of the US and Canada, but trends in California were not statistically significant.

The few long-term continuous O_3 measurements in Asia indicate increasing O_3 concentrations. In Japan, continuous measurements at Mt. Happo Observatory (1.9 km asl) show a springtime O_3 increase of 1.2 ± 0.3 ppb yr^{-1} from 1991 to 2006 (Tanimoto, 2009), and trends from other seasons are also larger than anywhere else in the world. However, 6 western Pacific rim sites (Tanimoto, 2009; Tanimoto et al., 2009) do not show significant trends. Ozone at these 6 sites is ~10 ppb greater than at eastern Pacific sites, where positive trends are observed (Parrish et al., 2009).

[INSERT FIGURE 2.24 HERE]

Figure 2.24: Springtime trends in surface O_3 mixing ratios measured in a) Europe and b) western North America and Japan. The lines (in color) are linear regressions fitted to the data, and the curves (in black) indicate quadratic polynomial fits to the three central European sites over the time span of the lines. Arkona and Zingst are close to the Baltic Sea. Mace Head is at the west coast of Ireland. Hohenpiessenberg (1.0 km asl) and Zugspitze (3.0 km asl) are in southern Germany, and Jungfraujoch (3.6 km asl) is in Switzerland. The North American data are from several sea level Pacific coastal sites and Lassen Volcanic National Park (1.8 km asl) near the west coast, and from the free troposphere over the western part of the continent. The Japanese data are from Mt. Happo (1.9 km asl) on the Japanese mainland and Rishiri, a northern (45°N) sea level island site (HTAP, 2010).

For Mauna Loa Observatory in Hawaii, Oltmans et al. (2006) found a positive trend of ca. 0.14 ± 0.06 ppb yr^{-1} for 1982–2004. The trend is mainly in autumn and winter, and possibly due to dynamical effects.

In the Southern Hemisphere, Oltmans et al. (2006) report increases of surface O_3 on the order of 0.3–0.5% yr^{-1} based on three time series covering 20 years. They point out that long-term O_3 trends vary in sign and magnitude among various regions, but they are broadly consistent with the expected behaviour of precursor emissions. (HTAP, 2010) states that qualitatively, but not quantitatively, models reproduce the observed trends of baseline O_3.

Relatively little progress has been made in the use of satellite retrievals for deriving trends of tropospheric O_3 columns. Thompson et al. (2001b) report strong El Niño signals, but no trends using Nimbus 7/TOMS data. Using a different technique, but the same instrument, Ziemke et al. (2005) show a statistically significant upward trend in the mid-latitudes of both hemispheres but not in the tropics. Model analysis by de Laat et al. (2005) suggests serious instrumental limitations for retrieving extratropical trends. Beig and Singh (2007) report TOMS derived tropospheric O_3 trends (1979–2005) of 0.4–0.9% yr^{-1} for some parts of south Asia. A new generation of satellites, TES (Tropospheric Emission Spectrometer) and OMI (Ozone Monitoring Instrument), operational since 2004, and IASI, operational since 2007, may in the near future allow more robust information on tropospheric O_3 trends (Keim et al., 2009; Liu et al., 2010; Zhang et al., 2010).

2.4.2.2 Stratospheric Ozone

AR4 did not extensively discuss stratospheric ozone trends, but instead reported the radiative forcing of stratospheric ozone between pre-industrial and 2005 to be –0.05 ± 0.10 W m^{-2}, with medium scientific understanding. The recent Scientific Assessment of Ozone Depletion (Ajavon et al., 2010), using various measurements, shows a rather consistent picture for changes of stratospheric ozone at mid-latitudes as well as polar ozone (Figure 2.25, adapted from Chapter 2 in Ajavon et al., 2010). In summary, average total ozone columns have remained at the same level for the past decade, about 3.5% below the 1964–1980 averages for the entire globe, and 2.5% for the latitudes 60°S–60°N. These results are consistent with the AR4 report, and the level of understanding of changes in stratospheric ozone is medium. For further discussion regarding changes in stratospheric dynamics see Section 2.6.7, and radiative forcing resulting from stratospheric ozone change see Chapter 8.

[INSERT FIGURE 2.25 HERE]

Figure 2.25: Trends in midlatitude a) and polar b) stratospheric ozone. Total ozone average of 63°–90° latitude in March (NH) and October (SH). Symbols indicate the satellite data that have been used in different years. The horizontal grey lines represent the average total ozone for the years prior to 1983 in March for the NH and in October in the SH.

2.4.2.3 Stratospheric H_2O Vapour

Stratospheric H_2O vapour has important roles in Earth's radiative balance and in stratospheric chemistry. Increased stratospheric H_2O vapour causes the troposphere to warm and the stratosphere to cool (Solomon et al., 2010), and, when halogen-containing compounds are present, it increases rates of O_3 loss. AR4 reported that stratospheric H_2O vapour showed significant long-term variability and an upward trend over the last half of the 20th Century, but no increase since 1996. This assessment identifies a significant decrease in stratospheric O_3 from 2000 to 2001 that was observed by independent measurement techniques, then an increase since 2005, and that this variability impacts surface temperatures.

The longest continuous time series of stratospheric water vapour abundance is from in situ measurements made with frost point hygrometers (FPH) starting in 1980 over Boulder, CO, USA (40°N, 105°W) (Oltmans et al., 2000; Scherer et al., 2008). These observations have been complemented by global satellite observations from SAGE II (1984–2005; Stratospheric Aerosol and Gas Experiment II), HALOE (1991–2005; HALogen Occultation Experiment), and Aura MLS (2004–present; Microwave Limb Sounder) (Read et al., 2007). Water vapour mixing ratios obtained using these different methods do not always agree, even in their trends. For example, offsets of up to 0.5 ppm in lower stratospheric water vapour mixing ratios exist between HALOE and Aura MLS retrievals during their 1-year period of overlap (2004 to 2005), i.e., the order of magnitude of interannual changes.

Hurst (2011) analyzed the Boulder FPH record for trends. They divided the record into 4 periods (1980–1989: period 1; 1990–2000: period 2; 2001–2005: period 3; and 2006–2010: period 4) and found statistically significant non-zero trends for all four periods in each of five 2-km altitude layers (16–26 km). Trends in all 5 layers were positive for periods 1, 2, and 4, and negative for period 3. Water vapour changes in the 5 layers for each of periods 1–4 averaged 0.32 ± 0.18 ppm, 0.57 ± 0.25 ppm, –0.35 ± 0.04 ppm and 0.49 ± 0.17 ppm, respectively. The 30-year net increase in these 5 layers (16–26 km), averaged 1.0 ± 0.2 ppm, with a vertical trend gradient of 0.07 ± 0.04 ppm km^{-1}. This pattern of increased growth with increasing altitude for the 1980–2010 period was also observed for periods 2 (0.08 ± 0.02 ppm km^{-1})) and 4 (0.03 ± 0.02 ppm km^{-1}), but the positive growth during period 1 weakened with altitude (-0.06 ± 0.02 ppm km^{-1}). The negative trends for period 3 showed no significant altitude dependence.

Solomon et al. (2010) showed that the stratospheric H_2O vapour decrease in 2000–2001 (start of period 3) slowed the rate of increase in global surface temperature by 25% compared to that which would have occurred due only to CO_2 and other GHGs. Data and trends reported by Hurst (2011) for H_2O vapour over Boulder are in agreement with the qualitative trends reported by Fujiwara et al. (2010) for the tropical stratosphere based on 1993-2009 data from balloon-borne frost point hygrometers. Agreement between the Boulder and HALOE mixing ratios and trends is poor for the 1990s; during period 2 in Hurst et al. (2011), HALOE showed no trend in stratospheric H_2O over Boulder (Scherer et al., 2008). In contrast, Boulder FPH and Aura MLS mixing ratios and trends remain in good agreement since the 2004 start of MLS data. From 2000 to 2005, the Boulder and HALOE stratospheric H_2O records both show negative trends, which have been explained by anomalously low tropical tropopause temperatures (Fueglistaler and Haynes, 2005; Randel et al., 2006; Rosenlof and Reid, 2008; Randel and Wu, 2010). About 30% of the positive trend in stratospheric H_2O determined by FPHs during the 1990s (Hurst, 2011; Fujiwara et al., 2010) can be explained by increased production of H_2O from CH_4 oxidation (Rohs et al., 2006), but the remainder can not be explained by changes in tropical tropopause temperatures. The cause of the period 4 increase in stratospheric H_2O seen in both the FPH and Aura MLS records has not yet been established.

Since AR4, new studies characterize the uncertainties in measurements from individual types of *in situ* H_2O sensors (Vomel et al., 2007a; Vomel et al., 2007b; Weinstock et al., 2009), but discrepancies between different instruments (on order of 50 to 100% at H_2O mixing ratios less than 10 ppm), particular for high-altitude measurements from aircraft, remain unexplained.

In summary, balloon-borne observations are in reasonable agreement with satellite observations from 2000 to present, but a discrepancy exists in trends for the 1990s that cannot be fully explained by trends in tropical tropopause temperatures and methane oxidation. Long-term balloon-borne observations from Boulder, Colorado indicate a net increase of 1 ppm for 1980–2010 while global satellite data suggest a net decrease of 0.2 ppm for 1992–2010, primarily related to a step-like decrease after 2000 and increases since 2005. There are unfortunately limited data sets for evaluating the long-term variability and trends in stratospheric water vapour. There is good understanding of the relationship between stratospheric water vapour trends and tropical tropopause temperature changes (see Figure 2.26), as Randel et al. (2006) demonstrated for the period 3 water vapour decrease, but the longer-term net increase in stratospheric water vapour over Boulder is not well understood.

[INSERT FIGURE 2.26 HERE]

Figure 2.26: Top) Deseasonalized stratospheric water vapor anomalies from HALOE (black) and MLS (blue). Bottom) Temperature anomalies over the time span as the top panel from near-equatorial radiosonde stations (black), and a shorter record (after 2001) based on GPS radio occultation (red).

2.4.2.4 Hydroxyl Radical (OH)

AR4 reported no detectable change in [OH] from 1979 to 2004. Recent studies do not agree on trends and variability, so confidence in reported trends in OH is low.

Rigby et al. (2008) report a general decline in [OH] from 2004 to 2007, but uncertainties are large. For example, they report a change in globally, annually averaged [OH] from 2006 to 2007 of 4 ± 14% and uncertainties in annually averaged [OH] of ~16%. Because of the large uncertainties, there is no statistically significant trend in [OH] at the 90% c.l.

Montzka et al. (2011b)) analyzed time series of 6 tracers to show that interannual variability (IAV) in globally averaged [OH] from 2000 to 2007 is small, ~2%. When variability in CH_4 only was considered, they showed that this small IAV in [OH] has existed since 1984. Small IAV in global [OH] does not preclude larger regional variations in [OH] as shown by (Manning et al., 2005) for the western Pacific in mid- to high-latitudes of the Southern Hemisphere based on measurments of ^{14}CO at Baring Head, New Zealand.

OH is important in climate change, because it initiates oxidation of many reduced LLGHGs (CH_4, HFCs, and HCFCs), and knowledge of its concentration combined and rate coefficients for relevant reactions are used to determine atmospheric lifetimes of these gases. In a model study that used methyl chloroform observations, (Wang et al., 2008) found that the lifetime of methyl chloroform due to OH from 1988 to 1994 was 11 to 21% longer than found in other studies. If confirmed, this study would indicate that lifetimes for CH_4, HFCs, and HCFCs used to calculate GWPs (see Chapter 8) should be longer than those currently considered, increasing their influence on climate relative to CO_2.

2.4.2.5 Carbon Monoxide (CO)

CO does not have a direct affect on radiative forcing, but it has an indirect effect on climate through its impact on OH (which affects the lifetimes of CH_4, HFCs, and HCFCs) and on tropospheric O_3 abundance. AR4 did not assess current trends in atmospheric CO based on observations. The major sources of atmospheric CO are in situ production by oxidation of hydrocarbons (mostly CH_4 and isoprene) and direct emission resulting from incomplete combustion of carbon-based fuels like biomass and fossil fuels. Analysis of CO data from the NOAA ESRL GMD global cooperative air sampling network (data path: ftp://ftp.cmdl.noaa.gov/ccg/co/flask/) indicates a small decrease in globally averaged CO from 2006 to 2010. The observations are consistent with estimates of a slight decline in global anthropogenic CO emissions over the same time (Granier and al., 2011).

2.4.2.6 Observations of NO_2

Nitrogen oxides (NO_x=NO+NO_2) from anthropogenic emissions are one of the most important contributors to the formation of tropospheric O_3. Due to its short atmospheric lifetime (hours), NO_x concentrations are highly variable in time and space. AR4 described the potential of satellite observations of NO_2 to verify and improve NO_x emission inventories and their trends and reported strong NO_2 increases by 50% over the industrial areas of China from 1996–2004. An extension of this analysis reveals increases between a factor of 1.7 and 3.2 over parts of China, while over Europe and the US NO_2 has decreased by 30 to 50% between 1996 and 2010. Increasingly, satellite data are used to derive trends in anthropogenic NO_x emissions.

Figure 2.27, updated from (Richter et al., 2005), shows the relative changes in tropospheric NO_2 columns, normalized for 1996, derived from measurements of two instruments, the Global Ozone Monitoring Experiment (GOME) until the end of 2002 and the Scanning Imaging Spectrometer for Atmospheric Chartography (SCIAMACHY) until 2010. The main results show a strong upward trend over Central Eastern China and an overall downward trend in Europe and the US. The decreases over Western Europe and Poland are only observed until 2003, with only small changes afterwards. In contrast, NO_2 reductions in the US are most pronounced after 2004, related to differences in effectiveness of NO_x emission abatements in the US and Europe. van der A et al. (2008) apply a similar methodology to derive linear trends in NO_x emissions, with reported Asian emission increases of up to 29% per year, and reductions in North America and Europe

up to 7% per year for the period 1996–2006. Using data for 2006–2009 from SCIAMACHY, (Lamsal et al., 2011) report increases in global NOx terrestrial emissions by 9.2%, largely driven by the 18.8% increases in East Asia, while taking into account the non-linear feedback of NO_2 on its lifetime. Focussing on the shipping transport sector, (de Ruyter de Wildt et al., 2011) use SCIAMACHY, OMI and GOME-2 data to derive significant increases in NO_2 columns (60–100%) in the 2002–2008 period, and substantial decreases in 2009–2010, in pace with changes in international trade volume.

[INSERT FIGURE 2.27 HERE]

Figure 2.27: Relative changes in tropospheric NO_2 columns, normalized for 1996, derived from two instruments, the Global Ozone Monitoring Experiment (GOME) until the end of 2002 and the Scanning Imaging Spectrometer for Atmospheric Chartography (SCIAMACHY) until 2010. Updated from Richter et al. (2005)

2.4.3 Aerosols

This section assesses trends in aerosol resulting from both anthropogenic and natural emissions. Due to the short life-time of aerosol (days to week) trends in anthropogenic aerosol are mainly confined to the high emission regions in the Northern Hemisphere. Natural aerosols (such as desert dust, seasalts, and biogenic aerosols) are important in both hemispheres, are also important for both direct and indirect aerosol interactions, and changes in natural aerosols are likely to result from climate and land-use use change (Carslaw et al., 2010). However, data on the trends in natural aerosols are even more limited compared to those for anthropogenic aerosols (Mahowald et al., 2010). Long-term measurements from aerosol components and parameters measured in-situ and obtained from remote sensing will be discussed, with a focus on the trends influenced by anthropogenic emissions.

2.4.3.1 Global and Regional Trends of Aerosol Optical Depth (AOD) from Remote Sensing

AR4 qualitatively described the early attempts to retrieve AOD from satellite data, and the first results from the newer generation instruments available since 2001. AR4 did not provide trend estimates. Since AR4, new long-term remotely sensed datasets of aerosol are becoming available. These datasets indicate a continuing decrease of AOD in the US, Europe, and Japan, and a continuing increase of AOD over Eastern and Southern Asia since the 1980s, which is consistent with estimated anthropogenic emission temporal trends. Some studies report negative trends over the global oceans, but these trends may be less certain due to instrumental issues, the length of the data-record, and the influence of natural variability. *Confidence* on trends in AOD from remote sensing *is* globally *low*, and in some regions medium. Some progress has been made detecting trends attributable to changes in anthropogenic emissions.

An extensive discussion on various optical properties derived from passive remote sensing data, which address aerosol amount, size and composition is given in Chapter 7. This section mainly discusses trends of AOD derived from passive remote sensing of mid-visible wavelengths.

AOD can be relatively accurately measured from ground sites by measuring the direct solar intensity (e.g., by sun-photometry) in cloud-free conditions. AOD is determined from the relative change in direct solar intensity, either from changes in atmospheric pathlength or in reference to the extrapolated value at the top of the atmosphere. AERONET (AErosol RObotic NETwork) is a network of ground-based sun-/sky-photometers which provides accurate multi-annual statistics on aerosol column properties simultaneously at more than 200 surface sites (Holben et al., 1998). The first instruments were deployed in the mid-1990s with a rapidly increasing density over the last 10 years. Presently there are only few stations that provide continuous time series for a decade or longer, however. In addition to direct beam solar observations (irradiance), AERONET and Skynet (distributed over Asia) also measure brightness of the sky as a function of angle (radiance). When AOD is large enough, these observations can be used to estimate size-distribution and absorption. In Japan, a recent study using ground-based broadband radiometers suggests an increase of optical thickness until the mid-1980s, followed by a decrease until the late 1990s and almost constant values in the 2000s (Kudo et al., 2011). A consistent analysis of long-term (longer than ca. 10 years) AERONET AOD for large regions and multiple stations has not been compiled, and, as spatial coverage of sun-photometer data is sparse and globally uneven, detected local trends may not be applicable for large regions.

For the last decade, dedicated satellite sensors provide continuous global data-records of aerosol properties. AOD is estimated from satellite sensor data using changes to sunlight reflected to space under cloud-free conditions. Satellite data offer quantitative information on AOD spatial distributions on global scales when it is validated with higher quality observations from ground-based remote sensing.

Linking trends to anthropogenic activities is difficult because long-term, (multi-) decadal changes in aerosol properties are usually small compared to seasonal and inter-annual variability. Variability may be strongly influenced by wet removal processes and by large variations of sources. On average about half of today's atmospheric AOD and most of the AOD variability can be linked to natural aerosol (e.g., dust, sea-salt, volcanoes). At present there are a number of 10 year data-records produced by satellite sensors (e.g., MODIS, MISR) with support from local monitoring by sun-photometer networks (e.g., AERONET, SkyNET, GAW). For example, the seasonal AOD maps derived from MISR sensor samples for individual years from 2000 to 2009 for the Atlantic Ocean and Africa shown in Figure 2.28 (Kahn et al., 2010) demonstrate significant seasonality and inter-annual variability associated with the outflow Saharan dust over the Atlantic. Abundances of natural aerosol are strongly linked to meteorological (e.g., near surface winds) or land- surface conditions (e.g., soil moisture, erosion). In addition, in certain years large volcanic eruptions (e.g., Mt. Pinatubo in 1991) can add aerosol to the stratosphere leading to stratospheric AOD values comparable to those of the troposphere, although volcanic contributions of such magnitude have not occurred during the last 10 years.

[INSERT FIGURE 2.28 HERE]

Figure 2.28: Mid-visible seasonal AOD data from 2000 to 2009 data over Africa and the Atlantic as detected by MISR samples. Updated from Kahn et al. (2010), courtesy MISR Team, Jet Propulsion Lab/Caltech and NASA Goddard Space Flight Center

Natural variability makes it difficult to quantify from measurements the trends in AOD fraction attributable to anthropogenic sources. Satellite retrievals over oceans (but not over land) can usually make some distinctions between AOD from larger and smaller aerosol, often associated with natural and anthropogenic aerosol. Therefore, anthropogenic AOD trend detection is most promising over coastal outflow regions of urban-industrial regions.

Uncertainties in AOD retrievals from satellite arise from poorly constrained aerosol absorption and surface solar reflection. Moreover, if retrieval models do not account for inter-annual changes to these properties (e.g., changes in aerosol mixture or changes to vegetation characteristics), erroneous trends may be derived. For such satellite sensor data analysis, careful evaluations of noise, bias, and calibration within and among sensors, are needed, while also retrieval issues such as the assumptions on surface characterization, sampling issues, cloud contamination and the aerosol models used in the inversion procedure, may also influence the retrieval of trends (Zhang and Reid, 2010). For example, instrumental degradation or errors leading to sensitivity loss in selected spectral bands, as recently detected for the MODIS sensors on Terra (Levy et al., 2010), can lead to erroneous trend estimates. The identification of decadal trends in AOD by satellite instruments remains challenging. A variety of satellite instruments provide long-term information on aerosol. Satellite aerosol observations with the longest data records going back to the early 1980s used TOMS and AVHRR sensors with limited capabilities with respect to aerosol retrieval. TOMS data are based on retrievals in the UV portion of the solar spectrum, where surface contributions to the detected signal are also small over land, so that retrievals over continents are possible not only for AOD, but also for estimates on aerosol absorption. Commonly, a qualitative measure for absorbing aerosol is used, the so called absorbing aerosol index product, to assess the variability of dust sources (Prospero et al., 2002) and biomass burning (Thompson et al., 2001a).

For anthropogenic AOD trends, regions with expected anthropogenic change are of interest, such as regions over or near eastern Asia and the eastern US. During the 1980s and 1990s TOMS data, whose UV retrieval permits estimates for AOD and absoption even over continents, indicate continued AOD and absorption increases during the dry fall/winter season over eastern Asia (Torres et al., 2002). From the mid-1980s onwards AVHRR data indicate continued AOD decreases and slightly decreasing aerosol sizes over coastal waters off the eastern US coast (Mishchenko et al., 2003).

AVHRR data are based on retrievals in the visible and, due to complications over land, AOD values are only retrieved over (deep) oceans. For total (natural plus anthropogenic) aerosol, the 23 year data record ((Mishchenko et al., 2007) indicates an overall decreasing total AOD trend. On a hemispheric basis AVHRR data show no trend before 1995 but between 1995 and 2005 a decrease of 0.02 for total AOD over oceans. A qualitative analysis of PATMOSx and AVHRR/GAPC data (Cermak et al., 2010) also suggests negative AOD trends over most ocean regions starting from the beginning of 1990s, supporting the global brightening hypothesis (see Section 2.5).

Detection of more reliable anthropogenic trends for the last 10 years is possible for aerosol dedicated satellite sensors deployed at the turn of the century, at least over oceans. This view is contested by more recent analyses of mid-visible bias-corrected MODIS (Moderate Resolution Imaging Spectro-radiometer) and MISR (Multi-angle Imaging Spectro-radiometer) level 2 time series (Zhang and Reid, 2010). MODIS and MISR, using wavelengths more suitable for aerosol retrieval, do not detect significant global AOD trends for the 2000–2009 period.

Mid-visible bias-corrected MODIS and MISR level 2 time series were examined for regional trends (Zhang and Reid, 2010). Consistent with emission trends, AOD over the last 10 years (Figure 2.29) displays strong positive trends over coastal water of southern and eastern Asia, and the sign of these changes is consistent with emission trends in Europe, North America and Asia (see Chapter 6, tbc).

Using MODIS retrieval at different visible wavelengths a separation of coarse (assumed natural) and fine (assumed anthropogenic) aerosol is possible.

[INSERT FIGURE 2.29 HERE]

Figure 2.29: Spatial distribution of ten year trends for the mid-visible total AOD (upper panel) and the derived anthropogenic AOD (lower panel) over oceans based on MODIS data trends (Zhang and Reid, 2010). Red boxes indicate regions with statistically significant trends.

2.4.3.2 Surface Aerosol Trends

AR4 did not report trends in long-term surface-based in-situ measurements of particulate matter or its components. In-situ ground based measurements of aerosol indicate a highly certain downward trend in inorganic (mainly SO_4) aerosol in parts of North America and Europe on the order of –3% yr^{-1} during the last 2–3 decades. In the USA almost all PM2.5 measurements indicated a downward trend on the order of 0 to –2.5% yr^{-1} during the last 2 decades. In Europe, downward trends in PM2.5 on the order of –2 to –3% yr^{-1} are found at a few locations. More long-term observations are available for PM10 measurements than for PM2.5; these indicate decreases on the order of –1 to –4% yr^{-1}. Likewise very few long-term equivalent black carbon (also called elemental carbon, depending on measurement technique) measurements are available, although total carbon observations in the USA indicate downward trends. In other parts of the world, coordinated surface aerosol measurements started, at best, in the early 2000s, and thus far these measurements do not provide a clear picture regarding trends of PM2.5 or aerosol components. There is high confidence in substantial downward trends of SO_4 and PM2.5 in the USA, medium confidence in Europe, and limited knowledge on trends elsewhere.

Regional aerosol and aerosol precursor emissions have changed and will continue to change due to economic development and implementation of air pollution controls, and they are drivers of variability and trends of aerosol surface and column abundances in polluted regions. Since at many continental locations a large fraction of the aerosol mass resides in the atmospheric boundary layer (Jaenicke, 1993), long term measurements at the Earth surface may also provide information on the aerosol columns and the resulting radiative perturbations driving climate change, provided that these measurements are representative for a larger region. Several studies, e.g., (Donkelaar van et al., 2010) have demonstrated a close relationship between satellite derived AOD and measured PM2.5. However, under marine outflow conditions, aircraft observations often show elevated aerosol levels above the boundary layer (Clarke and Kapustin, 2002; Osborne and Haywood, 2005), and surface measurements may not always accurately represent column changes. This section summarizes reported trends of PM2.5 (particulate matter with diameter <2.5 um) and two of the most widely measured climate relevant anthropogenic aerosol components, sulphate and equivalent black carbon or elemental carbon. Although more and longer time series of PM10 (d <10 um) are

available, their trends are probably less climate relevant than those of PM2.5, due to the influence of PM10 from local sources, and the smaller scattering efficiency of coarse aerosol. For a detailed discussion on observations and the role of other aerosol components and their properties, see Chapter 7, while Chapter 8 evaluates the radiative forcing of aerosol.

There are no true global networks of in-situ aerosol observations, and an overview and critical evaluation of worldwide, quality assured, aerosol trend measurement presently does not exist. A few long-term background measurements of aerosol properties are performed within the framework of the WMO GAW (Global Atmosphere Watch) program. Surface based remote sensing of aerosol is performed within AERONET and other networks, and it is discussed in Section 2.4.3.1.

In Asia, the Acid Deposition Network East Asia (EANET, 2011) has measured particulate matter and deposition since 2001, but thus far no trend studies have been published. In China, CAWNET and CARSNET recently started systematic aerosol observation, e.g., (Zhang et al., 2011b), however only few years of data are available. In some other Asian regions long-term measurements from individual research groups or small networks are becoming available, but it is often difficult to assess the significance of these measurements for larger regions. Air quality networks in North America and Europe are the most reliable source of information on long-term surface aerosol trends in these parts of the world.

In Europe, the EMEP network provides regionally representative measurements of aerosol composition since the 1980s; these measurements are described in annual reports, and they are available via www.emep.int. In North America, the U.S. Clean Air Status and Trends Network (CASTNET) and the Canadian Air and Precipitation Monitoring Network (CAPMoN) provide regionally-representative long term measurements of major ions in aerosols, including sulfate, but not PM2.5 mass. The U.S. Interagency Monitoring of Protected Visual Environments (IMPROVE) Network has measured PM2.5 and PM10 mass, total aerosol composition, and visibility at ca. 60 regional stations since 1989 (Hand et al., 2011).

2.4.3.2.1 PM2.5

In Europe, only a few PM2.5 time series longer than a decade are available, with the earliest measurements starting in 1997, but longer timeseries exist for PM10. Figure 2.30 updated from (EMEP, 2010) shows downward trends for the period 2001–2009 in PM2.5 at Penausende, Spain (–35%; or –3.9% yr^{-1}, Ispra, Italy (–31%; –3.4% yr^{-1}) and Schauinsland, Germany (–22%; –2.4% yr^{-1}), whereas at 5 other stations the trends were not significant.

[INSERT FIGURE 2.30 HERE]

Figure 2.30: Time series of annual average PM2.5 (ug m^{-3}) in Europe; updated from (EMEP, 2010)

In addition to PM2.5, substantially more regional PM10 measurements (updated from (EMEP, 2010)) provide additional information on European aerosol trends. Figure 2.31, shows significant reductions between –1.0 and –4.5% yr^{-1} for 11 out of 17 stations, mainly in Southern and Central Europe. With average ratios of PM2.5 to PM10 of 0.58–0.79 these declines are likely to be indicative for changes in PM2.5 as well.

[INSERT FIGURE 2.31 HERE]

Figure 2.31: Reduction of PM10 at European rural background sites. Adapted from (EMEP, 2010).

For Canada, annual mean PM2.5 for all urban measurement sites combined decreased by roughly 40% between 1985 and 2006 (Canada, 2011), corresponding to –3.6%/yr. This decline was to a large degree attributable to decreases in precursor emissions (SO_2 and NO_x) in eastern Canada and the eastern United States (Canada, 2011). In the USA, PM2.5 measurements obtained in IMPROVE (Hand et al., 2011) indicate highly significant ($p<0.05$) downward trends on the order of –2.5% yr^{-1} in most of the US, which are larger in winter than in summer (Figure 2.32).

[INSERT FIGURE 2.32 HERE]

Figure 2.32: IMPROVE (Hand et al., 2011) trends and significance of fine particulate matter levels in the USA.

2.4.3.2.2 Sulfate

Sulfate (SO_4) aerosol is an important mass fraction of PM2.5 (see Chapter 7). Currently, important sources are power generation, industry, and certain transport sectors (international shipping). SO_2 (the precursor gas of SO_4) emissions from industry and the energy sector, have been increasingly mitigated in response to acid deposition, and to reduce the impact of particulate matter on human health.

Figure 2.33 shows SO_4 trends (Pozzoli et al., 2011) for 1990–2005 from selected stations with long-time series for Europe (EMEP) and North America (CASTNET). Before 1990, the number of measurements was substantially less. Significant negative trends of SO_4 are found in eastern and northern Europe (–0.05 to –0.15 ug S m^{-3} yr^{-1}; or ~–2 to –6% yr^{-1}), and less (0 to –0.05 ug S m^{-3} yr^{-1}) in Scandinavia and Southern Europe. Pozzoli et al. (2011) attribute the trends in large part to emission changes, not to natural processes. Precipitation scavenging of aerosol provides another view of changes in aerosol column amounts. Consistent with the SO_4 aerosol trends, (Fowler et al., 2007) report declines in sulfate rainwater concentrations between 1980–2000 of about –3% yr^{-1} in eastern and southern Europe, and about –2% yr^{-1} elsewhere in Europe.

[INSERT FIGURE 2.33 HERE]

Figure 2.33: Observed SO_4 trends 1990–2005 (ug S m^{-3} yr^{-1}) in Europe and the US. Non-significant trends are denoted with red circle adapted from (Pozzoli et al., 2011).

The trends for the USA in Figure 2.33 are for non-urban sites (Pozzoli et al., 2011). SO_4 aerosol declines in the eastern United States ranging from 0 to –0.05 ug S m^{-3} yr^{-1} (0 to –3% yr^{-1}), and no significant trends in the western US. These trends are consistent with average trends reported by CASTNET (2010) of –0.045 ug S m^{-3} yr^{-1} for the period 1990–2008 in the eastern US, and a decrease of CASTNET aerosol sulphate concentrations by –21% in the east and northeast, –22% in the Midwest, and –20% in the south between the two periods 1990–1994 and 2000–2004 (Sickles and Shadwick, 2007b). Indirect evidence for declining sulfate particulate concentrations is found in an analysis of SO_4 wet deposition by 20–30% over a time period of 15 years (Sickles and Shadwick, 2007a), corresponding to a trend of about –1.4% to –2.1% yr^{-1}. In Canada, aerosol sulphate concentrations from 1991–1993 declined by –30 to –45% by 2004–2006 at non-urban CAPMoN sites in the eastern half of the country. Also IMPROVE (Murphy et al., 2011) , (Hand et al., 2011) reports overall declines of SO4 on the order of 2.5% yr^{-1}, and somewhat larger along the east and north-west coasts of the USA. SO4 declines in winter were somewhat larger than in other seasons.

These declines are consistent with the trends of inorganic aerosol components reported by Quinn et al. (2009) at Barrow, Alaska, ranging between –2.3% yr^{-1} for SO_4 to –6.4% for NH_4. Hidy and Pennell (2010) show remarkable agreement of PM2.5 and SO_4 declines in Canada, pointing to common emission sources of PM2.5 and SO_4

2.4.3.2.3 Black and elemental carbon trends

The terms black carbon (BC) and elemental carbon (EC) refer to the operational analysis methods: optical methods (aerosol light absorption) or filter measurements using thermal methods, respectively. The measurements are associated with large uncertainties; intercomparisons showed differences of a factor 2–3 for optical methods, and a factor of 4 for thermal methods (Vignati et al., 2010), which also renders quantitative comparison of BC time series uncertain. In addition, while there is a general lack of BC/EC measurements, long-term time series are even scarcer.

In Europe long term EC/BC are available at 2 stations (in Norway and Italy) starting in 2001 (EMEP, 2010), but thus far these time series have not been published. In North America, the IMPROVE network is measuring black carbon with optical techniques. However, due to an upgrade in measuring techniques around 2005, only long-term data for total carbon (TC=black carbon + organic carbon) are published (Hand et al., 2011; Hand et al, 2010). These TC measurements indicate highly significant ($p<0.05$) downward trends of total carbon between 2.5 and 7.5% yr^{-1} along the east and west coasts of the USA, and smaller and less significant ($p<0.15$) trends in other US regions from 1989–2008. Sharma et al. (2006) published long term measurements of equivalent BC at Alert, Canada and Barrow, Alaska, USA. Decreases were 54% at Alert and 27% at Barrow for 1989–2003; part of the trend difference was associated with changes in circulation patterns.

2.5 Radiation Budgets

The radiation budget of the Earth is the key energy driver of climate. In the mean, radiative processes alternately warm the surface and cool the atmosphere, requiring the hydrological cycle and sensible heating to compensate. Spatial and temporal energy imbalances due to radiation and latent heating produce the general circulation of the atmosphere and ocean. Anthropogenic interference with climate occurs first of all through a perturbation of the components of the Earth radiation budget.

The radiation budget at the top of atmosphere (TOA) defines the energy flows in and out of the global climate system. It includes the absorption of solar radiation by the Earth, determined as the difference between the incoming solar radiation at the TOA minus its reflected fraction, and the thermal outgoing radiation emitted from the Earth to space.

The surface radiation budget provides the energy for a variety of surface processes and largely determines the thermal and hydrological conditions at the Earth surface. The surface radiation budget takes into account the solar fluxes absorbed at the Earth surface, as well as the upwelling and downwelling thermal fluxes emitted by the surface and atmosphere, respectively.

2.5.1 Global Mean Radiation Budget

Since AR4 knowledge on the energy exchange between Sun, Earth and Space has been improved through new information from space-born platforms such as the Clouds and the Earth's Radiant Energy System (CERES, Wielicki et al., 1996) and the Solar Radiation and Climate Experiment (SORCE, Kopp and Lawrence, 2005) which are in operation since the turn of the millennium. Measurements of the total solar irradiance (TSI) incident at the TOA are now much better known, with the most recently launched SORCE Total Irradiance Monitor (TIM) reporting uncertainties as low as 0.035% (Kopp et al., 2005). For the 2008 solar minimum, the solar irradiance from SORCE/TIM is 1360.8 ± 0.5 W m^{-2} compared to 1365.5 ± 1.3 W m^{-2} from earlier missions (cf. Section 8.2.1). Kopp and Lean (2011) conclude that the SORCE/TIM value of total solar irradiance is the most credible value because it is validated by a NIST-calibrated cryogenic radiometer at full solar power levels while operating under vacuum (see Section 8.2.1 for a more detailed discussion). Distributed over the sphere of the globe and averaged over time this revised estimate corresponds to a total solar irradiance close to 340 W m^{-2} (Figure 2.34).

[INSERT FIGURE 2.34 HERE]

Figure 2.34: The global mean energy budget. Numbers state magnitudes of the individual energy flows in W m^{-2}, adjusted within their uncertainty ranges to close the energy budgets. Numbers in parentheses attached to the radiative fluxes cover the range of values in line with observational constraints.

The estimate for the reflected solar radiation at the TOA in Figure 2.34, 100 W m^{-2}, is a rounded value based on the CERES Energy Balanced and filled (EBAF) satellite data product (Loeb et al., 2009; Loeb et al., 2011) for the period 2001–2010. This data set adjusts the solar and thermal TOA fluxes within their range of uncertainty to be consistent with independent estimates of the global heating rate. This leaves 240 W m^{-2} of solar radiation absorbed by the globe, which is nearly balanced by thermal emission to space of about 239 W m^{-2} (based on CERES EBAF), considering a global heat storage of 0.6 W m^{-2} (residual term in Figure 2.34) (Loeb et al., 2011). The stated uncertainty in the solar reflected TOA fluxes from CERES due to uncertainty in absolute calibration alone is ~2% (2-sigma), or equivalently 2 W m^{-2} (Loeb et al., 2009). The uncertainty of the outgoing thermal flux at the TOA as measured by CERES (derived from the total channel at night and the difference between the total and shortwave channels during daytime) due to calibration is ~3.7 W m^{-2} (2-sigma). In addition to this, there is uncertainty in unfiltering the radiances, radiance-to-flux conversion, and time-space averaging, which adds up to another 1 W m^{-2} or more (Loeb et al., 2009).

Compared to the radiative energy flows in and out of the climate system at the TOA, which can be directly measured by satellites, the energy distribution *within* the climate system is less well known. Uncertainties in the components of the global mean surface radiation budget are thus generally larger and less well quantified than at the TOA. Since AR4, new estimates for the downward thermal radiation emerged, based on active space-born measurements which newly incorporate radar/lidar-derived cloud profiles and associated cloud-base heights, critical for an accurate determination of the downward thermal radiation (Kato et al., 2011

CloudSat-, and MODIS-derived cloud and aerosol properties; L'Ecuyer et al., 2008; Stephens et al., submitted-a). In line with earlier studies based on direct surface radiation measurements (Wild et al., 2001; Wild et al., 1998) these estimates suggest higher values of global mean downward thermal radiation than presented in previous IPCC assessments and typically found in climate models, on the order of 345 W m^{-2}, with an uncertainty of ±10 W m^{-2} (Figure 2.34).

Estimates of absorbed solar radiation at the Earth surface are still afflicted with considerable uncertainty. Global mean estimates derived from satellite retrievals, reanalyses and climate models range from below 160 W m^{-2} to above 170 W m^{-2}. Comparisons of models with surface observations as well as updated spectroscopic parameters and continuum absorption for water vapor favour values towards the lower bound of the range, near 160 W m^{-2} (Kim and Ramanathan, 2008; Trenberth et al., 2009; Wild, 2008; Wild et al., 1998), while some of the satellite-derived products indicate somewhat higher values (Stephens et al., submitted-b, and references therein).

The latent heat flux estimate, required to be around 90 W m^{-2} to close the surface energy balance in Figure 2.34, is higher than in previous assessments. This higher estimate (88 W m^{-2} as given in Stephens et al., submitted) is in line with the evidence for underestimations in the remote sensing based precipitation estimates (the latent heat flux corresponds to the energy equivalent of evaporation, which globally equals precipitation, and its magnitude is derived from the global precipitation estimates) (Berg et al., 2010; Ellis et al., 2009; Haynes et al., 2009; Stephens et al., submitted-b).

2.5.2 Changes in Top of Atmosphere Radiation Budget

Variations in TSI are discussed in Chapter 8, Section 8.2.1. The AR4 reported that large changes in tropical TOA radiation occurred between the 1980s and1990s. The results were based upon observations from the Earth Radiation Budget Experiment (ERBE, Barkstrom, 1984) Earth Radiation Budget Satellite (ERBS) Nonscanner Wide Field of View (WFOV) instrument (Wong et al., 2006). Net TOA radiation (the net radiation absorbed by the climate system) increased by 1.4 W m^{-2}, reflected solar radiation decreased by 2.1 W m^{-2} and emitted thermal radiation increased by 0.7 W m^{-2} over the period 1985–1998. Since the AR4, Andronova et al. (2009) extended the Wong et al. (2006) ERBS/WFOV record with observations from the Clouds and the Earth's Radiant Energy System (CERES) (Wielicki et al., 1996) on the Terra satellite. The longer record shows a continuation of these trends with tropical net TOA flux increasing by 2 W m^{-2} between 1985 and 2005 (Figure 2.35). By comparison, when thermal data based upon HIRS and ISCCP-FD are used in place of the ERBS/CERES thermal record, the net radiation increase is more pronounced, reaching 6 W m^{-2} for ISCCP-FD. ERBE and CERES employ broadband measurements that span most of the full SW and LW spectrum. The HIRS and ISCCP-FD estimates employ measurements with much more limited spectral coverage. The change in net radiation for ERBS/CERES is associated with a 3 W m^{-2} decrease in reflected solar radiation and an increase of 1 W m^{-2} in thermal emission. Comparisons between ERBS/CERES thermal radiation and that derived from the NOAA High Resolution Infrared Radiation Sounder (HIRS) Lee et al. (2004; 2007) show good agreement until approximately 1998, corroborating the reported rise of 0.7 W m^{-2}, after which HIRS thermal fluxes show much higher values. The discrepancy is likely due to changes in the channels used for HIRS/3 instruments launched after October 1998 compared to earlier HIRS instruments (Lee et al., 2007). While the underlying causes for the large decadal changes in tropical radiation remain uncertain, several studies have suggested links to decadal changes in atmospheric circulation (Allan and Slingo, 2002; Chen et al., 2002; Clement and Soden, 2005; Merrifield, 2011).

[INSERT FIGURE 2.35 HERE]

Figure 2.35: Comparison of net TOA flux and upper ocean heating rates. (a) Global annual average net TOA flux from CERES observations (based upon the EBAFTOA_ Ed2.6 product) and (b) ERA Interim reanalysis are anchored to an estimate of Earth's heating rate for 2006–2010. The Pacific Marine Environmental Laboratory/Jet Propulsion Laboratory/Joint Institute for Marine and Atmospheric Research (PMEL/JPL/JIMAR) ocean heating rate estimates (a) use data from Argo and World Ocean Database 2009; The gray bar (b) corresponds to one standard deviation about the 2001–2010 average net TOA flux of 15 CMIP3 models. From Loeb et al. (2011).

The extended records of reflected solar radiation from CERES covering the period 2001–2010 suggest that globally, the planetary albedo has been rather stable over the first decade of the 21th Century (Loeb et al., 2011).

On a global annual scale, interannual variations in net TOA radiation and ocean heating rate should be correlated, since oceans have a much larger heat capacity compared to land and the atmosphere and therefore serve as the main reservoir for heat added to the Earth-atmosphere system. Wong et al. (2006) showed that these two data sources are in good agreement for 1992–2003. In the ensuing 5 years, however, Trenberth and Fasullo (2010) note that the two diverge from one another. The satellite observations show an increase of about 1 W m^{-2} in the rate of absorbed net radiation at the TOA while the ocean in-situ measurements show a slowing of the increase in global ocean heat content. Loeb et al. (2011) show that the apparent decline in ocean heating rate is not statistically robust. Differences in variations in ocean heating rate and satellite net TOA flux are well within the uncertainty of the measurements. The variability in Earth's energy imbalance, relating to El Niño-Southern Oscillation (ENSO), is found to be consistent within uncertainties among the satellite measurements, a reanalysis model simulation and a new analysis of the ocean heat content records (Johnson et al., 2011) (Figure 2.35).

2.5.3 Changes in Surface Radiation Budget

2.5.3.1 Surface Solar Radiation

Changes in radiative fluxes at the surface can be traced further back in time than the satellite-based TOA fluxes, however not on a global scale but only at selected locations where long term records exist. Monitoring of radiative fluxes from surface stations began on a widespread basis in the mid-20th Century, predominantly measuring the downwelling solar component (also known as global radiation or surface solar radiation, hereafter referred to as SSR). However, the quality of these historic measurements is variable and not always well established. In view of the necessity for a reference network of surface radiation measurements with improved and defined accuracy, the Baseline Surface Radiation Network (BSRN) has been established in the early 1990s under the auspices of the World Climate Research Programme (WCRP) (Ohmura et al., 1998).

Various processes have the potential to alter SSR the Earth surface, such as changes in cloud characteristics, aerosol and water vapour. First indications for substantial decadal variations in the observational SSR records were reported in AR4. Specifically, a decline of surface solar radiation from the beginning of widespread measurements in the 1950s until the mid-1980s has been observed at many land-based sites (popularly known as "global dimming", Liepert, 2002; Stanhill and Cohen, 2001), and a partial recovery from the 1980s onward ("brightening", Wild et al., 2005) (cf. the long term SSR record of Potsdam in Figure 2.36 as an illustrative example).

Since AR4, numerous studies substantiated the findings of significant decadal SSR changes observed both at globally distributed sites (e.g., Dutton et al., 2006; Gilgen et al., 2009; Ohmura, 2009; Wild, 2009 and references therein) as well as in specific regions. Wild et al. (2008) estimated the SSR brightening over land surfaces at 2 W m^{-2} per decade for the period 1986–2000. In Europe, Norris and Wild (2007) noted a dimming from 1971 until the mid-1980s of 3.1 W m^{-2} per decade and subsequent brightening of 1.4 W m^{-2} per decade in a pan-European time series consisting of 75 sites. Similar tendencies were found at sites in Northern Europe (Stjern et al., 2009), Estonia (Russak, 2009) and Moscow (Abakumova et al., 2008). Chiacchio and Wild (2010) pointed out that dimming and subsequent brightening in Europe are mainly seen in spring and summer seasons. Brightening in Europe from the 1980s onward was further documented at sites in Switzerland and Germany (Ruckstuhl et al., 2008), as well as in Greece (Thessaloniki) (Zerefos et al., 2009). At continental US sites, Long et al. (2009) noted a significant brightening of SSR as well, of 8 W m^{-2} per decade between 1995 and 2007, and Riihimaki et al. (2009) found brightening at sites in Oregon over the extended period 1980–2007. The general pattern of dimming until the 1980s and brightening thereafter was also found at numerous sites in Japan (Norris and Wild, 2009; Ohmura, 2009; Wild et al., 2005). Analyses of observations from sites in China confirmed strong declines in SSR from the 1960s to 1980s on the order of 3–7 W m^{-2} per decade, which also did not persist in the 1990s (Che et al., 2005; Liang and Xia, 2005; Norris and Wild, 2009; Qian et al., 2006; Shi et al., 2008; Xia, 2010a). Dimming and subsequent brightening were not only found at sites on the Northern Hemisphere, but also in New Zealand (Liley, 2009). On the other hand, persistent dimming since the mid-20th Century with no evidence for a trend reversal was noted at sites in India (Kumari and Goswami, 2010; Kumari et al., 2007; Wild et al., 2005), and in the Canadian Prairie (Cutforth and Judiesch, 2007).

The longest observational SSR records, extending back to the 1920s and 1930s at a few sites in Europe, further indicate some brightening during the first half of the 20th Century, known as "early brightening" (cf. Figure 2.36) (Ohmura, 2009; Wild, 2009). This suggests that the decline in SSR, at least in Europe, was confined to a period between the 1950s and 1980s.

Updates on SSR changes observed at the Earth surface beyond the year 2000 suggest a continuation of the brightening at sites in Europe, U.S., and parts of Asia. Brightening seems to level off at sites in Japan and Antarctica after 2000, while indications for a renewed dimming are seen in China (Wild et al., 2009).

Alpert et al. (2005) and Alpert and Kishcha (2008) pointed out that the observed decline in surface solar radiation between 1960 and 1990 is larger in areas with dense population than in rural areas. The magnitude of this "urbanization effect" in the radiation data is not yet well quantified. Dimming and brightening is, however, also notable at remote and rural sites (Dutton et al., 2006; Karnieli et al., 2009; Liley, 2009; Russak, 2009; Wild, 2009).

While extended areas of the globe are not covered by surface measurements, satellite-derived fluxes can provide a near global picture. Such estimates are available since the early 1980s (Hatzianastassiou et al., 2005; Hinkelman et al., 2009; Pinker et al., 2005). Satellites do not directly measure the surface fluxes, but have to infer them from measurable top-of-atmosphere signals using empirical or physical models to remove atmospheric perturbations. Satellite-inferred SSR records may suffer from potential inhomogeneities due to changes in satellites, viewing geometries, inaccurate positioning, or sensor degradation, particularly in the earlier records (Evan et al., 2007). Available satellite-derived products qualitatively agree on a brightening from the mid-1980s to 2000 averaged globally as well as over oceans, on the order of 2–3 W m^{-2} per decade (Hatzianastassiou et al., 2005; Hinkelman et al., 2009; Pinker et al., 2005). Averaged over land, however, trends are positive or negative depending on the respective satellite product (Wild, 2009). Knowledge on the spatiotemporal variation of aerosol burdens and optical properties, which is required in satellite retrievals of SSR and considered relevant for dimming/brightening particularly over land, is very limited.

Reconstructions of SSR changes from more widely measured meteorological variables can help to increase their spatial and temporal coverage. Decadal SSR changes have been related to observed changes in sunshine duration, diurnal temperature range (DTR), and pan evaporation. Overall, these proxies provide independent evidence for the existence of large-scale decadal variations in SSR. Specifically, the dimming of SSR from the 1950s to the 1980s obtained additional support from widespread observations of concurrent declines in pan evaporation (Roderick and Farquhar, 2002) and DTR (Wild et al., 2007). The trend reversal of DTR observed over global land surfaces during the 1980s is in line with the transition from dimming to brightening (Wild et al., 2007). Over Europe, the dimming of SSR from the 1950s to the 1980s and brightening thereafter is consistent with concurrent declines and subsequent increases in sunshine duration (Sanchez-Lorenzo et al., 2008a), evaporation in energy limited environments (Teuling et al., 2009) and DTR (Makowski et al., 2009). The early brightening in the 1930s and 1940s seen in a few European radiation records is in line with corresponding changes in DTR and sunshine duration (Makowski et al., 2009; Sanchez-Lorenzo et al., 2008a). In China, the levelling off in SSR in the 1990s after decades of decline coincides with similar tendencies in the pan evaporation records, sunshine duration and DTR (Ding et al., 2007; Liu et al., 2004a; Liu et al., 2004b; Qian et al., 2006). Dimming up to the 1980s and brightening in the 1990s is also indicated in a set of 237 sunshine duration records in South America (Raichijk, 2011).

[INSERT FIGURE 2.36 HERE]

Figure 2.36: Annual mean surface solar radiation (in W m^{-2}) as observed at Potsdam, Germany, from 1937 to 2010. Five year moving average in blue. Extended phases of declines (1950s–1980s, "dimming") and increases (since 1980s, "brightening) can be seen, a characteristics found in many of the long term solar radiation records. There are also indications for an increase before the 1950s ("early brightening"). Updated from Wild (2009) and Ohmura (2009).

2.5.3.2 Surface Thermal Exchanges and Net Radiation

Long-term measurements of the thermal surface components as well as surface net radiation are available at much fewer sites than SSR. Downward thermal radiation observations started to become available during the early 1990s with the setup of the Baseline Surface Radiation Network (BSRN, Ohmura et al., 1998) at a limited number of sites. From these records, Wild et al. (2008) determined an overall increase of 2.6 W m^{-2}

per decade over the 1990s, in line with model projections and the expectations of an increasing greenhouse effect. Wang and Liang (2009) inferred an increase in downward thermal radiation of 2.2 W m^{-2} per decade over the period 1973–2008 from observations of temperature, humidity and cloud fraction at 3200 sites. Prata (2008) estimated a slightly lower increase of 1.7 W m^{-2} per decade for clear sky conditions over the earlier period 1964–1990, based on radiative transfer calculations using observed temperature and humidity profiles from radiosondes. Philipona et al. (2009; 2004) measured increasing downward thermal fluxes since the mid-1990s at eight stations in the Swiss Alps, corroborating an increasing greenhouse effect. The changes in the upward thermal radiation emitted by the Earth surface closely follow the changes in the surface temperature according to the Stefan-Boltzmann law (see Section 2.2). In addition, changes in soil moisture and vegetation will change the surface emissivity and hence the surface emitted thermal radiation.

Little is known about decadal changes in the surface net radiation, in large part because measurements of upwelling fluxes at the surface are made at only a few sites, and are hardly spatially representative over land. Wild et al. (2008; 2004) inferred a decline in the land surface net radiation on the order of 2 W m^{-2} per decade from the 1960s to the 1980s, and an increase at similar rate from the 1980s to 2000, respectively, based on estimated changes of the individual surface radiative components.

2.5.3.3 Relation to Observed Changes in Aerosol, Humidity and Clouds

The observed decadal variations in SSR cannot be explained by changes in the luminosity of the Sun, which are an order of magnitude smaller (Willson and Mordvinov, 2003). They therefore have to originate from alterations in the transparency of the atmosphere, which depends on the presence of clouds, aerosols, and radiatively active gases (Kim and Ramanathan, 2008; Kvalevag and Myhre, 2007). Cloud cover changes effectively modulate SSR on an interannual basis, but their contribution to the detected longer-term SSR trends is not always obvious. While cloud cover changes were found to explain the trends in some areas (e.g., Liley, 2009), this is not the case particularly in relatively polluted regions such as Europe and China (Norris and Wild, 2007, 2009; Qian et al., 2006; Wild, 2009). SSR dimming and brightening has also been observed under cloudless atmospheres at various locations, pointing to a prominent role of atmospheric aerosols (Norris and Wild, 2007, 2009; Ohvril et al., 2009; Russak, 2009; Wang et al., 2009a; Wild, 2009; Wild et al., 2005; Zerefos et al., 2009).

Aerosols can directly attenuate SSR by scattering and absorbing solar radiation (direct effect), or indirectly, through their ability to act as Cloud Condensation Nuclei (CCNs), thereby increasing cloud reflectivity and lifetime (first and second indirect effects) (Lohmann and Feichter, 2005; Ramanathan et al., 2001). The trend reversal from SSR dimming to brightening in the 1980s is reconcilable with trends in aerosol emission and aerosol optical depth, which also indicate a distinct reversal during the 1980s (Cermak et al., 2010; Mishchenko et al., 2007; Ohvril et al., 2009; Stern, 2006; Streets et al., 2006; Streets et al., 2009; Wild et al., 2005). However, direct aerosol effects alone may not be able to account for the full extent of the observed SSR changes, while indirect effects have not yet been well quantified.

Observed changes in atmospheric water vapour and other radiatively active gases are considered to be major contributors to the observed increases in downwelling thermal radiation (Allan, 2009; Philipona et al., 2009; Prata, 2008; Stephens et al., submitted-a).

2.5.3.4 Relation to the Hydrological Cycle

The Earth radiation balance is the key driver of the global hydrological cycle (Ramanathan et al., 2001; Stephens et al., submitted-b; Wild and Liepert, 2010). Global precipitation is constrained by the atmospheric and surface radiative energy balance to rise at around 2–3%/K (Allen and Ingram, 2002). Increased atmospheric moisture with warming (Willett et al., 2008) has been shown, using reanalyses and observationally-based methods, to enhance the LW radiative emission of the atmosphere to the surface (Allan, 2009; Philipona et al., 2009; Prata, 2008; Wang and Liang, 2009; Wild et al., 2008). The rises in atmospheric radiative emission with warming over interannual time-scales (John et al., 2009) are predominantly controlled by changes in the clear-sky atmosphere (Allan, 2009) and are consistent with enhanced precipitation with warming as part of radiative convective balance (Lambert and Webb, 2008; Stephens and Ellis, 2008). Links between global precipitation over land and the surface radiation balance are demonstrated by Wild et al. (2008) who argue that decreases in aerosol, also detected by satellite

measurements at the global scale (Mishchenko et al., 2007), and enhanced surface shortwave radiation provide the causal link. While scattering aerosol may influence global precipitation indirectly through surface temperature dependent responses, absorbing aerosols have the potential to directly influence changes in clouds and precipitation through radiative/convective adjustment (Andrews et al., 2009). Liepert and Previdi (2009) argue that large observed increases in global precipitation and ocean evaporation (Wentz et al., 2007) with warming of around 7% K^{-1} over the period 1987–2006 require an increase in net atmospheric radiative cooling of 0.7 W m^{-2} per decade to balance the global energy balance. While some evidence suggests enhanced radiative cooling to space over this period (Section 2.5.2.2; Wong et al., 2006; Zhang et al., 2007b) and a reversal of the weakening of the Walker circulation strength (Merrifield, 2011; Sohn and Park, 2010) statistical uncertainty is substantial and currently precludes definitive connection between these decadal changes.

2.5.4 Summary

The quantification of the global mean energy balance as presented in earlier assessments requires substantial revision. This revision includes updates in the magnitudes of a number of components, particularly the surface energy fluxes, as well as the attribution of uncertainty estimates, which were lacking in prior assessments.

Since the AR4, the satellite records of TOA radiation fluxes could be substantially expanded, and indicate a continuation of the decadal variations in the tropical radiation budget. Globally, no significant changes were measured in the planetary albedo since the turn of the millennium. The variability in the Earth's energy imbalance, relating to El Niño-Southern Oscillation (ENSO), is consistent with a new analysis of the ocean heat content records.

At the surface, since AR4 the evidence for widespread decadal changes in surface solar radiation has been substantiated. These changes are in line with observed changes in a variety of other related variables, such as sunshine duration, diurnal temperature range and hydrological quantities. There are also indications for increasing downward thermal and surface net radiation in recent decades.

2.6 Changes in Atmospheric Circulation and Patterns of Variability

Climatic changes at any given location depend not only on changes in the radiative forcing or local changes such as changes in land use, but also on changes in atmospheric circulation which themselves may in part be radiatively driven. Changes in atmospheric circulation and patterns of variability were assessed in AR4 (2007). Substantial multi-decadal variability was found in the large-scale atmospheric circulation over the Atlantic and the Pacific. A decrease was found in tropospheric geopotential height (GPH) over high latitudes of both hemispheres and an increase over the mid-latitudes in boreal winter for the period 1979–2001. These changes were found to be associated with an intensification and poleward displacement of Atlantic and southern polar front jet streams and enhanced storm track activity in the NH from the 1960s to at least the 1990s. Changes in the North Atlantic Oscillation (NAO) and the Southern Annular Mode (SAM) towards their positive phases were observed, but it was noted that the NAO returned to its long term mean state in the early 2000s. The new data sets and the longer time periods now better support the poleward motion of circulation features since the 1970s. At the same time, large decadal-to-multidecadal variability in atmospheric circulation is found.

In AR4, many studies based on reanalysis data were assessed. Since AR4, reanalyses have gained even more weight in the scientific literature (see Box 2.2). Also, more and improved observational data sets have been published (encompassing ground based, radiosonde, and space-borne data sets), and inaccuracies in all data sets are better understood. Finally, the time elapsed since AR4 extends the period for trend calculation, in particular since several data sets start only in (or are considered most reliable only after) 1979, when satellite information was included in many reanalyses data sets.

This section assesses observational evidence for changes in atmospheric circulation in fields of sea level pressure (SLP), GPH, and wind, in circulation features (such as the Hadley circulation or the jet streams), as well as in circulation variability modes. Monsoons are assessed in Chapter 14.

2.6.1 Sea Level Pressure

The spatial distribution of SLP represents the distribution of atmospheric mass, which is the surface imprint of the atmospheric circulation. Barometric measurements are made in weather stations or onboard ships, fields are produced from the observations by interpolation or using data assimilation. One of the most widely used observational data sets is HadSLP2 (Allan and Ansell, 2006), which integrates 2228 historical global terrestrial stations with marine observations from the International Comprehensive Ocean-Atmosphere Data Set (ICOADS) on a 5° x 5°grid. Although the quality of SLP data is generally considered good, there are discrepancies between gridded SLP data sets, in particular away from observations sites, e.g., over Antarctica (Jones and Lister, 2007).

AR4 concluded that DJF sea level pressure decreased between 1948 and 2005 in the Arctic, Antarctic and North Pacific. More recent studies using updated data for the period 1949–2009 (Gillett and Stott, 2009) also find decreases in SLP in the high latitudes of both hemispheres in all seasons and increasing SLP in the tropics and subtropics most of the year. Vecchi et al. (2006) found a weakening of the annual mean equatorial Pacific zonal SLP gradient based on marine data over the period 1861–1992. An increase in SLP over the Indian Ocean was found by Copsey et al. (2006) in two data sets over the period 1950–1996. However, trends strongly depend on the time period.

Prominent changes in strength and position are found for semi-permanent pressure centres on decadal time scales (Figure 2.37, top). The Azores high and the Icelandic low, as captured by the high and low SLP contours, were small (weak) in the 1960s, large (strong) in the 1980s, and again smaller (weaker) in the most recent decade. The weakening of the Icelandic low since the late 1980s has culminated in extremely high SLP averages in the winters 2009/2010 (Osborn, 2011) and 2010/2011 (see also Section 2.6.6). Favre and Gershunov (2006) find an eastward shift and intensification of the Aleutian low from the mid-1970s to 2001, which persisted during the 2000s (Figure 2.37). The Siberian High is strengthening again after decades of weakening (Panagiotopoulos et al., 2005), although trend magnitudes are data set dependent (Huang et al., 2010). The Western Pacific subtropical high has extended westward from 1980 to 1999 (Zhou et al., 2009).

[INSERT FIGURE 2.37 HERE]

Figure 2.37: Decadal averages for the 1960s, 1980s and 2000s of SLP (top) and 100 hPa GPH (bottom) for November to March (left) and May to October (right) shown by two selected contour lines. Each line represents a data set (listed in Box 2.3, Table 1, plus HadSLP2 for SLP; CFSR was only available up to 2009 and is not shown for the last period), the number of data sets is indicated with the coloured numbers. Topography above 2 km asl (as depicted in the Twentieth Century Reanalysis) is shaded in dark grey for the case of SLP.

On interannual time scales, variations in SLP have specific spatial characteristics known as “modes”. Trends in the indices that capture the strength of these modes are reported in Section 2.6.9.

2.6.2 Surface Winds

Surface wind is measured in-situ with anemometers or from space using the microwave band. Marine wind observations have been extracted from ship logbooks and are collected in ICOADS (currently version 2.5; Woodruff et al., 2011). Early observations were made using the Beaufort scale. Anemometer measurements were introduced starting in the 1950s. Growth in ship size is thought to be responsible for an upward trend in the (largely unreported) anemometer measurement heights and to cause a spurious increasing trend in wind speed estimates based on ICOADS data (Cardone et al., 1990; Gulev et al., 2007; Tokinaga and Xie, 2011a). This trend, being non-uniform in space and time because of varying proportion and unknown characteristics of anemometer measurements, has hindered most of research efforts to study long-term variability in winds from observations. For this reason, wind trends were assessed in AR4 mostly in the context of wave height observations, which showed increasing trends from 1950-2002 in most of the northern extratropics and decreasing trends in the western Pacific and tropical Atlantic.

New data sets are now available, however. Surface winds can be measured from space. While quality scatterometer-based satellite observations of marine surface winds only span a decade, recent efforts on homogenization of available SSM/I observations from satellites produced a wind data set that starts in July 1987 (Wentz et al., 2007). On the basis of this data set, high-resolution (0.25°) six-hourly wind products were developed that extend over more than two decades: Blended Sea Winds (Zhang et al., 2006) and Cross-

Calibrated Multi-Platform wind product (CCMP, Atlas et al., 2011). Tokinaga and Xie (2011a) attempted to correct biases in the ICOADS wind speed by using ICOADS surface wave information. Their product, covering the period 1950–2008, is called WASWind data set and consists of 4^{o} degree binned summaries of corrected ICOADS observations. A wind data set has also been constructued based on altimeter data of wave height back to 1991 (Young et al., 2011). Many of these data sets are newm and their accuracy is a subject of continued investigation.

Figure 2.38 shows linear trends in surface wind speeds over the oceans estimated from products based on the SSM/I wind data (Wentz et al., 2007): Blended Sea Winds and CCMP. The trend pattern is largely consistent with the corresponding trend in 20CR and with the WASWind product as well (the latter represents a major improvement compared with uncorrected ICOADS summaries, cf. Wentz et al. (2007), Tokinaga and Xie (2011a)). Decreasing wind speeds are found over certain areas in the North Atlantic, tropical and North Pacific, and increasing winds south of 40°S, over the central tropical Pacific, and over the Bering Sea (see alsoYoung et al., 2011).

Satellite products cover only the oceans. Over land, surface winds have been measured with anemometers on a global scale for a few decades, but until recently the data have been rarely used for trend analysis due to suspect quality. Century-long, homogenized instrumental records are rare (e.g., Usbeck et al., 2010). Winds near the surface can be derived from reanalysis products (see Box 2.3), but discrepancies are found when comparing trends therein with trends on land stations (McVicar et al., 2008; Smits et al., 2005).

Over land, a weakening of seasonal and annual as well as maximum winds is reported for many regions, including China (Guo et al., 2010; Xu et al., 2006b) and the Tibetan region (Zhang et al., 2007c) from the 1960s to the early 2000s, the Netherlands from 1962 to 2002 (Smits et al., 2005), much of the USA from 1973 to 2005 (Pryor et al., 2007), Australia from 1975 to 2006 (McVicar et al., 2008), and southern and western Canada from 1953 to 2006 (Wan et al., 2010). Increasing wind speeds were found at high latitudes in both hemispheres, namely in Alaska from 1921 to 2001 (Lynch et al., 2004), in parts of the Canadian Arctic from 1953 to 2006, and in Antarctica over the second half of the 20th Century (Turner et al., 2005).

Vautard et al. (2010) analysed a global land surface wind data sets from 1979 to 2008 after quality screening. They found decreasing trends on the order of –0.1 m/s per decade (termed “atmospheric stilling”), over large portions of Northern Hemispheric land areas which they could not find in geostrophic wind calculated from SLP fields and which they ascribed to an increased surface roughness.

[INSERT FIGURE 2.38 HERE]

Figure 2.38: Surface 10m windspeed trends for the period July 1986 to August 2006. a) Blended Sea Winds (Zhang et al., 2006), b) CCMP (Atlas et al., 2011), c) 20th Century Reanalysis (Compo et al., 2011), and d) WASWind (Tokinaga and Xie, 2011a).

2.6.3 Upper-Air Winds

In contrast to surface winds, which were discussed in previous assessment reports, upper level winds got little attention. Radiosondes and pilot balloon observations are available on a global scale from around the 1930s onwards (Stickler et al., 2010). While radiosonde wind records contain temporal inhomogeneities, they are far less common than those in temperature records (Gruber and Haimberger, 2008), at least from about 1960 onwards.

In the past few years, interest in an accurate depiction of upper air winds has grown since they are essential for estimating the state and changes of the general atmospheric circulation and for explaining changes in the surface winds (Vautard et al., 2010). In contrast to the wind stilling at the surface, no or much weaker trends were found for lower tropospheric winds from balloon data or reanalyses. Allen and Sherwood (2008) diagnosed significantly increasing vertical wind shear of up to 1 m/s per decade in the subtropics for the period 1979–2005, which has implications for upper tropical tropospheric temperature trends (see Section 2.2.5.6). At the tropopause, Wilcox et al. (2011) find increasing westerly winds over the Antarctic and decreasing westerly winds over the Arctic from 1989 to 2007. The recent weakening of surface wind speeds

over China is also found in the lower troposphere in radiosonde data and reanaylses (Jiang et al., 2010). However, systematic trend analyses of radiosonde winds are lacking.

Trends in upper-air winds in the extratropics from reanalysis data sets are studied mostly in the context of trends in the jet streams and storms. These studies are discussed in Sections 2.6.6 and 2.7, respectively.

2.6.4 Tropospheric Geopotential Height and Tropopause

Changes in GPH, which can be addressed using radiosonde data or reanalysis data, are an integral picture of SLP and temperature changes in the atmospheric levels below. At the same time the spatial gradients of the trend reflect changes in the upper-level circulation. AR4 concluded that over the NH between 1960 and 2000, boreal winter and annual means of tropospheric GPH decreased over high latitudes and increased over the mid-latitudes. Updated trends for 500 hPa GPH from 1979 to 2010 show that all statistically significant GPH trends are positive except at southern high latitudes in November to April, which is also found in radiosonde data. The high-latitude trends indicate changes in the polar vortices. Neff et al. (2008), analysing radiosonde data over the period 1957–2007, find asymmetric 500 hPa GPH trends over Antarctica, with falling GPH at East Antarctic stations in December-May, rising GPH over West Antarctica in May-December, and increasing GPH at the South Pole in all months. Over the Arctic (60°–90°N) from 1979 to 2003, tropospheric GPHs from radiosonde data decreased in winter and increased in fall (Forster et al., 2011 Chapter 4 in Scientific Assessment of Ozone Depletion: 2010). Angell (2006) found similar trends in NNR from 1963 to 2001.

Changes in the tropopause affect trace gas transport, chemistry, and radiative processes. Specifically, changes in the minimum temperatures near the tropical tropopause largely control stratospheric humidity (see Fueglistaler et al., 2009). Based on radiosonde data, Randel et al. (2006) found a decrease of tropical tropopause temperatures between the periods 1994–2000 and 2001–2004, which is consistent with changes in tropical upwelling (see Section 2.6.8). Trends in tropopause temperature are generally considered uncertain (Fueglistaler et al., 2009). However, Wilcox et al. (2011), using a new definition of the tropopause, find a decrease in global tropopause temperatures from 1989 to 2007 of 0.18 K per decade and a rising of 47 m per decade (with the Antarctic as the most notable exception). Trends are largest at the latitudes of the subtropical and largest in the eastern hemisphere.

2.6.5 The Tropical Circulation

This section assesses trends and variability in the strength of the Hadley and Walker circulations as well as the width of the tropical belt. Observational evidence is based on radiosonde and reanalyses data. Additionally, the tropical circulation imprints on other fields that are observed from space (e.g., total ozone, outgoing long-wave radiation). Changes in the water cycle also provide constraints for changes in the tropical circulation (Held and Soden, 2006; Schneider et al., 2010). In AR4, the tropical circulation was assessed. Large interannual variability of the Hadley and Walker circulation was highlighted, as well as the difficulty in addressing changes in these features in the light of discrepancies between data sets.

The additional data sets that became available since AR4 confirm this view. The strengths of the northern Hadley circulation and the Pacific Walker circulation in boreal winter (Figure 2.39) show substantial interannual variability, which is largely related to El Niño/Southern Oscillation (see Box 2.4). However, trends are less clear. Two widely used reanalysis data sets — NNR and ERA-40 — both have demonstrated shortcomings with respect to tropical circulation, hence their increases in the Hadley circulation strength since the 1970s might be artificial (Hu et al., 2011; Mitas and Clement, 2005; Song and Zhang, 2007). Additional reanalysis data sets (Bronnimann et al., 2009) as well as satellite humidity data (Sohn and Park, 2010) also suggest a strengthening from the mid 1970s to present, but the magnitude is strongly dataset dependent (Figure 2.39). The confidence in trends in the strength of the Hadley circulation is therefore low.

[INSERT FIGURE 2.39 HERE]

Figure 2.39: The strengths of the Pacific Walker circulation in September to January (top) and of the northern Hadley circulation in December to March (bottom) in different data sets. Monthly values of Hadley and Walker circulation strengths were defined similar as in Oort and Yienger (1996) as the maximum of the meridional mass stream function at 500 hPa between the equator and 40° N and the difference in the vertical velocity between [10°S to 10°N, 180°W to 100°W] and [10°S to 10°N, 100°E to 150°E], respectively. Time series show anomalies from the 1979/1980 to

2001/2002 mean values of each series (dots on the right). Reconstructions are based on historical upper-air and surface observations and extend NCEP/NCAR back in time (updated from Broennimann et al. (2009), and Compo et al. (2011)).

Vecchi et al. (2006) suggest a weakening of the Pacific Walker circulation based on changes of SLP gradients across the Pacific from 1861 to 1992 (see also Table 2.14). Boreal spring and summer contribute most strongly to the trend (Karnauskas et al., 2009). Nicholls (2008), over the period 1958–2007, finds an increasing trend in SLP at Darwin, Australia, in March-September, but not November-February, when the Walker circulation is strongest. Based on the vertical velocity at 500 hPa over the Pacific from reanalysis data sets and reconstructions, Compo et al. (2011) find no evidence for a change in the strength of the Walker circulation in boreal winter over the past century (Figure 2.39). As for the Hadley circulation, there are inconsistencies between ERA-40 and NNR (Chen et al., 2008). Deser et al.(2010a), based on marine air temperature and cloud cover over the Pacific, find a weakening of the Walker circulation during most of the 20th Century to be consistent with observations (see also Yu and Zwiers, 2010). However, since around 1980 the trend has reversed (cf. equatorial SOI linear trends and evolution in Table 2.7 and Box 2.4, Figure 1). Sohn and Park (2010) analysing water vapour flux from satellite and reanalysis data, find a strengthening of the Walker circulation over the period 1979–2006.

Observed changes in several atmospheric parameters suggest that the width of the tropical belt has increased at least since 1979 (Forster et al., 2011 Chapter 4 in Scientific Assessment of Ozone Depletion: 2010; Hu et al., 2011; Seidel et al., 2008). Since the AR4, wind, temperature, radiation, and ozone information from radiosondes, satellites, and reanalyses had been used to diagnose tropical edge latitudes and estimate their trends. Annual mean time series of the tropical belt width from various sources are shown in Figure 2.40.

[INSERT FIGURE 2.40 HERE]

Figure 2.40: Variations in annual mean tropical belt width (top) and tropical edge latitudes in each hemisphere (middle and bottom) during 1979–2009. The tropopause, Hadley cell, and jet stream metrics are based on reanalyses; outgoing longwave radiation and ozone metrics are based on satellite measurements. Adapted and updated from Seidel et al. (2008) using data presented in Davis and Rosenlof (2011). Where multiple datasets are available for a particular metric, all are shown as light solid lines, with shading showing their range and a heavy solid line showing their median.

Since 1979 the region of low column ozone values typical of the tropics has expanded in the NH (Hudson et al., 2006). Based on radiosonde observations and reanalyses, the region of high tropical tropopause has expanded since 1979, and possibly since 1960 (Birner, 2010; Seidel and Randel, 2007), although widening estimates from different reanalyses and using different methodologies show a range of magnitudes (Birner, 2010; Seidel and Randel, 2007). The widening is reflected in poleward motion of tropical 100 hPa GPH contours displayed in Figure 2.37, bottom. Wilcox et al. (2011), for the 1989–2007 period (using ERA-Interim data), find a broadening of the Tropics in the range 0.9–2.2° per decade based on tropopause altitude, zonal mean height, and zonal mean zonal wind.

Several lines of evidence indicate that climate features at the edges of the Hadley cell have also moved poleward since 1979. Subtropical jet metrics from reanalysis zonal winds (Archer and Caldeira, 2008a, 2008b; Strong and Davis, 2007, 2008b) and layer-average satellite temperatures (Fu and Lin, 2011; Fu et al., 2006) also indicate widening, although 1979–2009 wind-based trends (Davis and Rosenlof, 2011) are not statistically significant. Changes in subtropical outgoing longwave radiation, a surrogate for cloudiness, also suggest widening (Hu and Fu, 2007), but the methodology and results are disputed (Davis and Rosenlof, 2011). Precipitation patterns and subtropical high pressure regions also indicate widening (Davis and Rosenlof, 2011; Hu and Fu, 2007; Hu et al., 2011; Kang et al., 2011; Zhou et al., 2011)

The qualitative consistency of these observed changes in independent datasets suggests a widening of the tropical belt between at least 1979 and 2005 (Seidel et al., 2008), and possibly longer. Widening estimates range between around 0° and 3° latitude per decade, and their uncertainties have been only partially explored (Birner, 2010; Davis and Rosenlof, 2011).

2.6.6 Jets, Storm Tracks and Weather Types

2.6.6.1 Midlatitude and Subtropical Jets

Subtropical and midlatitude (eddy-driven) jet streams are three-dimensional entities that vary meridionally and vertically. GPH can be accurately determined from radiosonde measurements, hence wind speed estimates using quasi-geostrophic flow assumptions are considered reliable. However, a high vertical resolution is required for identification of jets. Using reanalysis data sets, it is possible to track 3-dimensional jet variations by identifying a surface of maximum wind (SMW).

Prior to AR4, no global or hemispheric-scale studies of jet stream variability had been conducted; most work was regional or dealt with overall vortex changes or large-scale patterns of trends in GPH. In NH summer, subtropical jets have lowered significantly over most of the tropics and subtropics from 1958 to 2004, particularly in the Eastern Hemisphere (Strong and Davis, 2006). Similar long-term trends in the SMW are not evident in boreal winter, where interannual jet variability is linked to monthly variations in the Arctic Oscillation or ENSO (Strong and Davis, 2008a).

Various analyses (from different reanalysis data sets that both include and exclude data from the pre-satellite era) indicate that the jet streams (midlatitude and subtropical) have been moving poleward in most regions (on both hemispheres) over the last three decades (Archer and Caldeira, 2008b; Fu et al., 2009b; Fu et al., 2006; Strong and Davis, 2007). This is also depicted in Figure 2.40. There is inconsistency with respect to speed trends based upon whether one uses an SMW-based or isobaric-based approach (Archer and Caldeira, 2008a, 2008b; Strong and Davis, 2007, 2008b). In general, eddy-driven jets have become more common (and jet speeds have increased) over Canada, the North Atlantic, and Europe (Barton and Ellis, 2009; Strong and Davis, 2007) — trends that are coupled with regional increases in GPH gradients and circumpolar vortex contraction (Angell, 2006; Frauenfeld and Davis, 2003). From a climate dynamics perspective, these trends are driven by regional patterns of tropospheric and lower stratospheric warming or cooling and thus are coupled to large-scale circulation variability. While jet speed trends are uncertain, it is *likely* that, at least in the NH, the jet core has been contracting towards the pole since the 1970s.

2.6.6.2 Storm Tracks and Frequency of Cyclones

Storm tracks are regions of enhanced synoptic activity due to the passage of cyclones. The main storm tracks stretch across the North Pacific, North Atlantic, and Southern Ocean. They are defined by applying band pass filtering or cyclone tracking to daily or sub-daily SLP data (station data, gridded data, or reanalyses) or to upper level fields from reanalyses. Trends have been shown to be sensitive to the method (Raible et al., 2008).

In AR4 changes in storm tracks were assessed. A poleward shift of the NH storm track was found, however, it was also noted that uncertainties are significant and that NNR and ERA-40 disagree in important aspects. For the North Atlantic, studies based on reanalysis data (Schneidereit et al., 2007), SLP measurements from ships (Chang, 2007) and sea level time series (Vilibic and Sepic, 2010) further support a poleward shift of the cyclone tracks from the 1950s to the early 2000s, with more wintertime high-latitude cyclones (see also Sorteberg and Walsh, 2008) but fewer at mid-latitudes. This is consistent with changes in the NAO to which the Atlantic storm track is associated (Schneidereit et al., 2007). However, storminess derived from SLP station triangles in Europe from the 1870s to 2005 shows large decadal variations (Matulla et al., 2008). Storminess and extreme winds are further discussed in Section 2.7.

Knapp and Soule (2007) find that over the period 1900-2004, summertime major midlatitude cyclones over the Northern Rockies have become less frequent and occur later in the season, due to more frequent mid-tropospheric ridging upstream from the Northern Rockies.

A southward shift of the SH storm track has been reported based on NNR data A decrease in storminess in south eastern Australia based on century plus records of measures derived from SLP is consistent with this shift (Alexander and Power, 2009; Alexander et al., 2011). However, ERA-40 and NNR differ with respect to SH storm tracks (Wang et al., 2006). Fredriksen and Fredriksen (2007) find a reduction in cyclogensis and southward deflection of storms when comparing the period 1975–1994 with 1949–1968.

2.6.6.3 Weather Types and Blocking

Changes in climate are associated with changes in weather. Changes in the frequency of weather types are of interest since weather extremes can be associated to specific weather types. For instance, persistent blocking is held responsible for the 2010 heat wave in Russia (Dole et al., 2011). Synoptic classifications or statistical clustering (Philipp et al., 2007) are used to classify the weather on a given day. Alternatively, feature-based methods have been developed (Croci-Maspoli et al., 2007a). These methods require daily SLP fields or upper-level fields from reanalyses.

In AR4, weather types were not assessed as such, but an increase in blocking frequency in the Western Pacific and a decrease in North Atlantic was noted. Trends in synoptic weather types have been best described for Europe. Comparing synoptic weather classifications for Central Europe for the two 30-year periods 1951–1980 and 1974–2003, Werner et al. (2008) found an increase of anticyclonic weather types in summer and cyclonic weather types in winter. Trnka et al. (2009) also found an increase by more than 80% of the frequency of drought-conducive weather types in central Europe from 1940–2005, with strongest changes during April to June. Applying a statistical clustering approach to daily SLP fields for Europe from 1850 to 2003, Philipp et al. (2007) found trends towards more frequent westerly circulation types and less frequent continental highs in winter, more frequent blocking over Great Britain in spring, and a retreated Azores high in summer. Changes in the frequency of occurrence of circulation types explain a significant amount of low-frequency variability of mean temperature over Europe, whereas low-frequency variability in extreme indices is governed by within-type variability (Jacobeit et al., 2009).

Using a feature-based approach, Croci-Maspoli et al. (2007a) found negative trends of blocking in winter over Greenland and in spring over the North Pacific during the period 1957–2001. Long-lasting blocking is closely associated with circulation modes such as the NAO or the PNA (Croci-Maspoli et al., 2007b), which is discussed in Section 2.6.9 Häkkinen et al. (2011) found a relation between the frequency of wintertime blocking between Greenland and Western Europe and a warmer, more saline subpolar North Atlantic on decadal scales. For the SH, Dong et al. (2008) found a decrease in number but increase in intensity of blocking days over the period 1948 to 1999.

2.6.7 Stratospheric Circulation

The stratosphere is coupled with the troposphere through fluxes of radiation, momentum, and mass. The most relevant characteristics of stratospheric circulation for climate and for trace gas distribution are the winter polar vortices, the Quasi-Biennial Oscillation, and the Brewer-Dobson circulation (BDC). Radiosonde observations, reanalysis data sets, and space-borne trace gas observations are used to address changes in the stratospheric circulation, but all of these sources of information carry large uncertainties.

Contours of the 100 hPa GPH surface (Figure 2.37) reveal zonally non-uniform poleward shifts that reflect both the warming of the troposphere beneath as well as changes in circulation. Changes in the polar vortices have been assessed in AR4 and more recently in the WMO assessment of ozone depletion (Forster et al., 2011 Chapter 4 in Scientific Assessment of Ozone Depletion: 2010). A significant decrease in lower-stratospheric GPH in summer over Antarctica since 1980 or earlier was found in AR4, whereas trends in the Northern Polar vortex were considered uncertain due to its large variability. This assessment was further corroborated in Forster et al. (2011 Chapter 4 in Scientific Assessment of Ozone Depletion: 2010). Cohen et al. (2009) report an increase in number of stratospheric sudden warmings (rapid warmings of the middle stratosphere accompanied by a collapse of the polar vortex and reversal of the flow) during the last two decades. However, interannual variability in the Arctic polar vortex is large and the uncertainties in the data products high (Tegtmeier et al., 2008). Langematz and Kunze (2008) find a strong dependence of stratospheric GPH trends over the Arctic on the time period, while the deepening of the Antarctic vortex was found to be more robust.

The BDC or stratospheric overturning circulation transports air upward in the tropics, poleward in the extratropics, and downward at middle and high latitudes. The BDC is relevant for the transport of trace gases and water vapour and affects their chemical and transport lifetime. However, the BDC is only indirectly observable via wave activity fluxes (which according to the current understanding are a major driver of the BDC), via the distribution of trace gases, or via determination of the “age of air” (i.e., the time an air parcel has resided in the stratosphere after its entry from the troposphere). All of these methods are subject to considerable uncertainties, and they might shed light only on some aspects of the BDC. For instance, wave

activity fluxes can be estimated from reanalysis data (see Box 2.4), however it is not clear whether long term trends are accurate. Randel et al. (2006), using observational data, found a sudden change in lower stratospheric water vapour and ozone around 2001 that is consistent with an increase in the mean tropical upwelling (see also Rosenlof and Reid, 2008). Engel et al. (2009) found no change in the age of air from measurements of chemically inert trace gases from 1975–2005, which however does not rule out trends in the lower stratospheric branch of the BDC (Bonisch et al., 2009).

[START BOX 2.4 HERE]

Box 2.4: Patterns and Indices of Climate Variability

Climate variability is not uniform in space: its major part can be described as a combination of "preferred" spatial patterns. The most prominent of these are known as *modes of climate variability* and impact weather and climate on many spatial and temporal scales. Individual climate modes historically have been identified through spatial *teleconnections*: relationships between regional climate variations at places far removed from each other. Subtracting climate anomalies calculated from meteorological records at stations exhibiting strongest effects of opposite signs (and adding records with the same sign effects), one could get an *index* describing temporal variations of the climate mode in question. By regressing on this index climate records from other places, one derives a spatial *climate pattern* characterizing this mode.

Since gridded fields of climate variables became available, appropriate regional averages or other statistics based on large domains replaced in many cases the use of individual station records for index definitions. On the other hand, indices defined in terms of station records can be re-defined for calculations with gridded fields as well: instead of a station record one can use a timeseries from the gridbox within which the station is located, or to interpolate the gridded field to the precise station location, etc.

While the relationship between the statistical and dynamical modes of climate system is complicated, important modes of climate variability are often responsible for a major part of variance of some climate variable and because of that appear as leading modes in statistical analyses of climate fields, e.g., in the principal component analysis (PCA). Indeed some climate indices are defined to begin with as principal components of a certain climate variable in an appropriately selected region.

Box 2.4, Table 1 lists some prominent modes of large-scale climate variability and indices used for defining them; changes in these indices are associated with large-scale climate variations. With some exceptions, indices included in Table 1 have been (1) used by a variety of authors, (2) are defined relatively simply from raw or statistically analyzed observations of a *single* climate variable, which (3) had a history of *surface* observations, so that for most of these indices at least a century-long record is available for climate research.

[INSERT BOX 2.4, TABLE 1 HERE]

Box 2.4, Table 1: Established indices of climate variability with global or regional influence. Columns are: (1) name of a climate phenomenon, (2) name of the index, (3) index definition, (4) primary references, (5) comments, including when available, characterization of the index or its spatial pattern as a dominant variability mode.

Box 2.4, Figure 1 illustrates climate modes listed in Box 2.4, Table 1 by showing temporal variability of their indices. Most climate modes are illustrated by several indices: they often behave similarly to each other albeit never identically. Spatial patterns of sea surface temperature (SST) or mean sea level pressure (MSLP) associated with these climate modes are illustrated in Box 2.4, Figure 2. These were obtained as regression patterns of SST or MSLP on the standardized index timeseries. (An index with the longest timeseries from those illustrated in Figure 1 was used for this purpose; linear trends were subtracted before regression). Therefore they can be interpreted as a change in the SST or MSLP field associated with one standard deviation (s.d.) change in the index.

[INSERT BOX 2.4, FIGURE 1 HERE]

Box 2.4, Figure 1: Some indices of climate variability, as defined in Table 1. Where "HadISST1", "HadSLP2r", or "20C RA" are indicated, the indices were computed from the SST or MSLP values of the former two data sets or from 500 or 850 hPa geopotential height fields from the 20th Century Reanalysis, version 2. A data set reference given in the title of each panel applies to all indices shown in that panel. "CPC" indicated an index timeseries publicly available

from the NOAA Climate Prediction Center. Where no data set is specified, a publicly available regularly updated version of an index from the authors of a primary reference given in Table 1 was used. (Citations are given in panel legends only when needed for unambiguous identification of a particular index definition from Table 1; their presence or absence does not mean on its own that the index values obtained from the authors were or were not used here). All indices are shown as 12-month running means (r.m.) except when their resolution (e.g., "DJFM" for December-to-March averages) or smoothing level (e.g., 11-year LPF for a low-pass filter with half-power at 11 years) are explicitly indicated.

[INSERT BOX 2.4, FIGURE 2 HERE]

Box 2.4, Figure 2: Spatial patterns of climate modes listed in Table 1. The patterns shown here are obtained by regression of either SST or MSLP fields on the standardized indices climate modes. For each climate mode one of the indices shown in Figure 1 was used. SST and MSLP fields are from HadISST1 and HadSLP2r data sets (interpolated gridded products based on data sets of historical observations). All SST-based patterns are results of monthly regressions for the 1870–2010 period except for the PDO regression pattern, which was computed for 1900–2010. The MSLP-based patterns of NAO and PNA are regression coefficients of the DJFM means; PSA1 and PSA2 patterns are regressions of seasonal means; SAM pattern is from a monthly regression. For each pattern the data was linearly de-trended over the regression interval. All patterns are shown by color plots, except for PSA2, which is shown by white contours over the PSA1 color plot (contour steps are 0.5 hPa, zero contour is skipped, negative values are indicated by dash).

The multiplicity of indices defining each climate phenomenon arises from the multidimensional nature of climate phenomena and often reflects a scientific debate about the nature of this phenomenon. The difficulty of identifying a universally "best" index for any particular climate mode is due to the fact that none of simply defined indicator can achieve a perfect separation of the target phenomenon from all other effects occurring in the climate system. As a result, each index is affected by many climate phenomena whose relative contributions may change with a time period and with a data set used. Limited length and quality of the observational record further compound this problem. Thus the choices of indices are always application-specific.

[END BOX 2.4 HERE]

2.6.8 Changes in Indices of Climate Variability

Indices of climate variability are used to measure the strength of natural modes of climate variability and to summarize large fractions of spatio-temporal variability using a single time series. While it is possible that anthropogenic warming could force systematic changes in index values or in the character of their variability, definite inferences about such occurrences in observational data sets are not easy to make. The records are relatively short, prone to error, and indices are subject to natural multidecadal variability. Moreover, definitions of SST-based indices for "natural" modes of climate variability often explicitly include detrending of the entire record (e.g., Deser et al., 2010b); the trends for subperiods of the record still can be found for such indices. In AR4 patterns of atmospheric circulation variability were assessed in detail. Multidecadal variability was found in patterns referring to Pacific and Atlantic SSTs. The NAO and SAM were found to exhibit increasing trends (strengthened midlatitude westerlies) from the 1960s to 1990s, but the NAO has returned to its long-term mean state since then.

Table 2.14 summarizes observed changes in some well-known indices of climate variability. After returning to its normal state in the last decade, NAO index reached very low values in the winter of 2009/2010 (Osborn, 2011) and was below normal in the winter of 2010/2011 as well. As a result, with the exception of the PC-based NAO index, which still shows the 5%-significant positive trend from 1951 to present, other NAO or NAM indices do not show significant trends of either sign for the periods presented in Table 2.14. In contrast, the SAM has resumed its upward trend that was noted in AR4, peaking in a record high SAM index in austral winter 2010. Fogt et al. (2009) found a positive trend in the SAM index from 1957 to 2005, Visbeck (2009), in a station-based index, found an increase in recent decades (1970s to 2000s). PC-based AAO index presented in Table 2.14 shows growing trends in the last 60 and 110 years with 1% level of significance.

The observed detrended multidecadal SST anomaly averaged over the North Atlantic Ocean area is often called Atlantic Multidecadal Oscillation Index (AMO, see Box 2.4, Table 1) and has significant regional and

hemispheric climate impacts. Warm AMO phases occurred during the late 19th century, in 1925–1965 and since 1995. Cold phases occurred during 1900–1925 and 1965–1995. Because of the transition into the present warm phase, there is a very significant increasing trend since 1979 to present (Table 2.14).

PDO, IPO, and NPI indices also show significant changes (positive for NPI and negative for PDO and IPO) since the 1980s that are consistent with the surface pressure changes discussed in Section 2.6.1. This change, and the teleconnection between the Equator and midlatitudes, is consistent with reverting the trends in the Walker Circulation (Section 2.6.5), which was reported to have slowed down before 1992 (Vecchi et al., 2006), but now seems to have sped up again. Specifically, in the period 1861–1992 the standardized equatorial SOI was decreasing with a linear trend of –0.052 ± 0.027 s.d. per decade and was significant at 0.2% level in a two-sided Student's *t* test (with the reduced by autocorrelation effective sample size, Santer et al., 2008). Since this decrease was reversed after 1990, the trend for the entire period 1861–2010 dropped to –0.028 ± 0.027 s.d. per decade, which is barely significant at 10% level. Since the beginning of the 20th Century, Equatorial SOI does not show significant long term trends, but was growing really fast in the last 20 years (Table 2.14).

Bunge and Clarke (2009) found an increase in the NINO3.4 index since about the 1870s. NINO3.4 computed on the basis of one of the well-established analyses of SST (ERSSTv3b, see Section 2.2.2) shows significant increasing trends in the periods from 1876 to present (0.057 ± 0.033 s.d. per decade with 0.006 p-value, for the standardized index values), while NINO3.4 computed from HadISST1 and COBE SST, other well-established analyzed SST data set, do not show significant trends on multidecadal time scales (trends in these indices after 1901 are shown in Table 2.14). Furthermore, the sign of the trend in east-west SST gradient across the Pacific remains ambiguous as well (Bunge and Clarke, 2009; Deser et al., 2010a; Karnauskas et al., 2009; Vecchi and Soden, 2007) and SST data sets differ with respect to the zonal gradient trends in the tropical equatorial Pacific (Deser et al., 2010a; Karnauskas et al., 2009; Vecchi et al., 2008). Indeed, Power and Smith (2007) found that the period 1977–2006 showed the lowest SOI, the highest recorded value in mean sea-level pressure at Darwin, the weakest equatorial surface wind-stresses and the highest tropical sea-surface temperatures on record. The formal veracity of this statement is supported by visual inspection of Box 2.4, Figure 1, however, the high level of variability obvious in this plot suggest caution in interpreting such observed changes as secular variability.

Table 2.14: Linear trend slopes (standard deviation/decade) for selected indices listed in Box 2.4, Table 1. Except where DJFM averaging is noted, results are for the calendar year averages and are presented with their 5% to 95% confidence intervals. Trend slopes were estimated using ordinary least squares regression; lag-1 autocorrelation coefficient of the trend line residuals was taken into account for uncertainty calculation (Santer et al., 2008). Trend values that are different from zero in the two-sided Student's *t* tests with 5% and 1% significance level are underlined and shown in bold, respectively. Index records where the source is not explicitly indicated were computed from either HadISST1 (for SST-based indices), or HadSLP2r (for MSLP-based indices), or the 20th Century Reanalysis fields of 500hPa or 850hPa geopotential height. CoA stands for "Centers of Action" index definitions. "Present" in the trend periods designates 2008 for the Reanalysis-based indices and 2010 for all other indices. Index standardization period is for 1871–2008 for Reanalysis based indices, 1876–2010 for Troup and Darwin SOIs, 1900-2010 for PDO and NAO indices, and 1870–2010 for all other indices. Standardization was done on DJFM means for NAO and PNA, seasonal anomalies for PSA1,2, and monthly anomalies for all other indices.

Index name	1901-present	1951-present	1979-present
(–1)*SOI Troup, BOM records	0.019 ± 0.039	0.040 ± 0.103	–0.209 ± 0.251
SOI Darwin, BOM records	0.030 ± 0.037	0.095 ± 0.087	–0.100 ± 0.216
(–1)*EQSOI	0.015 ± 0.049	–0.040 ± 0.137	–0.512 ± 0.321
NINO34	0.001 ± 0.043	0.030 ± 0.109	–0.121 ± 0.304
NINO34 (ERSSTv3b)	0.071 ± 0.045	0.070 ± 0.107	–0.046 ± 0.285
NINO34 (COBE SST)	0.029 ± 0.042	0.026 ± 0.111	–0.114 ± 0.320
NINO4	0.033 ± 0.055	0.095 ± 0.149	–0.030 ± 0.414
EMI	–0.051 ± 0.062	–0.096 ± 0.202	–0.046 ± 0.653
TNI	–0.025 ± 0.053	–0.094 ± 0.175	–0.126 ± 0.608
PDO (Mantua et al., 1997)	–0.006 ± 0.072	0.160 ± 0.180	–0.386 ± 0.308
(–1)*NPI	–0.023 ± 0.022	0.025 ± 0.045	–0.143 ± 0.117

AMO revised	–0.035 ± 0.115	–0.066 ± 0.362	0.802 ± 0.305
NAO stations DJFM (Hurrell, 1995a)	–0.010 ± 0.065	0.146 ± 0.159	–0.160 ± 0.409
NAO PC DJFM (Hurrell, 1995a)	0.000 ± 0.063	0.198 ± 0.157	–0.099 ± 0.442
NAM PC-based	–0.070 ± 0.064	0.144 ± 0.153	0.099 ± 0.494
AAO PC-based	0.145 ± 0.038	0.204 ± 0.054	0.159 ± 0.142
PNA DJFM, CoA	0.057 ± 0.056	0.176 ± 0.131	–0.109 ± 0.365
PSA CoA as in Karoly (1989)	–0.059 ± 0.030	–0.124 ± 0.073	–0.263 ± 0.205
(–1)*PSA CoA as in Yuan and Li (2008)	–0.058 ± 0.028	–0.088 ± 0.063	–0.151 ± 0.196
PSA1	–0.010 ± 0.042	0.070 ± 0.100	0.052 ± 0.304
PSA2	0.068 ± 0.032	0.183 ± 0.100	0.321 ± 0.270
ATL3 detrended for 1870–2010	0.037 ± 0.044	0.141 ± 0.092	0.266 ± 0.205
AONM	0.067 ± 0.053	0.154 ± 0.116	0.427 ± 0.241
AMM	0.018 ± 0.059	–0.034 ± 0.159	0.295 ± 0.363
IOBM	0.076 ± 0.054	0.331 ± 0.089	0.243 ± 0.229
DMI detrended for 1870–2010	0.029 ± 0.033	0.068 ± 0.095	0.176 ± 0.236
IODM	–0.017 ± 0.035	–0.042 ± 0.100	–0.104 ± 0.226

In addition to possible changes in the mean values of climate indices, changes in the nature of variability are also possible. In particular, attempts to identify changes in the character of ENSO variability have received much attention but have resulted in limited success. In the recent years, however, there has been a growing appreciation of the multidimensional nature of ENSO phenomenon. Starting from the work of Trenberth and Stepaniak (2001), who proposed to characterize the evolution of ENSO events with the Trans-Niño Index (TNI), which is virtually uncorrelated with the standard ENSO index NINO3.4, other alternative ENSO indices have been introduced and proposals were made for classifying ENSO events according to the indices they primarily maximize. While a traditional, "canonical" El Niño event type is viewed as the "eastern Pacific" type, the alternative indices identify events that have central Pacific maxima and are called dateline El Niño (Larkin and Harrison, 2005), Modoki (Ashok et al., 2007), or Central Pacific El Niño (Kao and Yu, 2009). Distinguishing event types is important, because the influence of the central Pacific SST anomaly on the atmosphere appears to be different from that of the canonical eastern Pacific ENSO SST anomaly (Ashok and Yamagata, 2009; Kim et al., 2009; Weng et al., 2009). However, what classification of ENSO event types would be the most appropriate has not been definitely established. Takahashi et al. (2011) have recently represented many of the old and new ENSO indices as elements in a two-dimensional linear space spanned by two classical ENSO indices that summarize eastern and central Pacific SST anomalies: NINO1+2 and NINO4 (see Box 2.4, Table 1 for index definitions). In effect, this suggests that most ENSO events belong to a continuum, rather than to any two discrete types. (Takahashi et al. (2011) also group ENSO events in a more sophisticated way, by their strength and evolution). While the observational record suggests an increase in frequency and intensity of El Niño events with a central Pacific warm SST anomaly from the mid-20th Century onward (Lee and McPhaden, 2010), this tendency seems not inconsistent with natural variability, based on a statistical simulation (Na et al., 2011) and further observational analysis (McPhaden et al., 2011)

Table 2.14 also lists a positive PNA trend (significant at 5% level) over the last 60 years and negative and positive trends in the first and second PSA modes respectively, throughout the 20th Century. The level of significance of trends in the PSA1 mode clearly depends on the index definition. Robustness of trends in these modes needs futher investigation, with a special attention to their clean separation from their respective annular modes, which are extremely energetic and are known to be affected by multidecadal trends. This issue is particularly important for the PSA which seems to lack a commonly accepted and uniformly used definition for it indices and whose state of the art presentation is through the PC analysis of the Southern Hemisphere upper air variables: second and third PCs are taken as the PSA1 and PSA2 respectively (the first PC is essentially SAM, although it's usually defined using poleward of 20^{o}S domain).

Remaining indices with significant trends in Table 2.14 are tropical Atlantic and Indian Ocean regional modes. The increasing trend in ATL3 and AONM indices that represent Atlantic "Niño" mode is due to the east-intensified warming in the Tropical Atlantic that causes the the weakening of the Atlantic equatorial cold tongue: this trend over the last 60 years has been recently identified and interpreted by Tokinaga and Xie (2011b). The Indian Ocean Basin Mode has a strong 1%-significant warming trend since the middle of the 20th Century. This phenomenon is well-known (Du and Xie, 2008) and its consequences for the regional climate is a subject of active research (Du et al., 2009; Xie et al., 2009).

2.6.9 Synthesis

New and improved data sets are available for addressing changes in the large-scale atmospheric circulation, but large variability on interannual to decadal time scales and remaining differences between data sets precludes robust conclusions on long-term changes in many instances. Some trend features that appeared from the 1950s or earlier to the 1990s (e.g., an increase in the NAO index or a weakening of the Pacific Walker circulation) have reversed in more recent periods. Studies based on ERA-40 (which covers the period 1957–2001) represent a period of an increasing winter NAO index whereas studies addressing the past 20–25 years represent a period with decreasing NAO index.

Several changes could nevertheless be found over the past 30 years. It is *likely* that, in a zonal mean sense, circulation features have moved poleward (widening of the tropical belt, poleward shift of storm tracks and jet streams, contraction of the polar vortex) since the 1970s. These features are consistent with each other but are based on different data sets and approaches. It is *likely* that the SAM has strengthened since the 1950s. Both changes have been described in AR4.

2.7 Changes in Extreme Events

AR4 (Trenberth et al., 2007) highlighted the importance of understanding changes in extreme climatic events given their disproportionate impact on society and ecosystems compared to changes in mean climate (see also WGII AR4). More recently a comprehensive assessment of observed changes in extreme events was undertaken by the IPCC SREX report (Seneviratne et al., 2012). SREX defined extreme weather and climate events as those which occur above (or below) a threshold value near the upper (or lower) ends ("tails") of the range of observed values of a given climate variable. Definitions of thresholds vary, but values with less than a 5% or 1% or even lower chance of occurrence during a specified reference period (generally 1961–1990) are often used. Absolute thresholds often related to physical or biological processes (rather than relative thresholds based on the range of observed values of a variable) can also be used to identify extreme events.

Data availability, quality and consistency are of particular importance for the analysis of extreme events since errors in long-term climate data are likely to show up as "extreme" and some variables are particularly sensitive to changing measurement practices over time. For example, the historical tropical cyclone records are known to be heterogeneous due to changing observing technology and reporting protocols (e.g., Landsea et al., 2004). Further heterogeneity is introduced when records from multiple ocean basins are combined to explore global trends because data quality and reporting protocols vary substantially between regions (Knapp and Kruk, 2010). Similar problems have been discovered when analysing wind extremes because of the sensitivity of measurements to changing instrumentation and observing practice (e.g., Smits et al., 2005; Wan et al., 2010).

The definitions of extremes can be further complicated by the changing nature of the statistical properties of the probability distributions of a given climate variable particularly as might occur under non-stationary climate conditions. Many studies have shown that changes in probability distribution functions associated with changes in variance or skewness can be as or more important than changes in the mean although there is still limited evidence as to whether the climate has become "more extreme" (Seneviratne et al., 2012) with many regional studies indicating that the changes observed in the frequency of extremes can be explained or inferred by shifts in the overall probability distribution of the climate variable (Ballester et al., 2010; Griffiths et al., 2005; Simolo et al., 2011). However, note that these studies refer to counts of threshold exceedance (frequency, duration) which closely follow mean changes. Departures from high percentiles/return periods (intensity, severity, magnitude) are highly sensitive to changes in the shape and scale parameters of the distribution (Clark et al., 2006; Della-Marta et al., 2007a; Della-Marta et al., 2007b;

Fischer and Schar, 2010; Schar et al., 2004) and geographical location. Subsequently, in the following sections we assess the conclusions from both AR4 and SREX and comment on studies subsequent to those assessments.

[START BOX 2.5 HERE]

Box 2.5: Extremes Indices

SREX highlighted that a large amount of the available scientific literature on climate extremes is based on the use of so-called "extreme indices", which can either be based on the probability of occurrence of given quantities or on threshold exceedances. In this sense extreme indices do not represent indices that might be related to extreme events e.g., NINO3 (these are discussed in Section 2.6). Typical indices that are seen in the scientific literature include the number, percentage or fraction of cold/warm days/nights (days with maximum temperature (T_{max}) or minimum temperature (T_{min}) below or above the 10th percentile, or the 90th percentile, generally defined with respect to the 1961–1990 reference time period). Other definitions relate to e.g., the number of days above specific absolute temperature or precipitation thresholds, or more complex definitions related to the length or persistence of climate extremes. Box 2.5, Table 1 lists some of the common definitions for indices that are widely used in the scientific literature and for which near-global datasets exist (generally for the latter half of the twentieth Century). Extreme indices are more generally defined for (daily) temperature and precipitation characteristics, and are rarely applied to other weather and climate variables, such as wind speed, humidity, or physical impacts and phenomena. Some examples are available in the literature for wind-based (Della-Marta et al., 2009) and pressure-based (Beniston, 2009) indices, for health-relevant indices combining temperature and relative humidity characteristics (e.g., Diffenbaugh et al., 2007; Fischer and Schar, 2010) and for a range of dryness indices (e.g., Palmer Drought Severity Index (PDSI) Palmer, 1965; Standardised Precipitation Index (SPI), Standardised Precipitation Evapotranspiration Index (SPEI) Vicente-Serrano et al., 2010a).

Box 2.5, Table 1: Some of the common definitions that are used for extremes indices in the scientific literature.

Index	Commonly-used definitions
Cold days	The coldest daily maximum temperatures in a season/year or the percentage of days below a percentile threshold (usually 10%) or fixed threshold (dependent on region)
Warm days	The warmest daily maximum temperatures in a season/year or the percentage of days above a percentile threshold (usually 90%) or fixed threshold (dependent on region)
Cold nights (including frost)	The coldest daily minimum temperatures in a season/year or the percentage of days below a percentile threshold (usually 10%) or fixed threshold (dependent on region)
Warm nights	The warmest daily minimum temperatures in a season/year or the percentage of days above a percentile threshold (usually 90%) or fixed threshold (dependent on region)
Cold spells	Period of several consecutive low temperature days/nights using a fixed or percentile-based threshold
Warm spells	Period of several consecutive high temperature days/nights using a fixed or percentile-based threshold. Can be classified within just the summer season (heat wave) or can define any unusually warm period at any time of the year
Heavy precipitation	Measure of precipitation falling above a percentile threshold (commonly 95%) or fixed threshold (dependent on region) or can also relate to the contribution to annual total or wet-day precipitation falling from events above given threshold
Dryness	The maximum number of dry days (usually <1mm) in a season/year; Palmer Drought Severity Index (PDSI); Standardised Precipitation Index (SPI); SPEI.

Some advantages of using predefined extreme indices are that they allow some comparability across observational and modelling studies and across regions. Moreover, in the case of observations, derived indices may be easier to obtain than is the case with daily temperature and precipitation data, which are not always distributed by meteorological services. Peterson and Manton (2008) discuss collaborative international efforts to monitor extremes by employing extreme indices. Typically, although not exclusively, extreme indices used in the scientific literature reflect "moderate" extremes, e.g., events occurring as often as

5% or 10% of the time. More extreme "extremes" can be better investigated using Extreme Value Theory (Coles, 2001) and a growing body of literature is exploring its use within the climate sciences (Brown et al., 2008; Zhang et al., 2011a; Zwiers and Kharin, 1998).

While indices may be similarly calculated with similar names, definitions may not be identical and this means that indices calculated by different groups are not always directly comparable (Zhang et al., 2011a). For instance percentile-based temperature indices that include exceedance rates of temperature smaller than the 10th percentile or larger than 90th percentile can be computed based on all available data (Haylock and Goodess, 2004) or using consecutive 5-day moving windows centred on that calendar day from the base period (Klein Tank et al., 2002). The former definition represents long-term changes in the 10th and 90th percentile exceedance and would therefore largely reflect mean winter and summer temperature changes, respectively, at most locations except those at very low latitudes or some coastal regions. The latter approach means, for example, that a location could experience what would be classified as a heat wave in the middle of winter. Note that splitting indices by season can be helpful for both impacts studies and to characterize variations in extremes due to climate dynamics (Kenyon and Hegerl, 2010).

The choice of index may be influenced by the application – an absolute annual index may be most suitable for many impacts applications, whereas relative indices may be best for assessing changes in synoptic situations favourable for extreme temperatures. Hence the term "heat wave" can mean very different things depending on the index formulation for the application for which it is required.

In addition to the complication of defining an index, the way in which indices are calculated to create global averages for example also adds an additional complication to their calculation. For example, the spatial patterns of trends in the hottest day of the year differ slightly between datasets although when globally averaged the trends are similar over the second half of the twentieth Century (see Box 2.5, Figure 1). Further discussion of the parametric and structural uncertainties in datasets is given in Box 2.1.

[**INSERT BOX 2.5, FIGURE 1 HERE**]

Box 2.5, Figure 1: Trends (°C/decade) in the warmest day of the year using different datasets for the periods indicated. The datasets are (a) HadEX (Alexander et al., 2006), (b) HadGHCND (Caesar et al., 2006) using data updated to 2009) and (c) global average timeseries plots (thin solid lines) for each dataset with associated decadal variations (thick solid lines). Also shown is the globally averaged timeseries for HadEX masked to the gridboxes where HadGHCND data are available.

[END BOX 2.5 HERE]

2.7.1 Temperature

AR4 (Trenberth et al., 2007) concluded that it was *very likely* that a large majority of global land areas analysed to date had experienced decreases in cold extremes including frosts and increases in warm extremes since the middle of the 20th Century consistent with warming in global mean temperatures. In addition globally averaged multi-day heat events had *likely* exhibited increases over a similar period. SREX (Seneviratne et al., 2012) updated information from AR4 and came to similar conclusions based on more recently available evidence. Further evidence since then indicates that the level of confidence that the majority of warm and cool extremes show warming remains high particularly for minimum temperature extremes.

A large amount of evidence exists that most global land areas analysed have experienced significant increases in warm nights and significant decreases in cold nights since about 1950 (Seneviratne et al., 2012; Trenberth et al., 2007). Changes in the occurrence of cold and warm days also show warming, but generally less marked except in some regions where the El Niño-Southern Oscillation tends to dominate maximum temperature variability (e.g., Alexander et al., 2009; Kenyon and Hegerl, 2008). Different datasets using different gridding methods and/or input data indicate large coherent trends in temperature extremes globally, associated with warming (Figure 2.41). Over the common period when all datasets have available data, 1951 to 2003, trends (%/decade) in (a) cold nights are –1.139 ± 0.194, –1.287 ± 0.254, –1.121 ± 0.207; (b) cold days are –0.583 ± 0.171, –0.753 ± 0.245, –0.599 ± 0.182, (c) warm nights are 1.339 ± 0.370, 1.620 ± 0.509,

1.241 ± 0.377 and (d) warm days are 0.658 ± 0.336, 0.902 ± 0.572, 0.765 ± 0.445 (HadEX; Alexander et al., 2006), (HadGHCND; Caesar et al., 2006), and (Duke; Morak et al., 2011) respectively.

However it is clear that some differences exist. These differences are most likely due to (i) the different input station data that are used to create each dataset – HadEX and Duke use almost identical input data but different averaging methods (Morak et al., 2011) while HadGHCND uses data solely from the Global Historical Climatology Network-Daily (GHCND) dataset (Durre et al., 2010) and (ii) in one case the indices are calculated from a daily gridded temperature dataset (HadGHCND) while in the other two cases indices are first calculated at the station level and then gridded. Comparison of these three datasets presents a measure of the structural uncertainty that exists when estimating trends in global temperature extremes (see Box 2.1) while still in all cases indicating a robust warming trend over the latter part of the 20th Century.

[**INSERT FIGURE 2.41 HERE**]

Figure 2.41: Maps show observed trends (% per decade) in the frequency of extreme temperatures, over the period 1951 to 2009, for: (a) cool nights (10th percentile), (b) cool days (10th percentile), (c) warm nights (90th percentile) and (d) warm days (90th percentile). Trends were calculated only for grid boxes that had at least 30 years of data during this period. The data source for trend maps is HadGHCND (Caesar et al., 2006). Beside each map are the global annual time series of anomalies with respect to 1961 to 1990 (thin solid lines) along with decadal variations (thick solid lines) for three global datasets: HadEX (Alexander et al., 2006), HadGHCND (Caesar et al., 2006) and Duke (Morak et al., 2011). Trends are significant at the 5% level for all the global indices shown.

A faster increase in T_{min} compared to T_{max} (as indicated by HadEX and Duke datasets), would have lead to a reduction in diurnal temperature range (DTR) since 1951. This is seen in many regions although with a somewhat flatter signature since the mid-1980s, mixed regional variations and questions related to the reliability of data (see Section 2.2.1.3). Changes in both local and global sea surface temperature patterns and large scale circulation patterns have been shown to be associated with regional changes in temperature extremes (e.g., Alexander and Arblaster, 2009; Barrucand et al., 2008) particularly in regions around the Pacific Rim (Kenyon and Hegerl, 2008).

Some regions have experienced close to a doubling (or halving) of the occurrence of warm and cold nights e.g., parts of the Asia-Pacific region (e.g., Choi et al., 2009), parts of Eurasia (e.g., Klein Tank et al., 2006) although this is not the case across all regions. Recent studies covering central and eastern Europe (Bartholy and Pongracz, 2007; Kurbis et al., 2009), the Mediterranean (Efthymiadis et al., 2011), the Tibetan Plateau (You et al., 2008), China (You et al., 2010), Australia (Alexander and Arblaster, 2009), western central Africa (Aguilar et al., 2009), North America (Peterson and Manton, 2008) and southern South America (Marengo et al., 2009), show significant increases in unusually warm nights and/or reductions in unusually cold nights.

SREX highlighted some exceptions to this including central North America, eastern USA (e.g., Alexander et al., 2006; Kunkel et al., 2008; Peterson et al., 2008) and some parts of South America (e.g., Alexander et al., 2006; Rusticucci and Renom, 2008) which indicate changes in these extremes consistent with the observed cooling. However this conclusion appears to be mostly associated with changes in maximum temperatures. The so-called “warming hole” in central North America and eastern USA where temperatures have cooled relative to the significant warming elsewhere on the continent has been ascribed to changes in the hydrological cycle, possibly linked to soil moisture and/or aerosol feedbacks (e.g., Pan et al., 2004; Portmann et al., 2009) or decadal variability linked with the Interdecadal Pacific Oscillation (Meehl et al., 2011).

AR4 based on the study of Alexander et al. (2006) found that over 70% of the global land area sampled showed a significant decrease in the annual occurrence of cold nights and a significant increase in the annual occurrence of warm nights (see Figure 2.41). Record daily maximum temperatures averaged across the USA now outnumber record daily minimum temperatures by a ratio of 2:1 in recent decades compared to preceding decades (Meehl et al., 2009) while in Australia, Trewin and Vermont (2010) found a marked tendency for low temperature records to outnumber high temperature records in the 1957–1966 decade, and for high temperature records to outnumber low temperature records in the 1997–2009 period. Rahmstorf and Coumou (2011) find using a theoretical statistical framework that the number of record-breaking events increases approximately in proportion to the ratio of warming trend to short-term standard deviation.

AR4 found a widespread reduction in the occurrences of frosts in mid-latitude regions since the mid-twentieth Century although SREX did not assess changes in frosts. Updating the AR4 assessment, there continues to be strong evidence for widespread decreases in the number of frost days since about 1950 over those parts of the globe where frosts can be defined e.g., in Asia (Alexander et al., 2006; Liu et al., 2006; Yang et al., 2011a; You et al., 2008); Europe (Alexander et al., 2006; Bartholy and Pongracz, 2007; Scaife et al., 2008); and large parts of North America (Alexander et al., 2006; Brown et al., 2010). Globally, there is evidence of large-scale warming trends in the extremes of temperature, especially minimum temperature, since the beginning of the 20th Century (Horton et al., 2001).

Since AR4 many studies (which were assessed for SREX) have analysed local to regional changes in multi-day temperature extremes in more detail, specifically addressing different heat wave aspects such as frequency, intensity, duration and spatial extent. Several studies suggest that the increase in the temperature mean accounts for most of the changes in heat wave frequency and duration (Ballester et al., 2010; Barnett et al., 2006). However, heat wave intensity/amplitude is highly sensitive to changes in temperature variability and shape (Clark et al., 2006; Della-Marta et al., 2007a; Della-Marta et al., 2007b; Fischer and Schar, 2010; Schar et al., 2004).

Heat waves are often associated with quasi-stationary anticyclonic circulation anomalies that produce subsidence, light winds, clear skies, warm-air advection, and prolonged hot conditions at the surface (Black and Sutton, 2007; Garcia-Herrera et al., 2010). Long-term changes in the persistence of anticyclonic summer circulation, which potentially have large effects on the duration of heat waves, are still relatively poorly understood (see also Section 2.6). Heat waves can also be amplified by pre-existing dry soil conditions in transitional climate zones (Ferranti and Viterbo, 2006; Fischer et al., 2007b) resulting from a precipitation deficit (Della-Marta et al., 2007b; Vautard et al., 2010; Vautard et al., 2007), low-cloudiness producing a higher evaporative demand (Black and Sutton, 2007; Fischer et al., 2007a), and earlier vegetation onset (Zaitchik et al., 2006). This amplification of soil moisture-temperature feedbacks is suggested to have enhanced the duration of extreme summer heat waves in southeastern Europe during the latter part of the 20th Century (Hirschi et al., 2011).

Regional studies have generally found statistically significant increasing trends in heat waves and decreasing trends in cold spells for example, over USA (Kunkel et al., 2008), China (Ding et al., 2010), Iran (Rahimzadeh et al., 2009), and Australia (Tryhorn and Risbey, 2006) primarily over the latter part of the twentieth Century. However over the USA for example on longer timescales, while there is a strong increase in heat waves since 1960, the 1930s remain the dominant decade in the 1985 to 2005 time series and is also associated with extreme drought conditions (Kunkel et al., 2008). However, while daytime temperatures were extremely high in the 1930s, night-time temperatures were not as unusual (Karl et al., 2008 Hawaii, Caribbean, and U.S. Pacific Islands). In Europe there is some suggestion that trends calculated in earlier studies may have been underestimated due to poor quality and/or consistency of data (e.g., Della-Marta et al. (2007a) over Western Europe; Kuglitsch et al. (2009; 2010) over the Mediterranean). Over Asia spatially consistent patterns of changes in warm spell duration were apparent over roughly the past five decades (Choi et al., 2009), increasing by 1–6 days per decade in numerous homogenized station series in Japan, Republic of Korea, China, Mongolia, Vietnam, Thailand, and Malaysia. A long station series for Hong Kong showed a trend towards longer heat waves over the period 1885–2008 (Lee et al., 2011). Ding et al. (2010) reported increasing numbers of heat waves over most of China for the 1961–2007 period. Significant increases in warm spell duration have further been identified at several weather stations in Iran (Rahimzadeh et al., 2009). For Africa there is insufficient evidence regarding changes in heat waves.

In summary, analyses continue to support the AR4 and SREX conclusions since 1950 it is *very likely* that there has been an overall decrease in the number of cold days and nights and an overall increase in the number of warm days and nights on the global scale, i.e., for land areas with sufficient data. It is *likely* that such changes have also occurred at the continental scale in North America, Europe, and Australia. In addition to SREX conclusions, it is *likely* that the occurrence of frost days have decreased in regions where frosts can be defined. There is *medium confidence* of a warming trend in daily temperature extremes in much of Asia although *likely* increases in warm days and nights and decreases in cold days and nights have been observed in central Asia. There is *low* to *medium confidence* in historical trends in daily temperature extremes in Africa and South America as there is either insufficient data or trends vary across regions. Globally, in many (but not all) regions with sufficient data there is *medium confidence* that the length or

number of warm spells, including heat waves, has increased since the middle of the 20th Century although there is *high confidence* that this is *likely* that this is the case for large parts of Europe.

2.7.2 Hydrological Cycle

AR4 concluded that it was *likely* that annual heavy precipitation events had disproportionately increased compared to mean changes between 1951 and 2003 over many mid-latitude regions even where there had been a reduction in annual total precipitation. Rare precipitation events were likely to have increased over regions with sufficient data since the late 19th Century. SREX supported this view as have subsequent analyses although noting that there is large spatial variability within and between regions. However AR4 also reported that very dry areas globally had more than doubled in extent since 1970 but this conclusion was primarily based on the analysis of one study and one index (PDSI; Dai et al., 2004). Other analyses assessed in SREX have since come to light which highlight that there are still large uncertainties in observed global-scale trends in meteorological droughts.

The Hydrological cycle refers to the continuous movement of water around the Earth. In Section 2.3 mean state changes in different aspects of the hydrological cycle are discussed. In this section we focus on the more extreme aspects of the cycle including extreme rainfall, severe local weather events like hail, flooding and droughts. Extreme events associated with tropical and extratropical storms are discussed in Sections 2.7.3 and 2.7.4 respectively.

Given the diverse climates across the globe it has been difficult to provide a universally valid definition of "extreme precipitation". However, in general statistical tests indicate changes in precipitation extremes are consistent with a wetter climate although with a less spatially coherent pattern of change than temperature change, that is, large areas showing both increasing and decreasing trends and a lower level of statistical significance (e.g., Alexander et al., 2006).

SREX gave a thorough assessment of observed regional changes in extreme precipitation (see Table 3.2 P128 of Seneviratne et al. (2012)). For North and Central America studies of heavy precipitation extremes indicate an increasing trend over the last half century in many areas (DeGaetano, 2009; Gleason et al., 2008; Kunkel et al., 2008; Pryor et al., 2009) while results for fewer studies for South America indicate both positive and negative trends over a similar period. Studies for European countries indicate general increases in the intensity and frequency of extreme precipitation especially in winter during the last four decades however there are inconsistencies between studies, regions and seasons.

For analyses of North America, Peterson et al. (2008) reported that heavy precipitation increased between 1950 and 2004 in Canada, the U.S., and Mexico as well as the average amount of precipitation falling on days with precipitation. DeGaetano (2009) showed a 20% reduction in the return period for extreme precipitation over 1950 to 2007 while Gleason et al. (2008) reported an increasing trend in the area experiencing a much above-normal proportion of heavy daily precipitation from 1950 to 2006. Pryor et al. (2009) provided evidence of increases in rainfall intensity above the 95th percentile during the 20th Century, particularly at the end of the century. The central plains/northwestern Midwest regions showed the largest trends towards increased annual total precipitation, number of rainy days and intense precipitation (e.g., fraction of precipitation derived from events in excess of the 90th percentile value). In northwest Mexico, statistically significant positive trends were found in daily precipitation intensity and the seasonal contribution of daily precipitation greater than its 95th percentile in mountain sites for the period 1961–1998. However, no statistically significant changes were found in coastal stations (Cavazos et al., 2008).

In South America, positive trends in extreme rainfall events were identified in the southeast of the continent, north central Argentina, northwest Peru and Ecuador and Sao Paulo, Brazil (Dufek and Ambrizzi, 2008; Marengo et al., 2009; Re and Barros, 2009) however negative trends were observed in winter extreme precipitation in some regions (Penalba and Robledo, 2010).

For Europe, winter extreme precipitation appears to have increased in Central-Western Europe and European Russia (Zolina et al., 2008), but the trend in summer precipitation has been weak or not spatially coherent (Bartholy and Pongracz, 2007; Costa and Soares, 2009; Durao et al., 2010; Kysely, 2009; Maraun et al., 2008; Moberg et al., 2006; Pavan et al., 2008; Rodda et al., 2010; Zolina et al., 2008). Zolina et al. (2010)

indicated that there has been a 15–20% increase in the persistence of wet spells over most of Europe over the last 60 years not associated with an increase of the total number of wet days. Increasing trends were found between 1901 and 2000 in 90th, 95th and 98th percentiles of daily winter precipitation (Moberg et al., 2006), which has been confirmed by more detailed country-based studies for the United Kingdom (Maraun et al., 2008), Germany (Zolina et al., 2008), Belgium (Ntegeka and Willems, 2008), Central and Eastern Europe (Bartholy and Pongracz, 2007; Kysely, 2009), while decreasing trends have been found in some regions such as northern Italy (Pavan et al., 2008), Poland (Lupikasza, 2010) and some Mediterranean coastal sites (Toreti et al., 2010). Uncertainties are overall larger in Southern Europe and the Mediterranean, where there is low confidence in the trends.

Observations at 143 weather stations in ten Asia-Pacific Network countries from 1955 to 2007 did not indicate systematic, regional trends in the frequency and duration of extreme precipitation events (Choi et al., 2009). However, other studies have suggested significant trends in extreme precipitation at sub-regional scales in the Asia-Pacific region and during monsoon seasons over Indian subcontinent (Krishnamurthy et al., 2009; Pattanaik and Rajeevan, 2010; Rajeevan et al., 2008; Sen Roy, 2009). Zhai et al. (2005) found significant increases over the period 1951–2000 in extreme precipitation in western China, and in parts of the southwest and south China coastal area, but a significant decrease in extremes is observed in north China and the Sichuan Basin. Several recent studies focused on Africa, in general, have not found significant trends in extreme precipitation (Aguilar et al., 2009; Kruger, 2006; New et al., 2006; Seleshi and Camberlin, 2006).

Above studies generally use indices which reflect "moderate" extremes (see Box 2.5), e.g., events occurring as often as 5% or 10% of the time. Only a few regions have sufficient data to assess trends in rarer precipitation events reliably, e.g., events occurring on average once in several decades. Using Extreme Value Theory, DeGaetano (2009) showed a 20% reduction in the return period for extreme precipitation events over the contiguous USA from 1950 to 2007. For Europe from 1951 to 2010, (Van den Besselaar et al., submitted) reported a median reduction in 5 to 20 year return periods of 18%, with a range between -4% and 59% depending on the subregion and season. This overall decrease in waiting times for rare extremes is qualitatively similar to the increase in moderate extremes for these regions reported above, and also consistent with earlier local results for the extreme tail of the distribution (Trenberth et al., 2007).

Another extreme aspect of the hydrological cycle is severe local weather phenomena such as hail or thunder storms. These are not well observed in many parts of the world since the density of surface meteorological observing stations required for detection is too coarse to measure all such events. Moreover, homogeneity of existing station series is questionable (Doswell et al., 2005). Alternatively, measures of severe thunderstorms or hailstorms can be derived by assessing the environmental conditions that are favourable for their formation but this method is associated with high uncertainty. SREX (Seneviratne et al., 2012) highlighted studies such as Brooks and Dotzek (2008) who found significant variability but no clear trend in the past 50 years in severe thunderstorms in a region east of the Rocky Mountains in the United States, Cao (2008) who found an increasing frequency of severe hail events in Ontario, Canada during the period 1979–2002 and Kunz et al. (2009) who found that hail days significantly increased during the period 1974–2003 in southwest Germany. In China between 1961 and 2005, the number of hail days has been found to generally decrease, with the highest occurrence between 1960 and 1980 but with a sharp drop since the mid-1980s (CMA, 2007; Xie et al., 2008).

AR4 noted that while flood damage was increasing (Kundzewicz et al., 2007), there was not a general global trend in the incidence of floods. There is however an abundance of evidence indicating that there has been an earlier occurrence of spring peak river flows in snow-dominated regions (Rosenzweig et al., 2007). For example, Cunderlik and Ouarda (2009), find that snow-melt spring floods are coming significantly earlier in southern Canada. While the most evident flood trends appear to be in northern high latitudes, where warming trends have been largest in the observational record, there are regions where no evidence of a trend in extreme flooding has been found e.g., over Russia based on daily river discharge (e.g., Shiklomanov et al., 2007). Other studies for Europe (e.g., Benito et al., 2005; Petrow and Merz, 2009) and Asia (e.g., Delgado et al., 2010; Jiang et al., 2008) show evidence for upward, downward or no trend in the magnitude and frequency of floods so we conclude that there is currently no clear and widespread evidence for observed changes in flooding (except for the earlier spring flow in snow-dominated regions).

SREX provided a comprehensive assessment of changes in observed droughts and updated the conclusions provided by AR4. SREX considered three types of drought in their assessment: i) Meteorological drought (abnormal precipitation deficit usually relative to some 'normal' amount); ii) Agricultural drought (also soil-moisture drought – a precipitation shortage during the growing season that affects agriculture or ecosystem functions); and iii) Hydrological drought (precipitation shortage affecting surface (e.g., run-off) or subsurface water supply). Depending on the type of drought considered and because of the complexities in defining drought this can substantially affect the conclusions regarding trends on a global scale.

AR4, based largely on the results of one study i.e., Dai et al. (2004), concluded that droughts (as defined by PDSI) had become more common, especially in the tropics and sub-tropics since about 1970. Based on evidence since AR4 (including studies by (Dai, 2011a; Dai, 2011b; Sheffield and Wood, 2008; Vicente-Serrano et al., 2010b), SREX somewhat revised this stating that there were not enough direct observations of dryness to suggest high confidence in observed trends although there was medium confidence that since the 1950s some regions of the world have experienced more intense and longer droughts. Analyses subsequent to SREX have not updated these conclusions further.

Similarly to heatwaves (see Section 2.7.1), droughts can be affected by land-atmosphere feedbacks and interactions (Nicholls and Larsen, 2011; Seneviratne et al., 2010) as well as the combined effects of multiple climate variables on multiple timescales such as precipitation, temperature, wind, solar radiation, and soil condition. However, because there are very few direct measurements of drought related variables, such as soil moisture (Robock et al., 2000) drought proxies (e.g., PDSI, SPI, SPEI) are often used to assess drought conditions. However analyses of these indirect indices come with substantial uncertainties. To alleviate some of these uncertainties in PDSI, which may not be comparable across climate zones, Wells et al. (2004) introduced the self-calibrating (sc-)PDSI by replacing the fixed empirical constants in PDSI with values representative of the local climate.

Using the sc-PDSI van der Schrier et al. (2006) found no statistically significant soil moisture trends in Europe. SREX indicated that there were inconsistent trends in drought related variables across most other continents (see Table 3.2, P128 of Seneviratne et al. (2012). For example, in North and Central America an overall slight decrease in dryness has been observed since 1950 (see Figure 2.42a) although regional variability and the 1930s drought in the USA dominate the signal (Aguilar et al., 2005; Alexander et al., 2006; Dai, 2011a; Dai, 2011b; Kunkel et al., 2008; Sheffield and Wood, 2008) while in Africa while there has been a general increase in drought indices (see Figure 2.42a), the 1970s prolonged Sahel drought dominates the signal (Dai, 2011a; Dai, 2011b; Sheffield and Wood, 2008).

It should be noted however that because drought is a complex variable and can at best be incompletely represented by commonly used drought indices, this can lead to potential discrepancies in the interpretation of changes. For example, globally Sheffield and Wood (2008) found decreasing trends in the duration, intensity and severity of drought (although this was using a hydrological model forced with observations). Conversely, Dai (2011a; 2011b) found a general global increase in drought although with substantial regional variation (see Figure 2.42a).

A recent study by Giorgi et al. (2011) also indicates that hydroclimatic intensity has increased over the latter part of the 20th Century in response to a warming climate. Using a measure which combines precipitation intensity and dry spell length they show that trends are most marked in Europe, India and East Asia although trends appear to have decreased in Australia (see Figure 2.42b). However data availability, quality and length of record remain issues in drawing conclusions on a global scale.

[**INSERT FIGURE 2.42 HERE**]

Figure 2.42: Spatial trends in (a) an annual drought index using the self-calibrated PDSI (change per 50 years) with the Penman-Monteith potential evaporation calculated over the period 1950 to 2008 (red indicates drying - from Dai, 2011b) and (b) hydroclimatic intensity (HY-INT: a multiplicative measure of length of dry spell and precipitation intensity) over the period 1976 to 2000 (from Giorgi et al. (2011)). An increase (decrease) in HY-INT reflects an increase (decrease) in the length of drought and /or extreme precipitation events.

In summary, analyses continue to support the AR4 and SREX conclusions that it is *likely* that there has been statistically significant increases in the number of heavy precipitation events (e.g., 95th percentile) in more regions than there has been statistically significant decreases, but there are strong regional and subregional

variations in the trends. In particular, many regions present statistically non-significant or negative trends, and, where seasonal changes have been assessed, there are also variations between seasons (e.g., more consistent trends in winter than in summer in Europe). The overall most consistent trends towards heavier precipitation events are found in North America (*likely* increase over the continent). There continues to be a lack of evidence and thus *low confidence* regarding the sign of trend in the magnitude and/or frequency of floods on a global scale. The current assessment does not support the AR4 conclusions regarding global increasing trends in droughts but rather concludes that there is not enough evidence at present to suggest high confidence in observed trends in dryness due to lack of direct observations, some geographical inconsistencies in the trends, and some dependencies of inferred trends on the index choice. There is *low confidence* in observed trends in small scale severe weather phenomena such as hail because of historical data inhomogeneities and inadequacies in monitoring systems.

2.7.3 Tropical Storms

AR4 concluded that it was *likely* that a trend had occurred in intense tropical cyclone activity since 1970 in some regions (IPCC, 2007b). In more detail it was stated that 'there is observational evidence for an increase in intense tropical cyclone activity in the North Atlantic since about 1970, correlated with increases of tropical SSTs. There are also suggestions of increased intense tropical cyclone activity in some other regions where concerns over data quality are greater. Multi-decadal variability and the quality of the tropical cyclone records prior to routine satellite observations in about 1970 complicate the detection of long-term trends in tropical cyclone activity. There is no clear trend in the annual numbers of tropical cyclones'. Subsequent assessments, including SREX and more recent literature (e.g., Vecchi and Knutson, 2011) indicate that the AR4 assessment needs to be somewhat revised.

There have been no significant trends observed in global tropical cyclone frequency records, including over the present 40-year period of satellite observations (e.g., Webster et al., 2005). Regional trends in tropical cyclone frequency have been identified in the North Atlantic, but the fidelity of these trends is debated (Holland and Webster, 2007; Landsea, 2007; Landsea et al., 2006; Mann et al., 2007b). Different methods for estimating undercounts in the earlier part of the North Atlantic tropical cyclone record provide mixed conclusions (Chang and Guo, 2007; Kunkel et al., 2008; Mann et al., 2007a; Vecchi and Knutson, 2008); . Figure 2.43 highlights how linear trends can change once undercounts in the early part of the observing record have been accounted for, in this case in the Atlantic hurricane storm counts. In the unadjusted timeseries there are upward trends in the frequency of both hurricane and tropical storms which flatten out or become negative once adjustments have been added (Vecchi and Knutson, 2011). Regional trends have not been detected in other oceans (Chan and Xu, 2009; Kubota and Chan, 2009) although Callaghan and Power (2011) do indicate a decrease in Eastern Australia land-falling tropical cyclones. It thus remains uncertain whether any reported long-term increases in tropical cyclone frequency are robust, after accounting for past changes in observing capabilities (Knutson et al., 2010).

[**INSERT FIGURE 2.43 HERE**]

Figure 2.43: Atlantic hurricane frequency changes using raw and adjusted data. Filled lines indicate the normalized 5-year running means, during 1878–2008, with straight dashed lines indicating the linear least squares trends. The blue-shaded curve represent unadjusted hurricane counts (HURDAT; (Landsea et al., 2008). The red curve includes time dependent adjustments for missing storms based on ship track density (Landsea et al., 2010; Vecchi and Knutson, 2008) and for the adjusted hurricane count record from Vecchi and Knutson (2011). Vertical axis ticks represent one standard deviation, with all series normalized to unit standard deviation after a 5-year running mean was applied (Vecchi and Knutson, 2011).

Whereas frequency estimation requires only that a tropical cyclone be identified and reported at some point in its lifetime, intensity estimation requires a series of specifically targeted measurements over the entire duration of the tropical cyclone (e.g., Landsea et al., 2006). Consequently, intensity values in the historical records are especially sensitive to changing technology and improving methodology, which heightens the challenge of detecting trends within the backdrop of natural variability. Global reanalyses of tropical cyclone intensity using a homogenous satellite record have suggested that changing technology has introduced a non-stationary bias that inflates trends in measures of intensity (Kossin et al., 2007), but a significant upward trend in the intensity of the strongest tropical cyclones remains after this bias is accounted for (Elsner et al., 2008).

Time series of power dissipation, an aggregate compound of tropical cyclone frequency, duration, and intensity that measures total energy consumption by tropical cyclones, show upward trends in the North Atlantic and weaker upward trends in the western North Pacific over the past 25 years (Emanuel, 2007), but interpretation of longer-term trends is again constrained by data quality concerns. Since 2005, accumulated cyclone energy, which is an integrated metric analogous to power dissipation, has been declining globally and is presently at a 40-year low point (Maue, 2009).

Based on research subsequent to AR4, which further elucidated the scope of uncertainties in historical tropical cyclone data, more recent assessments (Knutson et al., 2010) do not conclude that it is *likely* that annual numbers of tropical storms, hurricanes and major hurricanes counts have increased over the past 100 years in the North Atlantic basin, nor do they conclude that the Atlantic Power Dissipation Index increase is 'likely substantial' since the 1950s and 1960s. However there is evidence of an increase in the most intense tropical cyclones since the 1970s but the record is too short at present to be reliable. This assessment does not revise the SREX conclusion that there is *low confidence* that any reported long-term increases in tropical cyclone activity are robust, after accounting for past changes in observing capabilities.

2.7.4 Extratropical Storms

AR4 noted a *likely* net increase in frequency/intensity of Northern Hemisphere extreme extratropical cyclones and a poleward shift in storm tracks since the 1950s (Trenberth et al., 2007, Table 3.8), reporting on several papers showing increases in the number or strength of intense extratropical cyclones in the North Pacific and the North Atlantic (Trenberth et al., 2007, p. 312). SREX further consolidated the AR4 assessment of poleward shifting storm tracks but somewhat revised the assessment of regional changes in the intensity of extreme extratropical cyclones.

Studies using reanalyses continue to support a northward and eastward shift in the Atlantic cyclone activity during the last 60 years with both more frequent and more intense wintertime cyclones in the high-latitude Atlantic (Raible et al., 2008; Schneidereit et al., 2007; Vilibic and Sepic, 2010) and fewer in the mid-latitude Atlantic (Raible et al., 2008; Wang et al., 2006). As noted in SREX, there are inconsistencies however among studies of extreme cyclones in reanalyses. Some studies show an increase in intensity and number of extreme Atlantic cyclones (Geng and Sugi, 2001; Lehmann et al., 2011; Paciorek et al., 2002) while others show a reduction (Gulev et al., 2001). Differences can be partly explained by sensitivities in identification schemes and/or different definitions for extreme cyclones (Leckebusch et al., 2006; Pinto et al., 2006).

In the North Pacific studies using reanalyses and in situ data for the last 50 years have noted an increase in the number and intensity of wintertime intense extratropical cyclone systems since the 1950s (Graham and Diaz, 2001; Raible et al., 2008; Simmonds and Keay, 2002) and cyclone activity (Zhang et al., 2004), but signs of some of the trends disagreed when different tracking algorithms or reanalysis products are used (Raible et al., 2008). A slight positive trend has been found in north Pacific extreme cyclones (Geng and Sugi, 2001; Gulev et al., 2001; Paciorek et al., 2002).

Over continental land areas most studies of severe storms or storminess have been performed for Europe where there are long running in situ pressure and wind observations. SREX indicated that studies using long homogenous historical records of European storminess proxies show no clear trends over the last century or longer (Allan et al., 2009; Barring and Fortuniak, 2009; Hanna et al., 2008; Matulla et al., 2008) although Wang et al. (2009b) note some seasonal trends. Subsequently an updated study by Wang et al. (2011) extending analysis to cover a wider region of western Europe found substantial decadal and longer fluctuations and considerable seasonal and regional differences when assessing extreme geostrophic wind speeds. Figure 2.44 shows some of these changes for boreal winter indicating that decreasing trends outnumber increasing trends. However, there is some evidence the 140-year Twentieth Century Reanalysis (Compo et al., 2011) indicates significant increases in both the strength and frequency of wintertime storms for large parts of Europe (Donat et al., 2011) but it is unclear at present whether this is an artefact of the way in which the reanalyses are produced. Studies using wind proxies in the North Atlantic and Europe indicate that there is a tendency for increased storminess around 1900 and in the 1990s, while the 1960s and 1970s were periods of low storm activity (Allan et al., 2009; Wang et al., 2009b). Links identified between positive (negative) NAM/NAO to stronger (weaker) Atlantic/European cyclone activity (e.g., Chang, 2009; Pinto et al., 2009) have proved to be somewhat intermittent in a long historical context due to interdecadal shifts in

the location of the positions of the NAO pressure centres (Vicente-Serrano and Lopez-Moreno, 2008; Zhang et al., 2008).

[**INSERT FIGURE 2.44 HERE**]

Figure 2.44: Triangles show regions where geostrophic wind speeds have been calculated from in situ surface pressure observations. Within each pressure triangle, Gaussian low-pass filtered curves and estimated linear trends of the 99th percentile of these geostrophic wind speeds for winter are shown. The ticks of the time (horizontal) axis range from 1875 to 2005, with an interval of 10 years. Disconnections in lines show periods of missing data. Red and magenta (blue and cyan) trend lines indicate upward (downward) trends of at least 5 and 20% significance, respectively. From Wang et al. (2011).

There are still insufficient studies to make robust conclusions about changes in extratropical cyclone activity in Asia. SREX noted however that available studies using reanalyses indicate a decrease in extratropical cyclone activity (Zhang et al., 2004) and intensity (Wang et al., 2009c; Zhang et al., 2004) over the last 50 years has been reported for northern Eurasia (60–40°N) with a possible northward shift with increased cyclone frequency in the higher latitudes (50–45°N) and decrease in the lower latitudes (south of 45°N). The decrease at lower latitudes is also supported by a study of severe storms by Zou et al. (2006b) who used sub-daily in situ pressure data from a number of stations across China.

SREX also notes that based on reanalyses North American cyclone numbers have increased over the last 50 years, with no statistically significant change in cyclone intensity (Zhang et al., 2004). Hourly MSLP data from Canadian stations showed that winter cyclones have become significantly more frequent, longer lasting, and stronger in the lower Canadian Arctic over the last 50 years (1953–2002), but less frequent and weaker in the south, especially along the southeast and southwest Canadian coasts (Wang et al., 2006). Further south, a tendency toward weaker low-pressure systems over the past few decades was found for U.S. east coast winter cyclones using reanalyses, but no statistically significant trends in the frequency of occurrence of systems (Hirsch et al., 2001).

In the Southern Hemisphere, studies using in situ pressure observations indicate a significant decline in storminess since the mid-19th Century (Alexander and Power, 2009; Alexander et al., 2011), strengthening the evidence of a southward shift in storm tracks previously noted using reanalyses (Fyfe, 2003; Hope et al., 2006). Frederiksen and Frederiksen (2007) linked the reduction in cyclogenesis at 30°S and southward shift to a decrease in the vertical mean meridional temperature gradient. SREX notes some inconsistency among reanalysis products for the Southern Hemisphere regarding trends in the frequency of intense extratropical cyclones (Pezza et al. (2007), (Lim and Simmonds, 2009) although studies tend to agree on a trend towards more intense systems. Recent studies support a tendency for more cyclones around Antarctica when the Southern Annular Mode (SAM) is in its positive phase and a shift of cyclones toward midlatitudes when the SAM is in its negative phase (Pezza and Simmonds, 2008). Additionally, more intense (and fewer) cyclones seem to occur when the Pacific Decadal Oscillation (PDO) is strongly positive and vice versa (Pezza et al., 2007).

Extreme wind events are often associated with extratropical and tropical cyclones and other extreme phenomena such as thunderstorm downbursts or tornadoes. Changes in wind extremes may occur from changes in the intensity or location of their associated phenomena or from others changes in the climate system (e.g., a change in local convective activity). Recent studies that have examined trends in wind extremes from observations tend to point to declining trends in extremes in mid-latitudes (Pirazzoli and Tomasin, 2003; Pryor et al., 2007; Smits et al., 2005; Zhang et al., 2007c) and increasing trends in high latitudes (Hundecha et al., 2008; Lynch et al., 2004; Turner et al., 2005). Other recent studies have compared the trends from observations with reanalysis data and reported differing or even opposite trends in the reanalysis products (e.g., McVicar et al., 2008; Smits et al., 2005). On the other hand, declining trends reported by Xu et al. (2006b) over China were generally consistent with trends in NCEP reanalysis. The accuracy of trends extracted from reanalysis products however remains a source of debate since data assimilation methods can induce artificial trends (e.g., Bengtsson et al., 2004).

In summary, research subsequent to the AR4 and SREX continues to support a *likely* poleward shift of extratropical cyclones since the 1950s. However unlike AR4, here it is assessed that there is *low confidence* of regional changes in the intensity of extreme extratropical cyclones. Over the last century there is *low confidence* of a clear trend in storminess proxies due to inconsistencies between studies or lack of long-term

data in some parts of the world (particularly in the Southern Hemisphere). There is *low confidence* in trends in extreme winds due to quality and consistency issues with analysed data.

[START FAQ 2.2 HERE]

FAQ 2.2: Have there been any Changes in Climate Extremes?

For temperature extremes, particularly those related to minimum temperature, there is strong evidence that there have been statistically significant changes associated with warming since the mid-20th Century. For other extremes such as tropical cyclone frequency we have low confidence that there have been discernable changes over the observed record.

There is no consistent definition in scientific literature of what constitutes an extreme climatic event (Seneviratne et al., 2012) and this makes a global assessment difficult. In an absolute sense an extreme climate event will vary from place to place (e.g., a hot day in the tropics will be a different temperature than a hot day in mid-latitudes). Extremes in some climate variables (e.g., droughts or floods) may not necessarily be induced by extremes in meteorological variables (precipitation, temperature), but may be the result of an accumulation of moderate weather or climate events. It has been difficult to provide a precise definition of an extreme because events can vary between locations and can depend on the application for which analysis is required. For example, it has been difficult to define a universally valid critical threshold globally for defining a heat wave and differences exist between impact-dictated definitions (e.g., mortality rates) and physical definitions (e.g., temperature threshold and duration-driven definitions). Generally definitions have consisted of a certain number of consecutive days with temperatures exceeding percentile-based or fixed temperature thresholds (see Box 2.5).

Primarily extremes are defined as the infrequent events at the high and low end of the range of values of a particular variable. Whether these "tails" are calculated using percentile or fixed-thresholds, with respect to specific return frequencies (e.g., "100-year event"), what statistical model is used or what time period is considered, is dependent on the application for which analysis is required. Since the early IPCC assessments, efforts and progress have been made in defining consistent measures to allow comparability across modelling and observational studies and across regions (Nicholls and Alexander, 2007; Peterson and Manton, 2008; Box 2.5).

Studies which have used consistent definitions for cold (<10th percentile) and warm (>90th percentile) nights indicate changes associated with warming for most regions of the globe, a few exceptions being central North America and eastern USA and southern South America. Within uncertainty ranges, all point to changes associated with warming which is generally most apparent in minimum temperature extremes.

Warm spells or heat waves containing a series of consecutive extremely hot days or nights, have substantially larger impacts than individual hot days, although fewer studies have investigated heat wave characteristics compared to changes in warm days or nights. FAQ 2.2, Figure 1a indicates that most global land areas with available data indicate increasing trends in heat waves since the middle of the twentieth Century. One exception is the south-eastern USA where this measure of heat wave duration shows cooling (see Section 2.7.1 for more discussion of this "warming hole"). For parts of the globe with long historical temperature reconstructions such as Europe, indications are that some regions have experienced a disproportionate number of extreme heatwave events in more recent decades in records spanning several hundred years. The historical evolution of the hottest summers in Europe (see FAQ 2.2, Figure 1b) may suggest that the period from 2001-2010 stands substantially above any other 10-year period since 1500.

[**INSERT FAQ 2.2, FIGURE 1 HERE**]

FAQ 2.2, Figure 1: (a) Trends (days/decade) in a heatwave duration measure (WSDI - see Zhang et al., 2011a), over the period 1951 to 2009 (using updated HadGHCND data from Caesar et al. (2006)). Stippling indicates where trends are significant at 5% level. (b) European summer temperatures for the period 1500 to 2010 represented by a statistical frequency distribution of best-guess reconstructed and instrument based European ([35°N, 70°N], [25°W, 40°E]) summer land temperature anomalies (°C, relative to the 1970 to 1999 period). The five warmest and coldest summers are highlighted. Gray bars represent the distribution for the 1500–2002 period, with a Gaussian fit in black (Barriopedro et al., 2011).

For other climate extremes there are generally less coherent changes than for temperature, either because of lack of data, quality of data, inconsistency between studies, regions and/or seasons. However, for precipitation extremes for example, changes are consistent with a wetter (and warmer) climate. Analyses indicate that based on analysis of land areas with sufficient data since about 1950 that there have been increases in more extreme precipitation events in more recent decades but results are very regionally and seasonally dependent. However, studies analysing droughts do not agree on the sign of trend on the global scale.

Considering other extremes such as tropical cyclones, the latest assessments show that after accounting for past changes in observing capabilities, there is *low confidence* that any reported long-term increases in tropical cyclone activity are robust. FAQ 2.2, Figure 2a and 2b indicates that in two ocean basins, the north Atlantic and the south Pacific, that there have been slight decreases in the frequency of tropical cyclones over about the last 130 years when uncertainties in observing methods have been considered. In the north Pacific (FAQ2.2, Figure 2c), land falling typhoons in China appear to have increased since 1948 but with little evidence of a longer term trend in this ocean basin (Kubota and Chan, 2009).

[**INSERT FAQ 2.2, FIGURE 2 HERE**]

FAQ 2.2, Figure 2: Filled lines indicate the normalized 5-yr running means of the number of (a) land falling eastern Australian cyclones tropical cyclones, 1872/1873 to 2010/2011 (adapted from Callaghan and Power (2011) and updated to include 2010/2011 season) and (b) land falling U.S. hurricanes (adjusted to account for under-reporting in early part of record), 1878 to 2008 (adapted from Vecchi and Knutson, 2011) and (c) land falling Chinese typhoons, 1948 to 2010 (adapted from (CMA, 2007). Vertical axis major ticks represent one standard deviation, with all series normalized to unit standard deviation after a 5-year running mean was applied. The dashed lines are trends calculated using ordinary least squares regression.

Overall all the most robust changes in climate extremes globally are seen in measures of temperature, including frosts and to some extent heatwaves. Precipitation extremes also appear to be increasing in a manner consistent with a warming climate however there is large spatial inconsistency and observed trends in droughts are still uncertain. There is limited evidence that there have been changes in extremes associated with other climate variables.

[END FAQ 2.2 HERE]

2.8 Consistency Across Observations and Conclusions

Comparing trends and variability across independently measured climate variables can help assess whether the observed changes are consistent. If the estimated changes are consistent with each other, this can enhance confidence in the observations and the overall assessment of change. Observed inter-relationships among different variables described in this chapter include:

- Globally averaged surface temperatures for land, sea surface and marine air all show significant warming trends, as do upper air observations from radiosondes and satellites.

- Changes in extremes of temperature are consistent with warming, showing decreases in cold extremes and increases in warm extremes.

- Land-based precipitation observations since 1900 are consistent with the most recent and comprehensive analyses of streamflow, in that, globally, neither show significant trends during the 20th Century.

- Over land, a strong negative correlation is observed between precipitation and surface temperature in summer and at low latitudes throughout the year, and areas that have become wetter, such as the eastern USA and Argentina, have not warmed as much as other land areas.

- Surface specific humidity has generally increased in close association with higher temperatures over both land and ocean. Upper-tropospheric water vapour has also increased and in turn, widespread

observed increases in the fraction of heavy precipitation events (e.g., 95th percentile) are consistent with the increased water vapour amounts.

- Increasing zonal flow observed until the mid-1990s in the NH brought milder maritime air into Europe and much of high-latitude Asia from the North Atlantic in winter, enhancing warming there. In recent decades, these trends have reversed and warming has slowed in these regions.

- Widespread decadal changes in surface solar radiation (dimming until the 1980s and subsequent brightening) are in line with observed changes in a variety of other related variables, such as sunshine duration and hydrological quantities. These changes appear to be consistent also with increasing and decreasing aerosol loadings.

References

Abakumova, G. M., E. V. Gorbarenko, E. I. Nezval, and O. A. Shilovtseva, 2008: Fifty years of actinometrical measurements in Moscow. *International Journal of Remote Sensing*, **29**, 2629-2665.

Ackerman, S. A., R. E. Holz, R. Frey, E. W. Eloranta, B. C. Maddux, and M. McGill, 2008: Cloud detection with MODIS. Part II: Validation. *Journal of Atmospheric and Oceanic Technology*, **25**, 1073-1086.

Adam, J. C., and D. P. Lettenmaier, 2008: Application of new precipitation and reconstructed streamflow products to streamflow trend attribution in northern Eurasia. *Journal of Climate*, **21**, 1807-1828.

Adler, R. F., et al., 2003: The version-2 global precipitation climatology project (GPCP) monthly precipitation analysis (1979-present). *Journal of Hydrometeorology*, **4**, 1147-1167.

Aguilar, E., et al., 2009: Changes in temperature and precipitation extremes in western central Africa, Guinea Conakry, and Zimbabwe, 1955-2006. *Journal of Geophysical Research-Atmospheres*, **114**.

Aguilar, E., et al., 2005: Changes in precipitation and temperature extremes in Central America and northern South America, 1961-2003. *Journal of Geophysical Research-Atmospheres*, **110**.

Ajavon, A. L., P. A. Newman, J. Pyle, and A. R. Ravishankara, 2010: Scientific Assessment of ozone depletion: 2010.

Alexander, L. V., and J. M. Arblaster, 2009: Assessing trends in observed and modelled climate extremes over Australia in relation to future projections. *International Journal of Climatology*, **29**, 417-435.

Alexander, L. V., and S. Power, 2009: Severe storms inferred from 150 years of sub-daily pressure observations along Victoria's "Shipwreck Coast". *Australian Meteorological and Oceanographic Journal*, **58**, 129-133.

Alexander, L. V., P. Uotila, and N. Nicholls, 2009: Influence of sea surface temperature variability on global temperature and precipitation extremes. *Journal of Geophysical Research-Atmospheres*, **114**.

Alexander, L. V., X. L. L. Wang, H. Wan, and B. Trewin, 2011: Significant decline in storminess over southeast Australia since the late 19th century. *Australian Meteorological and Oceanographic Journal*, **61**, 23-30.

Alexander, L. V., et al., 2006: Global observed changes in daily climate extremes of temperature and precipitation. *Journal of Geophysical Research-Atmospheres*, **111**.

Allan, R., and T. Ansell, 2006: A new globally complete monthly historical gridded mean sea level pressure dataset (HadSLP2): 1850-2004. *Journal of Climate*, **19**, 5816-5842.

Allan, R., S. Tett, and L. Alexander, 2009: Fluctuations in autumn-winter severe storms over the British Isles: 1920 to present. *International Journal of Climatology*, **29**, 357-371.

Allan, R., P. Brohan, G. P. Compo, R. Stone, J. Luterbacher, and S. Bronnimann, 2011: The International Atmospheric Circulation Reconstructions over the Earth (ACRE) Initiative. *Bulletin of the American Meteorological Society*, 10.1175/2011BAMS218.1.

Allan, R. P., 2009: Examination of Relationships between Clear-Sky Longwave Radiation and Aspects of the Atmospheric Hydrological Cycle in Climate Models, Reanalyses, and Observations. *Journal of Climate*, **22**, 3127-3145.

Allan, R. P., and A. Slingo, 2002: Can current climate model forcings explain the spatial and temporal signatures of decadal OLR variations? *Geophysical Research Letters*, **29**, 1141.

Allan, R. P., B. J. Soden, V. O. John, W. Ingram, and P. Good, 2010: Current changes in tropical precipitation. *Environmental Research Letters*, **5**.

Allen, M. R., and W. J. Ingram, 2002: Constraints on future changes in climate and the hydrologic cycle. *Nature*, **419**, 224-+.

Allen, R. J., and S. C. Sherwood, 2007: Utility of radiosonde wind data in representing climatological variations of tropospheric temperature and baroclinicity in the western tropical Pacific. *Journal of Climate*, **20**, 5229-5243.

——, 2008: Warming maximum in the tropical upper troposphere deduced from thermal winds. *Nature Geoscience*, **1**, 399-403.

Alpert, P., and P. Kishcha, 2008: Quantification of the effect of urbanization on solar dimming. *Geophysical Research Letters*, **35**, L08801.

Alpert, P., P. Kishcha, Y. J. Kaufman, and R. Schwarzbard, 2005: Global dimming or local dimming?: Effect of urbanization on sunlight availability. *Geophysical Research Letters*, **32**, L17802.

Andreadis, K. M., and D. P. Lettenmaier, 2006: Trends in 20th century drought over the continental United States. *Geophysical Research Letters*, **33**.

Andrews, T., P. M. Forster, and J. M. Gregory, 2009: A Surface Energy Perspective on Climate Change. *Journal of Climate*, **22**, 2557-2570.

Andronova, N., J. E. Penner, and T. Wong, 2009: Observed and modeled evolution of the tropical mean radiation budget at the top of the atmosphere since 1985. *Journal of Geophysical Research-Atmospheres*, **114**, -.

Angell, J. K., 2006: Changes in the 300-mb North Circumpolar Vortex, 1963-2001. *Journal of Climate*, **19**, 2984-2994.

Anthes, R. A., et al., 2008: The COSMOC/FORMOSAT-3 - Mission early results. *Bulletin of the American Meteorological Society*, **89**, 313-+.

Archer, C. L., and K. Caldeira, 2008a: Historical trends in the jet streams. *Geophysical Research Letters*, **35**.

——, 2008b: Reply to comment by Courtenay Strong and Robert E. Davis on "Historical trends in the jet streams". *Geophysical Research Letters*, **35**.

Arndt, D. S., J. Blunden, and M. O. Baringer, 2011: STATE OF THE CLIMATE IN 2010. *Bulletin of the American Meteorological Society*, **92**, S17-+.

Ashok, K., and T. Yamagata, 2009: CLIMATE CHANGE The El Nino with a difference. *Nature*, **461**, 481-+.
Ashok, K., S. K. Behera, S. A. Rao, H. Y. Weng, and T. Yamagata, 2007: El Nino Modoki and its possible teleconnection. *Journal of Geophysical Research-Oceans*, **112**.
Atlas, R., R. Hoffman, J. Ardizzone, S. Leidner, J. Jusem, D. Smith, and D. Gombos, 2011: A CROSS-CALIBRATED MULTIPLATFORM OCEAN SURFACE WIND VELOCITY PRODUCT FOR METEOROLOGICAL AND OCEANOGRAPHIC APPLICATIONS. *Bulletin of the American Meteorological Society*, **92**, 157-+.
Ballester, J., F. Giorgi, and X. Rodo, 2010: Changes in European temperature extremes can be predicted from changes in PDF central statistics. *Climatic Change*, **98**, 277-284.
Baringer, M. O., D. S. Arndt, and M. R. Johnson, 2010: STATE OF THE CLIMATE IN 2009. *Bulletin of the American Meteorological Society*, **91**, S1-+.
Barkstrom, B. R., 1984: The Earth Radiation Budget Experiment (Erbe). *Bulletin of the American Meteorological Society*, **65**, 1170-1185.
Barnes, N., and D. Jones, 2011: Clear Climate Code: Rewriting Legacy Science Software for Clarity. *IEEE Software*, **28**, 36-42.
Barnett, D. N., S. J. Brown, J. M. Murphy, D. M. H. Sexton, and M. J. Webb, 2006: Quantifying uncertainty in changes in extreme event frequency in response to doubled CO2 using a large ensemble of GCM simulations. *Climate Dynamics*, **26**, 489-511.
Barnston, A. G., and R. E. Livezey, 1987: Classification, seasonality and persistence of low-frequency atmospheric circulation patterns. *Monthly Weather Review*, **115**, 1083-1126.
Barring, L., and K. Fortuniak, 2009: Multi-indices analysis of southern Scandinavian storminess 1780-2005 and links to interdecadal variations in the NW Europe-North Sea region. *International Journal of Climatology*, **29**, 373-384.
Barriopedro, D., E. M. Fischer, J. Luterbacher, R. Trigo, and R. Garcia-Herrera, 2011: The Hot Summer of 2010: Redrawing the Temperature Record Map of Europe. *Science*, **332**, 220-224.
Barrucand, M., M. Rusticucci, and W. Vargas, 2008: Temperature extremes in the south of South America in relation to Atlantic Ocean surface temperature and Southern Hemisphere circulation. *Journal of Geophysical Research-Atmospheres*, **113**.
Bartholy, J., and R. Pongracz, 2007: Regional analysis of extreme temperature and precipitation indices for the Carpathian Basin from 1946 to 2001. *Global and Planetary Change*, **57**, 83-95.
Barton, N. P., and A. W. Ellis, 2009: Variability in wintertime position and strength of the North Pacific jet stream as represented by re-analysis data. *International Journal of Climatology*, **29**, 851-862.
Baumer, D., and B. Vogel, 2007: An unexpected pattern of distinct weekly periodicities in climatological variables in Germany. *Geophysical Research Letters*, **34**.
Beig, G., and V. Singh, 2007: Trends in tropical tropospheric column ozone from satellite data and MOZART model. *Geophys. Res. Lett.*, **34**, L17801.
Bell, G. D., and M. S. Halpert, 1998: Climate assessment for 1997. *Bulletin of the American Meteorological Society*, **79**, S1-S50.
Bengtsson, L., and K. I. Hodges, 2011: On the evaluation of temperature trends in the tropical troposphere. *Climate Dynamics*, **36**, 419-430.
Bengtsson, L., S. Hagemann, and K. I. Hodges, 2004: Can climate trends be calculated from reanalysis data? *Journal of Geophysical Research-Atmospheres*, **109**.
Beniston, M., 2009: Decadal-scale changes in the tails of probability distribution functions of climate variables in Switzerland. *International Journal of Climatology*, **29**, 1362-1368.
Benito, G., T. Ouarda, and A. Bardossy, 2005: Applications of palaeoflood hydrology and historical data in flood risk analysis. *Journal of Hydrology*, **313**, 1-2.
Berg, W., T. L'Ecuyer, and J. M. Haynes, 2010: The distribution of rainfall over oceans from spaceborne radars. (vol 49, pg 535, 2010). *Journal of Applied Meteorology and Climatology*, **49**, 1063-1063.
Berry, D. I., and E. C. Kent, 2009: A NEW AIR-SEA INTERACTION GRIDDED DATASET FROM ICOADS WITH UNCERTAINTY ESTIMATES. *Bulletin of the American Meteorological Society*, **90**, 645-+.
Berry, D. I., E. C. Kent, and P. K. Taylor, 2004: An analytical model of heating errors in marine air temperatures from ships. *Journal of Atmospheric and Oceanic Technology*, **21**, 1198-1215.
Birner, T., 2010: Recent widening of the tropical belt from global tropopause statistics: Sensitivities. *Journal of Geophysical Research-Atmospheres*, **115**.
Bitz, C. M., and Q. Fu, 2008: Arctic warming aloft is data set dependent. *Nature*, **455**, E3-E4.
Black, E., and R. Sutton, 2007: The influence of oceanic conditions on the hot European summer of 2003. *Climate Dynamics*, **28**, 53-66.
Boden, T. A., G. Marland, and R. J. Andres, 10.3334/CDIAC/00001_V2010. Global, Regional, and National Fossil-Fuel CO_2 Emissions.
Bohm, R., P. D. Jones, J. Hiebl, D. Frank, M. Brunetti, and M. Maugeri, 2010: The early instrumental warm-bias: a solution for long central European temperature series 1760-2007. *Climatic Change*, **101**, 41-67.
Bonisch, H., A. Engel, J. Curtius, T. Birner, and P. Hoor, 2009: Quantifying transport into the lowermost stratosphere using simultaneous in-situ measurements of SF6 and CO2. *Atmospheric Chemistry and Physics*, **9**, 5905-5919.
Bosilovich, M. G., Robertson, F. R., Chen, J., 2011: Global Energy and Water Budgets in MERRA. *J. Climate*, **24**, 5721-5739.

Bottomley, M., C. K. Folland, J. Hsiung, R. E. Newell, and D. E. Parker, 1990: Global ocean surface temperature atlas "GOSTA", 20pp pp.
Bousquet, P., 2011: Source attribution of the changes in atmospheric methane for 2006–2008. *Atmos. Chem. Phys. Discuss.*, **10**, 27603-27630.
Brogniez, H., R. Roca, and L. Picon, 2009: Study of the Free Tropospheric Humidity Interannual Variability Using Meteosat Data and an Advection-Condensation Transport Model. *Journal of Climate*, **22**, 6773-6787.
Brohan, P., R. Allan, J. E. Freeman, A. M. Waple, D. Wheeler, C. Wilkinson, and S. Woodruff, 2009: MARINE OBSERVATIONS OF OLD WEATHER. *Bulletin of the American Meteorological Society*, **90**, 219-+.
Bronnimann, S., 2009: Early twentieth-century warming. *Nature Geoscience*, **2**, 735-736.
Bronnimann, S., et al., 2009: Variability of large-scale atmospheric circulation indices for the northern hemisphere during the past 100 years. *Meteorologische Zeitschrift*, **18**, 379-396.
Brooks, H. E., and N. Dotzek, 2008: The spatial distribution of severe convective storms and an analysis of their secular changes. *Climate Extremes and Society*, H. F. Diaz, and R. J. Murnane, Eds., Cambridge University Press, 35-53.
Brown, P. J., R. S. Bradley, and F. T. Keimig, 2010: Changes in Extreme Climate Indices for the Northeastern United States, 1870-2005. *Journal of Climate*, **23**, 6555-6572.
Brown, S. J., J. Caesar, and C. A. T. Ferro, 2008: Global changes in extreme daily temperature since 1950. *Journal of Geophysical Research-Atmospheres*, **113**.
Brownscombe, J. L., J. Nash, G. Vaughan, and C. F. Rogers, 1985: SOLAR TIDES IN THE MIDDLE ATMOSPHERE .1. DESCRIPTION OF SATELLITE-OBSERVATIONS AND COMPARISON WITH THEORETICAL CALCULATIONS AT EQUINOX. *Quarterly Journal of the Royal Meteorological Society*, **111**, 677-689.
Brunet, M., and P. Jones, 2011: Data rescue initiatives: bringing historical climate data into the 21st century. *Climate Research*, **47**, 29-40.
Brunet, M., et al., 2011: The minimization of the screen bias from ancient Western Mediterranean air temperature records: an exploratory statistical analysis. *International Journal of Climatology*, **31**, 1879-1895.
Bunge, L., and A. J. Clarke, 2009: A Verified Estimation of the El Nino Index Nino-3.4 since 1877. *Journal of Climate*, **22**, 3979-3992.
Burn, D. H., and N. M. Hesch, 2007: Trends in evaporation for the Canadian prairies. *Journal of Hydrology*, **336**, 61-73.
Caesar, J., L. Alexander, and R. Vose, 2006: Large-scale changes in observed daily maximum and minimum temperatures: Creation and analysis of a new gridded data set. *Journal of Geophysical Research-Atmospheres*, **111**.
Callaghan, J., and S. B. Power, 2011: Variability and decline in the number of severe tropical cyclones making land-fall over eastern Australia since the late nineteenth century. *Climate Dynamics*, **37**, 647-662.
Canada, 2011: Canadian Smog Science Assessment - Highlights and Key Messages., tbd pp.
Canadell, J., et al., 2007: Contributions to accelerating atmospheric CO2 growth from economic activity, carbon intensity, and efficiency of natural sinks. *Proceedings of the National Academy of Sciences of the United States of America*, DOI 10.1073/pnas.0702737104. 18866-18870.
Cane, M. A., 1986: EL-NINO. *Annual Review of Earth and Planetary Sciences*, **14**, 43-70.
Cane, M. A., S. E. Zebiak, and S. C. Dolan, 1986: Experimental forecasts of El Nino. *Nature*, **321**, 827-832.
Cao, Z. H., 2008: Severe hail frequency over Ontario, Canada: Recent trend and variability. *Geophysical Research Letters*, **35**.
Cardone, V. J., J. G. Greenwood, and M. A. Cane, 1990: ON TRENDS IN HISTORICAL MARINE WIND DATA. *Journal of Climate*, **3**, 113-127.
Carslaw, K. S., O. Boucher, D. Spracklen, G. Mann, J. G. Rae, S. Woodward, and M. Kumala, 2010: A review of natural aerosol interactions and feedbacks within the Earth System,. *Atmospheric Chemistry and Physics*, **10**, 1701-1737.
Casey, K. S., T. B. Brandon, P. Cornillon, and R. Evans, 2010: The Past, Present and Future of the AVHRR Pathfinder SST Program. *Oceanography from Space: Revisited*, V. Barale, J. F. R. Gower, and L. Alberotanza, Eds., Springer.
CASTNET, 2010: Clean Air Status and Trends Network (CASTNET) 2008 Annual Report, 80 pp.
Cavazos, T., C. Turrent, and D. P. Lettenmaier, 2008: Extreme precipitation trends associated with tropical cyclones in the core of the North American monsoon. *Geophysical Research Letters*, **35**.
Cermak, J., M. Wild, R. Knutti, M. I. Mishchenko, and A. K. Heidinger, 2010: Consistency of global satellite-derived aerosol and cloud data sets with recent brightening observations. *Geophys. Res. Lett.*, **37**, L21704.
Chan, E., 2009: Regional ground-level ozone trends in the context of meteorological influences across Canada and the eastern United States from 1997 to 2006. *J. Geophys. Res.*, **114**, D05301.
Chan, E., and R. J. Vet, 2010: Baseline levels and trends of ground level ozone in Canada and the United States. *Atmos. Chem. Phys.*, **10**, 8629-8647.
Chan, J. C. L., and M. Xu, 2009: Inter-annual and inter-decadal variations of landfalling tropical cyclones in East Asia. Part I: time series analysis. *International Journal of Climatology*, **29**, 1285-1293.
Chandler, R. E., and E. M. Scott, 2011: *Statistical Methods for Trend Detection and Analysis in the Environmental Sciences.* Wiley.

Chang, E. K. M., 2007: Assessing the increasing trend in Northern Hemisphere winter storm track activity using surface ship observations and a statistical storm track model. *Journal of Climate*, **20**, 5607-5628.
——, 2009: Are band-pass variance statistics useful measures of storm track activity? Re-examining storm track variability associated with the NAO using multiple storm track measures. *Climate Dynamics*, **33**, 277-296.
Chang, E. K. M., and Y. J. Guo, 2007: Is the number of North Atlantic tropical cyclones significantly underestimated prior to the availability of satellite observations? *Geophysical Research Letters*, **34**.
Che, H. Z., et al., 2005: Analysis of 40 years of solar radiation data from China, 1961-2000. *Geophysical Research Letters*, **32**, L06803.
Chen, J. Y., B. E. Carlson, and A. D. Del Genio, 2002: Evidence for strengthening of the tropical general circulation in the 1990s. *Science*, **295**, 838-841.
Chen, J. Y., A. D. Del Genio, B. E. Carlson, and M. G. Bosilovich, 2008: The spatiotemporal structure of twentieth-century climate variations in observations and reanalyses. Part I: Long-term trend. *Journal of Climate*, **21**, 2611-2633.
Chiacchio, M., and M. Wild, 2010: Influence of NAO and clouds on long-term seasonal variations of surface solar radiation in Europe. *Journal of Geophysical Research-Atmospheres*, **115**, D00d22.
Choi, G., et al., 2009: Changes in means and extreme events of temperature and precipitation in the Asia-Pacific Network region, 1955-2007. *International Journal of Climatology*, **29**, 1906-1925.
Christy, J. R., and W. B. Norris, 2006: Satellite and VIZ-radiosonde intercomparisons for diagnosis of nonclimatic influences. *Journal of Atmospheric and Oceanic Technology*, **23**, 1181-1194.
——, 2009: Discontinuity Issues with Radiosonde and Satellite Temperatures in the Australian Region 1979-2006. *Journal of Atmospheric and Oceanic Technology*, **26**, 508-522.
Christy, J. R., W. B. Norris, and R. T. McNider, 2009: Surface Temperature Variations in East Africa and Possible Causes. *Journal of Climate*, **22**, 3342-3356.
Christy, J. R., W. B. Norris, K. Redmond, and K. P. Gallo, 2006: Methodology and results of calculating central california surface temperature trends: Evidence of human-induced climate change? *Journal of Climate*, **19**, 548-563.
Christy, J. R., W. B. Norris, R. W. Spencer, and J. J. Hnilo, 2007: Tropospheric temperature change since 1979 from tropical radiosonde and satellite measurements. *Journal of Geophysical Research-Atmospheres*, **112**.
Christy, J. R., D. E. Parker, S. J. Brown, I. Macadam, M. Stendel, and W. B. Norris, 2001: Differential trends in tropical sea surface and atmospheric temperatures since 1979. *Geophysical Research Letters*, **28**, 183-186.
Christy, J. R., Herman, B, Pielke, R., Klotzbach, P., McNider, R. T., Hnilo, J. J., Spencer, R. W., Chase, T., Douglass, D., 2010: What do observational datasets say about modeled tropospheric temperature trends since 1979? , 2148-2169.
Christy, J. R., Spencer, R. W., Norris, W. B., 2011: The role of remote sensing in monitoring global bulk tropospheric temperatures.
Chuang, H., X. Huang, and K. Minschwaner, 2010: Interannual variations of tropical upper tropospheric humidity and tropical rainy-region SST: Comparisons between models, reanalyses, and observations. *Journal of Geophysical Research-Atmospheres*, **115**, -.
Chung, E. S., and B. J. Soden, 2010: Investigating the Influence of Carbon Dioxide and the Stratosphere on the Long-Term Tropospheric Temperature Monitoring from HIRS. *Journal of Applied Meteorology and Climatology*, **49**, 1927-1937.
Chung, E. S., D. Yeomans, and B. J. Soden, 2010: An assessment of climate feedback processes using satellite observations of clear-sky OLR. *Geophysical Research Letters*, **37**.
Clark, R. T., S. J. Brown, and J. M. Murphy, 2006: Modeling northern hemisphere summer heat extreme changes and their uncertainties using a physics ensemble of climate sensitivity experiments. *Journal of Climate*, **19**, 4418-4435.
Clarke, A. D., and V. N. Kapustin, 2002: A Pacific Aerosol Survey. Part I: A Decade of Data on Particle Production, Transport, Evolution, and Mixing in the Troposphere*. *Journal of the Atmospheric Sciences*, **59**, 363-382.
Clement, A. C., and B. Soden, 2005: The sensitivity of the tropical-mean radiation budget. *Journal of Climate*, **18**, 3189-3203.
Clement, A. C., R. Burgman, and J. R. Norris, 2009: Observational and Model Evidence for Positive Low-Level Cloud Feedback. *Science*, **325**, 460-464.
CMA, 2007: Atlas of China disastrous weather and climate.
Cohen, J., M. Barlow, and K. Saito, 2009: Decadal Fluctuations in Planetary Wave Forcing Modulate Global Warming in Late Boreal Winter. *Journal of Climate*, **22**, 4418-4426.
Cohn, T. A., and H. F. Lins, 2005: Nature's style: Naturally trendy. *Geophysical Research Letters*, **32**.
Coles, S., 2001: *An Introduction to Statistical Modeling of Extreme Values.* Springer-Verlag, 208 pp.
Compo, G. P., et al., 2011: The Twentieth Century Reanalysis Project. *Q. J. Roy. Meteorol. Soc.*, **137**, 1-28.
Cooper, O. R., et al., 2010: Increasing springtime ozone mixing ratios in the free troposphere over western North America. *Nature*, **463**, 344-348.
Copsey, D., R. Sutton, and J. R. Knight, 2006: Recent trends in sea level pressure in the Indian Ocean region. *Geophysical Research Letters*, **33**.

Costa, A. C., and A. Soares, 2009: Trends in extreme precipitation indices derived from a daily rainfall database for the South of Portugal. *International Journal of Climatology*, **29**, 1956-1975.
Croci-Maspoli, M., C. Schwierz, and H. C. Davies, 2007a: A multifaceted climatology of atmospheric blocking and its recent linear trend. *Journal of Climate*, **20**, 633-649.
——, 2007b: Atmospheric blocking: space-time links to the NAO and PNA. *Climate Dynamics*, **29**, 713-725.
Crutzen, P., A. Mosier, K. Smith, and W. Winiwarter, 2008: N2O release from agro-biofuel production negates global warming reduction by replacing fossil fuels. *Atmospheric Chemistry and Physics*. 389-395.
Cui, J., S. Pandey Deolal, M. Sprenger, S. Henne, J. Staehelin, M. Steinbacher, and P. Nédélec, 2010: Free tropospheric ozone changes over Europe as observed at Jungfraujoch (1990-2008): An analysis based on backward trajectories. *J. Geophys. Res.*, **116**, D10304.
Cunderlik, J. M., and T. Ouarda, 2009: Trends in the timing and magnitude of floods in Canada. *Journal of Hydrology*, **375**, 471-480.
Cutforth, H. W., and D. Judiesch, 2007: Long-term changes to incoming solar energy on the Canadian Prairie. *Agricultural and Forest Meteorology*, **145**, 167-175.
Dai, A., 2006: Recent climatology, variability, and trends in global surface humidity. *Journal of Climate*, **19**, 3589-3606.
Dai, A., 2011a: Characteristics and trends in various forms of the Palmer Drought Severity Index during 1900-2008. *Journal of Geophysical Research-Atmospheres*, **116**.
Dai, A., K. E. Trenberth, and T. T. Qian, 2004: A global dataset of Palmer Drought Severity Index for 1870-2002: Relationship with soil moisture and effects of surface warming. *Journal of Hydrometeorology*, **5**, 1117-1130.
Dai, A., T. T. Qian, K. E. Trenberth, and J. D. Milliman, 2009: Changes in Continental Freshwater Discharge from 1948 to 2004. *Journal of Climate*, **22**, 2773-2792.
Dai, A. G., 2011b: Drought under global warming: a review. *Wiley Interdisciplinary Reviews-Climate Change*, **2**, 45-65.
Dai, A. G., J. H. Wang, P. W. Thorne, D. E. Parker, L. Haimberger, and X. L. L. Wang, 2011: A New Approach to Homogenize Daily Radiosonde Humidity Data. *Journal of Climate*, **24**, 965-991.
Das, L., J. D. Annan, J. C. Hargreaves, and S. Emori, 2011: Centennial scale warming over Japan: are the rural stations really rural? *Atmospheric Science Letters*, 10.1002/asl.350.
Davidson, E., 2009: The contribution of manure and fertilizer nitrogen to atmospheric nitrous oxide since 1860. *Nature Geoscience*, **2**, 659-662.
Davis, S. M., and K. H. Rosenlof, 2011: A multi-diagnostic intercomparison of tropical width time series using reanalyses and satellite observations. *J. Climate*. doi: http://dx.doi.org/10.1175/JCLI-D-1111-00127.00121.
De Laat, A. T. J., and A. N. Maurellis, 2006: Evidence for influence of anthropogenic surface processes on lower tropospheric and surface temperature trends. *International Journal of Climatology*, **26**, 897-913.
de Laat, A. T. J., I. Aben, and G. J. Roelofs, 2005: A model perspective on total tropospheric O3 column variability and implications for satellite observations. *J. Geophys. Res.*, **110**, D13303.
de Ruyter de Wildt, M., H. J. Eskes, and K. F. Boersma, 2011: The global economic cycle and satellite-derived NO2 trends over shipping lanes,. *Geophys. Res. Lett.,*, **2011GL049541, submitted**.
Dee, D. P., et al., 2011: The ERA-Interim reanalysis: configuration and performance of the data assimilation system. *Quarterly Journal of the Royal Meteorological Society*, **137**, 553-597.
Deeds, D., et al., 2008: Evidence for crustal degassing of CF4 and SF6 in Mojave Desert groundwaters. *Geochimica Et Cosmochimica Acta*, DOI 10.1016/j.gca.2007.11.027. 999-1013.
DeGaetano, A. T., 2009: Time-Dependent Changes in Extreme-Precipitation Return-Period Amounts in the Continental United States. *Journal of Applied Meteorology and Climatology*, **48**, 2086-2099.
Delgado, J. M., H. Apel, and B. Merz, 2010: Flood trends and variability in the Mekong river. *Hydrology and Earth System Sciences*, **14**, 407-418.
Della-Marta, P. M., M. R. Haylock, J. Luterbacher, and H. Wanner, 2007a: Doubled length of western European summer heat waves since 1880. *Journal of Geophysical Research-Atmospheres*, **112**.
Della-Marta, P. M., J. Luterbacher, H. von Weissenfluh, E. Xoplaki, M. Brunet, and H. Wanner, 2007b: Summer heat waves over western Europe 1880-2003, their relationship to large-scale forcings and predictability. *Climate Dynamics*, **29**, 251-275.
Della-Marta, P. M., H. Mathis, C. Frei, M. A. Liniger, J. Kleinn, and C. Appenzeller, 2009: The return period of wind storms over Europe. *International Journal of Climatology*, **29**, 437-459.
Deser, C., A. S. Phillips, and M. A. Alexander, 2010a: Twentieth century tropical sea surface temperature trends revisited. *Geophysical Research Letters*, **37**.
Deser, C., M. A. Alexander, S. P. Xie, and A. S. Phillips, 2010b: Sea Surface Temperature Variability: Patterns and Mechanisms. *Annual Review of Marine Science*, **2**, 115-143.
Dessler, A. E., 2010: A Determination of the Cloud Feedback from Climate Variations over the Past Decade. *Science*, **330**, 1523-1527.
Dessler, A. E., Z. Zhang, and P. Yang, 2008: Water-vapor climate feedback inferred from climate fluctuations, 2003-2008. *Geophysical Research Letters*, **35**.
Diffenbaugh, N. S., J. S. Pal, F. Giorgi, and X. J. Gao, 2007: Heat stress intensification in the Mediterranean climate change hotspot. *Geophysical Research Letters*, **34**.

Ding, T., W. H. Qian, and Z. W. Yan, 2010: Changes in hot days and heat waves in China during 1961-2007. *International Journal of Climatology*, **30**, 1452-1462.
Ding, Y. H., G. Y. Ren, Z. C. Zhao, Y. Xu, Y. Luo, Q. P. Li, and J. Zhang, 2007: Detection, causes and projection of climate change over China: An overview of recent progress. *Advances in Atmospheric Sciences*, **24**, 954-971.
Dlugokencky, E., et al., 2009: Observational constraints on recent increases in the atmospheric CH4 burden. *Geophysical Research Letters*, ARTN L18803, DOI 10.1029/2009GL039780. -.
Dole, R., et al., 2011: Was there a basis for anticipating the 2010 Russian heat wave? *Geophysical Research Letters*, **38**.
Donat, M. G., D. Renggli, S. Wild, L. V. Alexander, G. C. Leckebusch, and U. Ulbrich, 2011: Reanalysis suggests long-term upward trends in European storminess since 1871. *Geophysical Research Letters*, **38**.
Dong, L., T. J. Vogelsang, and S. J. Colucci, 2008: Interdecadal trend and ENSO-related interannual variability in Southern Hemisphere blocking. *Journal of Climate*, **21**, 3068-3077.
Donkelaar van, A., R. V. Martin, M. Brauer, R. Kahn, R. Levy, Verduzco, and P. J. Villeneuve, 2010: Global Estimates of Ambient Fine Particulate Matter Concentrations from Satellite-Based Aerosol Optical Depth: Development and Application. *Environmental Health Perspecitives*, **118, doi: 10.1289/ehp.0901623**, 847–855.
Donlon, C., et al., 2007: The global ocean data assimilation experiment high-resolution sea surface temperature pilot project. *Bulletin of the American Meteorological Society*, **88**, 1197-1213.
Doswell, C. A., H. E. Brooks, and M. P. Kay, 2005: Climatological estimates of daily local nontornadic severe thunderstorm probability for the United States. *Weather and Forecasting*, **20**, 577-595.
Douglass, A., et al., 2008a: Relationship of loss, mean age of air and the distribution of CFCs to stratospheric circulation and implications for atmospheric lifetimes. *Journal of Geophysical Research-Atmospheres*, ARTN D14309, DOI 10.1029/2007JD009575. -.
Douglass, D. H., J. R. Christy, B. D. Pearson, and S. F. Singer, 2008b: A comparison of tropical temperature trends with model predictions. *International Journal of Climatology*, **28**, 1693-1701.
Du, Y., and S. Xie, 2008: Role of atmospheric adjustments in the tropical Indian Ocean warming during the 20th century in climate models. *Geophysical Research Letters*, **35**, -.
Du, Y., S. Xie, G. Huang, and K. Hu, 2009: Role of Air-Sea Interaction in the Long Persistence of El Nino-Induced North Indian Ocean Warming. *Journal of Climate*, **22**, 2023-2038.
Duan, A. M., and G. X. Wu, 2006: Change of cloud amount and the climate warming on the Tibetan Plateau. *Geophysical Research Letters*, **33**.
Dufek, A. S., and T. Ambrizzi, 2008: Precipitation variability in Sao Paulo State, Brazil. *Theoretical and Applied Climatology*, **93**, 167-178.
Durao, R. M., M. J. Pereira, A. C. Costa, J. Delgado, G. del Barrio, and A. Soares, 2010: Spatial-temporal dynamics of precipitation extremes in southern Portugal: a geostatistical assessment study. *International Journal of Climatology*, **30**, 1526-1537.
Durre, I., C. N. Williams, X. G. Yin, and R. S. Vose, 2009: Radiosonde-based trends in precipitable water over the Northern Hemisphere: An update. *Journal of Geophysical Research-Atmospheres*, **114**.
Durre, I., M. J. Menne, B. E. Gleason, T. G. Houston, and R. S. Vose, 2010: Comprehensive Automated Quality Assurance of Daily Surface Observations. *Journal of Applied Meteorology and Climatology*, **49**, 1615-1633.
Dutton, E. G., D. W. Nelson, R. S. Stone, D. Longenecker, G. Carbaugh, J. M. Harris, and J. Wendell, 2006: Decadal variations in surface solar irradiance as observed in a globally remote network. *Journal of Geophysical Research-Atmospheres*, **111**, D19101.
EANET, 2011: EANET Data Report on the Acid Deposition in the East Asian Region 2009.
Easterling, D., and M. Wehner, 2009: Is the climate warming or cooling? *Geophysical Research Letters*, ARTN L08706, DOI 10.1029/2009GL037810. -.
Eastman, R., S. G. Warren, and C. J. Hahn, submitted: Variations in cloud cover and cloud types over the ocean from surface observations, 1954-2008. *J. Climate*.
Efthymiadis, D., C. M. Goodess, and P. D. Jones, 2011: Trends in Mediterranean gridded temperature extremes and large-scale circulation influences. *Natural Hazards and Earth System Sciences*, **11**, 2199-2214.
Efthymiadis, D. A., and P. D. Jones, 2010: Assessment of Maximum Possible Urbanization Influences on Land Temperature Data by Comparison of Land and Marine Data around Coasts. *Atmosphere*, **1**, 51-61.
Ellis, T. D., T. L'Ecuyer, J. M. Haynes, and G. L. Stephens, 2009: How often does it rain over the global oceans? The perspective from CloudSat. *Geophysical Research Letters*, **36**.
Elsner, J. B., J. P. Kossin, and T. H. Jagger, 2008: The increasing intensity of the strongest tropical cyclones. *Nature*, **455**, 92-95.
Emanuel, K., 2007: Environmental factors affecting tropical cyclone power dissipation. *Journal of Climate*, **20**, 5497-5509.
Embury, O., and C. J. Merchant, 2011: Reprocessing for Climate of Sea Surface Temperature from the Along-Track Scanning Radiometers: A New Retrieval Scheme. *Remote Sensing Environment*, 10.1016/j.rse.2010.11.020.
Embury, O., C. J. Merchant, and G. K. Corlett, 2011: A reprocessing for Climate of Sea Surface Temperature from the Along-Track Scanning Radiometers: Preliminary validation, accounting for skin and diurnal variability. *Remote Sensing Environment*, 10.1016/j.rse.2011.02.028.
EMEP, 2010: EMEP Status report 4/2010, Transboundary Particulate Matter in Europe.

Emery, W. J., D. J. Baldwin, P. Schlussel, and R. W. Reynolds, 2001: Accuracy of in situ sea surface temperatures used to calibrate infrared satellite measurements. *Journal of Geophysical Research-Oceans*, **106**, 2387-2405.
Endo, N., and T. Yasunari, 2006: Changes in low cloudiness over China between 1971 and 1996. *Journal of Climate*, **19**, 1204-1213.
Enfield, D. B., A. M. Mestas-Nunez, and P. J. Trimble, 2001: The Atlantic multidecadal oscillation and its relation to rainfall and river flows in the continental US. *Geophysical Research Letters*, **28**, 2077-2080.
Engel, A., et al., 2009: Age of stratospheric air unchanged within uncertainties over the past 30 years. *Nature Geoscience*, **2**, 28-31.
Etheridge, D., L. Steele, R. Francey, and R. Langenfelds, 1998: Atmospheric methane between 1000 AD and present: Evidence of anthropogenic emissions and climatic variability. *Journal of Geophysical Research-Atmospheres*. 15979-15993.
Etheridge, D. M., L. P. Steele, R. L. Langenfelds, R. J. Francey, J. M. Barnola, and V. I. Morgan, 1996: Natural and anthropogenic changes in atmospheric CO2 over the last 1000 years from air in Antarctic ice and firn. *Journal of Geophysical Research-Atmospheres*. 4115-4128.
Evan, A. T., A. K. Heidinger, and D. J. Vimont, 2007: Arguments against a physical long-term trend in global ISCCP cloud amounts. *Geophysical Research Letters*, **34**, L04701.
Fall, S., D. Niyogi, A. Gluhovsky, R. A. Pielke, E. Kalnay, and G. Rochon, 2010: Impacts of land use land cover on temperature trends over the continental United States: assessment using the North American Regional Reanalysis. *International Journal of Climatology*, **30**, 1980-1993.
Fall, S., A. Watts, J. Nielsen-Gammon, E. Jones, D. Niyogi, J. R. Christy, and R. A. Pielke, 2011: Analysis of the impacts of station exposure on the US Historical Climatology Network temperatures and temperature trends. *Journal of Geophysical Research-Atmospheres*, **116**.
Favre, A., and A. Gershunov, 2006: Extra-tropical cyclonic/anticyclonic activity in North-Eastern Pacific and air temperature extremes in Western North America. *Climate Dynamics*, **26**, 617-629.
Fekete, B. M., C. J. Vorosmarty, and W. Grabs, 2002: High-resolution fields of global runoff combining observed river discharge and simulated water balances. *Global Biogeochemical Cycles*, **16**.
Feng, S., and Q. Hu, 2007: Changes in winter snowfall/precipitation ratio in the contiguous United States. *Journal of Geophysical Research-Atmospheres*, **112**.
Ferranti, L., and P. Viterbo, 2006: The European summer of 2003: Sensitivity to soil water initial conditions. *Journal of Climate*. 3659-3680.
Ferretti, D., et al., 2005: Unexpected changes to the global methane budget over the past 2000 years. *Science*, DOI 10.1126/science.1115193. 1714-1717.
Fischer, E. M., and C. Schar, 2010: Consistent geographical patterns of changes in high-impact European heatwaves. *Nature Geoscience*, **3**, 398-403.
Fischer, E. M., S. I. Seneviratne, D. Luthi, and C. Schar, 2007a: Contribution of land-atmosphere coupling to recent European summer heat waves. *Geophysical Research Letters*, **34**.
Fischer, E. M., S. I. Seneviratne, P. L. Vidale, D. Luthi, and C. Schar, 2007b: Soil moisture - Atmosphere interactions during the 2003 European summer heat wave. *Journal of Climate*, **20**, 5081-5099.
Foelsche, U., B. Pirscher, M. Borsche, G. Kirchengast, and J. Wickert, 2009: Assessing the Climate Monitoring Utility of Radio Occultation Data: From CHAMP to FORMOSAT-3/COSMIC. *Terrestrial Atmospheric and Oceanic Sciences*, **20**, 155-170.
Fogt, R. L., J. Perlwitz, A. J. Monaghan, D. H. Bromwich, J. M. Jones, and G. J. Marshall, 2009: Historical SAM Variability. Part II: Twentieth-Century Variability and Trends from Reconstructions, Observations, and the IPCC AR4 Models. *Journal of Climate*, **22**, 5346-5365.
Folland, C. K., and D. E. Parker, 1995: CORRECTION OF INSTRUMENTAL BIASES IN HISTORICAL SEA-SURFACE TEMPERATURE DATA. *Quarterly Journal of the Royal Meteorological Society*, **121**, 319-367.
Folland, C. K., D. E. Parker, A. Colman, and W. R., 1999: Large scale modes of ocean surface temperature since the late nineteenth century. *Beyond El Nino: Decadal and Interdecadal Climate Variability*, A. Navarra, Ed., Springer-Verlag, 73-102.
Folland, C. K., J. Knight, H. W. Linderholm, D. Fereday, S. Ineson, and J. W. Hurrell, 2009: The Summer North Atlantic Oscillation: Past, Present, and Future. *Journal of Climate*, **22**, 1082-1103.
Forster, P. M., et al., 2011: Stratospheric changes and climate, Chapter 4 in Scientific Assessment of Ozone Depletion: 2010, 516 pp. pp.
Forster, P. M. D., and S. Solomon, 2003: Observations of a "weekend effect" in diurnal temperature range. *Proceedings of the National Academy of Sciences of the United States of America*, **100**, 11225-11230.
Fowler, D., R. Smith, J. Muller, N. Cape, M. Sutton, J. W. Erisman, and H. Fagerli, 2007: Long Term Trends in Sulphur and Nitrogen Deposition in Europe and the Cause of Non-linearities. *Water Air Soil Pollution*, **7**, 41–47.
Frankenberg, C., et al., 2011: Global column-averaged methane mixing ratios from 2003 to 2009 as derived from SCIAMACHY: Trends and variability. *Journal of Geophysical Research-Atmospheres*, **116**.
Frauenfeld, O. W., and R. E. Davis, 2003: Northern Hemisphere circumpolar vortex trends and climate change implications. *Journal of Geophysical Research-Atmospheres*, **108**.
Frederiksen, J. S., and C. S. Frederiksen, 2007: Interdecadal changes in southern hemisphere winter storm track modes. *Tellus Series a-Dynamic Meteorology and Oceanography*, **59**, 599-617.

Free, M., D. J. Seidel, J. K. Angell, J. Lanzante, I. Durre, and T. C. Peterson, 2005: Radiosonde Atmospheric Temperature Products for Assessing Climate (RATPAC): A new data set of large-area anomaly time series. *Journal of Geophysical Research-Atmospheres*, **110**.

Fu, G. B., S. P. Charles, and J. J. Yu, 2009a: A critical overview of pan evaporation trends over the last 50 years. *Climatic Change*, **97**, 193-214.

Fu, G. B., S. P. Charles, J. J. Yu, and C. M. Liu, 2009b: Decadal Climatic Variability, Trends, and Future Scenarios for the North China Plain. *Journal of Climate*, **22**, 2111-2123.

Fu, Q., and P. Lin, 2011: Poleward shift of subtropical jets inferred from satellite-observed lower stratospheric temperatures. *J. Climate*, **24**, 5597-5603.

Fu, Q., C. M. Johanson, S. G. Warren, and D. J. Seidel, 2004: Contribution of stratospheric cooling to satellite-inferred tropospheric temperature trends. *Nature*, **429**, 55-58.

Fu, Q., C. M. Johanson, J. M. Wallace, and T. Reichler, 2006: Enhanced mid-latitude tropospheric warming in satellite measurements. *Science*, **312**, 1179-1179.

Fueglistaler, S., and P. H. Haynes, 2005: Control of interannual and longer-term variability of stratospheric water vapor. *Journal of Geophysical Research-Atmospheres*, **110**.

Fueglistaler, S., A. E. Dessler, T. J. Dunkerton, I. Folkins, Q. Fu, and P. W. Mote, 2009: TROPICAL TROPOPAUSE LAYER. *Reviews of Geophysics*, **47**.

Fujibe, F., 2009: Detection of urban warming in recent temperature trends in Japan. *International Journal of Climatology*, **29**, 1811-1822.

Fujiwara, M., et al., 2010: Seasonal to decadal variations of water vapor in the tropical lower stratosphere observed with balloon-borne cryogenic frost point hygrometers. *Journal of Geophysical Research-Atmospheres*, **115**.

Fyfe, J. C., 2003: Extratropical southern hemisphere cyclones: Harbingers of climate change? *Journal of Climate*, **16**, 2802-2805.

Garcia-Herrera, R., J. Diaz, R. M. Trigo, J. Luterbacher, and E. M. Fischer, 2010: A Review of the European Summer Heat Wave of 2003. *Critical Reviews in Environmental Science and Technology*, **40**, 267-306.

Geng, Q. Z., and M. Sugi, 2001: Variability of the North Atlantic cyclone activity in winter analyzed from NCEP-NCAR reanalysis data. *Journal of Climate*, **14**, 3863-3873.

Gettelman, A., and Q. Fu, 2008: Observed and simulated upper-tropospheric water vapor feedback. *Journal of Climate*, **21**, 3282-3289.

Gilge, S., C. Plass-Duelmer, W. Fricke, A. Kaiser, L. Ries, B. Buchmann, and M. Steinbacher, 2010: Ozone, carbon monoxide and nitrogen oxides time series at four alpine GAW mountain stations in central Europe. *Atmospheric Chemistry and Physics*, **10**, 12295-12316.

Gilgen, H., A. Roesch, M. Wild, and A. Ohmura, 2009: Decadal changes in shortwave irradiance at the surface in the period from 1960 to 2000 estimated from Global Energy Balance Archive Data. *Journal of Geophysical Research-Atmospheres*, **114**, D00d08.

Gillett, N. P., and P. A. Stott, 2009: Attribution of anthropogenic influence on seasonal sea level pressure. *Geophysical Research Letters*, **36**.

Giorgi, F., and R. Francisco, 2000: Evaluating uncertainties in the prediction of regional climate change. *Geophysical Research Letters*, **27**, 1295-1298.

Giorgi, F., E. S. Im, E. Coppola, N. S. Diffenbaugh, X. J. Gao, L. Mariotti, and Y. Shi, 2011: Higher Hydroclimatic Intensity with Global Warming. *Journal of Climate*, **24**, 5309-5324.

Gleason, K. L., J. H. Lawrimore, D. H. Levinson, T. R. Karl, and D. J. Karoly, 2008: A revised US Climate Extremes Index. *Journal of Climate*, **21**, 2124-2137.

Gloor, M., J. Sarmiento, and N. Gruber, 2010: What can be learned about carbon cycle climate feedbacks from the CO2 airborne fraction? *Atmospheric Chemistry and Physics*, DOI 10.5194/acp-10-7739-2010. 7739-7751.

Gong, D. Y., and S. W. Wang, 1999: Definition of Antarctic Oscillation Index. *Geophysical Research Letters*, **26**, 459-462.

Gong, D. Y., C. H. Ho, D. L. Chen, Y. Qian, Y. S. Choi, and J. W. Kim, 2007: Weekly cycle of aerosol-meteorology interaction over China. *Journal of Geophysical Research-Atmospheres*, **112**, 9.

Graham, N. E., and H. F. Diaz, 2001: Evidence for intensification of North Pacific winter cyclones since 1948. *Bulletin of the American Meteorological Society*, **82**, 1869-1893.

Granier, C., and e. al., 2011: Evolution of anthropogenic and biomass burning emissions of air pollutants at global and regional scales during the 1980–2010 period. *Climatic Change*, **109**, 28.

Grant, A. N., S. Bronnimann, and L. Haimberger, 2008: Recent Arctic warming vertical structure contested. *Nature*, **455**, E2-E3.

Graversen, R. G., T. Mauritsen, M. Tjernstrom, E. Kallen, and G. Svensson, 2008: Vertical structure of recent Arctic warming. *Nature*, **451**, 53-U54.

Greally, B., et al., 2007: Observations of 1,1-difluoroethane (HFC-152a) at AGAGE and SOGE monitoring stations in 1994-2004 and derived global and regional emission estimates. *Journal of Geophysical Research-Atmospheres*, **112**, -.

Griffiths, G. M., et al., 2005: Change in mean temperature as a predictor of extreme temperature change in the Asia-Pacific region. *International Journal of Climatology*, **25**, 1301-1330.

Grody, N. C., K. Y. Vinnikov, M. D. Goldberg, J. T. Sullivan, and J. D. Tarpley, 2004: Calibration of multisatellite observations for climatic studies: Microwave Sounding Unit (MSU). *Journal of Geophysical Research-Atmospheres*, **109**.

Gruber, C., and L. Haimberger, 2008: On the homogeneity of radiosonde wind time series. *Meteorologische Zeitschrift*, **17**, 631-643.

Gulev, S., T. Jung, and E. Ruprecht, 2007: Estimation of the impact of sampling errors in the VOS observations on air-sea fluxes. Part II: Impact on trends and interannual variability. *Journal of Climate*, **20**, 302-315.

Gulev, S. K., O. Zolina, and S. Grigoriev, 2001: Extratropical cyclone variability in the Northern Hemisphere winter from the NCEP/NCAR reanalysis data. *Climate Dynamics*, **17**, 795-809.

Guo, H., M. Xu, and Q. Hub, 2010: Changes in near-surface wind speed in China: 1969–2005. *Int. J. Climatol.*, 10.1002/joc.2091.

Haimberger, L., 2004: Checking the temporal homogeneity of radiosonde data in the Alpine region using ERA-40 analysis feedback data. *Meteorologische Zeitschrift*, **13**, 123-129.

——, 2007: Homogenization of radiosonde temperature time series using innovation statistics. *Journal of Climate*, **20**, 1377-1403.

Haimberger, L., C. Tavolato, and S. Sperka, 2008: Toward elimination of the warm bias in historic radiosonde temperature records - Some new results from a comprehensive intercomparison of upper-air data. *Journal of Climate*, **21**, 4587-4606.

Haimberger, L., C. Tavolato, and S. Sperka, Submitted: Homogenization of the global radiosonde dataset through combined comparison with reanalysis background series and neighboring stations. *Journal of Climate*.

Hajj, G. A., et al., 2004: CHAMP and SAC-C atmospheric occultation results and intercomparisons. *Journal of Geophysical Research-Atmospheres*, **109**.

Häkkinen, S., P. B. Rhines, and D. L. Worthen, 2011: Atmospheric Blocking and Atlantic Multidecadal Ocean variability. *Science*, **334**, 655-659.

Hand, J. L., et al., 2011: IMPROVE, Spatial and Seasonal Patterns and Temporal Variability of Haze and its Constituents in the United States,, ISSN 0737-5352-0787 pp.

Hanna, E., J. Cappelen, R. Allan, T. Jonsson, F. Le Blancq, T. Lillington, and K. Hickey, 2008: New Insights into North European and North Atlantic Surface Pressure Variability, Storminess, and Related Climatic Change since 1830. *Journal of Climate*, **21**, 6739-6766.

Hansen, J., R. Ruedy, M. Sato, and K. Lo, 2010: GLOBAL SURFACE TEMPERATURE CHANGE. *Reviews of Geophysics*, **48**.

Hansen, J., et al., 2001: A closer look at United States and global surface temperature change. *Journal of Geophysical Research-Atmospheres*, **106**, 23947-23963.

Harries, J. E., and J. M. Futyan, 2006: On the stability of the Earth's radiative energy balance: Response to the Mt. Pinatubo eruption. *Geophysical Research Letters*, **33**.

Hatzianastassiou, N., C. Matsoukas, A. Fotiadi, K. G. Pavlakis, E. Drakakis, D. Hatzidimitriou, and I. Vardavas, 2005: Global distribution of Earth's surface shortwave radiation budget. *Atmospheric Chemistry and Physics*, **5**, 2847-2867.

Haylock, M. R., and C. M. Goodess, 2004: Interannual variability of european extreme winter rainfall and links with mean large-scale circulation. *International Journal of Climatology*, **24**, 759-776.

Haynes, J. M., T. S. L'Ecuyer, G. L. Stephens, S. D. Miller, C. Mitrescu, N. B. Wood, and S. Tanelli, 2009: Rainfall retrieval over the ocean with spaceborne W-band radar. *Journal of Geophysical Research-Atmospheres*, **114**.

He, W. Y., S. P. Ho, H. B. Chen, X. J. Zhou, D. Hunt, and Y. H. Kuo, 2009: Assessment of radiosonde temperature measurements in the upper troposphere and lower stratosphere using COSMIC radio occultation data. *Geophysical Research Letters*, **36**.

Heidinger, A. K., and M. J. Pavolonis, 2009: Gazing at Cirrus Clouds for 25 Years through a Split Window. Part I: Methodology. *Journal of Applied Meteorology and Climatology*, **48**, 1100-1116.

Held, I. M., and B. J. Soden, 2006: Robust responses of the hydrological cycle to global warming. *Journal of Climate*, **19**, 5686-5699.

Hess, P. G., and R. Zbinden, 2011: Stratospheric impact on tropospheric ozone variability and trends: 1990–2009. *Atmos. Chem. Phys. Discuss.*, **11**, 22719-22770.

Hidy, G. M., and G. T. Pennell, 2010: Multipollutant Air Quality Management: 2010 Critical Review. *J. Air & Waste Management Assocciation*, **60, DOI:10.3155/1047-3289.60.6.645**, 645–674.

Hinkelman, L. M., P. W. Stackhouse, B. A. Wielicki, T. P. Zhang, and S. R. Wilson, 2009: Surface insolation trends from satellite and ground measurements: Comparisons and challenges. *Journal of Geophysical Research-Atmospheres*, **114**, D00d20.

Hirsch, M. E., A. T. DeGaetano, and S. J. Colucci, 2001: An East Coast winter storm climatology. *Journal of Climate*, **14**, 882-899.

Hirschi, M., et al., 2011: Observational evidence for soil-moisture impact on hot extremes in southeastern Europe. *Nature Geoscience*, **4**, 17-21.

Ho, C. H., Y. S. Choi, and S. K. Hur, 2009a: Long-term changes in summer weekend effect over northeastern China and the connection with regional warming. *Geophysical Research Letters*, **36**.

Ho, S. P., W. He, and Y. H. Kuo, 2009b: *Construction of Consistent Temperature Records in the Lower Stratosphere Using Global Positioning System Radio Occultation Data and Microwave Sounding Measurements.* 10.1007/978-3-642-00321-9_17. 207-217 pp.

Ho, S. P., Y. H. Kuo, Z. Zeng, and T. C. Peterson, 2007: A comparison of lower stratosphere temperature from microwave measurements with CHAMP GPS RO data. *Geophysical Research Letters*, **34**.

Ho, S. P., M. Goldberg, Y. H. Kuo, C. Z. Zou, and W. Schreiner, 2009c: Calibration of Temperature in the Lower Stratosphere from Microwave Measurements Using COSMIC Radio Occultation Data: Preliminary Results. *Terrestrial Atmospheric and Oceanic Sciences*, **20**, 87-100.

Ho, S. P., et al., 2009d: Estimating the uncertainty of using GPS radio occultation data for climate monitoring: Intercomparison of CHAMP refractivity climate records from 2002 to 2006 from different data centers. *Journal of Geophysical Research-Atmospheres*, **114**.

Holben, B. N., et al., 1998: AERONET--A Federated Instrument Network and Data Archive for Aerosol Characterization. *Remote Sensing of Environment*, **66**, 1-16.

Holland, G. J., and P. J. Webster, 2007: Heightened tropical cyclone activity in the North Atlantic: natural variability or climate trend? *Philosophical Transactions of the Royal Society a-Mathematical Physical and Engineering Sciences*, **365**, 2695-2716.

Hope, P. K., W. Drosdowsky, and N. Nicholls, 2006: Shifts in the synoptic systems influencing southwest Western Australia. *Climate Dynamics*, **26**, 751-764.

Horton, E. B., C. K. Folland, and D. E. Parker, 2001: The changing incidence of extremes in worldwide and Central England temperatures to the end of the twentieth century. *Climatic Change*, **50**, 267-295.

Hsu, J., and M. Prather, 2010: Global long-lived chemical modes excited in a 3-D chemistry transport model: Stratospheric N2O, NOy, O-3 and CH4 chemistry. *Geophysical Research Letters*, ARTN L07805 DOI 10.1029/2009GL042243. -.

HTAP, 2010: Hemispheric Transport of Airpollution: Part A: Ozone and Particulate Matter, 278 pp pp.

Hu, Y., and Q. Fu, 2007: Observed poleward expansion of the Hadley circulation since 1979. *Atmospheric Chemistry and Physics*, **7**, 5229-5236.

Hu, Y. C., W. J. Dong, and Y. He, 2010: Impact of land surface forcings on mean and extreme temperature in eastern China. *Journal of Geophysical Research-Atmospheres*, **115**, 11.

Hu, Y. Y., C. Zhou, and J. P. Liu, 2011: Observational evidence for the poleward expansion of the Hadley circulation. *Adv. Atmos. Sci.*, **28**, 33-44.

Huang, J., et al., 2008: Estimation of regional emissions of nitrous oxide from 1997 to 2005 using multinetwork measurements, a chemical transport model, and an inverse method. *Journal of Geophysical Research-Atmospheres*, ARTN D17313, DOI 10.1029/2007JD009381. -.

Huang, W.-R., S.-Y. Wang, and J. C. L. Chan, 2010: Discrepancies between global reanalyses and observations in the interdecadal variations of Southeast Asian cold surge. *Int. J. Climatol.*, 10.1002/joc.2234.

Hudson, R. D., M. F. Andrade, M. B. Follette, and A. D. Frolov, 2006: The total ozone field separated into meteorological regimes - Part II: Northern Hemisphere mid-latitude total ozone trends. *Atmospheric Chemistry and Physics*, **6**, 5183-5191.

Hundecha, Y., A. St-Hilaire, T. Ouarda, S. El Adlouni, and P. Gachon, 2008: A Nonstationary Extreme Value Analysis for the Assessment of Changes in Extreme Annual Wind Speed over the Gulf of St. Lawrence, Canada. *Journal of Applied Meteorology and Climatology*, **47**, 2745-2759.

Hurrell, J. W., 1995a: Decadal trends in the North Atlantic Oscillation: Regional temperatures and precipitation. *Science*, **269**, 676-679.

——, 1995b: DECADAL TRENDS IN THE NORTH-ATLANTIC OSCILLATION - REGIONAL TEMPERATURES AND PRECIPITATION. *Science*, **269**, 676-679.

Hurst, D., 2011: Stratospheric water vapor trends over Boulder, Colorado: Analysis of the 30 year Boulder record. *J. Geophys. Res.*, **116**.

Idso, S. B., and A. J. Brazel, 1984: RISING ATMOSPHERIC CARBON-DIOXIDE CONCENTRATIONS MAY INCREASE STREAMFLOW. *Nature*, **312**, 51-53.

IPCC, 2001: Climate Change 2001: The scientific basis. *Contribution of working group I to the Third assessment report of the Intergovernmental Panel on Climate*, J. T. Houghton, et al., Eds., Cambridge University Press.

——, 2007a: *Climate Change 2007: The Physical Science Basis. Contribution of Working Group I to the Fourth Assessment Report of the Intergovernmental Panel on Climate Change (IPCC).* Cambridge University Press, 996 pp pp.

——, 2007b: *Summary for Policymakers, In: Climate Change 2007: The Physical Science Basis. Contribution of Working Group I to the Fourth Assessment Report of the Intergovernmental Panel on Climate Change.* Cambridge University Press.

Ishii, M., A. Shouji, S. Sugimoto, and T. Matsumoto, 2005: Objective analyses of sea-surface temperature and marine meteorological variables for the 20th century using icoads and the Kobe collection. *International Journal of Climatology*, **25**, 865-879.

Ishijima, K., et al., 2007: Temporal variations of the atmospheric nitrous oxide concentration and its delta N-15 and delta O-18 for the latter half of the 20th century reconstructed from firn air analyses. *Journal of Geophysical Research-Atmospheres*, ARTN D03305, DOI 10.1029/2006JD007208. -.

Ishijima, K., et al., 2010: Stratospheric influence on the seasonal cycle of nitrous oxide in the troposphere as deduced from aircraft observations and model simulations. *Journal of Geophysical Research-Atmospheres*, ARTN D20308, DOI 10.1029/2009JD013322. -.

Jacobeit, J., J. Rathmann, A. Philipp, and P. D. Jones, 2009: Central European precipitation and temperature extremes in relation to large-scale atmospheric circulation types. *Meteorologische Zeitschrift*, **18**, 397-410.

Jacobowitz, H., L. L. Stowe, G. Ohring, A. Heidinger, K. Knapp, and N. R. Nalli, 2003: The advanced very high resolution radiometer Pathfinder Atmosphere (PATMOS) climate dataset - A resource for climate research. *Bulletin of the American Meteorological Society*, **84**, 785-+.

Jaenicke, R., 1993: Tropospheric Aerosols. *International Geophysics*, **54**, 1-31.

Jaffe, D., and J. Ray, 2007: Increase in surface ozone at rural sites in the western US. *Atmospheric Environment*, **41**, 5452-5463.

Jhajharia, D., S. Shrivastava, D. Sarkar, and S. Sarkar, 2009: Temporal characteristics of pan evaporation trends under humid conditions of northeast India. *Agricultural and Forest Meteorology*, **336**, 61-73.

Jiang, T., Z. W. Kundzewicz, and B. Su, 2008: Changes in monthly precipitation and flood hazard in the Yangtze River Basin, China. *International Journal of Climatology*, **28**, 1471-1481.

Jiang, X., W. Ku, R. Shia, Q. Li, J. Elkins, R. Prinn, and Y. Yung, 2007: Seasonal cycle of N2O: Analysis of data. *Global Biogeochemical Cycles*, ARTN GB1006, DOI 10.1029/2006GB002691. -.

Jiang, Y., Y. Luo, Z. C. Zhao, and S. W. Tao, 2010: Changes in wind speed over China during 1956-2004. *Theoretical and Applied Climatology*, **99**, 421-430.

Jin, S. G., J. U. Park, J. H. Cho, and P. H. Park, 2007: Seasonal variability of GPS-derived zenith tropospheric delay (1994-2006) and climate implications. *Journal of Geophysical Research-Atmospheres*, **112**.

John, V. O., R. P. Allan, and B. J. Soden, 2009: How robust are observed and simulated precipitation responses to tropical ocean warming? *Geophysical Research Letters*, **36**.

John, V. O., G. Holl, R. P. Allan, S. A. Buehler, D. E. Parker, and B. J. Soden, 2011: Clear-sky biases in satellite infrared estimates of upper tropospheric humidity and its trends. *Journal of Geophysical Research-Atmospheres*, **116**.

Johnson, G. C., J. M. Lyman, J. K. Willis, S. Levitus, T. Boyer, J. Antonov, and S. A. Good, 2011: [Global Oceans] Ocean heat content [in "State of the Climate in 2010"]. S161–S163.

Jones, P. D., and D. H. Lister, 2007: Intercomparison of four different Southern Hemisphere sea level pressure datasets. *Geophysical Research Letters*, **34**.

——, 2009: The urban heat island in Central London and urban-related warming trends in Central London since 1900. *Weather*, **64**, 323-327.

Jones, P. D., T. Jonsson, and D. Wheeler, 1997: Extension to the North Atlantic Oscillation using early instrumental pressure observations from Gibraltar and south-west Iceland. *International Journal of Climatology*, **17**, 1433-1450.

Jones, P. D., D. H. Lister, and Q. Li, 2008: Urbanization effects in large-scale temperature records, with an emphasis on China. *Journal of Geophysical Research-Atmospheres*, **113**.

Jones, P. D., D. H. Lister, T. J. Osborn, H. C., S. M., and C. P. Morice, Submitted: Hemispheric and large-scale land surface air temperature variations: An extensive revision and an update to 2010. *Journal of Geophysical Research*.

Jonson, J. E., D. Simpson, H. Fagerli, and S. Solberg, 2006: Can we explain the trends in European ozone levels? *Atmos. Chem. Phys.*, **6**, 51-66.

Joshi, M. M., J. M. Gregory, M. J. Webb, D. M. H. Sexton, and T. C. Johns, 2008: Mechanisms for the land/sea warming contrast exhibited by simulations of climate change. *Climate Dynamics*, **30**, 455-465.

Jung, M., et al., 2010: Recent decline in the global land evapotranspiration trend due to limited moisture supply. *Nature*, **467**, 951-954.

Kahn, R. A., B. J. Gaitley, M. J. Garay, D. J. Diner, T. F. Eck, A. Smirnov, and B. N. Holben, 2010: Multiangle Imaging SpectroRadiometer global aerosol product assessment by comparison with the Aerosol Robotic Network. *J. Geophys. Res.*, **115**, D23209.

Kanamitsu, M., W. Ebisuzaki, J. Woollen, S. K. Yang, J. J. Hnilo, M. Fiorino, and G. L. Potter, 2002: NCEP-DOE AMIP-II reanalysis (R-2). *Bulletin of the American Meteorological Society*, **83**, 1631-1643.

Kang, S. M., L. M. Polvani, J. C. Fyfe, and M. Sigmond, 2011: Impact of Polar Ozone Depletion on Subtropical Precipitation. *Science*, **332**, 951-954.

Kao, H. Y., and J. Y. Yu, 2009: Contrasting Eastern-Pacific and Central-Pacific Types of ENSO. *Journal of Climate*, **22**, 615-632.

Karl, T. R., G. A. Meehl, D. M. Christopher, S. J. Hassol, A. M. Waple, and W. L. Murray, 2008: *Weather and Climate Extremes in a Changing Climate. Regions of Focus: North America, Hawaii, Caribbean, and U.S. Pacific Islands.* A Report by the U.S. Climate Change Science Program and the Subcommittee on Global Change Research, 164 pp.

Karnauskas, K. B., R. Seager, A. Kaplan, Y. Kushnir, and M. A. Cane, 2009: Observed Strengthening of the Zonal Sea Surface Temperature Gradient across the Equatorial Pacific Ocean. *Journal of Climate*, **22**, 4316-4321.

Karnieli, A., et al., 2009: Temporal trend in anthropogenic sulfur aerosol transport from central and eastern Europe to Israel. *Journal of Geophysical Research-Atmospheres*, **114**, D00d19.

KAROLY, D., 1989: SOUTHERN-HEMISPHERE CIRCULATION FEATURES ASSOCIATED WITH ELNINO - SOUTHERN OSCILLATION EVENTS. *Journal of Climate*, **2**, 1239-1252.
Kato, S., et al., 2011: Improvements of top-of-atmosphere and surface irradiance computations with CALIPSO-, CloudSat-, and MODIS-derived cloud and aerosol properties. *Journal of Geophysical Research-Atmospheres*, **116**, doi:10.1029/2011JD016050.
Kawai, Y., and A. Wada, 2007: Diurnal sea surface temperature variation and its impact on the atmosphere and ocean: A review. *Journal of Oceanography*, **63**, 721-744.
Keeling, C. D., Bacastow, R. B., Bainbridge, A. E., Ekdahl, C. A., Guenther, P. R., Waterman, L. S., 1976: Atmospheric carbon dioxide variations at Mauna Loa Observatory, Hawaii. 538-551.
Keim, C., et al., 2009: Tropospheric ozone from IASI: comparison of different inversion algorithms and validation with ozone sondes in the northern middle latitudes. *Atmos. Chem. Phys.*, **9**, 9329-9347.
Kennedy, J. J., P. Brohan, and S. F. B. Tett, 2007: A global climatology of the diurnal variations in sea-surface temperature and implications for MSU temperature trends. *Geophysical Research Letters*, **34**.
Kennedy, J. J., N. A. Rayner, and R. O. Smith, 2011a: Using AATSR data to assess the quality of in situ sea surface temperature observations for climate studies. *Remote Sensing Environ.*, **in press**.
Kennedy, J. J., N. A. Rayner, R. O. Smith, M. Saunby, and D. E. Parker, 2011b: Reassessing biases and other uncertainties in sea surface temperature observations since 1850, part 1: Measurement and sampling uncertainties. *J. Geophys. Res.*, **submitted**.
——, 2011c: Reassessing biases and other uncertainties in sea surface temperature observations since 1850, part 2: Biases and homogenization. *J. Geophys. Res.*, **submitted**.
Kent, E. C., and D. I. Berry, 2005: Quantifying random measurement errors in voluntary observing ships' meteorological observations. *International Journal of Climatology*, **25**, 843-856.
Kent, E. C., and P. G. Challenor, 2006: Toward estimating climatic trends in SST. Part II: Random errors. *Journal of Atmospheric and Oceanic Technology*, **23**, 476-486.
Kent, E. C., and D. I. Berry, 2008: Assessment of the Marine Observing System (ASMOS): Final Report, 55pp pp.
Kent, E. C., P. G. Challenor, and P. K. Taylor, 1999: A statistical determination of the random observational errors present in voluntary observing ships meteorological reports. *Journal of Atmospheric and Oceanic Technology*, **16**, 905-914.
Kent, E. C., S. D. Woodruff, and D. I. Berry, 2007: Metadata from WMO publication no. 47 and an assessment of voluntary observing ship observation heights in ICOADS. *Journal of Atmospheric and Oceanic Technology*, **24**, 214-234.
Kent, E. C., J. J. Kennedy, D. I. Berry, and R. O. Smith, 2010: Effects of instrumentation changes on sea surface temperature measured in situ. *Wiley Interdisciplinary Reviews: Climate Change*, **1**, 718-728.
Kenyon, J., and G. C. Hegerl, 2008: Influence of modes of climate variability on global temperature extremes. *Journal of Climate*, **21**, 3872-3889.
——, 2010: Influence of Modes of Climate Variability on Global Precipitation Extremes. *Journal of Climate*, **23**, 6248-6262.
Kim, D. Y., and V. Ramanathan, 2008: Solar radiation budget and radiative forcing due to aerosols and clouds. *Journal of Geophysical Research-Atmospheres*, **113**.
Kim, H. M., P. J. Webster, and J. A. Curry, 2009: Impact of Shifting Patterns of Pacific Ocean Warming on North Atlantic Tropical Cyclones. *Science*, **325**, 77-80.
Kistler, R., et al., 2001: The NCEP-NCAR 50-year reanalysis: Monthly means CD-ROM and documentation. *Bulletin of the American Meteorological Society*, **82**, 247-267.
Klein Tank, A., et al., 2002: Daily dataset of 20th-century surface air temperature and precipitation series for the European Climate Assessment. *International Journal of Climatology*, **22**, 1441-1453.
Klein Tank, A. M. G., et al., 2006: Changes in daily temperature and precipitation extremes in central and south Asia. *Journal of Geophysical Research-Atmospheres*, **111**.
Knapp, K. R., and M. C. Kruk, 2010: Quantifying Interagency Differences in Tropical Cyclone Best-Track Wind Speed Estimates. *Monthly Weather Review*, **138**, 1459-1473.
Knapp, P. A., and P. T. Soule, 2007: Trends in midlatitude cyclone frequency and occurrence during fire season in the Northern Rockies: 1900-2004. *Geophysical Research Letters*, **34**.
Knorr, W., 2009: Is the airborne fraction of anthropogenic CO2 emissions increasing? *Geophysical Research Letters*, ARTN L21710, DOI 10.1029/2009GL040613. -.
Knowles, N., M. D. Dettinger, and D. R. Cayan, 2006: Trends in snowfall versus rainfall in the Western United States. *Journal of Climate*, **19**, 4545-4559.
Knutson, T. R., et al., 2010: Tropical cyclones and climate change. *Nature Geoscience*, **3**, 157-163.
Kobayashi, S., M. Matricardi, D. Dee, and S. Uppala, 2009: Toward a consistent reanalysis of the upper stratosphere based on radiance measurements from SSU and AMSU-A. *Quarterly Journal of the Royal Meteorological Society*, **135**, 2086-2099.
Kopp, G., and G. Lawrence, 2005: The Total Irradiance Monitor (TIM): Instrument design. *Solar Physics*, **230**, 91-109.
Kopp, G., and J. L. Lean, 2011: A new, lower value of total solar irradiance: Evidence and climate significance. *Geophysical Research Letters*, **38**.

Kopp, G., G. Lawrence, and G. Rottman, 2005: The Total Irradiance Monitor (TIM): Science results. *Solar Physics*, **230**, 129-139.
Kossin, J. P., K. R. Knapp, D. J. Vimont, R. J. Murnane, and B. A. Harper, 2007: A globally consistent reanalysis of hurricane variability and trends. *Geophysical Research Letters*, **34**.
Krishnamurthy, C. K. B., U. Lall, and H. H. Kwon, 2009: Changing Frequency and Intensity of Rainfall Extremes over India from 1951 to 2003. *Journal of Climate*, **22**, 4737-4746.
Kruger, A. C., 2006: Observed trends in daily precipitation indices in South Africa: 1910-2004. *International Journal of Climatology*, **26**, 2275-2285.
Kubota, H., and J. C. L. Chan, 2009: Interdecadal variability of tropical cyclone landfall in the Philippines from 1902 to 2005. *Geophysical Research Letters*, **36**.
Kudo, R., A. Uchiyama, A. Yamazaki, T. Sakami, and O. Ijima, 2011: Decadal changes in aerosol optical thickness and single scattering albedo estimated from ground-based broadband radiometers: A case study in Japan. *J. Geophys. Res.*, **116**, D03207.
Kuglitsch, F. G., A. Toreti, E. Xoplaki, P. M. Della-Marta, J. Luterbacher, and H. Wanner, 2009: Homogenization of daily maximum temperature series in the Mediterranean. *Journal of Geophysical Research-Atmospheres*, **114**.
Kuglitsch, F. G., A. Toreti, E. Xoplaki, P. M. Della-Marta, C. S. Zerefos, M. Turkes, and J. Luterbacher, 2010: Heat wave changes in the eastern Mediterranean since 1960. *Geophysical Research Letters*, **37**.
Kumari, B. P., and B. N. Goswami, 2010: Seminal role of clouds on solar dimming over the Indian monsoon region. *Geophysical Research Letters*, **37**, -.
Kumari, B. P., A. L. Londhe, S. Daniel, and D. B. Jadhav, 2007: Observational evidence of solar dimming: Offsetting surface warming over India. *Geophysical Research Letters*, **34**, L21810.
Kundzewicz, Z. W., et al., 2007: Freshwater resources and their management. *Climate Change 2007: Impacts, Adaptation and Vulnerability. Contribution of Working Group II to the Fourth Assessment Report of the Intergovernmental Panel on Climate Change*, Cambridge University Press.
Kunkel, K. E., M. A. Palecki, K. G. Hubbard, D. A. Robinson, K. T. Redmond, and D. R. Easterling, 2007: Trend identification in twentieth-century US snowfall: The challenges. *Journal of Atmospheric and Oceanic Technology*, **24**, 64-73.
Kunkel, K. E., M. A. Palecki, L. Ensor, D. Easterling, K. G. Hubbard, D. Robinson, and K. Redmond, 2009: Trends in Twentieth-Century US Extreme Snowfall Seasons. *Journal of Climate*, **22**, 6204-6216.
Kunkel, K. E., et al., 2008: Observed Changes in Weather and Climate Extremes. *Weather and Climate Extremes in a Changing Climate. Regions of Focus: North America, Hawaii, Caribbean, and U.S. Pacific Islands.*, T. R. Karl, G. A. Meehl, D. M. Christopher, S. J. Hassol, A. M. Waple, and W. L. Murray, Eds., A Report by the U.S. Climate Change Science Program and the Subcommittee on Global Change Research, 222.
Kunz, M., J. Sander, and C. Kottmeier, 2009: Recent trends of thunderstorm and hailstorm frequency and their relation to atmospheric characteristics in southwest Germany. *International Journal of Climatology*, **29**, 2283-2297.
Kuo, Y. H., W. S. Schreiner, J. Wang, D. L. Rossiter, and Y. Zhang, 2005: Comparison of GPS radio occultation soundings with radiosondes. *Geophysical Research Letters*, **32**.
Kuo, Y. H., T. K. Wee, S. Sokolovskiy, C. Rocken, W. Schreiner, D. Hunt, and R. A. Anthes, 2004: Inversion and error estimation of GPS radio occultation data. *Journal of the Meteorological Society of Japan*, **82**, 507-531.
Kurbis, K., M. Mudelsee, G. Tetzlaff, and R. Brazdil, 2009: Trends in extremes of temperature, dew point, and precipitation from long instrumental series from central Europe. *Theoretical and Applied Climatology*, **98**, 187-195.
Kvalevag, M. M., and G. Myhre, 2007: Human impact on direct and diffuse solar radiation during the industrial era. *Journal of Climate*, **20**, 4874-4883.
Kysely, J., 2009: Trends in heavy precipitation in the Czech Republic over 1961-2005. *International Journal of Climatology*, **29**, 1745-1758.
L'Ecuyer, T. S., N. B. Wood, T. Haladay, G. L. Stephens, and P. W. Stackhouse, 2008: Impact of clouds on atmospheric heating based on the R04 CloudSat fluxes and heating rates data set. *Journal of Geophysical Research-Atmospheres*, **113**, 15.
Labat, D., Y. Godderis, J. L. Probst, and J. L. Guyot, 2004: Evidence for global runoff increase related to climate warming. *Advances in Water Resources*, **27**, 631-642.
Lacis, A., G. Schmidt, D. Rind, and R. Ruedy, 2010: Atmospheric CO2: Principal Control Knob Governing Earth's Temperature. *Science*, DOI 10.1126/science.1190653. 356-359.
Ladstadter, F., A. K. Steiner, U. Foelsche, L. Haimberger, C. Tavolato, and G. Kirchneb=ngast, 2011: An assessment of differences in lower stratospheric temperature records from (A)MSU, radiosondes and GPS radio occultation. *Atmospheric Measurement Techniques*, **4**, 1965-1977.
Lambert, F. H., and M. J. Webb, 2008: Dependency of global mean precipitation on surface temperature. *Geophysical Research Letters*, **35**.
Lamsal, L. N., et al., 2011: Application of satellite observations for timely updates to global anthropogenic NOx emission inventories. *Geophys. Res. Lett.*
Landsea, C. W., 2007: Counting Atlantic tropical cyclones back to 1900. *EOS Transactions (AGU)*, **88**, 197-202.
Landsea, C. W., B. A. Harper, K. Hoarau, and J. A. Knaff, 2006: Can we detect trends in extreme tropical cyclones? *Science*, **313**, 452-454.

Landsea, C. W., G. A. Vecchi, L. Bengtsson, and T. R. Knutson, 2010: Impact of Duration Thresholds on Atlantic Tropical Cyclone Counts. *Journal of Climate*, **23**, 2508-2519.
Landsea, C. W., et al., 2004: The Atlantic hurricane database re-analysis project: Documentation for the 1851-1910 alterations and additions to the HURDAT database. *Hurricanes and Typhoons: Past, Present and Future*, R. J. Murnane, and K. B. Liu, Eds., Columbia University Press, 177-221.
Landsea, C. W., et al., 2008: A reanalysis of the 1911-20 Atlantic hurricane database. *Journal of Climate*, **21**, 2138-2168.
Langematz, U., and M. Kunze, 2008: Dynamical changes in the Arctic and Antarctic stratosphere during spring. *Climate Variability and Extremes during the Past 100 Years. Advances in Global Change Research*, S. Brönnimann, J. Luterbacher, T. Ewen, H. F. Diaz, R. S. Stolarski, and U. Neu, Eds., 293-301.
Lanzante, J. R., 1996: Resistant, robust and non-parametric techniques for the analysis of climate data: Theory and examples, including applications to historical radiosonde station data. *International Journal of Climatology*, **16**, 1197-1226.
Larkin, N. K., and D. E. Harrison, 2005: On the definition of El Nino and associated seasonal average US weather anomalies. *Geophysical Research Letters*, **32**.
Laube, J., et al., 2010: Accelerating growth of HFC-227ea (1,1,1,2,3,3,3-heptafluoropropane) in the atmosphere. *Atmospheric Chemistry and Physics*, **10**, 5903-5910.
Laux, P., and H. Kunstmann, 2008: Detection of regional weekly weather cycles across Europe. *Environmental Research Letters*, **3**.
Lawrimore, J. H., M. J. Menne, B. E. Gleason, C. N. Williams, D. B. Wuertz, R. S. Vose, and J. Rennie, 2011: An overview of the Global Historical Climatology Network monthly mean temperature data set, version 3. *Journal of Geophysical Research-Atmospheres*, **116**, doi:10.1029/2011jd016187.
Le Quere, C., et al., 2009: Trends in the sources and sinks of carbon dioxide. *Nature Geoscience*, DOI 10.1038/ngeo689. 831-836.
Leakey, A. D. B., M. Uribelarrea, E. A. Ainsworth, S. L. Naidu, A. Rogers, D. R. Ort, and S. P. Long, 2006: Photosynthesis, productivity, and yield of maize are not affected by open-air elevation of CO2 concentration in the absence of drought. *Plant Physiology*, **140**, 779-790.
Leckebusch, G. C., B. Koffi, U. Ulbrich, J. G. Pinto, T. Spangehl, and S. Zacharias, 2006: Analysis of frequency and intensity of European winter storm events from a multi-model perspective, at synoptic and regional scales. *Climate Research*, **31**, 59-74.
Lee, H. T., A. Heidinger, A. Gruber, and R. G. Ellingson, 2004: The HIRS outgoing longwave radiation product from hybrid polar and geosynchronous satellite observations. *Climate Change Processes in the Stratosphere, Earth-Atmosphere-Ocean Systems, and Oceanographic Processes from Satellite Data*, **33**, 1120-1124.
Lee, H. T., A. Gruber, R. G. Ellingson, and I. Laszlo, 2007: Development of the HIRS outgoing longwave radiation climate dataset. *Journal of Atmospheric and Oceanic Technology*, **24**, 2029-2047.
Lee, T., and M. J. McPhaden, 2010: Increasing intensity of El Nino in the central-equatorial Pacific. *Geophysical Research Letters*, **37**.
Lee, T. C., H. S. Chan, E. W. L. Ginn, and M. C. Wong, 2011: Long-Term Trends in Extreme Temperatures in Hong Kong and Southern China. *Advances in Atmospheric Sciences*, **28**, 147-157.
Lehmann, A., K. Getzlaff, and J. Harlass, 2011: Detailed assessment of climate variability in the Baltic Sea area for the period 1958 to 2009. *Climate Research*, **46**, 185-196.
Levin, I., et al., 2010: The global SF6 source inferred from long-term high precision atmospheric measurements and its comparison with emission inventories. *Atmospheric Chemistry and Physics*. 2655-2662.
Levy, R. C., L. A. Remer, R. G. Kleidman, S. Mattoo, C. Ichoku, R. Kahn, and T. F. Eck, 2010: Global evaluation of the Collection 5 MODIS dark-target aerosol products over land. *Atmos. Chem. Phys.*, **10**, 10399-10420.
Liang, F., and X. A. Xia, 2005: Long-term trends in solar radiation and the associated climatic factors over China for 1961-2000. *Annales Geophysicae*, **23**, 2425-2432.
Liepert, B. G., 2002: Observed reductions of surface solar radiation at sites in the United States and worldwide from 1961 to 1990. *Geophysical Research Letters*, **29**, 4.
Liepert, B. G., and M. Previdi, 2009: Do Models and Observations Disagree on the Rainfall Response to Global Warming? *Journal of Climate*, **22**, 3156-3166.
Liley, J. B., 2009: New Zealand dimming and brightening. *Journal of Geophysical Research-Atmospheres*, **114**, D00d10.
Lim, E. P., and I. Simmonds, 2009: Effect of tropospheric temperature change on the zonal mean circulation and SH winter extratropical cyclones. *Climate Dynamics*, **33**, 19-32.
Lim, Y. K., M. Cai, E. Kalnay, and L. Zhou, 2008: Impact of vegetation types on surface temperature change. *Journal of Applied Meteorology and Climatology*, **47**, 411-424.
Lindzen, R. S., and Y. S. Choi, 2009: On the determination of climate feedbacks from ERBE data. *Geophysical Research Letters*, **36**.
Liu, B. H., M. Xu, M. Henderson, and W. G. Gong, 2004a: A spatial analysis of pan evaporation trends in China, 1955-2000. *Journal of Geophysical Research-Atmospheres*, **109**, D15102.
Liu, B. H., M. Xu, M. Henderson, Y. Qi, and Y. Q. Li, 2004b: Taking China's temperature: Daily range, warming trends, and regional variations, 1955-2000. *Journal of Climate*, **17**, 4453-4462.

Liu, Q. H., and F. Z. Weng, 2009: Recent Stratospheric Temperature Observed from Satellite Measurements. *Sola*, **5**, 53-56.
Liu, X., Z.-Y. Yin, X. Shao, and N. Qin, 2006: Temporal trends and variability of daily maximum and minimum, extreme temperature events, and growing season length over the eastern and central Tibetan Plateau during 1961-2003. *Journal of Geophysical Research-Atmospheres*, **111**.
Liu, X., P. K. Bhartia, K. Chance, R. J. D. Spurr, and T. P. Kurosu, 2010: Ozone profile retrievals from the Ozone Monitoring Instrument. *Atmos. Chem. Phys.*, **10**, 2521-2537.
Loeb, N. G., et al., 2009: Toward Optimal Closure of the Earth's Top-of-Atmosphere Radiation Budget. *Journal of Climate*, **22**, 748-766.
Loeb, N. G., et al., 2011: Observing Changes in Earth's Energy Budget during the Past Decade. *Nature Geoscience*. submitted.
Loeb, N. G., et al., 2007: Multi-instrument comparison of top-of-atmosphere reflected solar radiation. *Journal of Climate*, **20**, 575-591.
Logan, J. A., et al., 2011: Changes in Ozone over Europe since 1990: analysis of ozone measurements from sondes, regular Aircraft (MOZAIC), and alpine surface sites. *submitted to JGR*.
Lohmann, U., and J. Feichter, 2005: Global indirect aerosol effects: a review. *Atmospheric Chemistry and Physics*, **5**, 715-737.
Long, C. N., E. G. Dutton, J. A. Augustine, W. Wiscombe, M. Wild, S. A. McFarlane, and C. J. Flynn, 2009: Significant decadal brightening of downwelling shortwave in the continental United States. *Journal of Geophysical Research-Atmospheres*, **114**, D00d06.
Lupikasza, E., 2010: Spatial and temporal variability of extreme precipitation in Poland in the period 1951-2006. *International Journal of Climatology*, **30**, 991-1007.
Lynch, A. H., J. A. Curry, R. D. Brunner, and J. A. Maslanik, 2004: Toward an integrated assessment of the impacts of extreme wind events on Barrow, Alaska. *Bulletin of the American Meteorological Society*, **85**, 209-+.
Lynch, P., and X. Y. Huang, 1992: INITIALIZATION OF THE HIRLAM MODEL USING A DIGITAL-FILTER. *Monthly Weather Review*, **120**, 1019-1034.
Mahowald, N., et al., 2010: Observed 20th century desert dust variability: impact on climate and biogeochemistry. *Atmospheric Chemistry and Physics*, **10**, 10875-10893.
Makowski, K., E. B. Jaeger, M. Chiacchio, M. Wild, T. Ewen, and A. Ohmura, 2009: On the relationship between diurnal temperature range and surface solar radiation in Europe. *Journal of Geophysical Research-Atmospheres*, **114**, D00d07.
Mann, M. E., T. A. Sabbatelli, and U. Neu, 2007a: Evidence for a modest undercount bias in early historical Atlantic tropical cyclone counts. *Geophysical Research Letters*, **34**.
Mann, M. E., K. A. Emanual, G. J. Holland, and P. J. Webster, 2007b: Atlantic tropical cyclones revisited. *Eos Transactions (AGU)*, **88**, 349-350.
Manning, M., D. Lowe, R. Moss, G. Bodeker, and W. Allan, 2005: Short-term variations in the oxidizing power of the atmosphere. *Nature*, **436**, 1001-1004.
Mantua, N. J., S. R. Hare, Y. Zhang, J. M. Wallace, and R. C. Francis, 1997: A Pacific interdecadal climate oscillation with impacts on salmon production. *Bulletin of the American Meteorological Society*, **78**, 1069-1079.
Maraun, D., T. J. Osborn, and N. P. Gillett, 2008: United Kingdom daily precipitation intensity: improved early data, error estimates and an update from 2000 to 2006. *International Journal of Climatology*, **28**, 833-842.
Marengo, J. A., R. Jones, L. M. Alves, and M. C. Valverde, 2009: Future change of temperature and precipitation extremes in South America as derived from the PRECIS regional climate modeling system. *International Journal of Climatology*, **29**, 2241-2255.
Marshall, G. J., 2003: Trends in the southern annular mode from observations and reanalyses. *Journal of Climate*, **16**, 4134-4143.
Martinerie, P., et al., 2009: Long-lived halocarbon trends and budgets from atmospheric chemistry modelling constrained with measurements in polar firn. *Atmospheric Chemistry and Physics*. 3911-3934.
Matulla, C., W. Schoner, H. Alexandersson, H. von Storch, and X. L. Wang, 2008: European storminess: late nineteenth century to present. *Climate Dynamics*, **31**, 125-130.
Maue, R. N., 2009: Northern Hemisphere tropical cyclone activity. *Geophysical Research Letters*, **36**.
McCarthy, M. P., P. W. Thorne, and H. A. Titchner, 2009: An Analysis of Tropospheric Humidity Trends from Radiosondes. *Journal of Climate*, **22**, 5820-5838.
McCarthy, M. P., H. A. Titchner, P. W. Thorne, S. F. B. Tett, L. Haimberger, and D. E. Parker, 2008: Assessing bias and uncertainty in the HadAT-adjusted radiosonde climate record. *Journal of Climate*, **21**, 817-832.
McKitrick, R., and P. J. Michaels, 2004: A test of corrections for extraneous signals in gridded surface temperature data. *Climate Research*, **26**, 159-173.
McKitrick, R. R., and P. J. Michaels, 2007: Quantifying the influence of anthropogenic surface processes and inhomogeneities on gridded global climate data. *Journal of Geophysical Research-Atmospheres*, **112**.
McPhaden, M., T. Lee, and D. McClurg, 2011: El Nino and its relationship to changing background conditions in the tropical Pacific Ocean. *Geophysical Research Letters*, **38**, -.

McVicar, T. R., T. G. Van Niel, L. T. Li, M. L. Roderick, D. P. Rayner, L. Ricciardulli, and R. J. Donohue, 2008: Wind speed climatology and trends for Australia, 1975-2006: Capturing the stilling phenomenon and comparison with near-surface reanalysis output. *Geophysical Research Letters*, **35**.

Mears, C. A., and F. J. Wentz, 2009a: Construction of the Remote Sensing Systems V3.2 Atmospheric Temperature Records from the MSU and AMSU Microwave Sounders. *Journal of Atmospheric and Oceanic Technology*, **26**, 1040-1056.

——, 2009b: Construction of the RSS V3.2 Lower-Tropospheric Temperature Dataset from the MSU and AMSU Microwave Sounders. *Journal of Atmospheric and Oceanic Technology*, **26**, 1493-1509.

Mears, C. A., C. E. Forest, R. W. Spencer, R. S. Vose, and R. W. Reynolds, 2006: What is ourunderstanding of the contribution made by observational or methodological uncertainties to the previously reported vertical differences in temperature trends? *Temperature Trends in the Lower Tmosphere: Steps for Understanding and Reconciling Differences*, T. R. Karl, S. J. Hassol, C. D. Miller, and W. L. Murray, Eds.

Mears, C. A., B. D. Santer, F. J. Wentz, K. E. Taylor, and M. F. Wehner, 2007: Relationship between temperature and precipitable water changes over tropical oceans. *Geophysical Research Letters*, **34**.

Mears, C. A., Wentz, F. J., Thorne, P., Bernie, D., 2011: Assessing uncertainty in estimates of atmospheric temperature changes from MSU and AMSU using a monte-carlo estimation technique.

Meehl, G. A., J. M. Arblaster, and G. Branstator, 2011: Understanding the U.S. east-west differential of heat extremes in terms of record temperatures and the warming hole. *Journal of Climate*. submitted.

Meehl, G. A., C. Tebaldi, G. Walton, D. Easterling, and L. McDaniel, 2009: Relative increase of record high maximum temperatures compared to record low minimum temperatures in the U. S. *Geophysical Research Letters*, **36**.

Menne, M. J., and C. N. Williams, 2009: Homogenization of Temperature Series via Pairwise Comparisons. *Journal of Climate*, **22**, 1700-1717.

Menne, M. J., C. N. Williams, and R. S. Vose, 2009: THE US HISTORICAL CLIMATOLOGY NETWORK MONTHLY TEMPERATURE DATA, VERSION 2. *Bulletin of the American Meteorological Society*, **90**, 993-1007.

Menne, M. J., C. N. Williams, and M. A. Palecki, 2010: On the reliability of the US surface temperature record. *Journal of Geophysical Research-Atmospheres*, **115**.

Merrifield, M. A., 2011: A Shift in Western Tropical Pacific Sea Level Trends during the 1990s. *Journal of Climate*, **24**, 4126-4138.

Mieruch, S., S. Noel, H. Bovensmann, and J. P. Burrows, 2008: Analysis of global water vapour trends from satellite measurements in the visible spectral range. *Atmospheric Chemistry and Physics*, **8**, 491-504.

Milewska, E. J., 2004: Baseline cloudiness trends in Canada 1953-2002. *Atmosphere-Ocean*, **42**, 267-280.

Miller, B., R. Weiss, P. Salameh, T. Tanhua, B. Greally, J. Muhle, and P. Simmonds, 2008: Medusa: A sample preconcentration and GC/MS detector system for in situ measurements of atmospheric trace halocarbons, hydrocarbons, and sulfur compounds. *Analytical Chemistry*, DOI 10.1021/ac702084k. 1536-1545.

Miller, B., et al., 2010: HFC-23 (CHF3) emission trend response to HCFC-22 (CHClF2) production and recent HFC-23 emission abatement measures. *Atmospheric Chemistry and Physics*, DOI 10.5194/acp-10-7875-2010. 7875-7890.

Milliman, J. D., K. L. Farnsworth, P. D. Jones, K. H. Xu, and L. C. Smith, 2008: Climatic and anthropogenic factors affecting river discharge to the global ocean, 1951-2000. *Global and Planetary Change*, **62**, 187-194.

Mishchenko, M. I., et al., 2007: Long-Term Satellite Record Reveals Likely Recent Aerosol Trend. *Science*, **315**, 1543-1543.

Mishchenko, M. I., et al., 2003: Aerosol retrievals from AVHRR radiances: effects of particle nonsphericity and absorption and an updated long-term global climatology of aerosol properties. *Journal of Quantitative Spectroscopy and Radiative Transfer*, **79-80**, 953-972.

Mitas, C. M., and A. Clement, 2005: Has the Hadley cell been strengthening in recent decades? *Geophysical Research Letters*, **32**.

Mo, K., and J. Paegle, 2001: The Pacific-South American modes and their downstream effects. *International Journal of Climatology*, **21**, 1211-1229.

Mo, T., 2009: A study of the NOAA-15 AMSU-A brightness temperatures from 1998 through 2007. *Journal of Geophysical Research-Atmospheres*, **114**.

Moberg, A., et al., 2006: Indices for daily temperature and precipitation extremes in Europe analyzed for the period 1901-2000. *Journal of Geophysical Research-Atmospheres*, **111**.

Montzka, S., B. Hall, and J. Elkins, 2009: Accelerated increases observed for hydrochlorofluorocarbons since 2004 in the global atmosphere. *Geophysical Research Letters*, ARTN L03804, DOI 10.1029/2008GL036475. -.

Montzka, S., E. Dlugokencky, and J. Butler, 2011a: Non-CO2 greenhouse gases and climate change. *Nature*, **476**, 43-50.

Montzka, S., M. Krol, E. Dlugokencky, B. Hall, P. Jockel, and J. Lelieveld, 2011b: Small Interannual Variability of Global Atmospheric Hydroxyl. *Science*, DOI 10.1126/science.1197640. -.

Montzka, S., L. Kuijpers, M. Battle, M. Aydin, K. Verhulst, E. Saltzman, and D. Fahey, 2010: Recent increases in global HFC-23 emissions. *Geophysical Research Letters*, ARTN L02808, DOI 10.1029/2009GL041195. -.

Morak, S., G. C. Hegerl, and J. Kenyon, 2011: Detectable regional changes in the number of warm nights. *Geophysical Research Letters*, **38**, 5.

Morice, C. P., J. J. Kennedy, N. A. Rayner, and P. D. Jones, Submitted: Quantifying uncertainties in global and regional temperature change using an ensemble of observational estimates: the HadCRUT4 dataset. *Journal of Geophysical Research*.
Mueller, B., et al., 2011: Evaluation of global observations-based evapotranspiration datasets and IPCC AR4 simulations. *Geophysical Research Letters*, **38**.
Muhle, J., et al., 2009: Sulfuryl fluoride in the global atmosphere. *Journal of Geophysical Research-Atmospheres*, ARTN D05306, DOI 10.1029/2008JD011162. -.
Muhle, J., et al., 2010: Perfluorocarbons in the global atmosphere: tetrafluoromethane, hexafluoroethane, and octafluoropropane. *Atmospheric Chemistry and Physics*, DOI 10.5194/acp-10-5145-2010. 5145-5164.
Muller, R. A., et al., submitted: Earth Atmospheric Land Surface Temperature and Station Quality in the United States. *Journal of Geophysical Research-Atmospheres*. submitted.
Murphy, D. M., 2010: Constraining climate sensitivity with linear fits to outgoing radiation. *Geophysical Research Letters*, **37**.
Murphy, D. M., et al., 2011: Decreases in elemental carbon and fine particle mass in the United States. *Atmos. Chem. Phys.*, **11**, 4679-4686.
Na, H., B. Jang, W. Choi, and K. Kim, 2011: Statistical simulations of the future 50-year statistics of cold-tongue El Nio and warm-pool El Nio. *Asia-Pacific Journal of Atmospheric Sciences*, **47**, 223-233.
Nan, S., and J. P. Li, 2003: The relationship between the summer precipitation in the Yangtze River valley and the boreal spring Southern Hemisphere annular mode. *Geophysical Research Letters*, **30**.
Neff, W., J. Perlwitz, and M. Hoerling, 2008: Observational evidence for asymmetric changes in tropospheric heights over Antarctica on decadal time scales. *Geophysical Research Letters*, **35**.
Nevison, C., 2011: Abiotic and biogeochemical signals derived from the seasonal cycles of tropospheric nitrous oxide. *Atmos. Chem. Phys. Discuss.*, **10**, 25803-25839.
Nevison, C., N. Mahowald, R. Weiss, and R. Prinn, 2007: Interannual and seasonal variability in atmospheric N2O. *Global Biogeochemical Cycles*, ARTN GB3017, DOI 10.1029/2006GB002755. -.
New, M., et al., 2006: Evidence of trends in daily climate extremes over southern and west Africa. *Journal of Geophysical Research-Atmospheres*, **111**.
Nicholls, N., 2008: Recent trends in the seasonal and temporal behaviour of the El Nino-Southern Oscillation. *Geophysical Research Letters*, **35**.
Nicholls, N., and L. Alexander, 2007: Has the climate become more variable or extreme? Progress 1992-2006. *Progress in Physical Geography*, **31**, 77-87.
Nicholls, N., and S. Larsen, 2011: Impact of drought on temperature extremes in Melbourne, Australia. *Australian Meteorological and Oceanographic Journal*, **61**, 113-116.
Nisbet, E., and R. Weiss, 2010: Top-Down Versus Bottom-Up. *Science*, DOI 10.1126/science.1189936. 1241-1243.
Norris, J. R., and M. Wild, 2007: Trends in aerosol radiative effects over Europe inferred from observed cloud cover, solar "dimming" and solar "brightening". *Journal of Geophysical Research-Atmospheres*, **112**.
——, 2009: Trends in aerosol radiative effects over China and Japan inferred from observed cloud cover, solar dimming, and solar brightening. *Journal of Geophysical Research-Atmospheres*, **114**, D00d15.
Ntegeka, V., and P. Willems, 2008: Trends and multidecadal oscillations in rainfall extremes, based on a more than 100-year time series of 10 min rainfall intensities at Uccle, Belgium. *Water Resources Research*, **44**.
O'Carroll, A. G., J. R. Eyre, and R. W. Saunders, 2008: Three-way error analysis between AATSR, AMSR-E, and in situ sea surface temperature observations. *Journal of Atmospheric and Oceanic Technology*, **25**, 1197-1207.
O'Dell, C. W., F. J. Wentz, and R. Bennartz, 2008: Cloud liquid water path from satellite-based passive microwave observations: A new climatology over the global oceans. *Journal of Climate*, **21**, 1721-1739.
O'Doherty, S., et al., 2009: Global and regional emissions of HFC-125 (CHF2CF3) from in situ and air archive atmospheric observations at AGAGE and SOGE observatories. *Journal of Geophysical Research-Atmospheres*, ARTN D23304, DOI 10.1029/2009JD012184. -.
Ohmura, A., 2009: Observed decadal variations in surface solar radiation and their causes. *Journal of Geophysical Research-Atmospheres*, **114**, D00d05.
Ohmura, A., et al., 1998: Baseline Surface Radiation Network (BSRN/WCRP): New precision radiometry for climate research. *Bulletin of the American Meteorological Society*, **79**, 2115-2136.
Ohvril, H., et al., 2009: Global dimming and brightening versus atmospheric column transparency, Europe, 1906-2007. *Journal of Geophysical Research-Atmospheres*, **114**, D00d12.
Oltmans, S., H. Vomel, D. Hofmann, K. Rosenlof, and D. Kley, 2000: The increase in stratospheric water vapor from balloonborne, frostpoint hygrometer measurements at Washington, DC, and Boulder, Colorado. *Geophysical Research Letters*. 3453-3456.
Oltmans, S. J., A. S. Lefohn, J. M. Harris, and D. S. Shadwick, 2008: Background ozone levels of air entering the west coast of the US and assessment of longer-term changes. *Atmospheric Environment*, **42**, 6020-6038.
Oltmans, S. J., et al., 2006: Long-term changes in tropospheric ozone. *Atmospheric Environment*, **40**, 3156-3173.
Onogi, K., et al., 2007: The JRA-25 reanalysis. *Journal of the Meteorological Society of Japan*, **85**, 369-432.
Oort, A. H., and J. J. Yienger, 1996: Observed interannual variability in the Hadley circulation and its connection to ENSO. *Journal of Climate*, **9**, 2751-2767.

Osborn, T. J., 2011: Winter 2009/2010 temperatures and a record breaking North Atlantic Oscillation index. *Weather*, **66**, 19-21.
Osborne, S. R., and J. M. Haywood, 2005: Aircraft observations of the microphysical and optical properties of major aerosol species. *Atmospheric Research*, **73**, 173-201.
Paciorek, C. J., J. S. Risbey, V. Ventura, and R. D. Rosen, 2002: Multiple indices of Northern Hemisphere cyclone activity, winters 1949-99. *Journal of Climate*, **15**, 1573-1590.
Palmer, W. C., 1965: Meteorological drought.
Paltridge, G., A. Arking, and M. Pook, 2009: Trends in middle- and upper-level tropospheric humidity from NCEP reanalysis data. *Theoretical and Applied Climatology*, **98**, 351-359.
Pan, Z. T., R. W. Arritt, E. S. Takle, W. J. Gutowski, C. J. Anderson, and M. Segal, 2004: Altered hydrologic feedback in a warming climate introduces a "warming hole". *Geophysical Research Letters*, **31**.
Panagiotopoulos, F., M. Shahgedanova, A. Hannachi, and D. B. Stephenson, 2005: Observed trends and teleconnections of the Siberian high: A recently declining center of action. *Journal of Climate*, **18**, 1411-1422.
Parker, D., C. Folland, A. Scaife, J. Knight, A. Colman, P. Baines, and B. Dong, 2007: Decadal to multidecadal variability and the climate change background. *Journal of Geophysical Research-Atmospheres*, **112**, -.
Parker, D. E., 2006: A demonstration that large-scale warming is not urban. *Journal of Climate*, **19**, 2882-2895.
——, 2010: Urban heat island effects on estimates of observed climate change. *Wiley Interdisciplinary Reviews-Climate Change*, **1**, 123-133.
Parker, D. E., 2011: Recent land surface air temperature trends assessed using the 20th Century Reanalysis. *Journal of Geophysical Research - Atmospheres*, **116**, D20125.
Parker, D. E., P. Jones, T. C. Peterson, and J. Kennedy, 2009: Comment on "Unresolved issues with the assessment of multidecadal global land surface temperature trends" by Roger A. Pielke Sr. et al. *Journal of Geophysical Research-Atmospheres*, **114**.
Parrish, D. D., D. B. Millet, and A. H. Goldstein, 2009: Increasing ozone in marine boundary layer inflow at the west coasts of North America and Europe. *Atmos. Chem. Phys.*, **9**, 1303-1323.
Pattanaik, D. R., and M. Rajeevan, 2010: Variability of extreme rainfall events over India during southwest monsoon season. *Meteorological Applications*, **17**, 88-104.
Pavan, V., R. Tomozeiu, C. Cacciamani, and M. Di Lorenzo, 2008: Daily precipitation observations over Emilia-Romagna: mean values and extremes. *International Journal of Climatology*, **28**, 2065-2079.
Penalba, O. C., and F. A. Robledo, 2010: Spatial and temporal variability of the frequency of extreme daily rainfall regime in the La Plata Basin during the 20th century. *Climatic Change*, **98**, 531-550.
Peterson, T. C., and M. J. Manton, 2008: Monitoring changes in climate extremes - A tale of international collaboration. *Bulletin of the American Meteorological Society*, **89**, 1266-1271.
Peterson, T. C., K. M. Willett, and P. W. Thorne, 2011: Observed changes in surface atmospheric energy over land. *Geophysical Research Letters*, **38**.
Peterson, T. C., X. B. Zhang, M. Brunet-India, and J. L. Vazquez-Aguirre, 2008: Changes in North American extremes derived from daily weather data. *Journal of Geophysical Research-Atmospheres*, **113**.
Peterson, T. C., et al., 2009: State of the Climate in 2008. *Bulletin of the American Meteorological Society*, **90**, S13-+.
Petrow, T., and B. Merz, 2009: Trends in flood magnitude, frequency and seasonality in Germany in the period 1951-2002. *Journal of Hydrology*, **371**, 129-141.
Pezza, A. B., and I. Simmonds, 2008: Large-scale Factors in Tropical. and Extratropical Cyclone Transition and Extreme Weather Events. *Trends and Directions in Climate Research*, L. Gimeno, R. GarciaHerrera, and R. M. Trigo, Eds., 189-211.
Pezza, A. B., I. Simmonds, and J. A. Renwick, 2007: Southern Hemisphere cyclones and anticyclones: Recent trends and links with decadal variability in the Pacific Ocean. *International Journal of Climatology*, **27**, 1403-1419.
Philipona, R., K. Behrens, and C. Ruckstuhl, 2009: How declining aerosols and rising greenhouse gases forced rapid warming in Europe since the 1980s. *Geophysical Research Letters*, **36**, L02806.
Philipona, R., B. Durr, C. Marty, A. Ohmura, and M. Wild, 2004: Radiative forcing - measured at Earth's surface - corroborate the increasing greenhouse effect. *Geophysical Research Letters*, **31**, L03202.
Philipp, A., P. M. Della-Marta, J. Jacobeit, D. R. Fereday, P. D. Jones, A. Moberg, and H. Wanner, 2007: Long-term variability of daily North Atlantic-European pressure patterns since 1850 classified by simulated annealing clustering. *Journal of Climate*, **20**, 4065-4095.
Pielke, R. A., Sr., et al., 2007: Unresolved issues with the assessment of multidecadal global land surface temperature trends. *Journal of Geophysical Research-Atmospheres*, **112**.
Pinker, R. T., B. Zhang, and E. G. Dutton, 2005: Do satellites detect trends in surface solar radiation? *Science*, **308**, 850-854.
Pinto, J. G., T. Spangehl, U. Ulbrich, and P. Speth, 2006: Assessment of winter cyclone activity in a transient ECHAM4-OPYC3 GHG experiment. *Meteorologische Zeitschrift*, **15**, 279-291.
Pinto, J. G., S. Zacharias, A. H. Fink, G. C. Leckebusch, and U. Ulbrich, 2009: Factors contributing to the development of extreme North Atlantic cyclones and their relationship with the NAO. *Climate Dynamics*, **32**, 711-737.
Pirazzoli, P. A., and A. Tomasin, 2003: Recent near-surface wind changes in the central Mediterranean and Adriatic areas. *International Journal of Climatology*, **23**, 963-973.

Portmann, R. W., S. Solomon, and G. C. Hegerl, 2009: Linkages between climate change, extreme temperature and precipitation across the United States. *Proceedings of the National Academy of Sciences*, **106**, 7324-7329.
Power, S., T. Casey, C. Folland, A. Colman, and V. Mehta, 1999: Inter-decadal modulation of the impact of ENSO on Australia. *Climate Dynamics*, **15**, 319-324.
Power, S. B., and I. N. Smith, 2007: Weakening of the Walker Circulation and apparent dominance of El Nino both reach record levels, but has ENSO really changed? *Geophysical Research Letters*, **34**.
Pozzoli, L., et al., 2011: Reanalysis of tropospheric sulfate aerosol and ozone for the period 1980-2005 using the aerosol-chemistry-climate model ECHAM5-HAMMOZ. *Atmospheric Chemistry and Physics*, **11**, 9563-9594.
Prata, F., 2008: The climatological record of clear-sky longwave radiation at the Earth's surface: evidence for water vapour feedback? *International Journal of Remote Sensing*, **29**, 5247-5263.
Prather, M., and J. Hsu, 2008: NF3, the greenhouse gas missing from Kyoto. *Geophysical Research Letters*, ARTN L12810, DOI 10.1029/2008GL034542. -.
Prinn, R., et al., 2005: Evidence for variability of atmospheric hydroxyl radicals over the past quarter century. *Geophysical Research Letters*, ARTN L07809, DOI 10.1029/2004GL022228. -.
Prospero, J. M., P. Ginoux, O. Torres, S. E. Nicholson, and T. E. Gill, 2002: Environmental characterization of global sources of atmospheric soil dust identified with the Nimbus 7 Total Ozone Mapping Spectrometer (TOMS) absorbing aerosol product. *Reviews of Geophysics*, **40**.
Pryor, S. C., R. J. Barthelmie, and E. S. Riley, 2007: Historical evolution of wind climates in the USA - art. no. 012065. *Science of Making Torque from Wind*, M. O. L. Hansen, and K. S. Hansen, Eds., 12065-12065.
Pryor, S. C., et al., 2009: Wind speed trends over the contiguous United States. *Journal of Geophysical Research-Atmospheres*, **114**.
Qian, Y., D. P. Kaiser, L. R. Leung, and M. Xu, 2006: More frequent cloud-free sky and less surface solar radiation in China from 1955 to 2000. *Geophysical Research Letters*, **33**, L01812.
Quinn, P. K., T. S. Bates, K. Schulz, and G. E. Shaw, 2009: Decadal trends in aerosol chemical composition at Barrow, Alaska: 1976-2008. *Atmos. Chem. Phys.*, **9**, 8883-8888.
Rahimzadeh, F., A. Asgari, and E. Fattahi, 2009: Variability of extreme temperature and precipitation in Iran during recent decades. *International Journal of Climatology*, **29**, 329-343.
Rahmstorf, S., and D. Coumou, 2011: Increase of extreme events in a warming world. *Proceedings of the National Academy of Sciences of the United States of America*, **108**, 17905-17909.
Raible, C. C., P. M. Della-Marta, C. Schwierz, H. Wernli, and R. Blender, 2008: Northern hemisphere extratropical cyclones: A comparison of detection and tracking methods and different reanalyses. *Monthly Weather Review*, **136**, 880-897.
Raichijk, C., 2011: Observed trends in sunshine duration over South America. *Int. J. Climatol.*, DOI: 10.1002/joc.2296.
Rajeevan, M., J. Bhate, and A. K. Jaswal, 2008: Analysis of variability and trends of extreme rainfall events over India using 104 years of gridded daily rainfall data. *Geophysical Research Letters*, **35**.
Ramanathan, V., P. J. Crutzen, J. T. Kiehl, and D. Rosenfeld, 2001: Atmosphere - Aerosols, climate, and the hydrological cycle. *Science*, **294**, 2119-2124.
Randall, R. M., and B. M. Herman, 2008: Using limited time period trends as a means to determine attribution of discrepancies in microwave sounding unit-derived tropospheric temperature time series. *Journal of Geophysical Research-Atmospheres*, **113**.
Randel, W., and F. Wu, 2010: The Polar Summer Tropopause Inversion Layer. *Journal of the Atmospheric Sciences*, **67**, 2572-2581.
Randel, W. J., F. Wu, H. Vomel, G. E. Nedoluha, and P. Forster, 2006: Decreases in stratospheric water vapor after 2001: Links to changes in the tropical tropopause and the Brewer-Dobson circulation. *Journal of Geophysical Research-Atmospheres*, **111**.
Randel, W. J., et al., 2009: An update of observed stratospheric temperature trends. *Journal of Geophysical Research-Atmospheres*, **114**.
Rasmusson, E. M., and J. M. Wallace, 1983: Meteorological aspects of the El Nino - Southern Oscillation. *Science*, **222**, 1195-1202.
Raupach, M., J. Canadell, and C. Le Quere, 2008: Anthropogenic and biophysical contributions to increasing atmospheric CO2 growth rate and airborne fraction. *Biogeosciences*. 1601-1613.
Rausch, J., A. Heidinger, and R. Bennartz, 2010: Regional assessment of microphysical properties of marine boundary layer cloud using the PATMOS-x dataset. *Journal of Geophysical Research-Atmospheres*, **115**.
Ravishankara, A. R., J. S. Daniel, and R. W. Portmann, 2009: Nitrous Oxide (N(2)O): The Dominant Ozone-Depleting Substance Emitted in the 21st Century. *Science*, **326**, 123-125.
Rayner, D. P., 2007: Wind run changes: The dominant factor affecting pan evaporation trends in Australia. *Journal of Climate*, **20**, 3379-3394.
Rayner, N. A., et al., 2003: Global analyses of sea surface temperature, sea ice, and night marine air temperature since the late nineteenth century. *Journal of Geophysical Research-Atmospheres*, **108**.
Rayner, N. A., et al., 2006: Improved analyses of changes and uncertainties in sea surface temperature measured in situ sice the mid-nineteenth century: The HadSST2 dataset. *Journal of Climate*, **19**, 446-469.
Re, M., and V. R. Barros, 2009: Extreme rainfalls in SE South America. *Climatic Change*, **96**, 119-136.

Read, W. G., et al., 2007: Aura Microwave Limb Sounder upper tropospheric and lower stratospheric H2O and relative humidity with respect to ice validation. *Journal of Geophysical Research-Atmospheres*, **112**.
Ren, G. Y., Y. Q. Zhou, Z. Y. Chu, J. X. Zhou, A. Y. Zhang, J. Guo, and X. F. Liu, 2008: Urbanization effects on observed surface air temperature trends in north China. *Journal of Climate*, **21**, 1333-1348.
Reynolds, R. W., C. L. Gentemann, and G. K. Corlett, 2010: Evaluation of AATSR and TMI Satellite SST Data. *Journal of Climate*, **23**, 152-165.
Reynolds, R. W., N. A. Rayner, T. M. Smith, D. C. Stokes, W. Wang, and A. M. S. Ams, 2002: *An improved in situ and satellite SST analysis.* 146-148 pp.
Reynolds, R. W., T. M. Smith, C. Liu, D. B. Chelton, K. S. Casey, and M. G. Schlax, 2007: Daily high-resolution-blended analyses for sea surface temperature. *Journal of Climate*, **20**, 5473-5496.
Rhode, R., et al., submitted: Berkeley Earth Temperature Averaging Process. *Journal of Geophysical Reseach*. submitted.
Richter, A., J. P. Burrows, H. Nüß, C. Granier, and U. Niemeier, 2005: Increase in tropospheric nitrogen dioxide over China observed from space. *Nature*, **437,**, 129-132, d.
Rienecker, M. M., Suarez, M.J., Gelaro, R., Todling, R., Bacmeister, J., Liu, E., Bosilovich, M.G., Schubert, S.D., Takacs, L., Kim, G.-K., Bloom, S., Chen, J., Collins, D., Conaty, A., da Silva, A., Gu, W., Joiner, J., Koster, R.D., Lucchesi, R., Molod, A., Owens, T., Pawson, S., Pegion, P., Redder, C. R., Reichle, R., Robertson, F. R., Ruddick, A. G., Sienkiewicz, M., Woollen, J., 2011: MERRA: NASA's Modern-Era Retrospective Analysis for Research and Applications. *J. Climate*, **in press**.
Rigby, M., et al., 2008: Renewed growth of atmospheric methane. *Geophysical Research Letters*, ARTN L22805, DOI 10.1029/2008GL036037. -.
Rigby, M., et al., 2010: History of atmospheric SF6 from 1973 to 2008. *Atmospheric Chemistry and Physics*, DOI 10.5194/acp-10-10305-2010. 10305-10320.
Riihimaki, L. D., F. E. Vignola, and C. N. Long, 2009: Analyzing the contribution of aerosols to an observed increase in direct normal irradiance in Oregon. *Journal of Geophysical Research-Atmospheres*, **114**, D00d02.
Robock, A., et al., 2000: The Global Soil Moisture Data Bank. *Bulletin of the American Meteorological Society*, **81**, 1281-1299.
Rodda, J. C., M. A. Little, H. J. E. Rodda, and P. E. McSharry, 2010: A comparative study of the magnitude, frequency and distribution of intense rainfall in the United Kingdom. *International Journal of Climatology*, **30**, 1776-1783.
Roderick, M. L., and G. D. Farquhar, 2002: The cause of decreased pan evaporation over the past 50 years. *Science*, **298**, 1410-1411.
Roderick, M. L., L. D. Rotstayn, G. D. Farquhar, and M. T. Hobbins, 2007: On the attribution of changing pan evaporation. *Geophysical Research Letters*, **34**.
Rohs, S., et al., 2006: Long-term changes of methane and hydrogen in the stratosphere in the period 1978-2003 and their impact on the abundance of stratospheric water vapor. *Journal of Geophysical Research-Atmospheres*, **111**.
Rosenlof, K. H., and G. C. Reid, 2008: Trends in the temperature and water vapor content of the tropical lower stratosphere: Sea surface connection. *Journal of Geophysical Research-Atmospheres*, **113**.
Rosenzweig, C., et al., 2007: Assessment of observed changes and responses in natural and managed systems. *Climate Change 2007: Impacts, Adaptation and Vulnerability. Contribution of Working Group II to the Fourth Assessment Report of the Intergovernmental Panel on Climate Change*, M. L. Parry, O. F. Canziani, J. P. Palutikof, P. J. van der Linden, and C. E. Hanson, Eds., Cambridge University Press.
Rossow, W. B., and R. A. Schiffer, 1999: Advances in understanding clouds from ISCCP. *Bulletin of the American Meteorological Society*, **80**, 2261-2287.
Ruckstuhl, C., et al., 2008: Aerosol and cloud effects on solar brightening and the recent rapid warming. *Geophysical Research Letters*, **35**, L12708.
Ruddiman, W., 2003: The anthropogenic greenhouse era began thousands of years ago. *Climatic Change*. 261-293.
——, 2007: The early anthropogenic hypothesis: Challenges and responses. *Reviews of Geophysics*, ARTN RG4001, DOI 10.1029/2006RG000207. -.
Rudolf, B., A. Becker, U. Schneider, A. Meyer-Christoffer, and M. Ziese, 2011: New GPCC full data reanalysis version 5 provides high-quality gridded monthly precipitation data. *Gewex News*, **21**, 4-5.
Russak, V., 2009: Changes in solar radiation and their influence on temperature trend in Estonia (1955-2007). *Journal of Geophysical Research-Atmospheres*, **114**, D00d01.
Rusticucci, M., and M. Renom, 2008: Variability and trends in indices of quality-controlled daily temperature extremes in Uruguay. *International Journal of Climatology*, **28**, 1083-1095.
Saha, S., et al., 2010: THE NCEP CLIMATE FORECAST SYSTEM REANALYSIS. *Bulletin of the American Meteorological Society*, **91**, 1015-1057.
Saji, N. H., B. N. Goswami, P. N. Vinayachandran, and T. Yamagata, 1999: A dipole mode in the tropical Indian Ocean. *Nature*, **401**, 360-363.
Sakamoto, M., and J. R. Christy, 2009: The Influences of TOVS Radiance Assimilation on Temperature and Moisture Tendencies in JRA-25 and ERA-40. *Journal of Atmospheric and Oceanic Technology*, **26**, 1435-1455.
Sanchez-Lorenzo, A., J. Calbo, and J. Martin-Vide, 2008a: Spatial and Temporal Trends in Sunshine Duration over Western Europe (1938-2004). *Journal of Climate*, **21**, 6089-6098.

Sanchez-Lorenzo, A., J. Calbo, J. Martin-Vide, A. Garcia-Manuel, G. Garcia-Soriano, and C. Beck, 2008b: Winter "weekend effect" in southern Europe and its connections with periodicities in atmospheric dynamics. *Geophysical Research Letters*, **35**.

Santer, B., et al., 2008: Consistency of modelled and observed temperature trends in the tropical troposphere. *International Journal of Climatology*, **28**, 1703-1722.

Santer, B. D., et al., 2000: Statistical significance of trends and trend differences in layer-average atmospheric temperature time series. *Journal of Geophysical Research-Atmospheres*, **105**, 7337-7356.

Santer, B. D., et al., 2007: Identification of human-induced changes in atmospheric moisture content. *Proceedings of the National Academy of Sciences of the United States of America*, **104**, 15248-15253.

Santer, B. D., et al., 2011: Separating Signal and Noise in Atmospheric Temperature Changes: The Importance of Timescale. *Journal of Geophysical Research*, 10.1029/2011JD016263.

Scaife, A. A., C. K. Folland, L. V. Alexander, A. Moberg, and J. R. Knight, 2008: European climate extremes and the North Atlantic Oscillation. *Journal of Climate*, **21**, 72-83.

Scaife, A. A., J. Austin, N. Butchart, S. Pawson, M. Keil, J. Nash, and I. N. James, 2000: Seasonal and interannual variability of the stratosphere diagnosed from UKMO TOVS analyses. *Quarterly Journal of the Royal Meteorological Society*, **126**, 2585-2604.

Schar, C., P. L. Vidale, D. Luthi, C. Frei, C. Haberli, M. A. Liniger, and C. Appenzeller, 2004: The role of increasing temperature variability in European summer heatwaves. *Nature*, **427**, 332-336.

Scherer, M., H. Vomel, S. Fueglistaler, S. J. Oltmans, and J. Staehelin, 2008: Trends and variability of midlatitude stratospheric water vapour deduced from the re-evaluated Boulder balloon series and HALOE. *Atmospheric Chemistry and Physics*, **8**, 1391-1402.

Schmidt, G. A., 2009: Spurious correlations between recent warming and indices of local economic activity. *International Journal of Climatology*, **29**, 2041-2048.

Schneider, T., P. A. O'Gorman, and X. J. Levine, 2010: Water vapour and the dynamics of climate changes. Reviews of Geophysics, RG3001.

Schneidereit, A., R. Blender, K. Fraedrich, and F. Lunkeit, 2007: Icelandic climate and north Atlantic cyclones in ERA-40 reanalyses. *Meteorologische Zeitschrift*, **16**, 17-23.

Scinocca, J. F., D. B. Stephenson, T. C. Bailey, and J. Austin, 2010: Estimates of past and future ozone trends from multimodel simulations using a flexible smoothing spline methodology. *Journal of Geophysical Research-Atmospheres*, **115**.

Seidel, D. J., and J. R. Lanzante, 2004: An assessment of three alternatives to linear trends for characterizing global atmospheric temperature changes. *Journal of Geophysical Research-Atmospheres*, **109**.

Seidel, D. J., and W. J. Randel, 2007: Recent widening of the tropical belt: Evidence from tropopause observations. *Journal of Geophysical Research-Atmospheres*, **112**.

Seidel, D. J., Q. Fu, W. J. Randel, and T. J. Reichler, 2008: Widening of the tropical belt in a changing climate. *Nature Geoscience*, **1**, 21-24.

Seidel, D. J., Gillett, N. P., Lanzante, J. R., Shine, K. P., Thorne, P. W., 2011: Stratospheric temperature trends: Our evolving understanding.

Seleshi, Y., and P. Camberlin, 2006: Recent changes in dry spell and extreme rainfall events in Ethiopia. *Theoretical and Applied Climatology*, **83**, 181-191.

SEN, P., 1968: ESTIMATES OF REGRESSION COEFFICIENT BASED ON KENDALLS TAU. *Journal of the American Statistical Association*, **63**, 1379-&.

Sen Roy, S., 2009: A spatial analysis of extreme hourly precipitation patterns in India. *International Journal of Climatology*, **29**, 345-355.

Sen Roy, S., and R. C. Balling, 2005: Analysis of trends in maximum and minimum temperature, diurnal temperature range, and cloud cover over India. *Geophysical Research Letters*, **32**.

Seneviratne, S. I., et al., 2010: Investigating soil moisture-climate interactions in a changing climate: A review. *Earth-Science Reviews*, **99**, 125-161.

Seneviratne, S. I., et al., 2012: Changes in Climate Extremes and their Impacts on the Natural Physical Environment. Chapter 3 of the IPCC Special Report: *Managing the Risks of Extreme Events and Disasters to Advance Climate Change Adaptation*. In press.

Serquet, G., C. Marty, J. P. Dulex, and M. Rebetez, 2011: Seasonal trends and temperature dependence of the snowfall/precipitation-day ratio in Switzerland. *Geophysical Research Letters*, **38**.

Sharma, S., E. Andrews, L. A. Barrie, J. A. Ogren, and D. Lavoué, 2006: Variations and sources of the equivalent black carbon in the high Arctic revealed by long-term observations at Alert and Barrow: 1989-2003. *J. Geophys. Res.*, **111**, D14208.

Sheffield, J., and E. F. Wood, 2007: Characteristics of global and regional drought, 1950-2000: Analysis of soil moisture data from off-line simulation of the terrestrial hydrologic cycle. *Journal of Geophysical Research-Atmospheres*, **112**.

——, 2008: Global trends and variability in soil moisture and drought characteristics, 1950-2000, from observation-driven Simulations of the terrestrial hydrologic cycle. *Journal of Climate*, **21**, 432-458.

Shekar, M., H. Chand, S. Kumar, K. Srinivasan, and A. Ganju, 2010: Climate change studies in the western Himalaya. *Annals of Glaciology*, **51**.

Shepherd, A., and D. Wingham, 2007: Recent sea-level contributions of the Antarctic and Greenland ice sheets. *Science*, **315**, 1529-1532.
Sherwood, S. C., 2007: Simultaneous detection of climate change and observing biases in a network with incomplete sampling. *Journal of Climate*, **20**, 4047-4062.
Sherwood, S. C., C. L. Meyer, R. J. Allen, and H. A. Titchner, 2008: Robust Tropospheric Warming Revealed by Iteratively Homogenized Radiosonde Data. *Journal of Climate*, **21**, 5336-5350.
Sherwood, S. C., H. A. Titchner, P. W. Thorne, and M. P. McCarthy, 2009: How do we tell which estimates of past climate change are correct. *International Journal of Climatology*, **29**, 1520-1523.
Shi, G. Y., et al., 2008: Data quality assessment and the long-term trend of ground solar radiation in China. *Journal of Applied Meteorology and Climatology*, **47**, 1006-1016.
Shiklomanov, A. I., R. B. Lammers, M. A. Rawlins, L. C. Smith, and T. M. Pavelsky, 2007: Temporal and spatial variations in maximum river discharge from a new Russian data set. *Journal of Geophysical Research-Biogeosciences*, **112**.
Shiklomanov, I. A., V. Y. Georgievskii, V. I. Babkin, and Z. A. Balonishnikova, 2010: Research Problems of Formation and Estimation of Water Resources and Water Availability Changes of the Russian Federation. *Russian Meteorology and Hydrology*, **35**, 13-19.
Shine, K. P., J. J. Barnett, and W. J. Randel, 2008: Temperature trends derived from Stratospheric Sounding Unit radiances: The effect of increasing CO2 on the weighting function. *Geophysical Research Letters*, **35**.
Sickles, J. E., II, and D. S. Shadwick, 2007a: Seasonal and regional air quality and atmospheric deposition in the eastern United States. *J. Geophys. Res.*, **112**, D17302.
——, 2007b: Changes in air quality and atmospheric deposition in the eastern United States: 1990-2004. *J. Geophys. Res.*, **112**, D17301.
Simmonds, I., and K. Keay, 2002: Surface fluxes of momentum and mechanical energy over the North Pacific and North Atlantic Oceans. *Meteorology and Atmospheric Physics*, **80**, 1-18.
Simmons, A. J., K. M. Willett, P. D. Jones, P. W. Thorne, and D. P. Dee, 2010: Low-frequency variations in surface atmospheric humidity, temperature, and precipitation: Inferences from reanalyses and monthly gridded observational data sets. *Journal of Geophysical Research-Atmospheres*, **115**.
Simolo, C., M. Brunetti, M. Maugeri, and T. Nanni, 2011: Evolution of extreme temperatures in a warming climate. *Geophysical Research Letters*, **38**, 6.
Smith, T. M., and R. W. Reynolds, 2002: Bias corrections for historical sea surface temperatures based on marine air temperatures. *Journal of Climate*, **15**, 73-87.
Smith, T. M., R. W. Reynolds, T. C. Peterson, and J. Lawrimore, 2008: Improvements to NOAA's historical merged land-ocean surface temperature analysis (1880-2006). *Journal of Climate*, **21**, 2283-2296.
Smith, T. M., P. A. Arkin, M. R. P. Sapiano, and C. Y. Chang, 2010: Merged Statistical Analyses of Historical Monthly Precipitation Anomalies Beginning 1900. *Journal of Climate*, **23**, 5755-5770.
Smits, A., A. Tank, and G. P. Konnen, 2005: Trends in storminess over the Netherlands, 1962-2002. *International Journal of Climatology*, **25**, 1331-1344.
Soden, B. J., D. L. Jackson, V. Ramaswamy, M. D. Schwarzkopf, and X. L. Huang, 2005: The radiative signature of upper tropospheric moistening. *Science*, **310**, 841-844.
Sohn, B. J., and S. C. Park, 2010: Strengthened tropical circulations in past three decades inferred from water vapor transport. *Journal of Geophysical Research-Atmospheres*, **115**.
Solomon, S., K. Rosenlof, R. Portmann, J. Daniel, S. Davis, T. Sanford, and G. Plattner, 2010: Contributions of Stratospheric Water Vapor to Decadal Changes in the Rate of Global Warming. *Science*, DOI 10.1126/science.1182488. 1219-1223.
Song, H., and M. H. Zhang, 2007: Changes of the boreal winter Hadley circulation in the NCEP-NCAR and ECMWF reanalyses: A comparative study. *Journal of Climate*, **20**, 5191-5200.
Sorteberg, A., and J. E. Walsh, 2008: Seasonal cyclone variability at 70 degrees N and its impact on moisture transport into the Arctic. *Tellus Series a-Dynamic Meteorology and Oceanography*, **60**, 570-586.
Spencer, R. W., and J. R. Christy, 1992: PRECISION AND RADIOSONDE VALIDATION OF SATELLITE GRIDPOINT TEMPERATURE ANOMALIES .2. A TROPOSPHERIC RETRIEVAL AND TRENDS DURING 1979-90. *Journal of Climate*, **5**, 858-866.
Spencer, R. W., and W. D. Braswell, 2010: On the diagnosis of radiative feedback in the presence of unknown radiative forcing. *Journal of Geophysical Research-Atmospheres*, **115**.
Stanhill, G., and S. Cohen, 2001: Global dimming: a review of the evidence for a widespread and significant reduction in global radiation with discussion of its probable causes and possible agricultural consequences. *Agricultural and Forest Meteorology*, **107**, 255-278.
Stark, J., C. Donlon, A. O'Carroll, and G. Corlett, 2008: Determination of AATSR biases using the OSTIA SST analysis system and a matchup database. *Journal of Atmospheric and Oceanic Technology*, **25**, 1208-1217.
Stemmler, K., et al., 2007: European emissions of HFC-365mfc, a chlorine-free substitute for the foam blowing agents HCFC-141b and CFC-11. *Environmental Science & Technology*, **41**, 1145-1151.
Stephens, G. L., and T. D. Ellis, 2008: Controls of Global-Mean Precipitation Increases in Global Warming GCM Experiments. *Journal of Climate*, **21**, 6141-6155.

Stephens, G. L., M. Wild, P. Stackhouse, T. L'Ecuyer, and S. Kato, submitted-a: The global character of the flux of downward longwave radiation. *J. Climate*. submitted.
Stephens, G. L., et al., submitted-b: The energy balance of the Earth's climate system. *Nature Geoscience*. submitted.
Stern, D. I., 2006: Reversal of the trend in global anthropogenic sulfur emissions. *Global Environmental Change-Human and Policy Dimensions*, **16**, 207-220.
Stickler, A., et al., 2010: THE COMPREHENSIVE HISTORICAL UPPER-AIR NETWORK. *Bulletin of the American Meteorological Society*, **91**, 741-+.
Stjern, C. W., J. E. Kristjansson, and A. W. Hansen, 2009: Global dimming and global brightening - an analysis of surface radiation and cloud cover data in northern Europe. *International Journal of Climatology*, **29**, 643-653.
Stohl, A., et al., 2009: An analytical inversion method for determining regional and global emissions of greenhouse gases: Sensitivity studies and application to halocarbons. *Atmospheric Chemistry and Physics*. 1597-1620.
Streets, D. G., Y. Wu, and M. Chin, 2006: Two-decadal aerosol trends as a likely explanation of the global dimming/brightening transition. *Geophysical Research Letters*, **33**, L15806.
Streets, D. G., et al., 2009: Anthropogenic and natural contributions to regional trends in aerosol optical depth, 1980-2006. *Journal of Geophysical Research-Atmospheres*, **114**.
Strong, C., and R. E. Davis, 2006: Temperature-related trends in the vertical position of the summer upper tropospheric surface of maximum wind over the Northern Hemisphere. *International Journal of Climatology*, **26**, 1977-1997.
——, 2007: Winter jet stream trends over the Northern Hemisphere. *Quarterly Journal of the Royal Meteorological Society*, **133**, 2109-2115.
——, 2008a: Variability in the position and strength of winter jet stream cores related to northern hemisphere teleconnections. *Journal of Climate*, **21**, 584-592.
——, 2008b: Comment on "Historical trends in the jet streams" by Cristina L. Archer and Ken Caldeira. *Geophysical Research Letters*. L24806 (24802 pp.).
Sun, B. M., T. R. Karl, and D. J. Seidel, 2007: Changes in cloud-ceiling heights and frequencies over the United States since the early 1950s. *Journal of Climate*, **20**, 3956-3970.
Sun, B. M., A. Reale, D. J. Seidel, and D. C. Hunt, 2010: Comparing radiosonde and COSMIC atmospheric profile data to quantify differences among radiosonde types and the effects of imperfect collocation on comparison statistics. *Journal of Geophysical Research-Atmospheres*, **115**.
Syakila, A., and C. Kroeze, 2011: The global nitrous oxide budget revisited. *Greenhouse Gas Measurement and Management*, **1**, 17-26.
Takahashi, K., A. Montecinos, K. Goubanova, and B. Dewitte, 2011: ENSO regimes: Reinterpreting the canonical and Modoki El Nino. *Geophysical Research Letters*, **38**, -.
Takeuchi, Y., Y. Endo, and S. Murakami, 2008: High correlation between winter precipitation and air temperature in heavy-snowfall areas in Japan. *Annals of Glaciology*, **49**, 7-10.
Tanimoto, H., 2009: Increase in springtime tropospheric ozone at a mountainous site in Japan for the period 1998-2006. *Atmospheric Environment*, **43**, 1358-1363.
Tanimoto, H., T. Ohara, and I. Uno, 2009: Asian anthropogenic emissions and decadal trends in springtime tropospheric ozone over Japan: 1998-2007. *Geophys. Res. Lett.*, **36**, L23802.
Tans, P., 2009: An Accounting of the Observed Increase in Oceanic and Atmospheric CO2 and an Outlook for the Future. *Oceanography*. 26-35.
Tegtmeier, S., K. Kruger, I. Wohltmann, K. Schoellhammer, and M. Rex, 2008: Variations of the residual circulation in the Northern Hemispheric winter. *Journal of Geophysical Research-Atmospheres*, **113**.
Teuling, A. J., et al., 2009: A regional perspective on trends in continental evaporation. *Geophysical Research Letters*, **36**, L02404.
Thompson, A. M., J. C. Witte, R. D. Hudson, H. Guo, J. R. Herman, and M. Fujiwara, 2001a: Tropical tropospheric biomass burning. *Science*, **291**, 2128-2132.
Thompson, A. M., J. C. Witte, R. D. Hudson, H. Guo, J. R. Herman, and M. Fujiwara, 2001b: Tropical Tropospheric Ozone and Biomass Burning. *Science*, **291**, 2128-2132.
Thompson, D. W. J., and J. M. Wallace, 1998: The Arctic Oscillation signature in the wintertime geopotential height and temperature fields. *Geophysical Research Letters*, **25**, 1297-1300.
——, 2000: Annular modes in the extratropical circulation. Part I: Month-to-month variability. *Journal of Climate*, **13**, 1000-1016.
Thompson, D. W. J., J. J. Kennedy, J. M. Wallace, and P. D. Jones, 2008: A large discontinuity in the mid-twentieth century in observed global-mean surface temperature. *Nature*, **453**, 646-U645.
Thorne, P. W., 2008: Arctic tropospheric warming amplification? *Nature*, **455**, E1-E2.
Thorne, P. W., and R. S. Vose, 2010: REANALYSES SUITABLE FOR CHARACTERIZING LONG-TERM TRENDS Are They Really Achievable? *Bulletin of the American Meteorological Society*, **91**, 353-+.
Thorne, P. W., D. E. Parker, J. R. Christy, and C. A. Mears, 2005a: Uncertainties in climate trends - Lessons from upper-air temperature records. *Bulletin of the American Meteorological Society*, **86**, 1437-+.
Thorne, P. W., D. E. Parker, S. F. B. Tett, P. D. Jones, M. McCarthy, H. Coleman, and P. Brohan, 2005b: Revisiting radiosonde upper air temperatures from 1958 to 2002. *Journal of Geophysical Research-Atmospheres*, **110**.
Thorne, P. W., et al., 2011a: A quantification of uncertainties in historical tropical tropospheric temperature trends from radiosondes. *Journal of Geophysical Research-Atmospheres*, **116**.

Thorne, P. W., et al., 2011b: Guiding the Creation of a Comprehensive Surface Temperature Resource for 21st Century Climate Science. *Bulletin of the American Meteorological Society*, 10.1175/2011BAMS3124.1.
Thorne, P. W., Brohan, P., Titchner, H. A., McCarthy, M. P., Sherwood, S. C., Peterson, T. C., Haimberger, L., Parker, D. E., Tett, S. F. B., Santer, B. D., Fereday, D. R., Kennedy, J. J., 2011a: A quantification of uncertainties in historical tropospheric temperature trends from radiosondes.
Thorne, P. W., Lanzante, J. R., Peterson, T. C., Seidel, D. J., Shine, K. P., 2011b: Tropospheric temperature trends: History of an ongoing controversy. 66-88.
Titchner, H. A., P. W. Thorne, M. P. McCarthy, S. F. B. Tett, L. Haimberger, and D. E. Parker, 2009: Critically Reassessing Tropospheric Temperature Trends from Radiosondes Using Realistic Validation Experiments. *Journal of Climate*, **22**, 465-485.
Tokinaga, H., and S.-P. Xie, 2011a: Wave and anemometer-based sea surface wind (WASWind) for climate change analysis (in press). *J. Clim.*
Tokinaga, H., and S. P. Xie, 2011b: Weakening of the equatorial Atlantic cold tongue over the past six decades. *Nature Geosci.*, 10.1038/NGEO1078.
Toreti, A., E. Xoplaki, D. Maraun, F. G. Kuglitsch, H. Wanner, and J. Luterbacher, 2010: Characterisation of extreme winter precipitation in Mediterranean coastal sites and associated anomalous atmospheric circulation patterns. *Natural Hazards and Earth System Sciences*, **10**, 1037-1050.
Torres, O., P. Barthia, J. Herman, A. Sinyuk, P. Ginoux, and B. Holben, 2002: A long-term record of aerosol optical depth from TOMS observations and comparison to AERONET measurements. *J.Atmos.Science*, **59,**, 398-413.
Trenberth, K. E., 1984: Signal versus noise in the Southern Oscillation. *Monthly Weather Review*, **112**, 326-332.
——, 1997: The definition of El Nino. *Bulletin of the American Meteorological Society*, **78**, 2771-2777.
Trenberth, K. E., and J. W. Hurrell, 1994: Decadal atmosphere-ocean variations in the Pacific. *Climate Dynamics*, **9**, 303-319.
Trenberth, K. E., and T. J. Hoar, 1996: The 1990-1995 El Nino Southern Oscillation event: Longest on record. *Geophysical Research Letters*, **23**, 57-60.
Trenberth, K. E., and D. P. Stepaniak, 2001: Indices of El Nino evolution. *Journal of Climate*, **14**, 1697-1701.
Trenberth, K. E., and D. J. Shea, 2006: Atlantic hurricanes and natural variability in 2005. *Geophysical Research Letters*, **33**.
Trenberth, K. E., and J. T. Fasullo, 2010: CLIMATE CHANGE Tracking Earth's Energy. *Science*, **328**, 316-317.
Trenberth, K. E., J. T. Fasullo, and J. Kiehl, 2009: EARTH'S GLOBAL ENERGY BUDGET. *Bulletin of the American Meteorological Society*, **90**, 311-+.
Trenberth, K. E., J. T. Fasullo, C. O'Dell, and T. Wong, 2010: Relationships between tropical sea surface temperature and top-of-atmosphere radiation. *Geophysical Research Letters*, **37**.
Trenberth, K. E., et al., 2007: Observations: Surface and Atmospheric Climate Change. *Climate Change 2007: The Physical Science Basis. Contribution of Working Group I to the Fourth Assessment Report of the Intergovernmental Panel on Climate Change*, Cambridge University Press.
Trewin, B., and H. Vermont, 2010: Changes in the frequency of record temperatures in Australia, 1957-2009. *Australian Meteorological and Oceanographic Journal*, **60**, 113-119.
Trnka, M., J. Kysely, M. Mozny, and M. Dubrovsky, 2009: Changes in Central-European soil-moisture availability and circulation patterns in 1881-2005. *International Journal of Climatology*, **29**, 655-672.
Troup, A. J., 1965: Southern Oscillation. *Quarterly Journal of the Royal Meteorological Society*, **91**, 490-&.
Tryhorn, L., and J. Risbey, 2006: On the distribution of heat waves over the Australian region. *Australian Meteorological Magazine*, **55**, 169-182.
Turner, J., et al., 2005: Antarctic climate change during the last 50 years. *International Journal of Climatology*, **25**, 279-294.
Uppala, S. M., et al., 2005: The ERA-40 re-analysis. *Quarterly Journal of the Royal Meteorological Society*, **131**, 2961-3012.
Usbeck, T., T. Wohlgemuth, C. Pfister, R. Volz, M. Beniston, and M. Dobbertin, 2010: Wind speed measurements and forest damage in Canton Zurich (Central Europe) from 1891 to winter 2007. *International Journal of Climatology*, **30**, 347-358.
Van den Besselaar, E. J. M., A. M. G. Klein Tank, and T. A. Buishand, submitted: Trends in European precipitation extremes. *Int. J. Climatol.*
van der A, R. J., et al., 2008: Trends, seasonal variability and dominant NOx source derived from a ten year record of NO2 measured from space. *J. Geophys. Res.*, **113, D04302, doi:10.1029/2007JD009021**.
van der Schrier, G., K. R. Briffa, P. D. Jones, and T. J. Osborn, 2006: Summer moisture variability across Europe. *Journal of Climate*, **19**, 2818-2834.
van Heerwaarden, C. C., J. V. G. de Arellano, and A. J. Teuling, 2010: Land-atmosphere coupling explains the link between pan evaporation and actual evapotranspiration trends in a changing climate. *Geophysical Research Letters*, **37**.
van Ommen, T. D., and V. Morgan, 2010: Snowfall increase in coastal East Antarctica linked with southwest Western Australian drought. *Nature Geoscience*, **3**, 267-272.
Vautard, R., J. Cattiaux, P. Yiou, J. N. The paut, and P. Ciais, 2010: Northern Hemisphere atmospheric stilling partly attributed to an increase in surface roughness. *Nature Geoscience*, 10.1038/ngeo979. 756-761.

Vautard, R., et al., 2007: Summertime European heat and drought waves induced by wintertime Mediterranean rainfall deficit. *Geophysical Research Letters*, **34**.

Vecchi, G. A., and B. J. Soden, 2007: Global warming and the weakening of the tropical circulation. *Journal of Climate*, **20**, 4316-4340.

Vecchi, G. A., and T. R. Knutson, 2008: On estimates of historical north Atlantic tropical cyclone activity. *Journal of Climate*, **21**, 3580-3600.

——, 2011: Estimating Annual Numbers of Atlantic Hurricanes Missing from the HURDAT Database (1878-1965) Using Ship Track Density. *Journal of Climate*, **24**, 1736-1746.

Vecchi, G. A., A. Clement, and B. J. Soden, 2008: Examining the tropical Pacific's response to global warming. *Eos, Trans. Amer. Geophys. Union*, 81-83.

Vecchi, G. A., B. J. Soden, A. T. Wittenberg, I. M. Held, A. Leetmaa, and M. J. Harrison, 2006: Weakening of tropical Pacific atmospheric circulation due to anthropogenic forcing. *Nature*, **441**, 73-76.

Velders, G., S. Andersen, J. Daniel, D. Fahey, and M. McFarland, 2007: The importance of the Montreal Protocol in protecting climate. *Proceedings of the National Academy of Sciences of the United States of America*, DOI 10.1073/pnas.0610328104. 4814-4819.

Velders, G., D. Fahey, J. Daniel, M. McFarland, and S. Andersen, 2009: The large contribution of projected HFC emissions to future climate forcing. *Proceedings of the National Academy of Sciences of the United States of America*, DOI 10.1073/pnas.0902817106. 10949-10954.

Venema, V. K., et al., 2011: Benchmarking monthly homogenization algorithms. *Climates of the Past Discussion*, **7**, 2655-2718.

Vicente-Serrano, S. M., and J. I. Lopez-Moreno, 2008: Nonstationary influence of the North Atlantic Oscillation on European precipitation. *Journal of Geophysical Research-Atmospheres*, **113**.

Vicente-Serrano, S. M., S. Begueria, and J. I. Lopez-Moreno, 2010a: A Multiscalar Drought Index Sensitive to Global Warming: The Standardized Precipitation Evapotranspiration Index. *Journal of Climate*, **23**, 1696-1718.

Vicente-Serrano, S. M., S. Begueria, J. I. Lopez-Moreno, M. Angulo, and A. El Kenawy, 2010b: A New Global 0.5 degrees Gridded Dataset (1901-2006) of a Multiscalar Drought Index: Comparison with Current Drought Index Datasets Based on the Palmer Drought Severity Index. *Journal of Hydrometeorology*, **11**, 1033-1043.

Vignati, E., M. Karl, M. Krol, J. Wilson, P. Stier, and F. Cavalli, 2010: Sources of uncertainties in modelling black carbon at the global scale. *Atmos. Chem. Phys.*, **10**, 2595-2611.

Vilibic, I., and J. Sepic, 2010: Long-term variability and trends of sea level storminess and extremes in European Seas. *Global and Planetary Change*, **71**, 1-12.

Visbeck, M., 2009: A Station-Based Southern Annular Mode Index from 1884 to 2005. *Journal of Climate*, **22**, 940-950.

Vollmer, M., S. Reimann, D. Folini, L. Porter, and L. Steele, 2006: First appearance and rapid growth of anthropogenic HFC-245fa (CHF2CH2CF3) in the atmosphere. *Geophysical Research Letters*, **33**, -.

Vomel, H., D. E. David, and K. Smith, 2007a: Accuracy of tropospheric and stratospheric water vapor measurements by the cryogenic frost point hygrometer: Instrumental details and observations. *Journal of Geophysical Research-Atmospheres*, **112**.

Vomel, H., et al., 2007b: Validation of Aura Microwave Limb Sounder water vapor by balloon-borne Cryogenic Frost point Hygrometer measurements. *Journal of Geophysical Research-Atmospheres*, **112**.

Von Storch, H., 1999: Misuses of Statistical Analysis in Climate Research. *Analysis of Climate Variability: Applications of Statistical Techniques*, 2nd Edition ed., H. Von Storch, and A. Navarra, Eds., Springer-Verlag, 11-26.

von Storch, H., and F. W. Zwiers, 1999: *Statistical Analysis in Climate Research.* Cambridge University Press, 484 pp.

Vose, R. S., D. R. Easterling, and B. Gleason, 2005a: Maximum and minimum temperature trends for the globe: An update through 2004. *Geophysical Research Letters*, **32**.

Vose, R. S., D. Wuertz, T. C. Peterson, and P. D. Jones, 2005b: An intercomparison of trends in surface air temperature analyses at the global, hemispheric, and grid-box scale. *Geophysical Research Letters*, **32**.

Vose, R. S., S. Applequist, M. J. Menne, C. N. Williams, and P. W. Thorne, Submitted-a: An Intercomparison of Temperature Trends in the U.S. Historical Climatology Network and Recent Atmospheric Reanalyses. *Geophysical Research Letters*.

Vose, R. S., Oak Ridge National Laboratory. Environmental Sciences Division., U.S. Global Change Research Program, United States. Dept. of Energy. Office of Health and Environmental Research., Carbon Dioxide Information Analysis Center (U.S.), and Martin Marietta Energy Systems Inc., 1992: *The Global historical climatology network : long-term monthly temperature, precipitation, sea level pressure, and station pressure data.* Carbon Dioxide Information Analysis Center Available to the public from N.T.I.S., 1 v. (various pagings) pp.

Vose, R. S., et al., Submitted-b: NOAA's Merged Land-Ocean Surface Temperature Analysis. *Bulletin of the American Meteorological Society*.

Wahba, G., 1990: *Spline models for observational data*. SIAM.

Wallace, J. M., and D. S. Gutzler, 1981: Teleconnections in the geopotential height field during the Northern Hemisphere winter. *Monthly Weather Review*, **109**, 784-812.

Wan, H., X. L. Wang, and V. R. Swail, 2010: Homogenization and Trend Analysis of Canadian Near-Surface Wind Speeds. *Journal of Climate*, **23**, 1209-1225.
Wang, J., M. McElroy, J. Logan, P. Palmer, W. Chameides, Y. Wang, and I. Megretskaia, 2008: A quantitative assessment of uncertainties affecting estimates of global mean OH derived from methyl chloroform observations. *Journal of Geophysical Research-Atmospheres*, **113**, -.
Wang, J. H., and L. Y. Zhang, 2008: Systematic errors in global radiosonde precipitable water data from comparisons with ground-based GPS measurements. *Journal of Climate*, **21**, 2218-2238.
——, 2009: Climate applications of a global, 2-hourly atmospheric precipitable water dataset derived from IGS tropospheric products. *Journal of Geodesy*, **83**, 209-217.
Wang, J. H., L. Y. Zhang, A. Dai, T. Van Hove, and J. Van Baelen, 2007: A near-global, 2-hourly data set of atmospheric precipitable water from ground-based GPS measurements. *Journal of Geophysical Research-Atmospheres*, **112**.
Wang, K. C., and S. L. Liang, 2009: Global atmospheric downward longwave radiation over land surface under all-sky conditions from 1973 to 2008. *Journal of Geophysical Research-Atmospheres*, **114**, -.
Wang, K. C., R. E. Dickinson, and S. L. Liang, 2009a: Clear Sky Visibility Has Decreased over Land Globally from 1973 to 2007. *Science*, **323**, 1468-1470.
Wang, K. C., R. E. Dickinson, M. Wild, and S. L. Liang, 2010: Evidence for decadal variation in global terrestrial evapotranspiration between 1982 and 2002: 2. Results. *Journal of Geophysical Research-Atmospheres*, **115**.
Wang, L., C.-Z. Zou, and H. Qian, Submitted: Construction of Stratospheric Temperature Data Records from Stratospheric Sounding Units. *Journal of Climate*.
Wang, X., et al., 2011: Trends and low-frequency variability of storminess over western Europe, 1878–2007. *Climate Dynamics*, 10.1007/s00382-011-1107-0. 1-17.
Wang, X. L. L., and V. R. Swail, 2001: Changes of extreme wave heights in Northern Hemisphere oceans and related atmospheric circulation regimes. *Journal of Climate*, **14**, 2204-2221.
Wang, X. L. L., V. R. Swail, and F. W. Zwiers, 2006: Climatology and changes of extratropical cyclone activity: Comparison of ERA-40 with NCEP-NCAR reanalysis for 1958-2001. *Journal of Climate*, **19**, 3145-3166.
Wang, X. L. L., F. W. Zwiers, V. R. Swail, and Y. Feng, 2009b: Trends and variability of storminess in the Northeast Atlantic region, 1874-2007. *Climate Dynamics*, **33**, 1179-1195.
Wang, X. M., P. M. Zhai, and C. C. Wang, 2009c: Variations in extratropical cyclone activity in northern East Asia. *Advances in Atmospheric Sciences*, **26**, 471-479.
Warren, S. G., R. M. Eastman, and C. J. Hahn, 2007: A survey of changes in cloud cover and cloud types over land from surface observations, 1971-96. *Journal of Climate*, **20**, 717-738.
Webster, P. J., G. J. Holland, J. A. Curry, and H. R. Chang, 2005: Changes in tropical cyclone number, duration, and intensity in a warming environment. *Science*, **309**, 1844-1846.
Weinstock, E. M., et al., 2009: Validation of the Harvard Lyman-alpha in situ water vapor instrument: Implications for the mechanisms that control stratospheric water vapor. *Journal of Geophysical Research-Atmospheres*, **114**.
Weiss, R., J. Muhle, P. Salameh, and C. Harth, 2008: Nitrogen trifluoride in the global atmosphere. *Geophysical Research Letters*, ARTN L20821, DOI 10.1029/2008GL035913. -.
Wells, N., S. Goddard, and M. J. Hayes, 2004: A self-calibrating Palmer Drought Severity Index. *Journal of Climate*, **17**, 2335-2351.
Weng, H. Y., S. K. Behera, and T. Yamagata, 2009: Anomalous winter climate conditions in the Pacific rim during recent El NiA +/- o Modoki and El NiA +/- o events. *Climate Dynamics*, **32**, 663-674.
Wentz, F. J., L. Ricciardulli, K. Hilburn, and C. Mears, 2007: How much more rain will global warming bring? *Science*, **317**, 233-235.
Werner, P. C., F. W. Gerstengarbe, and F. Wechsung, 2008: Grosswetterlagen and precipitation trends in the Elbe river catchment. *Meteorologische Zeitschrift*, **17**, 61-66.
Wibig, J., 2008: Cloudiness variations in Lodz in the second half of the 20th century. *International Journal of Climatology*, **28**, 479-491.
Wickham, C., et al., submitted: Influence of Urban Heating on the Global Temperature Land average Using Rural Sites Identified from MODIS Classifications. *Journal of Geophysical Research*. Submitted.
Wielicki, B. A., B. R. Barkstrom, E. F. Harrison, R. B. Lee, G. L. Smith, and J. E. Cooper, 1996: Clouds and the earth's radiant energy system (CERES): An earth observing system experiment. *Bulletin of the American Meteorological Society*, **77**, 853-868.
Wilby, R. L., P. D. Jones, and D. H. Lister, 2011: Decadal variations in the nocturnal heat island of London. *Weather*, **66**, 59-64.
Wilcox, L. J., B. J. Hoskins, and K. P. Shine, 2011: A global blended tropopause based on ERA data. Part II: Trends and tropical broadening. *Quarterly Journal of the Royal Meteorological Society*, DOI: 10.1002/qj.910.
Wild, M., 2008: Short-wave and long-wave surface radiation budgets in GCMs: a review based on the IPCC-AR4/CMIP3 models. *Tellus Series a-Dynamic Meteorology and Oceanography*, **60**, 932-945.
——, 2009: Global dimming and brightening: A review. *Journal of Geophysical Research-Atmospheres*, **114**.
Wild, M., and B. Liepert, 2010: The Earth radiation balance as driver of the global hydrological cycle. *Environmental Research Letters*, **5**.

Wild, M., A. Ohmura, and K. Makowski, 2007: Impact of global dimming and brightening on global warming. *Geophysical Research Letters*, **34**, L04702.
Wild, M., J. Grieser, and C. Schaer, 2008: Combined surface solar brightening and increasing greenhouse effect support recent intensification of the global land-based hydrological cycle. *Geophysical Research Letters*, **35**, L17706.
Wild, M., A. Ohmura, H. Gilgen, and D. Rosenfeld, 2004: On the consistency of trends in radiation and temperature records and implications for the global hydrological cycle. *Geophysical Research Letters*, **31**, L11201.
Wild, M., A. Ohmura, H. Gilgen, J. J. Morcrette, and A. Slingo, 2001: Evaluation of downward longwave radiation in general circulation models. *Journal of Climate*, **14**, 3227-3239.
Wild, M., A. Ohmura, H. Gilgen, E. Roeckner, M. Giorgetta, and J. J. Morcrette, 1998: The disposition of radiative energy in the global climate system: GCM-calculated versus observational estimates. *Climate Dynamics*, **14**, 853-869.
Wild, M., B. Truessel, A. Ohmura, C. N. Long, G. Konig-Langlo, E. G. Dutton, and A. Tsvetkov, 2009: Global dimming and brightening: An update beyond 2000. *Journal of Geophysical Research-Atmospheres*, **114**, D00d13.
Wild, M., et al., 2005: From dimming to brightening: Decadal changes in solar radiation at Earth's surface. *Science*, **308**, 847-850.
Wilks, D. S., 2006: *Statistical Methods in the Atmospheric Sciences.* 2nd Edition ed. Elsevier, 627 pp.
Willett, K. M., P. D. Jones, N. P. Gillett, and P. W. Thorne, 2008: Recent Changes in Surface Humidity: Development of the HadCRUH Dataset. *Journal of Climate*, **21**, 5364-5383.
Willett, K. M., P. D. Jones, P. W. Thorne, and N. P. Gillett, 2010: A comparison of large scale changes in surface humidity over land in observations and CMIP3 general circulation models. *Environmental Research Letters*, **5**.
Williams, C. A., M. J. Menne, and P. W. Thorne, Submitted: Benchmarking the performance of pairwise homogenization of surface temperatures in the United States. *Journal of Geophysical Research*.
Willson, R. C., and A. V. Mordvinov, 2003: Secular total solar irradiance trend during solar cycles 21-23. *Geophysical Research Letters*, **30**.
Wilson, R. C., et al., 2011: Have primary emission reduction measures reduced ozone across Europe? An analysis of European rural background ozone trends 1996–2005. *Atmos. Chem. Phys. Discuss.*, **11**, 18433-18485.
WMO, 2011: Scientific Assessment of Ozone Depletion: 2010, Global Ozone Research and Monitoring Project–Report No. 52.
Wong, T., B. A. Wielicki, R. B. Lee, ., G. L. Smith, K. A. Bush, and J. K. Willis, 2006: Reexamination of the observed decadal variability of the earth radiation budget using altitude-corrected ERBE/ERBS nonscanner WFOV data. *Journal of Climate*, **19**, 4028-4040.
Wood, S. N., 2006: *Generalized Additive Models: An Introduction with R*. CRC/Chapman & Hall.
Woodruff, S. D., et al., 2011: ICOADS Release 2.5: Extensions and Enhancements to the Surface Marine Meteorological Archive. *Int. J. Climatol.*, **31**, 951-967.
Worton, D., et al., 2007: Atmospheric trends and radiative forcings of CF4 and C2F6 inferred from firn air. *Environmental Science & Technology*, DOI 10.1021/es061710t. 2184-2189.
Wu, Z., N. E. Huang, J. M. Wallace, B. V. Smoliak, and X. Chen, 2011: On the time-varying trend in global-mean surface temperature. *Climate Dynamics*, **37**, 759-773.
Xavier, P. K., V. O. John, S. A. Buehler, R. S. Ajayamohan, and S. Sijikumar, 2010: Variability of Indian summer monsoon in a new upper tropospheric humidity data set. *Geophysical Research Letters*, **37**.
Xia, X., 2010a: A closer looking at dimming and brightening in China during 1961-2005. *Annales Geophysicae*, **28**, 1121-1132.
Xia, X. G., 2010b: Spatiotemporal changes in sunshine duration and cloud amount as well as their relationship in China during 1954-2005. *Journal of Geophysical Research-Atmospheres*, **115**.
Xie, B. G., Q. H. Zhang, and Y. Q. Wang, 2008: Trends in hail in China during 1960-2005. *Geophysical Research Letters*, **35**.
Xie, S., K. Hu, J. Hafner, H. Tokinaga, Y. Du, G. Huang, and T. Sampe, 2009: Indian Ocean Capacitor Effect on Indo-Western Pacific Climate during the Summer following El Nino. *Journal of Climate*, **22**, 730-747.
Xu, C. Y., L. B. Gong, J. Tong, and D. L. Chen, 2006a: Decreasing reference evapotranspiration in a warming climate - A case of Changjiang (Yangtze) River catchment during 1970-2000. *Advances in Atmospheric Sciences*, **23**, 513-520.
Xu, M., C. P. Chang, C. B. Fu, Y. Qi, A. Robock, D. Robinson, and H. M. Zhang, 2006b: Steady decline of east Asian monsoon winds, 1969-2000: Evidence from direct ground measurements of wind speed. *Journal of Geophysical Research-Atmospheres*, **111**.
Yang, T., et al., 2011a: Changes of climate extremes in a typical arid zone: Observations and multimodel ensemble projections. *Journal of Geophysical Research-Atmospheres*, **116**.
Yang, X. C., Y. L. Hou, and B. D. Chen, 2011b: Observed surface warming induced by urbanization in east China. *Journal of Geophysical Research-Atmospheres*, **116**, 12.
You, Q., et al., 2010: Changes in daily climate extremes in China and their connection to the large scale atmospheric circulation during 1961-2003. *Climate Dynamics*, 10.1007/s00382-009-0735-0.
You, Q. L., S. C. Kang, E. Aguilar, and Y. P. Yan, 2008: Changes in daily climate extremes in the eastern and central Tibetan Plateau during 1961-2005. *Journal of Geophysical Research-Atmospheres*, **113**.

Young, I. R., S. Zieger, and A. V. Babanin, 2011: Global Trends in Wind Speed and Wave Height. *Science*, **332**, 451-455.
Yu, B., and F. W. Zwiers, 2010: Changes in equatorial atmospheric zonal circulations in recent decades. *Geophysical Research Letters*, **37**.
Yuan, X., and C. Li, 2008: Climate modes in southern high latitudes and their impacts on Antarctic sea ice. *Journal of Geophysical Research-Oceans*, **113**, -.
Zaitchik, B. F., A. K. Macalady, L. R. Bonneau, and R. B. Smith, 2006: Europe's 2003 heat wave: A satellite view of impacts and land-atmosphere feedbacks. *International Journal of Climatology*, **26**, 743-769.
Zebiak, S. E., 1993: Air-sea interaction in the equatorial Atlantic region. *Journal of Climate*, **6**, 1567-1568.
Zelinka, M. D., and D. L. Hartmann, 2010: Why is longwave cloud feedback positive? *Journal of Geophysical Research-Atmospheres*, **115**.
Zerefos, C. S., et al., 2009: Solar dimming and brightening over Thessaloniki, Greece, and Beijing, China. *Tellus Series B-Chemical and Physical Meteorology*, **61**, 657-665.
Zhai, P. M., X. B. Zhang, H. Wan, and X. H. Pan, 2005: Trends in total precipitation and frequency of daily precipitation extremes over China. *Journal of Climate*, **18**, 1096-1108.
Zhang, H., J. Bates, and R. Reynolds, 2006: Assessment of composite global sampling: Sea srface wind speed. *Geophysical Research Letters*, **33**, -.
Zhang, J., and J. S. Reid, 2010: A decadal regional and global trend analysis of the aerosol optical depth using a data-assimilation grade over-water MODIS and Level 2 MISR aerosol products. *Atmos. Chem. Phys.*, **10**, 10949-10963.
Zhang, L., D. J. Jacob, X. Liu, J. A. Logan, K. Chance, A. Eldering, and B. R. Bojkov, 2010: Intercomparison methods for satellite measurements of atmospheric composition: application to tropospheric ozone from TES and OMI. *Atmos. Chem. Phys.*, **10**, 4725-4739.
Zhang, X., and F. Zwiers, 2004: Comment on "Applicability of prewhitening to eliminate the influence of serial correlation on the Mann-Kendall test" by Sheng Yue and Chun Yuan Wang. *Water Resources Research*, **40**, -.
Zhang, X., et al., 2007a: Detection of human influence on twentieth-century precipitation trends. *Nature*, **448**, 461-U464.
Zhang, X., et al., 2011a: Indices for monitoring changes in extremes based on daily temperature and precipitation data. *Wiley Interdisciplinary Reviews: Climate Change*, 10.1002/wcc.147. n/a-n/a.
Zhang, X. D., J. E. Walsh, J. Zhang, U. S. Bhatt, and M. Ikeda, 2004: Climatology and interannual variability of arctic cyclone activity: 1948-2002. *Journal of Climate*, **17**, 2300-2317.
Zhang, X. D., A. Sorteberg, J. Zhang, R. Gerdes, and J. C. Comiso, 2008: Recent radical shifts of atmospheric circulations and rapid changes in Arctic climate system. *Geophysical Research Letters*, **35**.
Zhang, X. Y., Y. Q. Wang, T. Niu, X. C. Zhang, S. L. Gong, Y. M. Zhang, and J. Y. Sun, 2011b: Atmospheric aerosol compositions in China: spatial/temporal variability, chemical signature, regional haze distribution and comparisons with global aerosols. *Atmos. Chem. Phys. Discuss.*, **11**, 26571-26615.
Zhang, Y., J. M. Wallace, and D. S. Battisti, 1997: ENSO-like interdecadal variability: 1900-93. *Journal of Climate*, **10**, 1004-1020.
Zhang, Y. C., W. B. Rossow, P. Stackhouse, A. Romanou, and B. A. Wielicki, 2007b: Decadal variations of global energy and ocean heat budget and meridional energy transports inferred from recent global data sets. *Journal of Geophysical Research-Atmospheres*, **112**.
Zhang, Y. Q., C. M. Liu, Y. H. Tang, and Y. H. Yang, 2007c: Trends in pan evaporation and reference and actual evapotranspiration across the Tibetan Plateau. *Journal of Geophysical Research-Atmospheres*, **112**.
Zhou, T. J., et al., 2009: Why the Western Pacific Subtropical High Has Extended Westward since the Late 1970s. *Journal of Climate*, **22**, 2199-2215.
Zhou, Y. P., K. M. Xu, Y. C. Sud, and A. K. Betts, 2011: Recent trends of the tropical hydrological cycle inferred from Global Precipitation Climatology Project and International Satellite Cloud Climatology Project data. *Journal of Geophysical Research-Atmospheres*, **116**.
Ziemke, J. R., S. Chandra, and P. K. Bhartia, 2005: A 25-year data record of atmospheric ozone in the Pacific from Total Ozone Mapping Spectrometer (TOMS) cloud slicing: Implications for ozone trends in the stratosphere and troposphere. *J. Geophys. Res.*, **110**, D15105.
Zolina, O., C. Simmer, S. K. Gulev, and S. Kollet, 2010: Changing structure of European precipitation: Longer wet periods leading to more abundant rainfalls. *Geophysical Research Letters*, **37**.
Zolina, O., C. Simmer, A. Kapala, S. Bachner, S. Gulev, and H. Maechel, 2008: Seasonally dependent changes of precipitation extremes over Germany since 1950 from a very dense observational network. *Journal of Geophysical Research-Atmospheres*, **113**.
Zou, C.-Z., and W. Wang, 2011: Inter-Satellite Calibration of AMSU-A Observations for Weather and Climate Applications. *Journal of Geophysical Research*, 10.1029/2011JD016205.
Zou, C. Z., and W. H. Wang, 2010: Stability of the MSU-Derived Atmospheric Temperature Trend. *Journal of Atmospheric and Oceanic Technology*, **27**, 1960-1971.
Zou, C. Z., M. Gao, and M. D. Goldberg, 2009: Error Structure and Atmospheric Temperature Trends in Observations from the Microwave Sounding Unit. *Journal of Climate*, **22**, 1661-1681.

Zou, C. Z., M. D. Goldberg, Z. H. Cheng, N. C. Grody, J. T. Sullivan, C. Y. Cao, and D. Tarpley, 2006a: Recalibration of microwave sounding unit for climate studies using simultaneous nadir overpasses. *Journal of Geophysical Research-Atmospheres*, **111**.

Zou, X., L. V. Alexander, D. Parker, and J. Caesar, 2006b: Variations in severe storms over China. *Geophysical Research Letters*, **33**.

Zwiers, F. W., and V. V. Kharin, 1998: Changes in the extremes of the climate simulated by CCC GCM2 under CO2 doubling. *Journal of Climate*, **11**, 2200-2222.

Tables

Table 2.13: Overview of O_3 trends reported in literature, using datasets with more than 8 years of data availability.

		Trend (ppb yr^{-1})	Period	Reference	Remark
Europe					
Europe, surface	Regional rural stations	0.27 ± 0.18 to 0.44 ± 0.15 (winter) –0.1 ± 0.28 to 0.04 ± 0.32 (summer)	1990–2005	(Pozzoli et al., 2011)	Linear regression, ca. 100 stations, lowest and highest trend estimate out of 4 European regions.
Europe, surface	Mace Head 53°N, 10°W	0.56 ± 0.36 (CS) 0.37 ± 0.13 (CS) 0.28 ± 0.33 (All) 0.18 ± 0.33 (All)	1990–2000 1990–2010 1990–2000 1990–2010	(Hess and Zbinden, 2011)	CS Clean sector selection. All: All measurements. Largest trend in winter and spring.
Europe, surface	Hohenpeissen-berg (48°N–11°E, 985 m)	0.31 ± 0.09	1971–2008	(Gilge et al., 2010)	Linear regression
Europe, free troposphere	Zugzpitze (47°N–11°E, 2962 m)	0.42 ± 0.09	1975–2008	(Gilge et al., 2010)	Linear regression
Europe, free troposphere	Jungfraujoch (46°N–8°E, 3580 m)	0.26 ± 0.16 (annual) 0.99 ± 0.45 0.69 ± 0.80	1986–2008 1990–1999 1990–1999	(Gilge et al., 2010) (Cui et al., 2010) (Cui et al., 2010)	Linear regression. Highest trends in winter, no significant trend in recent years.
Europe, free troposphere	MOZAIC (681 hPa)	0.18 ±0.18	1995–2008	(Logan et al., 2011)	Largest trends in winter and summmer
C. Europe, free troposphere	500 hPa	0.09 ± 0.44 0.02 ± 0.12	1990–2000 1990–2010	(Hess and Zbinden, 2011)	Composite of soundings and MOZAIC
N. Europe, free troposphere	500 hPa	0.61 ± 0.66 0.33 ± 0.26	1990–2000 1990–2010	(Hess and Zbinden, 2011)	Composite of soundings and MOZAIC
North America					
North America, surface	Regional rural stations	0.04 ± 0.18 to 0.22 ± 0.13 (winter) –0.4 ± 0.37 (Central US) to 0.4 ± 0.31 (W.US) (summer)	1990–2005	(Pozzoli et al., 2011)	Linear regression, ca. 100 stations, lowest and highest trend estimate for 5 US regions.
N. America, surface	Non-urban, multi net-work monitoring sites	–1.28 ± 0.41(SE US) to 0.3 ± 0.24 (Pacific)	1997–2006	(Chan, 2009; Chan and Vet, 2010)	97 sites; Principal component analysis, May- September, daily 8-hour maximu, 16 regions; Californian. Largest positive changes in winter
N. America, surface	Yreka, 42°N–123°W; Lassen Volcanic, 41–122°W; California	0.17 ± 0.04 (Yreka) 0.34 ± 0.06 (Lassen)	1981–2006 1987–2006	(Oltmans et al., 2008)	Partly baseline, partly influenced by local conditions. Cubic polynomial. Assume annual average of 33 and 42 ppb for conversion to ppb yr^{-1}
N. America, surface	8 Pacific US Stations	0.34 ± 0.09 (annual) 0.45 ± 0.13 (winter) 0.24 ± 0.16 (spring) 0.34 ± 0.09 (summer) 0.12 ± 0.14 (autumn)	8–25 years	(Parrish et al., 2009)	
N. America,	Western USA	0.63 ± 0.34	1995–2008	(Cooper et al.,	Various methods

free troposphere				2010)	
N. America, free troposphere	Eastern USA	1.60 ± 1.90 0.45 ± 0.51	1990–2000 1990–2010	(Hess and Zbinden, 2011)	
Asia					
Asia, surface	Mt. Happo, Japan	1.25 ± 0.53 springtime	1998–2007	(Tanimoto, 2009; Tanimoto et al., 2009)	Positive, but insigficant trends at 7 out of 9 Japanes stations.
Asia, troposphere	Continental South Asia	0.7–0.9% yr^{-1} of tropospheric column ozone	1997–2005	(Beig and Singh, 2007)	Satellite observations; further trends in China, and South East Asia.
Pacific, Free Tropopshere					
	Mauna Loa, Hawaii, 21°N, 157°W, 3400 m	0.14 ± 0.06	1973–2004	(Oltmans et al., 2006)	Mainly during autumn and winter, dynamical effect? Annual average 41 ppb for conversion.
Southern Hemisphere					
	Cape Point, 34°S, 18°E South Africa	0.11 ±	1982–2005	(Oltmans et al., 2006)	Yearly average ozone 22 ppb for conversion.

1
2

Box 2.4, Table 1: Established indices of climate variability with global or regional influence. Columns are: (1) name of a climate phenomenon, (2) name of the index, (3) index definition, (4) primary references, (5) comments, including when available, characterization of the index or its spatial pattern as a dominant variability mode.

Climate Phenomenon		Index name	Index Definition	Primary Refs	Characterization / Comments
El Niño – Southern Oscillation (ENSO)	Traditional indices of ENSO-related Tropical Pacific climate variability	NINO3	SST anomaly averaged over [5°S–5°N, 150°W–90°W]	Rasmusson (1983), Cane (1986)	Traditional SST-based ENSO index, "devised by the Climate Analysis Center of NOAA [*now: Climate Prediction Center*] because a warming in this region strongly influences the global atmosphere" Cane et al. (1986).
		NINO1	Same as above but for [10°S–5°S, 90°W–80°W]		Introduced along with NINO3 by NOAA's Climate Analysis Center (now: Climate Prediction Center) circa 1983–1984 to describe other details of ENSO-related tropical Pacific SST variability.
		NINO2	Same as above but for [5°S–0°, 90°W–80°W]		
		NINO1+2	Same as above but for [10°S–0°, 90°W–80°W]		
		NINO4	Same as above but for [5°S–5°N, 160°E–150°W]		
		NINO3.4	Same as above but for [5°S–5°N, 170°W–120°W]	Trenberth (1997)	Used by WMO, NOAA to define El Niño / La Niña events. Detrended form is close to the 1st PC of linearly detrended global field of monthly SST anomalies (Deser et al., 2010)
		Troup SOI	Standardized for each calendar month MSLP difference: Tahiti minus Darwin, x10	Troup (1965)	Used by Australian Bureau of Meteorology
		SOI	Standardized difference of standardized MSLP anomalies: Tahiti minus Darwin	Trenberth (1984)	Maximizes signal to noise ratio of linear combinations of Darwin / Tahiti records
		Darwin SOI	Standardized Darwin MSLP anomaly	Trenberth and Hoar (1996)	Introduced to avoid use of the Tahiti record, considered suspicious before 1935.
		Equatorial SOI (EQSOI)	Standardized difference of standardized MSLP anomalies over equatorial [5°S–5°N] Pacific Ocean: [130°W–80°W] minus [90°E–140°E]	Bell and Halpert (1998)	
	Indices of ENSO events evolution	Trans-Niño Index (TNI)	Standardized NINO1+2 minus standardized NINO4	Trenberth and Stepaniak (2001)	Nearly uncorrelated with NINO3.4

	and for identifying different types of events	El Niño Modoki Index (EMI)	SSTA: [165°E–140°W, 10°S–10°N] minus ½[110°W–70°W, 15°S–5°N] minus ½[125°E–145°E, 10°S–20°N]	Ashok et al. (2007)	Defines "typical El Niño Modoki events" as those with the seasonal EMI value (JJAS or DJF means) no less than 0.7σ, where σ is the seasonal EMI std.
		Indices of Eastern Pacific (EP) and Central Pacific (CP) types of ENSO events	EP Index: leading PC of the tropical Pacific SSTA with subtracted predictions from a linear regression on NINO4; CP index: same as EP but with NINO1+2 used in place of NINO4.	Kao and Yu (2009)	
		E and C Indices	45° orthogonal rotation of the two leading PCs of the equatorial Pacific SSTA. Approximate formulas: C=1.7*NINO4 - 0.1*NINO1+2, E = NINO1+2 - 0.5*NINO4	Takahashi et al. (2011)	Constructed to be mutually uncorrelated; many other SST-based ENSO indices are well approximated by linear combinations of E and C.
Pacific Decadal and Interdecadal Variability		Pacific Decadal Oscillation (PDO)	1st PC of monthly N. Pacific SST anomaly field [20°N–70°N] with subtracted global mean	Mantua et al. (1997); Zhang et al. (1997)	
		Intedecadal Pacific Oscillation (IPO)	Projection of a global SST anomaly field onto the IPO pattern, which is found as one of the leading EOFs of a low-pass filtered global SST field	Folland et al. (1999); Power et al. (1999) ; Parker et al. (2007)	IPO pattern was the 3rd EOF for 1911–1995 period and half power at 13.3 years; 2nd EOF for 1891–2005 data and 11 years half power
		North Pacific Index (NPI)	SLP [30°N–65°N; 160°E–140°W]	Trenberth and Hurrell (1994)	
NAO		Lisbon/ Ponta Delgada-Stykkisholmur/ Reykjavik North Atlantic Oscillation (NAO) Index	Lisbon/Ponta Delgada minus Stykkisholmur/ Reykjavik standardized MSLP anomalies	Hurrell (1995a)	A primary NH teleconnection both in MSLP and 500 hPa geopotential heigh (Z500) anomalies (Wallace and Gutzler, 1981); one of rotated PCs of NH Z500 (Barnston and Livezey, 1987). MSLP anomalies can be monthly, seasonal or annual averages, resulting in the NAO index of the same temporal resolution (Hurrell, 1995). In Jones et al. (1997) definition, temporal averaging is applied to monthly NAO index values. NAO index is typically interpreted for boreal winter season (e.g., DJFM or NDJFM means).
		Gibraltar – South-west Iceland NAO Index	Gibraltar minus South-west Icealnd / Reykjavik standardized monthly surface pressure anomalies	Jones et al. (1997)	
		PC-based NAO Index	Leading PC of MSLP anomalies over the Atlantic sector [20°N–80°N, 90°W–40°E]	Hurrell (1995a)	

		Summer NAO (SNAO)	Leading PC of daily MSLP anomalies for July and August over the North Atlantic region [25°N–70°N, 70°W–50°E]	Folland et al. (2009)	Calculations with daily, 10-day, or July-August mean MSLP data result in the same spatial pattern "characterized by a more northerly location and smaller spatial scale than its winter counterpart."
Annular modes	Arctic Oscillation (AO), a.k.a. Northern Annular Mode (NAM)	PC-based NAM (AO) index	1st PC of the monthly mean MSLP anomalies poleward of 20°N	Thompson and Wallace (1998, 2000)	Closely related to the NAO
	Antarctic Oscillation (AAO), a.k.a. Southern Annular Mode (SAM)	PC-based AAO index	1st PC of 850hPa or 700hPa height anomalies south of 20°S	Thompson and Wallace (2000)	
		Grid-based AAO index: 40°S–65°S difference	Difference between normalized zonal mean MSLP at 40°S and 65°S, using gridded SLP fields	Gong and Wang (1999)	
		Grid-based SAM index: 40°S–70°S difference	Same as above but uses latitudes 40°S and 70°S	Nan and Li (2003)	
		Station-based SAM index: 40°S–65°S	Difference in normalized zonal mean MSLP at 40°S and 65°S, using station data	Marshall et al. (2003)	
Pacific/North America (PNA) atmospheric teleconnection		PNA index based on centers of action	¼[Z(20°N, 160°W) - Z(45°N, 165°W) + Z(55°N, 115°W) - Z(30°N, 85°W)], Z is the location's standardized 500 hPa geopotential height anomaly	Wallace and Gutzler (1981)	A primary NH telecon-nection (Wallace and Gutzler, 1981) in MSLP and in 500 hPa geopotential height anomalies (Z500); 2nd leading rotated PC of the NH Z500 (Barnston and Livezey, 1987)
		RPC-based PNA	Amplitude of the PNA pattern in the decomposition of the 500 hPa geopotential (Z500) anomaly field into the set of leading rotated EOFs obtained from the RPCA analysis of the NH Z500 monthly anomalies	Barnston and Livezey (1987).	
Pacific/South America (PSA) atmospheric teleconnection		PSA1 and PSA2 mode indices (PC-based)	2nd and 3rd PCs respectively of SH 500 hPa seasonal geopotential height anomaly	Mo and Paegle (2001)	Calculation was done with NCEP-NCAR reanalysis for Jan 1949 - Mar 2000. First three PCs were explaining 20%, 13%, and 11% of the total variance, respectively. There many published variations on this procedure, involving temporal filtering, using austral winter data only, PC rotation, different variables (e.g., 200 hPa streamfunction). PSA1 is positive

				during El Niño events (sign-selecting convention).
	PSA index based on centers of action from the 1972-1982 El Niño events composite	[-Z(35°S, 150°W) + Z(60°S, 120°W) - Z(45°S, 60°W)], Z is the location's JJA 500 hPa geopotential height anomaly	Karoly (1989)	Approximates PSA1 of the previous definition
	PSA index based on centers of action and La Niña response sign	-[-Z(45°S, 170°W) + Z(67.5°S, 120°W) - Z(50°S, 45°W)]/3, Z is the location's 500 hPa geopotential height anomaly	Yuan and Li (2008)	Approximates (–1)*PSA1 of the PC-based definition above
Atlantic Ocean Themohaline circulation	Atlantic Multidecadal Oscillation (AMO) index	10-yr running mean of de-trended Atlantic mean SST anomalies [0°–70°N]	Enfield et al. (2001)	Called "virtually identical" to the smoothed leading rotated N. Atlantic PC
	Revised AMO index	As above, but subtracts global mean anomaly instead of de-trending	Trenberth and Shea (2006)	
Tropical Atlantic Ocean non-ENSO variability	Atlantic Niño Index, ATL3	SSTA [3°S–3°N, 20°W–0°]	Zebiak (1993)	Identified as the two leading PCs of detrended tropical Atlantic monthly SSTA (20°S–20°N): 38% and 25% variance respectively for HadISST1, 1900–2008 (Deser et al. 2010)
	Atlantic Niño Index, PC-based	1st PC of the detrended tropical Atlantic monthly SSTA (20°S–20°N)	Deser et al. (2010b)	
	Tropical Atlantic Meridional Mode (AMM)	2nd PC of the detrended tropical Atlantic monthly SSTA (20°S–20°N)		
Tropical Indian Ocean non-ENSO variability	Indian Ocean Basin Mode (IOBM) Index	The 1st PC of the IO detrended SST anomalies (40°E–110° E, 20°S–20°N)	Deser et al. (2010b)	Identified as the two leading PCs of detrended tropical Indian Ocean monthly SSTA (20°S–20°N): 39% and 12% of the variance, respectively, for HadISST1, 1900–2008 (Deser et al. 2010)
	Indian Ocean Dipole mode (IODM), PC-based index	The 2nd PC of the IO detrended SST anomalies (40°E–110° E, 20°S–20°N)		
	Indian Ocean Dipole Mode Index (DMI)	SST anomalies: [50°E–70°E, 10°S–10°N)]-[90°E–110°E, 10°S–0°]	Saji et al. (1999)	

1

Appendix 2.A: Methods of Estimating Linear Trends and Uncertainties

Several different methods of calculating linear trends and uncertainties have been applied to climate data sets to assess the sensitivity of trend estimates to the methodology. The methods are described briefly below. The conclusion of this analysis is that, for data sets like the ones addressed here, the trend line and uncertainty limits are very similar for most of the methods that take into account dependency in the data sets through an AR1 model. The results are also very similar to those given for the REML method used in AR4.

OLS: ordinary least squares, no reduction in degrees of freedom (DOF)

OLSdofrS: OLS, with DOF reduced as n --> nr=[n*(1-rho)/(1+rho)] andused in the formula for sigma (trend error estimate std). Hereinafterrho is lag-1 autocorrelation coefficient; it's estimated from asequence of the OLS residuals for all methods below except WS2001. (Itis assumed that the timeseries are avalable on a uniform time grid,without gaps). This OLSdofrS method is the same as the Santer et al. (2000) AdjSE method.

OLSdofrST: same as OLSdofrS, but nr replaces n also in t-statisticsDOF parameter, i.e., (1+-p)/2 quantiles of t(nr-2), not of t(n-2) areused to scale sigma for the boundaries of the p%-confidence intervalfor the trend slope. Same as Santer et al. (2000) AdjSE+AdjDF method.

GLS: generalized least squares approach, with the error covariancematrix V assumed to be proportional to that of the AR(1) process withautocorrelation rho (Vij=rho^|i-j|). To obtain the trend uncertaintyestimate this matrix is scaled by a factor s2=e'*inv(V)*e/(n-2), wheree is a vector of residuals. (This scaling factor s2 is what RMLEgives).

GLS-obs: a heuristic modification of GLS to take into accountuncertainties given with time series from Hadley Centre and used by AR4for trend calculation

Prewhtng: timeseries (y) is prewhitened as yw=(y(i+1)-rho*y(i))/(1-rho), and then the OLS is applied to yw. For this form of pre-whitening thelinear trend coefficient is the same for yw and y; given the trendcoefficient, the constant term can be estimated too.

Sen: Non parametric estimate of the linear trend based on Kendall'stau, from Sen (1968). Assumes independent observations. No DOFreduction is made.

WS2001: A method of trend calculation iterating between computing Sentrend slope for prewhitened (as above) timeseries, computing trendline residuals from the original timeseries and their rho, prewhitening, etc. proposed by (Wang and Swail, 2001), Appendix A). Compared with other method and recommended by (Zhang and Zwiers, 2004).

Among these methods Sen and WS2001 do non-parametric trend estimation. All other methods are least squares based, hence their interpretation is that the data is assumed to represent a linear trend line plus a AR(1) random process.

Reported are the following statistics:
tr(+-c/+u-d) [nr [rho]]

where

tr is a trend slope estimate (K/decade);
+-c is a half 90%-confidence interval (if symmetric);
+u -d - upper and lower parts of 90% confidence interval:
50%-95% and 5%-50%, respectively;
nr - reduced number of degrees of freedom (if computed);
rho - lag-1 autocorrelation coefficient for the trend fit residuals (if computed).

Lugina, land temperature, global average

[Data was taken from http://www.ipcc-data.org/obs/ar4_obs.html which brings one to http://cdiac.ornl.gov/ftp/trends/temp/lugina/90N-60S.dat which is a file with monthly data, averaged into annual values for this comparison.]

Lugina	1850-2005, n=125			1901-2005, n=105			1979-2005, n= 27		
GL	tr(+-c/+u-d)	[nr	[rho]]	tr(+-c/+u-d)	[nr	[rho]]	tr(+-c/+u-d)	[nr	[rho]]
AR4Tab3.2				0.069+-0.020			0.203+-0.058		
OLS				0.067+-0.009			0.200+-0.053		
OLSdofrS				0.067+-0.017	28	0.573	0.200+-0.061	21	0.120
OLSdofrST				0.067+-0.018	28	0.573	0.200+-0.061	21	0.120
GLS				0.068+-0.016		0.573	0.202+-0.059		0.120
Prewhtng				0.073+-0.016		0.573	0.210+-0.064		0.120
Sen				0.066+0.009-0.009			0.196+0.064-0.052		
WS2001				0.070+0.018-0.016	0.576		0.222+0.072-0.083	0.142	

HadSST2: hemispheric (NH,SH) and global(GL)annual SST averages

from the U.K. MetOffice website (Hadley Centre):
http://www.metoffice.gov.uk/hadobs/crutem3/diagnostics/

fname =**HadSST2_NH_annual.txt**

HadSST2	1850-2005, n=156			1901-2005, n=105			1979-2005, n= 27		
NH	tr(+-c/+u-d)	[nr	[rho]]	tr(+-c/+u-d)	[nr	[rho]]	tr(+-c/+u-d)	[nr	[rho]]
AR4Tab3.2	0.042+-0.016			0.071+-0.029			0.190+-0.134		
OLS	0.038+-0.005			0.065+-0.008			0.197+-0.041		
OLSdofrS	0.038+-0.013	25	0.717	0.065+-0.020	18	0.700	0.197+-0.059	14	0.307
OLSdofrST	0.038+-0.014	25	0.717	0.065+-0.021	18	0.700	0.197+-0.062	14	0.307
GLS	0.040+-0.012		0.717	0.066+-0.017		0.700	0.197+-0.053		0.307
GLS-obs	0.039+-0.012		0.717	0.066+-0.018		0.700	0.196+-0.063		0.307
Prewhtng	0.041+-0.012		0.717	0.072+-0.019		0.700	0.216+-0.058		0.307
Sen	0.037+0.005-0.005			0.065+0.009-0.009			0.195+0.047-0.040		
WS2001	0.043+0.013-0.013		0.725	0.077+0.021-0.022		0.717	0.221+0.062-0.061		0.326

fname =**HadSST2_SH_annual.txt**

HadSST2	1850-2005, n=156			1901-2005, n=105			1979-2005, n= 27		
SH	tr(+-c/+u-d)	[nr	[rho]]	tr(+-c/+u-d)	[nr	[rho]]	tr(+-c/+u-d)	[nr	[rho]]
AR4Tab3.2	0.036+-0.013			0.068+-0.015			0.089+-0.041		
OLS	0.034+-0.005			0.068+-0.007			0.089+-0.033		
OLSdofrS	0.034+-0.012	24	0.732	0.068+-0.014	26	0.593	0.089+-0.042	17	0.206
OLSdofrST	0.034+-0.013	24	0.732	0.068+-0.014	26	0.593	0.089+-0.043	17	0.206
GLS	0.035+-0.011		0.732	0.067+-0.012		0.593	0.088+-0.039		0.206
GLS-obs	0.035+-0.011		0.732	0.068+-0.013		0.593	0.088+-0.045		0.206
Prewhtng	0.037+-0.012		0.732	0.072+-0.013		0.593	0.095+-0.043		0.206

Sen	0.034+0.005-0.005			0.069+0.007-0.007			0.080+0.030-0.038		
WS2001	0.036+0.012-0.012		0.733	0.071+0.013-0.012		0.594	0.084+0.036-0.045		0.211

fname =**HadSST2_GL_annual.txt**

HadSST2	**1850-2005, n=156**			**1901-2005, n=105**			**1979-2005, n= 27**		
GL	tr(+-c/+u-d)	[nr	[rho]]	tr(+-c/+u-d)	[nr	[rho]]	tr(+-c/+u-d)	[nr	[rho]]
AR4Tab3.2	**0.038+-0.011**			**0.067+-0.015**			**0.133+-0.047**		
OLS	0.036+-0.004			0.067+-0.006			0.143+-0.034		
OLSdofrS	0.036+-0.012	23	0.734	0.067+-0.013	24	0.617	0.143+-0.045	16	0.254
OLSdofrST	0.036+-0.012	23	0.734	0.067+-0.014	24	0.617	0.143+-0.046	16	0.254
GLS	0.037+-0.010		0.734	0.066+-0.012		0.617	0.142+-0.042		0.254
GLS-obs	0.037+-0.011		0.734	0.067+-0.013		0.617	0.142+-0.048		0.254
Prewhtng	0.039+-0.011		0.734	0.071+-0.013		0.617	0.155+-0.046		0.254
Sen	0.036+0.005-0.004			0.067+0.007-0.007			0.139+0.037-0.036		
WS2001	0.041+0.011-0.012		0.742	0.072+0.014-0.013		0.623	0.147+0.053-0.051		0.253

Chapter 2: Observations: Atmosphere and Surface

Coordinating Lead Authors: Dennis Hartmann (USA), Albert Klein Tank (Netherlands), Matilde Rusticucci (Argentina)

Lead Authors: Lisa Alexander (Australia), Stefan Broennimann (Switzerland), Yassine Abdul-Rahman Charabi (Oman), Frank Dentener (EU / Netherlands), Ed Dlugokencky (USA), David Easterling (USA), Alexey Kaplan (USA), Nzioka John Muthama (Kenya), Brian Soden (USA), Peter Thorne (USA / UK), Martin Wild (Switzerland), Panmao Zhai (China)

Contributing Authors: Robert Adler (USA), Richard Allan (UK), Robert Allan (UK), Aiguo Dai (USA), Robert Davis (USA), Sean Davis (USA), Markus Donat (Australia), Vitali Filotev (Canada), Erich Fischer (Switzerland), Leopold Haimberger (Austria), Ben Ho (USA), John Kennedy (UK), Stefan Kinne (Germany), James Kossin (USA), Norman Loeb (USA), Carl Mears (USA), Christopher Merchant (UK), Steve Montzka (USA), Colin Morice (UK), Joel Norris (USA), David Parker (UK), Bill Randel (USA), Andreas Richter (Germany), Ben Santer (USA), Dian Seidel (USA), Tom Smith (USA), David Stephenson (UK), Ryan Teuling (Netherlands), Junhong Wang (USA), Ray Weiss (USA), Kate Willett (UK), Simon Wood (UK), Tingjun Zhang (China)

Review Editors: Jim Hurrell (USA), Jose Marengo (Brazil), Fredolin Tangang (Malaysia), Pedro Viterbo (Portugal)

Date of Draft: 16 December 2011

Notes: TSU Compiled Version

Figures

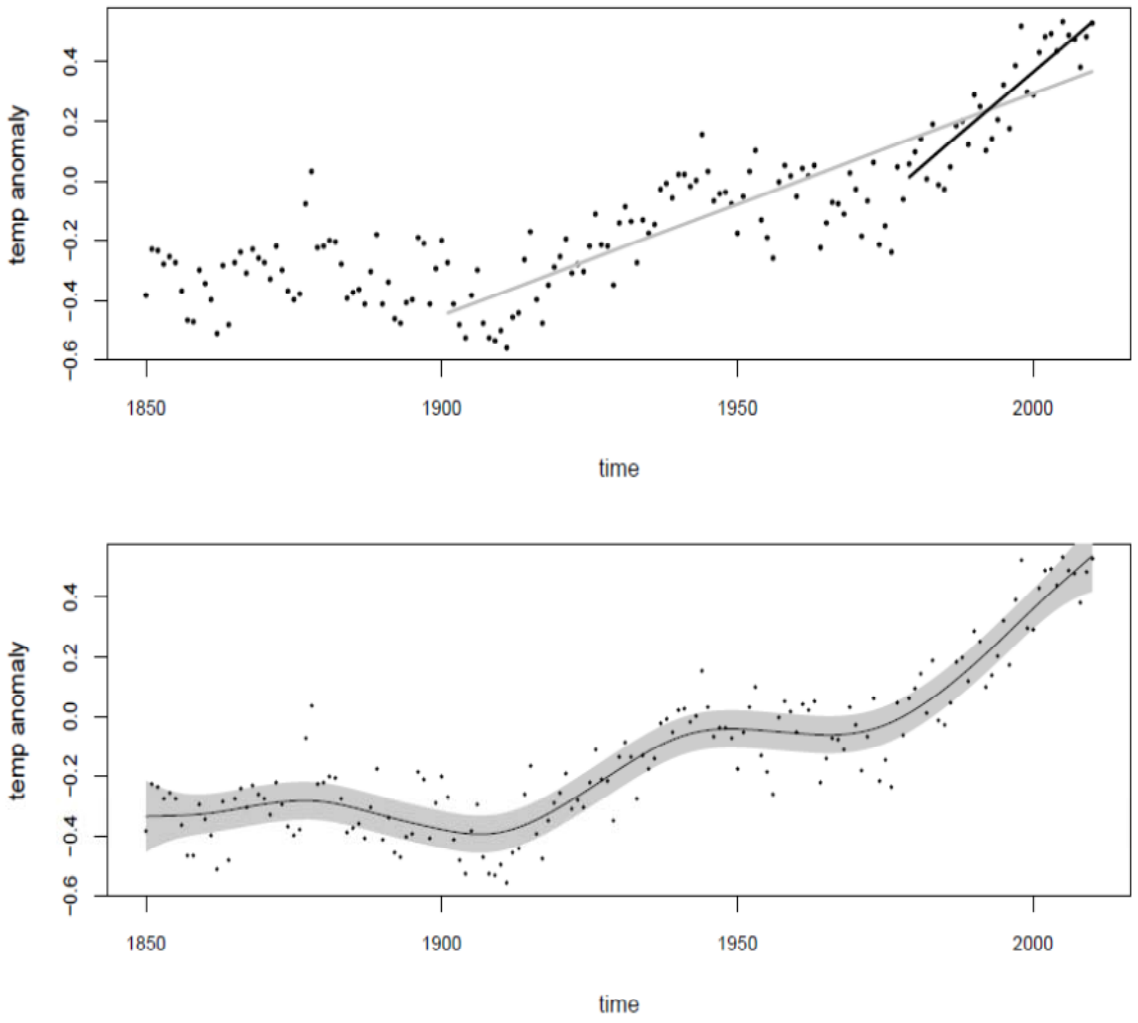

Box 2.2, Figure 1: (Top): HadCRUT4 global annual mean data from 1850 to 2010 (dots), grey line is a trend line for 1901–2010, black line is trend line for 1979–2010, both assuming AR1 errors. (Bottom): Same data as top, with spline smooth (solid curve) and the 95% confidence limits on the smooth curve, also assuming AR1 errors.

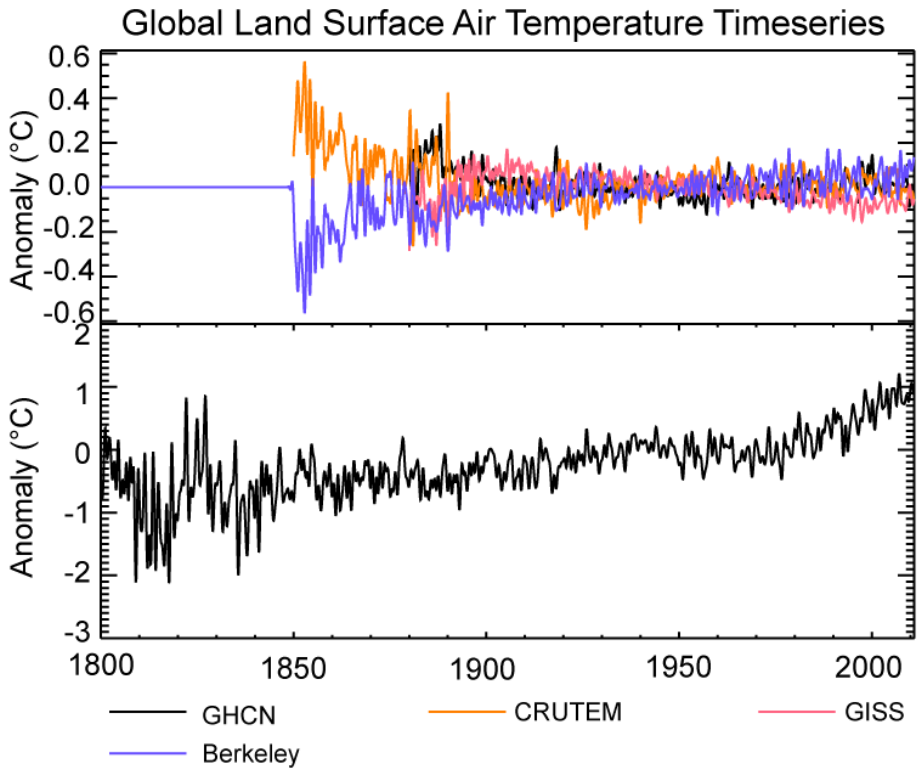

Figure 2.1: Global land surface temperature timeseries evolution estimates from 1800 to present. Lower panel shows the mean of all available datasets available at each timestep (which varies prior to 1880). The top panel shows offsets from this multi-dataset mean series behavior (datasets in this panel are denoted in the key). Note the top plot range is much reduced compared to the lower plot and that inter-dataset differences are much smaller than the long-term series changes. All timeseries have been smoothed with a digital filter (Lynch and Huang, 1992) to emphasize variations on interannual timescales. GISS land data series have had a land mask applied to avoid interpolation over oceans undertaken in their public dataset release, which provides a more like-for-like comparison.

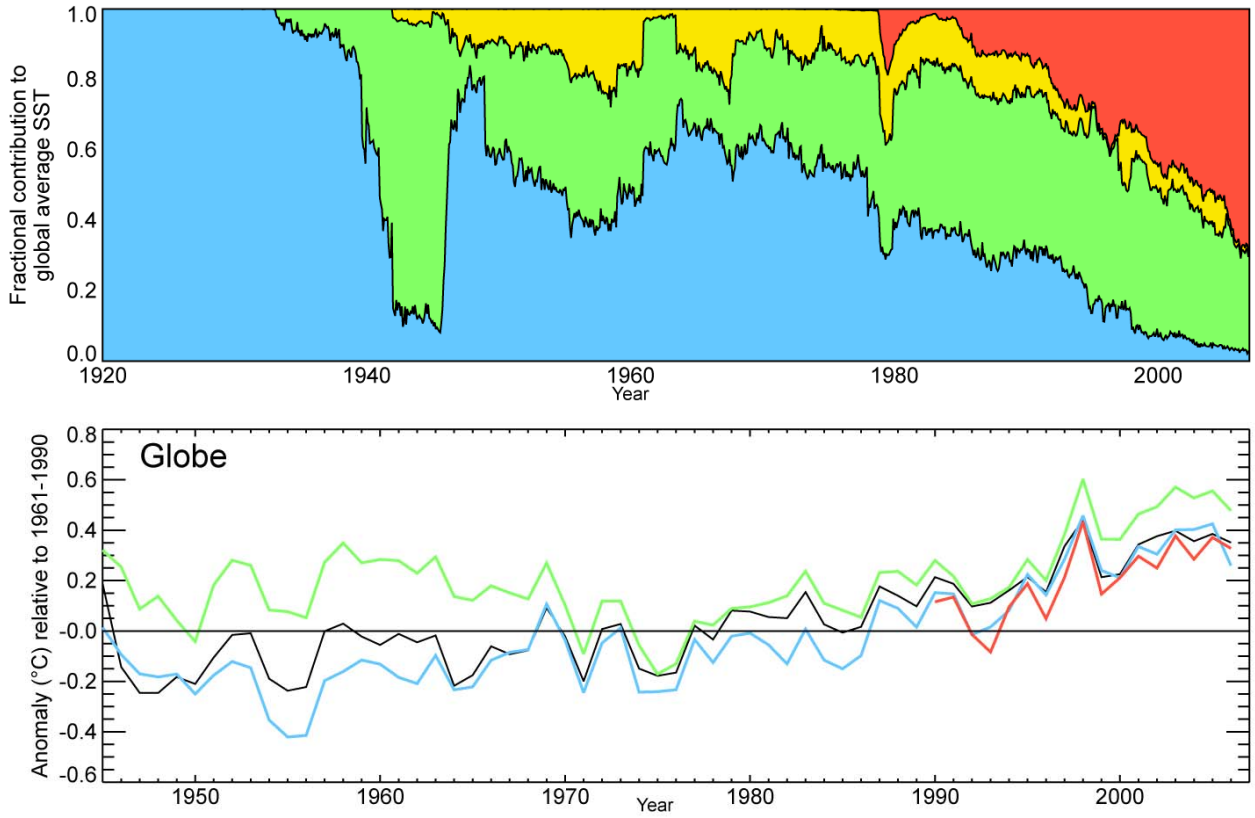

Figure 2.2: Temporal changes in the prevalence of different measurement methods in the ICOADS. (top) Fractional contributions of observations made by different measurement methods: bucket observations (blue), ERI and hull contact sensor observations (green), moored and drifting buoys (red), and unknown (yellow). (bottom) Global annual average SST anomaly based on different kinds of co-located data: ERI and hull contact sensor (green), bucket (blue), buoy (red), and all (black). Adapted from Kennedy et al., (2011b).

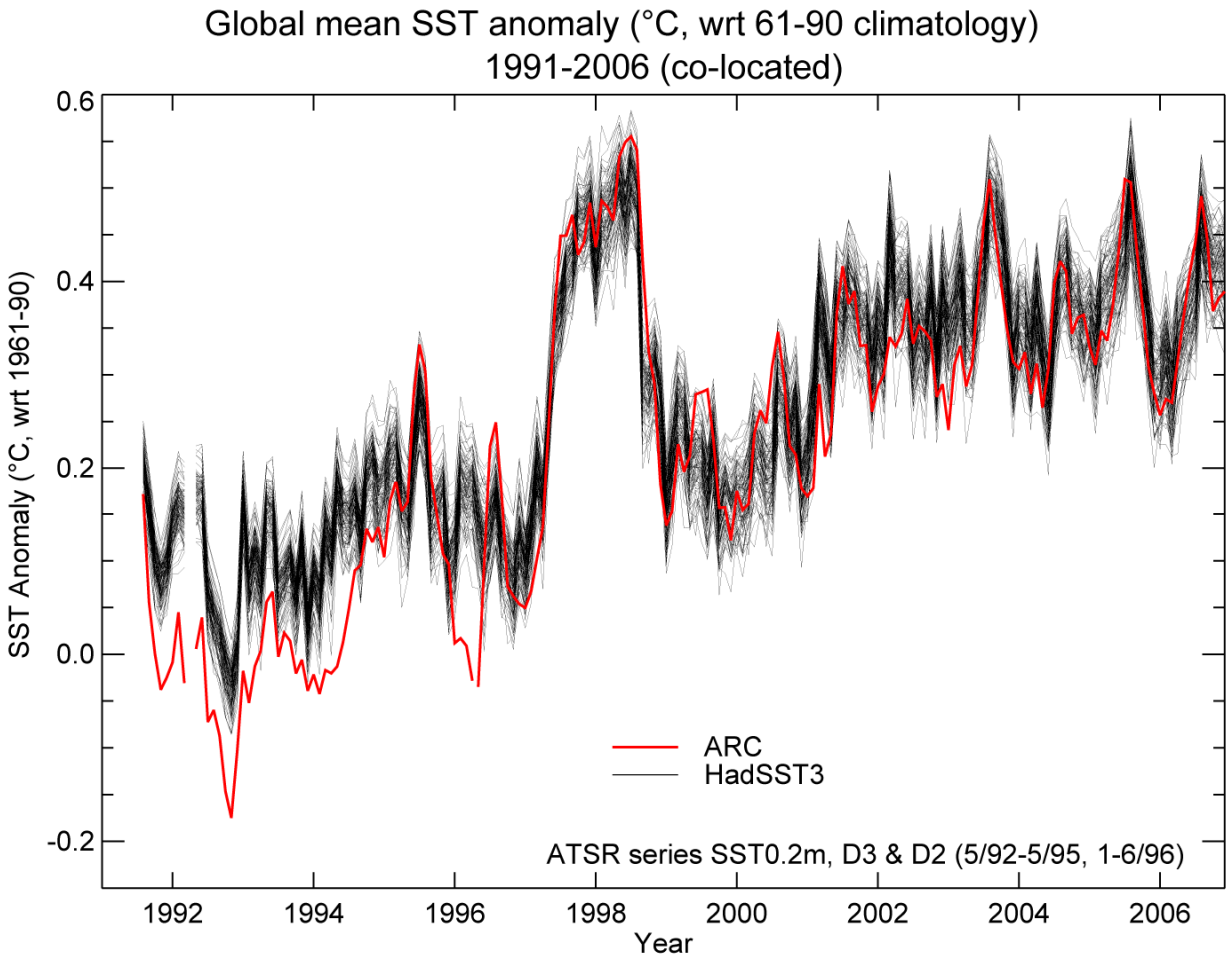

Figure 2.3: Global monthly mean SST anomalies measured from satellites (ATSRs) and *in situ* (HadSST3). Black lines: HadSST3 ensemble of 100. Red line: ATSR night-time SST timeseries from the ATSR Reprocessing for Climate (ARC) project. One month is missing in 1996 due to non-complete overlap of successive satellite missions.

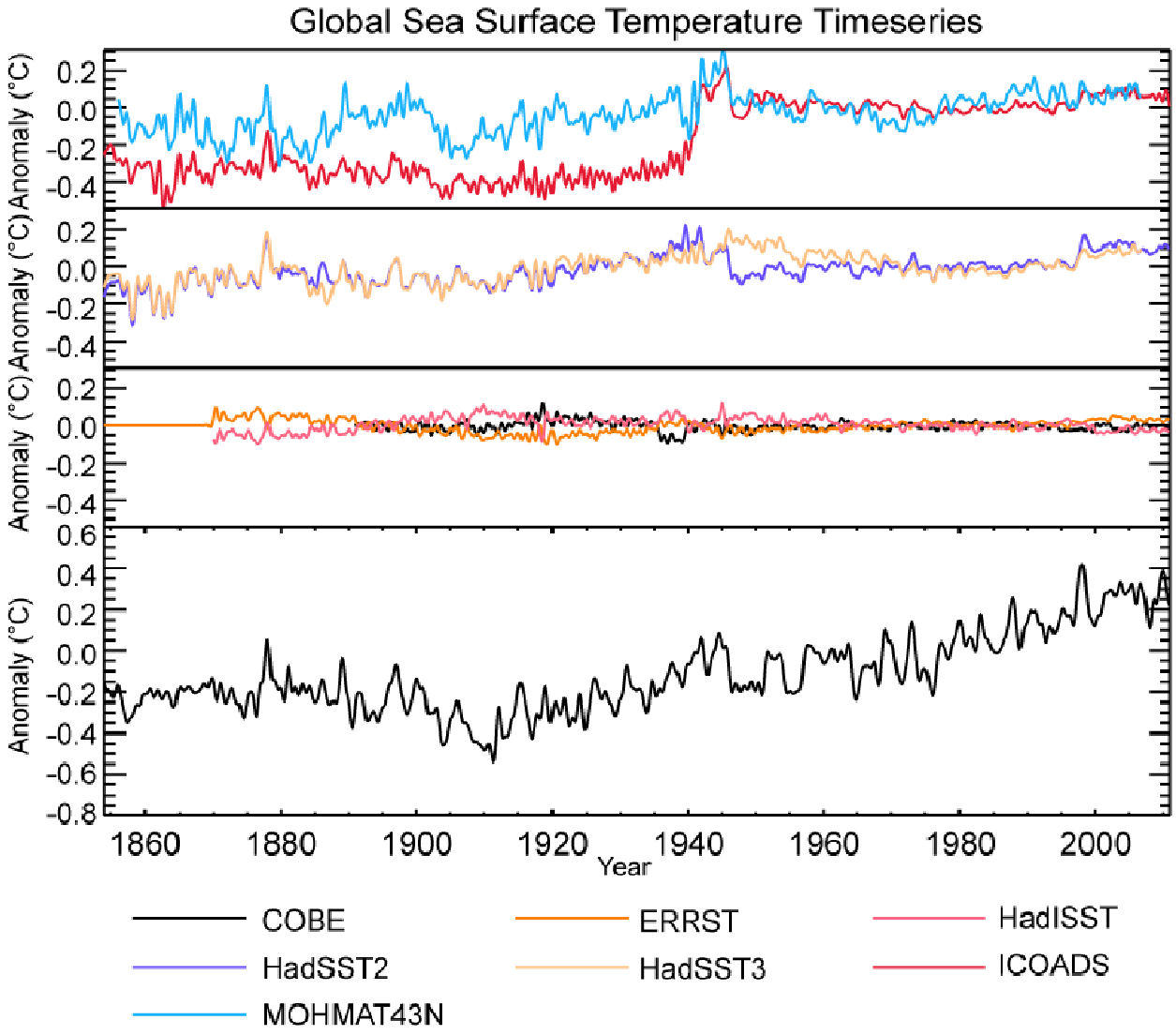

Figure 2.4: Global means of SST timeseries since 1854. Lower panel shows the mean on the three interpolated products (COBE, ERRSTv3b and HadISST). The top panel shows offsets from this average for two uninterpolated products (HadSST2 and HadSST3), the raw SST measurement archive (ICOADS) and night marine air temperatures (MOHMAT43N). The mean timeseries and the offset series have had a digital filter applied as described in Figure 2.1.

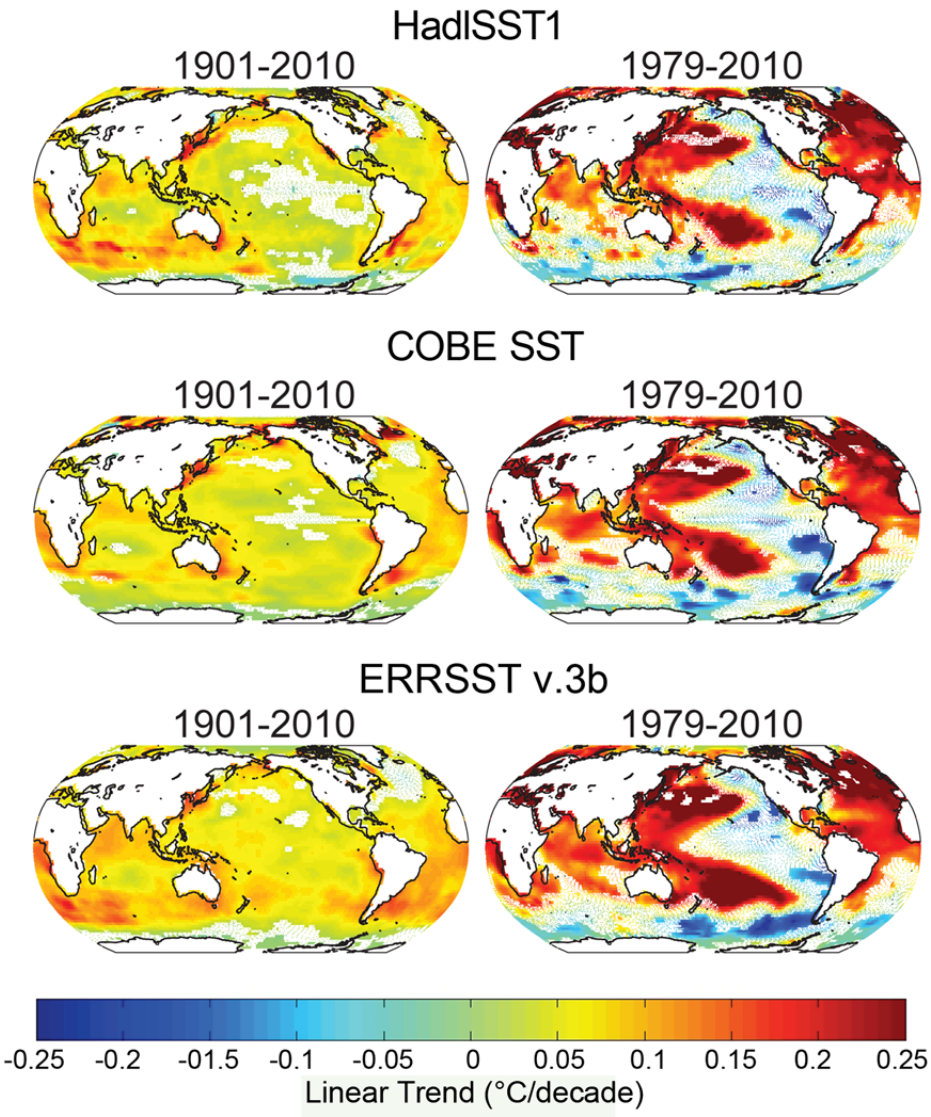

Figure 2.5: Linear trend slope estimates for 1901–2010 and 1979–2010 periods in the annual means of interpolated globally complete SST data sets. See Table 2.3 for data set details. Color patches show trends with higher than 90% confidence. In the areas where the 5% to 95% confidence interval for the slope contains zero, the field of slope estimates is shown by dotted color contours. Trend slopes were estimated using ordinary least squares regression with the lag-1 autocorrelation taken into account for the uncertainty calculation (Santer et al., 2000).

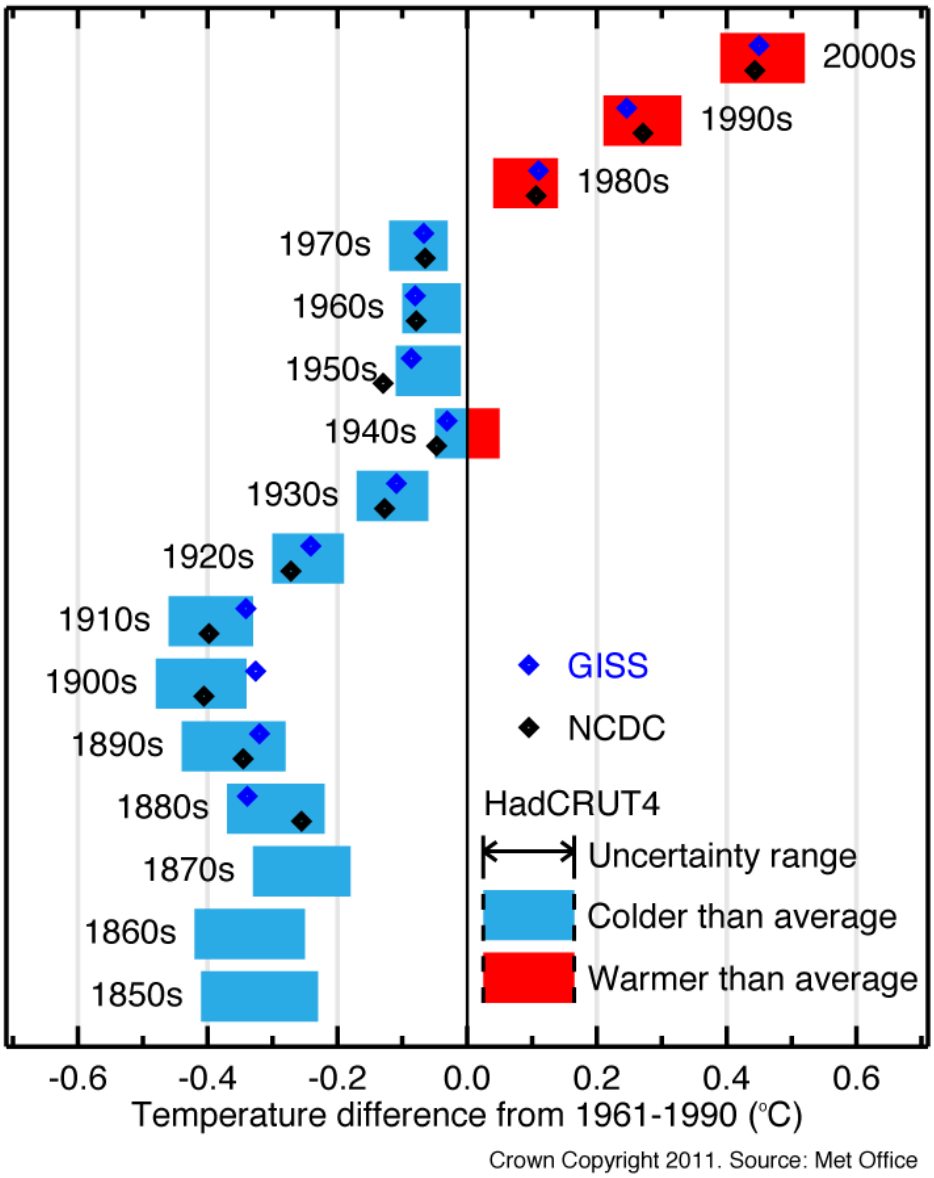

Figure 2.6: Decadal mean anomalies and associated uncertainties (2.5–97.5 percentile ranges) based upon the HadCRUT4 ensemble(Morice et al., Submitted). Anomalies are relative to a 1961–1990 climatology period. NCDC MLOSTand GISS dataset estimates are also shown and their uncertainties would yield grossly similar results and a similar conclusion that each of the last three decades in turn has been significantly warmer than all preceding decades in the record.

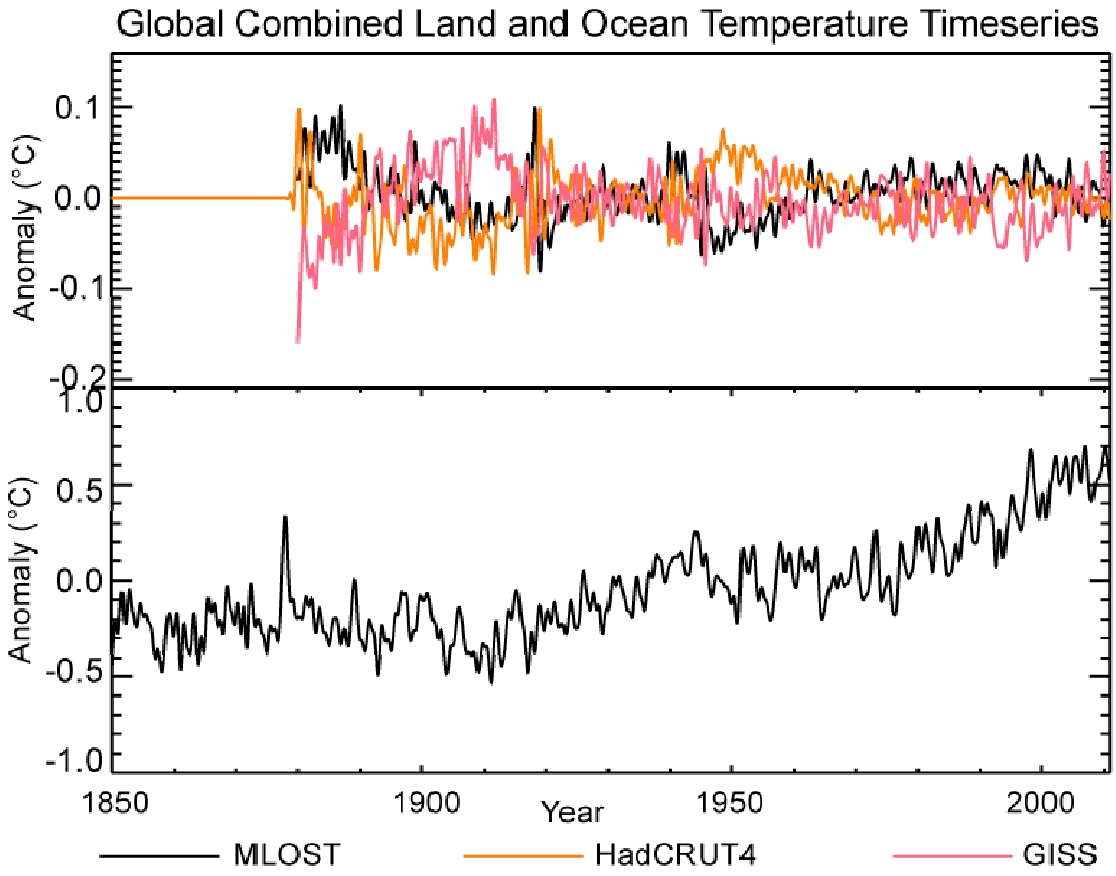

Figure 2.7: Global mean temperature series at annual resolution from a straight average of the three data products, plus differences between each product and this mean. For details of the smoothing applied refer to Figure 2.1.

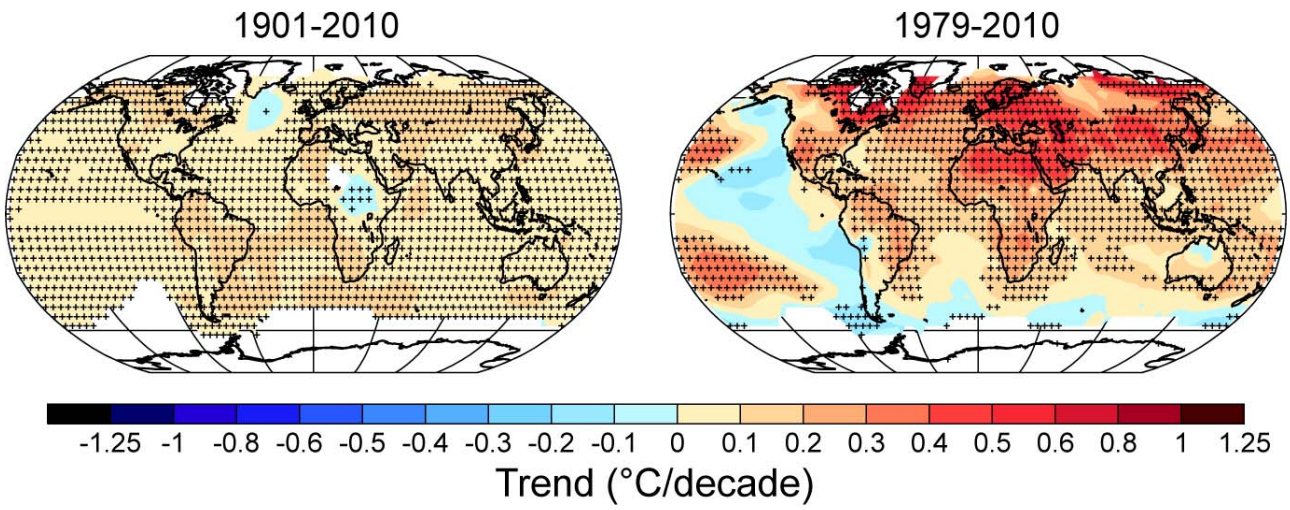

Figure 2.8: Global trend maps from NCDC MLOST surface record for 1901 to 2010 (left hand panel) and 1979 to 2010 (right hand panel). Trends have been calculated only for those gridboxes with greater than 70% complete records using OLS regression with standard errors adjusted for AR1 autocorrelation effects (Box 2.2). Gridboxes where the absolute trend is greater than 2 standard errors from zero are highlighted with a black cross.

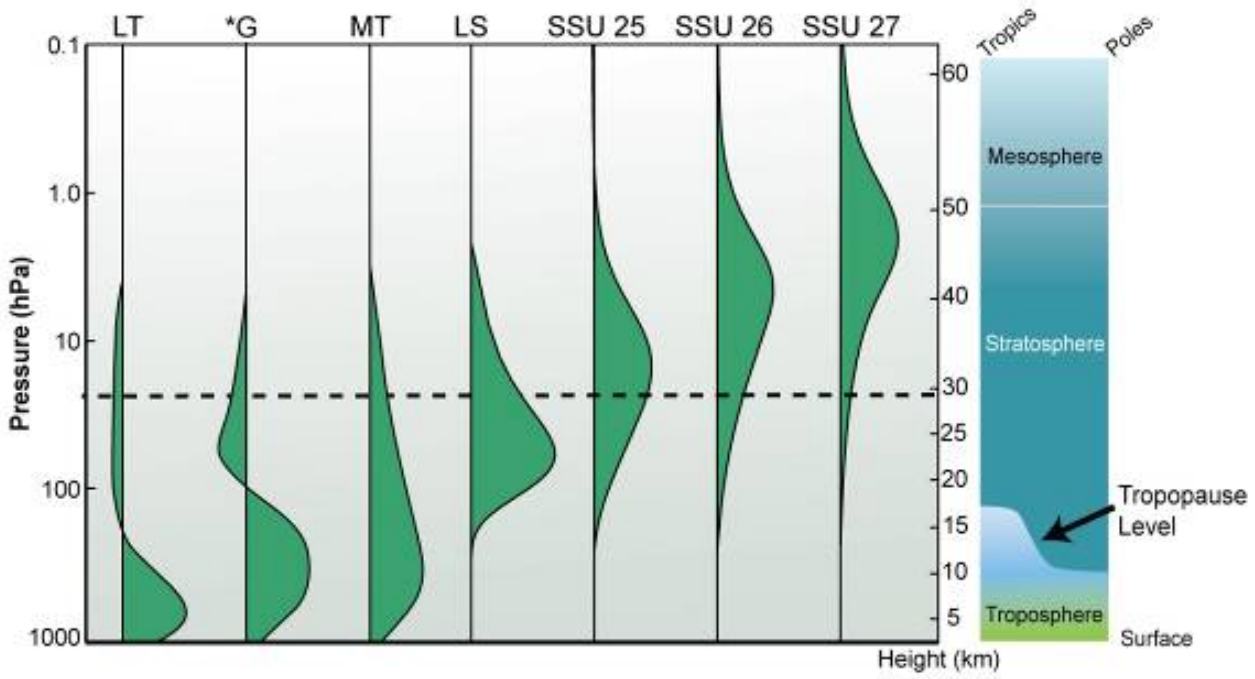

Figure 2.9: Vertical weighting functions for those satellite temperature retrievals discussed in this chapter. The dashed line indicates the typical maximum altitude achieved in the historical radiosonde record.

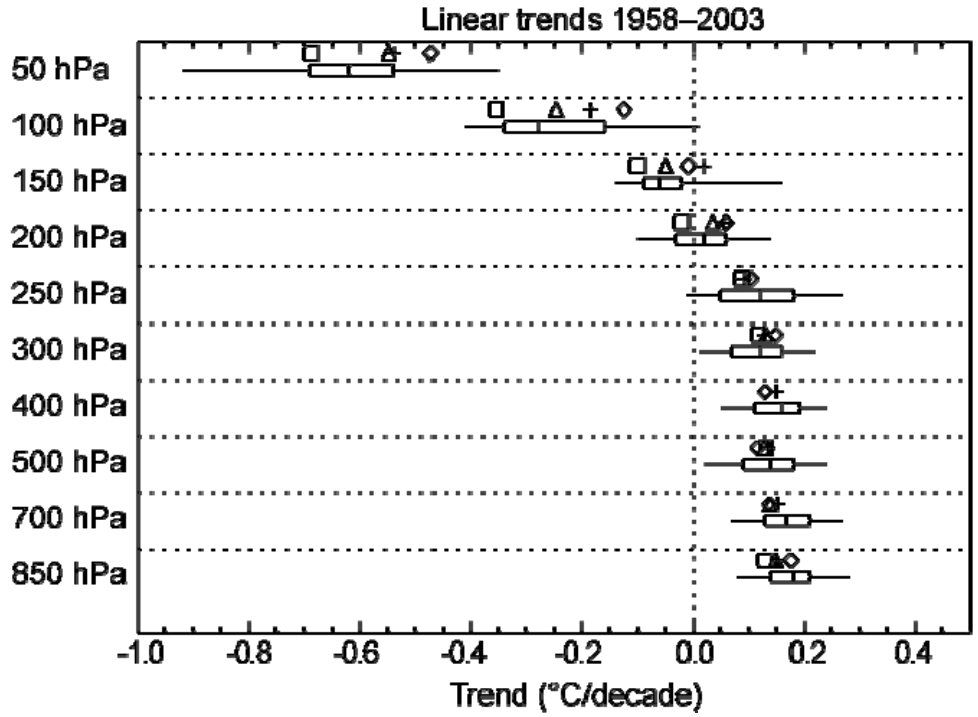

Figure 2.10: Radiosonde product global temperature trend estimates from four datasets (symbols) and the estimated structural uncertainty in the HadAT product from (Thorne et al., 2011a) (Box whiskers denote median estimator, 25–75th percentile and range) over the common period of record 1958–2003. All trend estimates are from median of pairwise slopes technique (Lanzante, 1996). Global averages were created by calculating zonal means and then weighting zonal anomalies by cos(lat). The four best estimates used are HadAT2 (Δ), IUK (□), RICH (+) and RAOBCORE (◊). [Note that new versions of RICH / RAOBCORE will be used in the SOD].

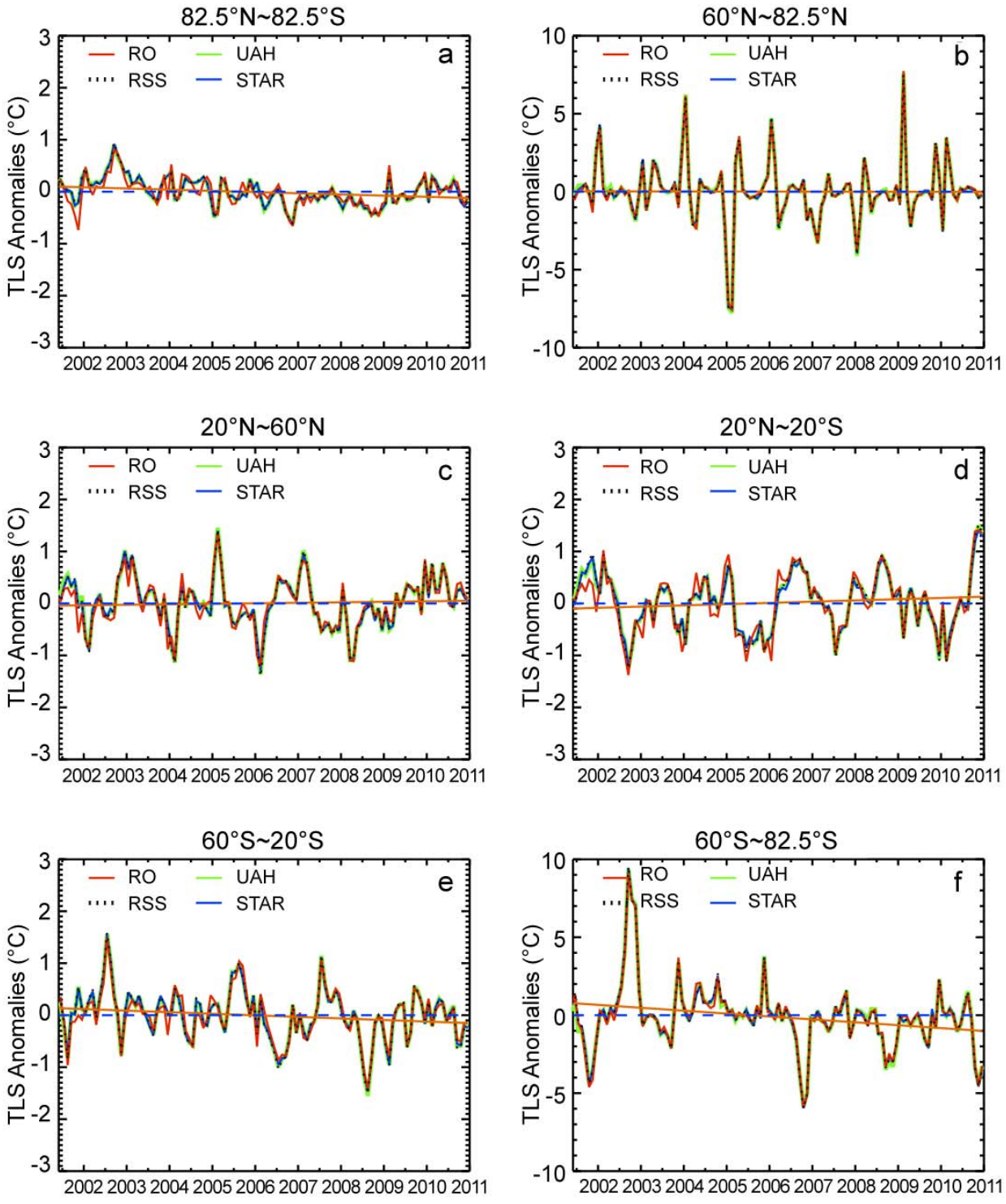

Figure 2.11: LS anomalies of RSS, UAH, STAR, and RO_AMSU for (a) the entire globe (82.5ºN–82.5ºS), b) 82.5ºN–60ºN, (c) 60ºN–20ºN, (d) 20ºN–20ºS, (e) 20ºS–60ºS, and (f) 60ºS–82.5ºS. The orange line indicates the mean trend for RO_AMSU.

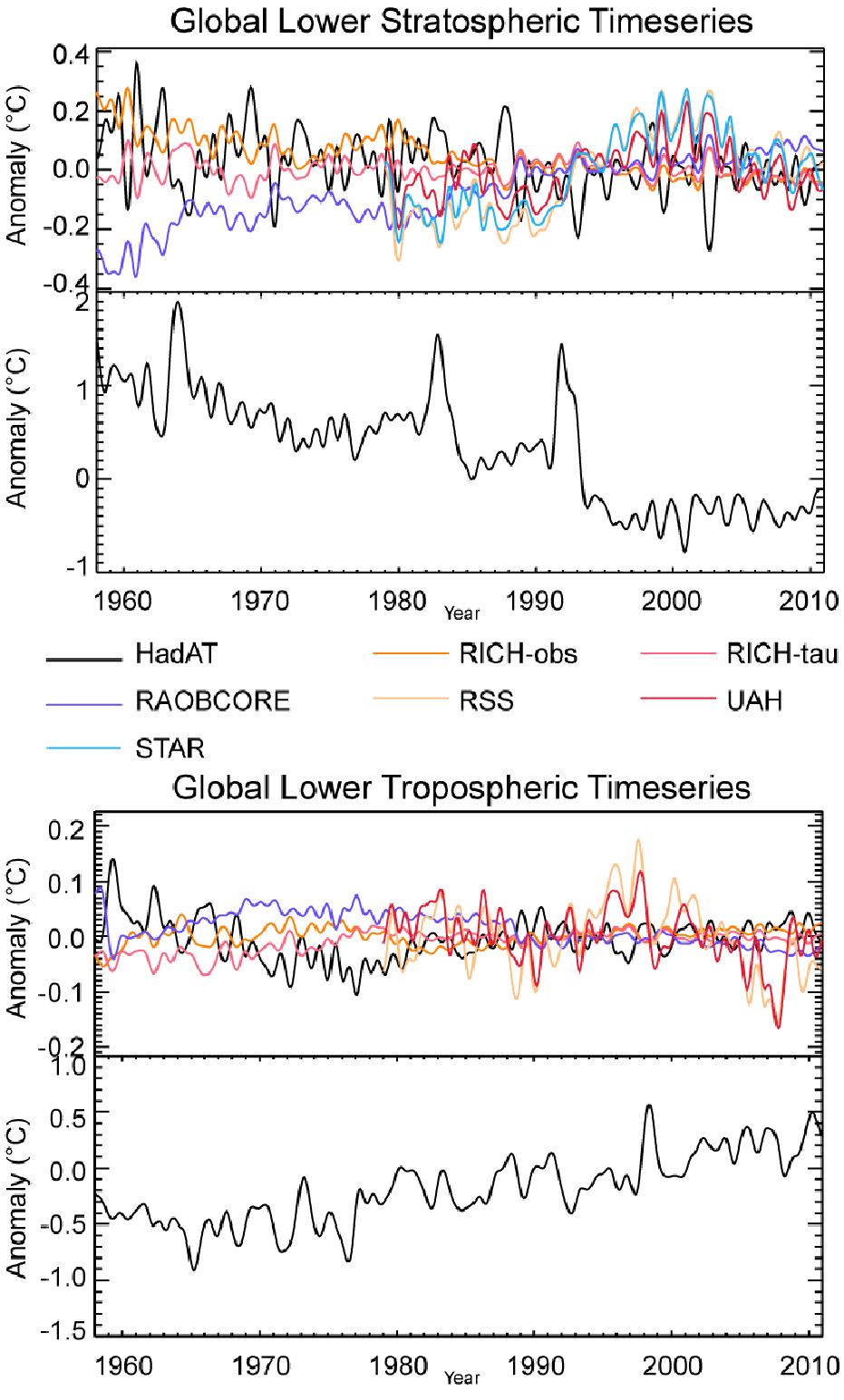

Figure 2.12: Global average lower stratospheric (top) and lower tropospheric (bottom) temperature anomaly timeseries for the mean of all included radiosonde datasets (HadAT, RICH and RAOBCORE(v1.4)) and offset therefrom the differences from this composite for each dataset. Note the difference in y-axis resolution between the various panels. All timeseries have been anomalized to a common 1981–2010 reference period.STAR do not produce a lower tropospheric temperature product. For details of the smoothing applied refer to Figure 2.1.

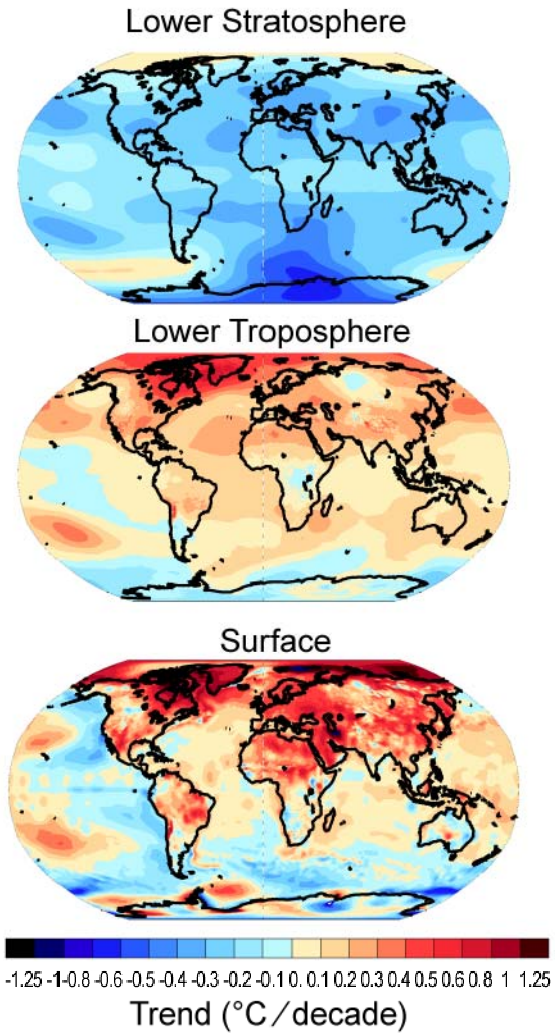

Figure 2.13: Linear trend estimates for the surface, lower troposphere and lower stratosphere estimated from the ERA-Interim reanalysis product over 1979–2010. Trends have been estimated as described in Box 2.2.

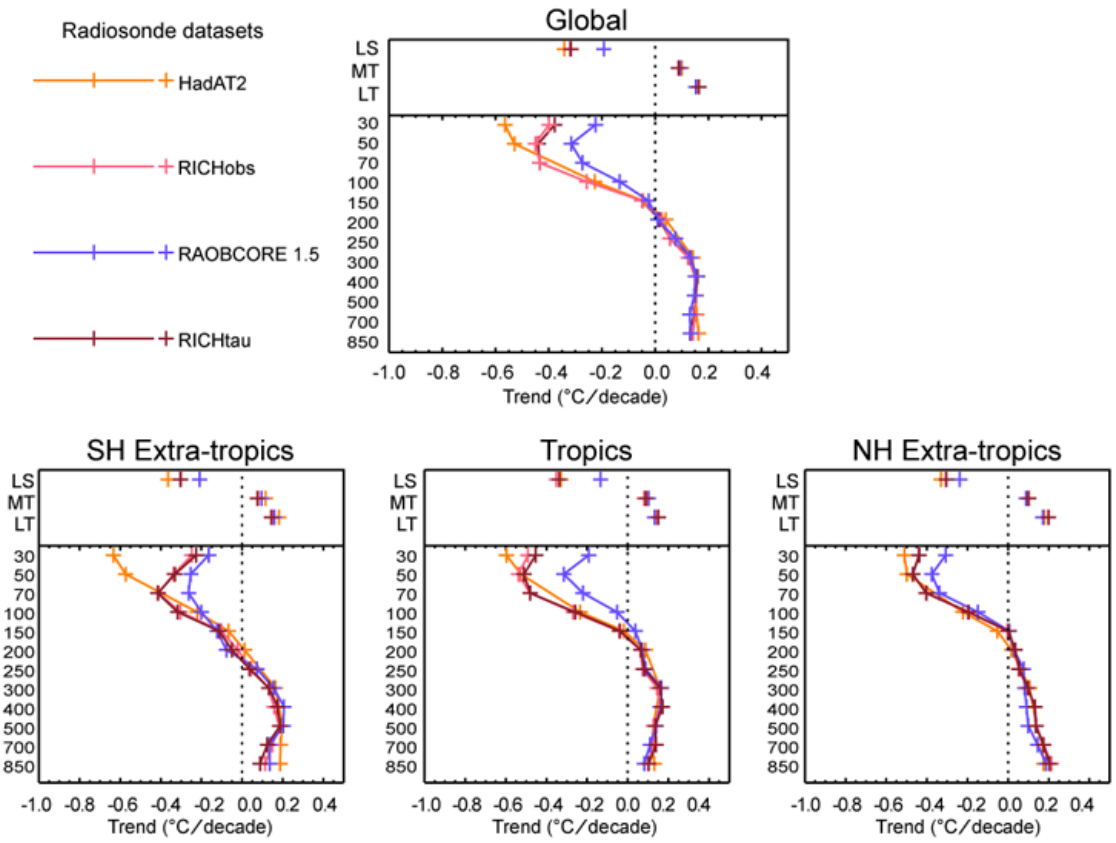

Figure 2.14: Linear trend estimates for all available data products that contain records for 1958–2010 for the globe (top) and tropics and extra-tropics (bottom). The bottom panel trace in each case is for trends on distinct pressure levels. Note that the pressure axis is not linear. The top panel points show MSU layer equivalent measure trends over the same period. MSU layer equivalents have been processed using the method of Thorne et al. (2005b). No attempts have been made to sub-sample to a common data mask.

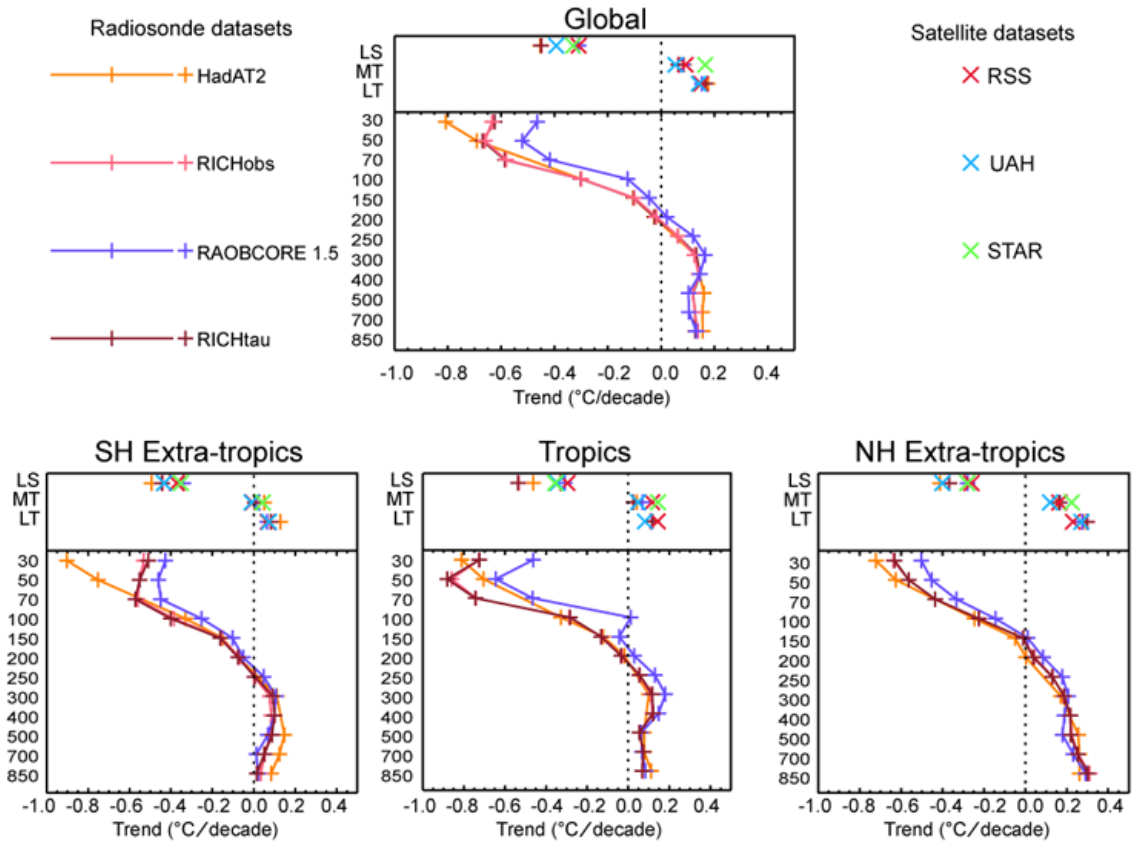

Figure 2.15: As Figure 2.14 except for the satellite era 1979–2010 period.

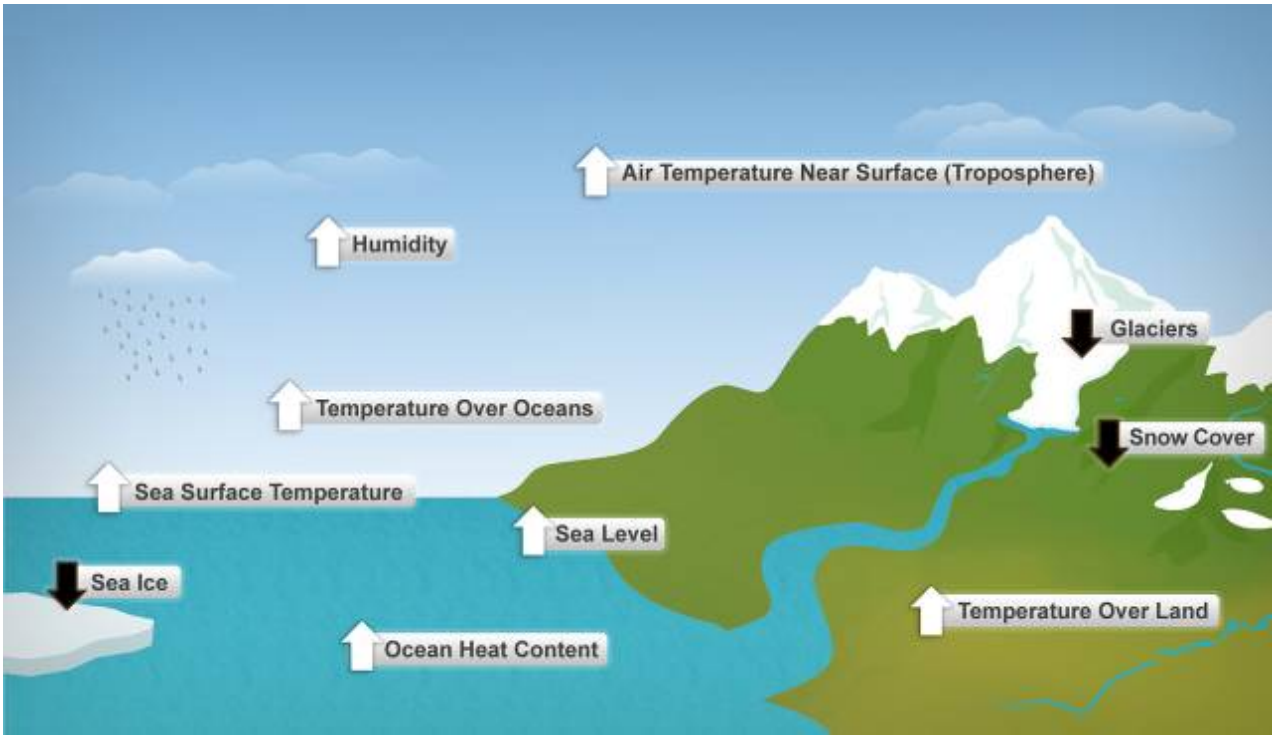

FAQ 2.1, Figure 1: Schematic of those climate elements that have been measured quasi-globally and on multi-decadal timescales that would be expected to change if the world were indeed warming; and the direction in which they would be expected to change.

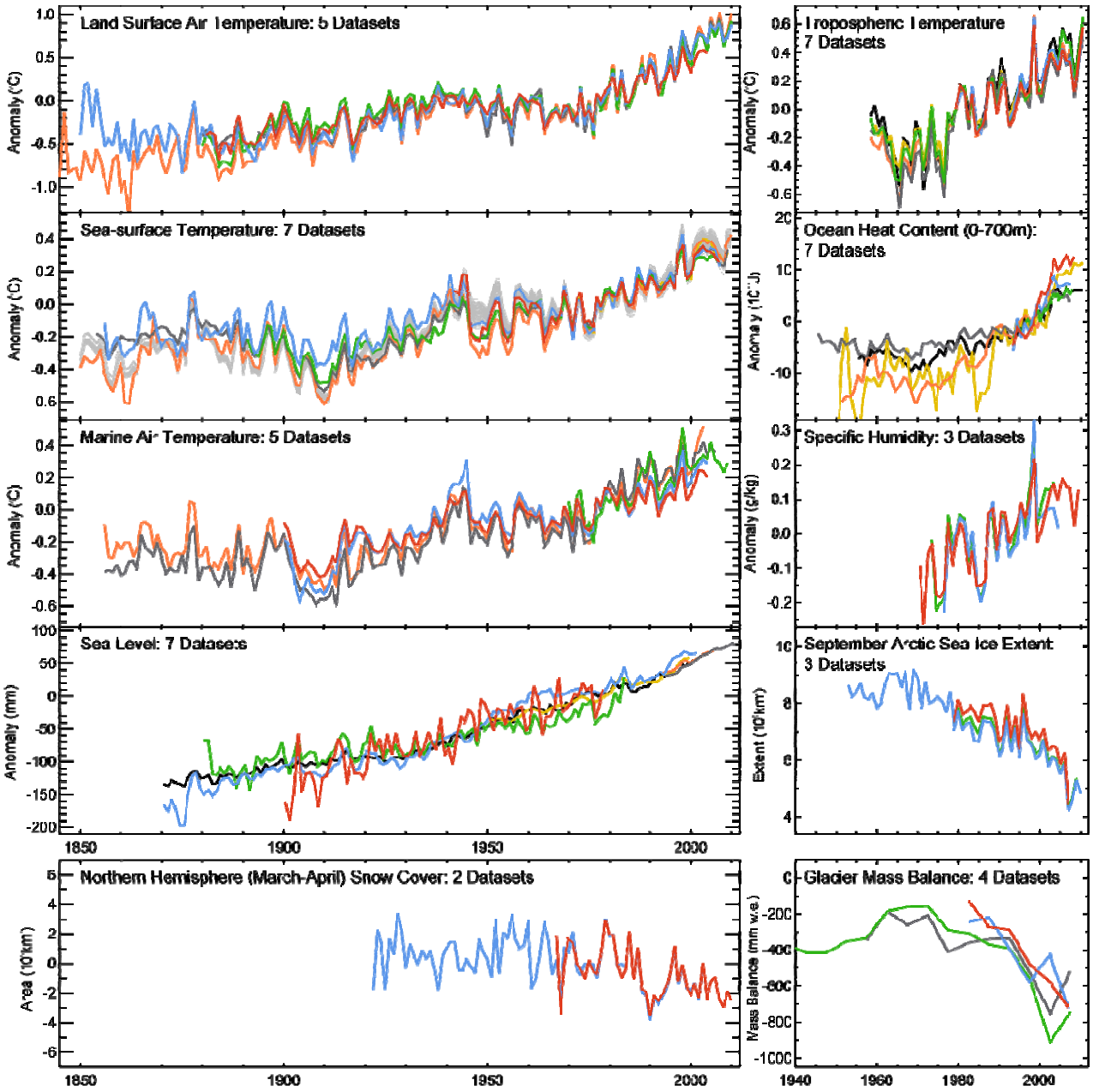

FAQ 2.1, Figure 2: Multiple redundant indicators of a changing global climate. Each line represents an independently derived estimate of change in the climate element. All publically available, documented, datasets known to the authors have been used in their latest version with no further screening criteria applied. Further details are given in (Baringer et al., 2010).

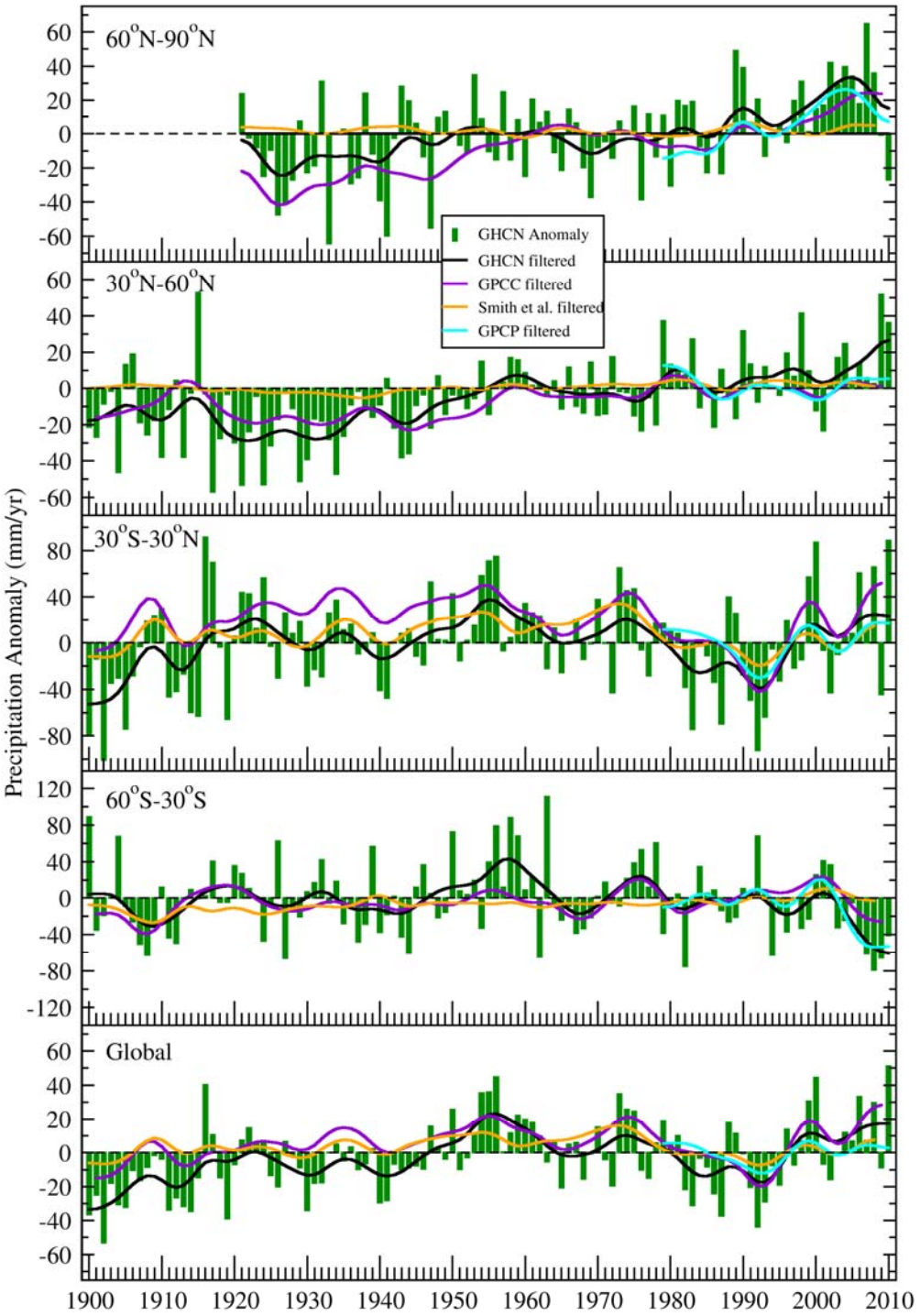

Figure 2.16: Annual precipitation averaged over land areas for four latitudinal bands and the globe from GHCN (green bars) with respect to the 1981–2000 base period. Smoothed curves (see Appendix 3.A from Trenberth et al., 2007) for GHCN and other global precipitation data sets as listed. [PLACEHOLDER FOR SECOND ORDER DRAFT: Figure to be updated with latest data.]

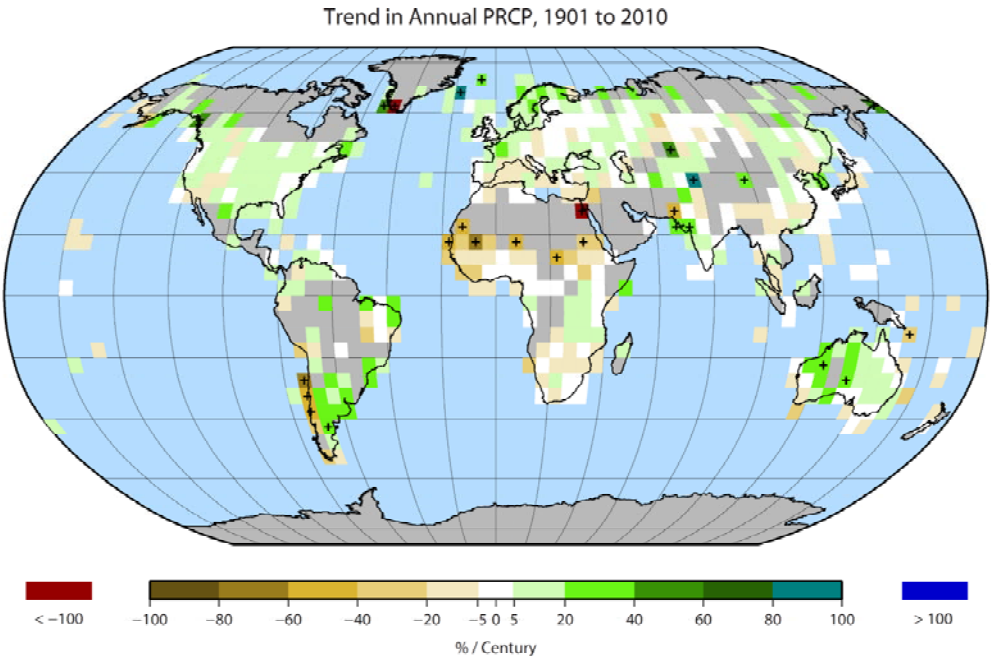

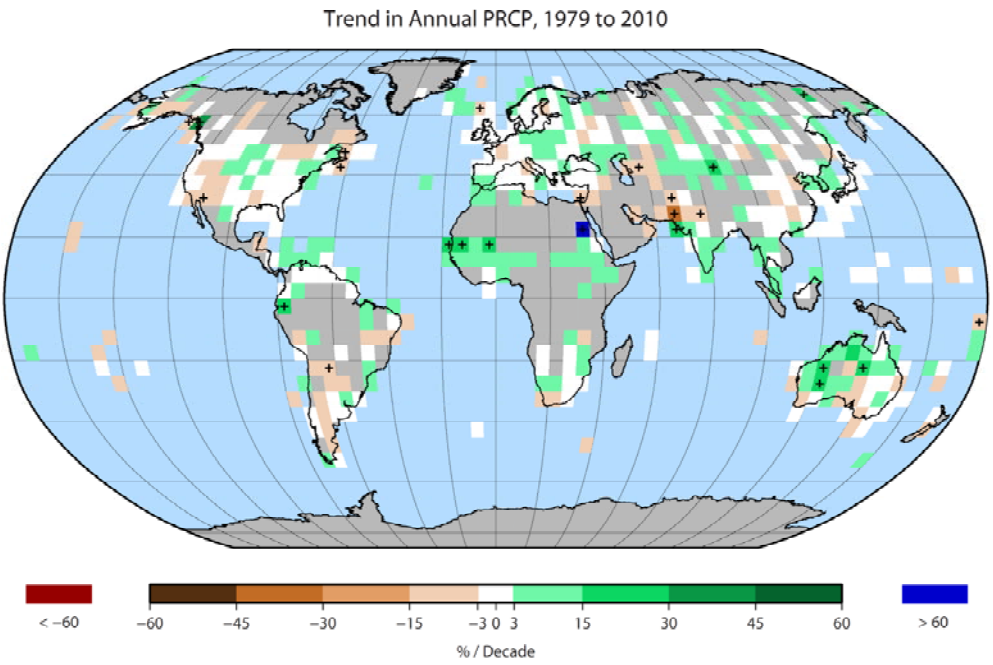

Figure 2.17: Linear trend, in % per century for annual precipitation from the GHCN data set for 1901–2010 (top) and 1979–2010 (bottom). Grid boxes with statistically significant trends at the 5% level are indicated by +. [Note that a slightly different trend calculation method than described in Appendix 2.A has been used; PLACEHOLDER FOR SECOND ORDER DRAFT: updated results will be included.]

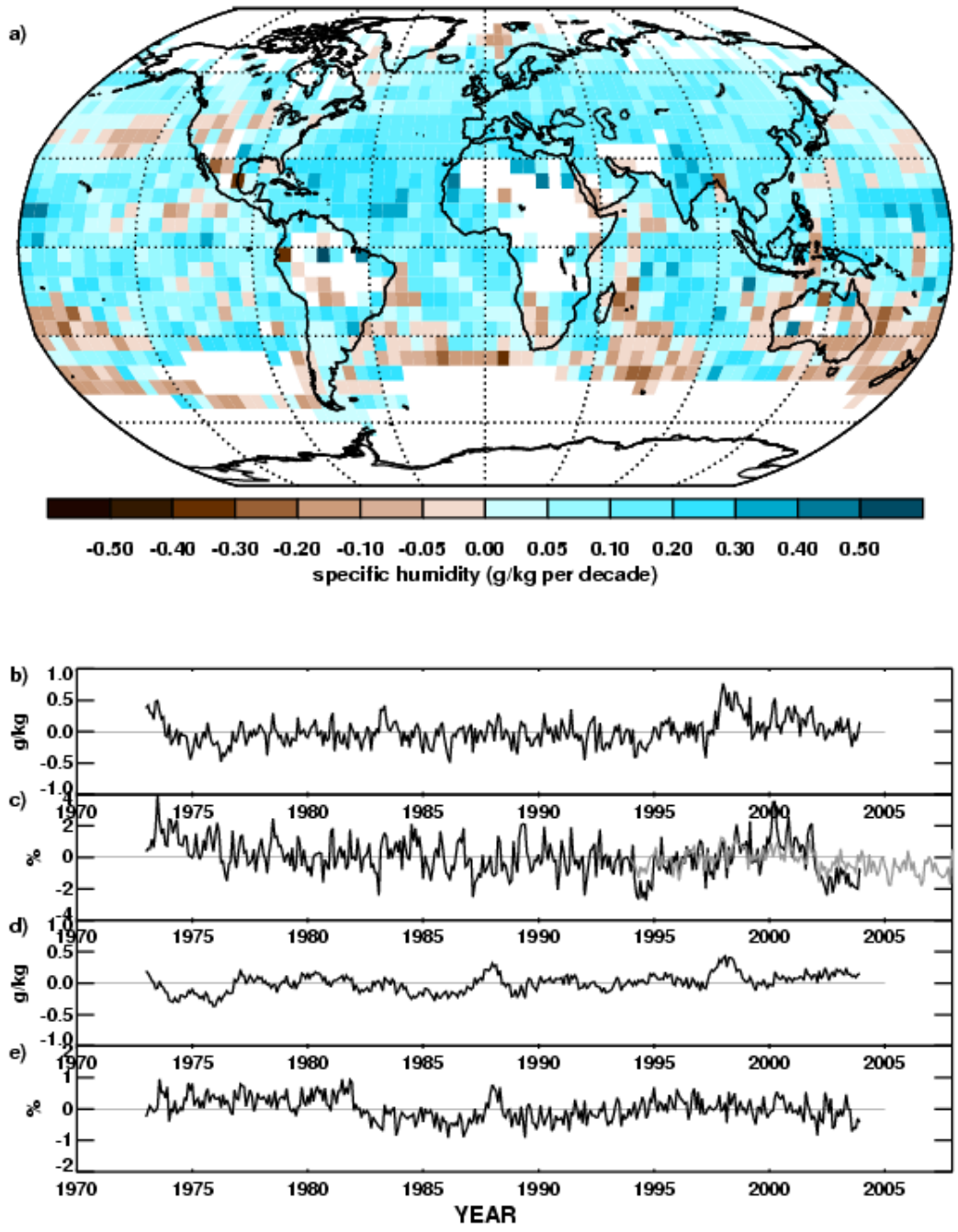

Figure 2.18: Trends and variability in surface humidity. a) Decadal trends in surface specific humidity in g kg^{-1} per decade from HadCRUH over 1973–2003. b) Globally averaged monthly mean anomaly time series of land surface specific humidity. c) Globally averaged monthly mean anomaly time series of land surface relative humidity. d) Globally averaged monthly mean anomaly time series of marine surface specific humidity. e) Globally averaged monthly mean anomaly time series of marine surface relative humidity. Time series show data from HadCRUH (solid thick black) and HadCRUHext (solid thick grey). [PLACEHOLDER FOR SECOND ORDER DRAFT: additional datasets will be included.]

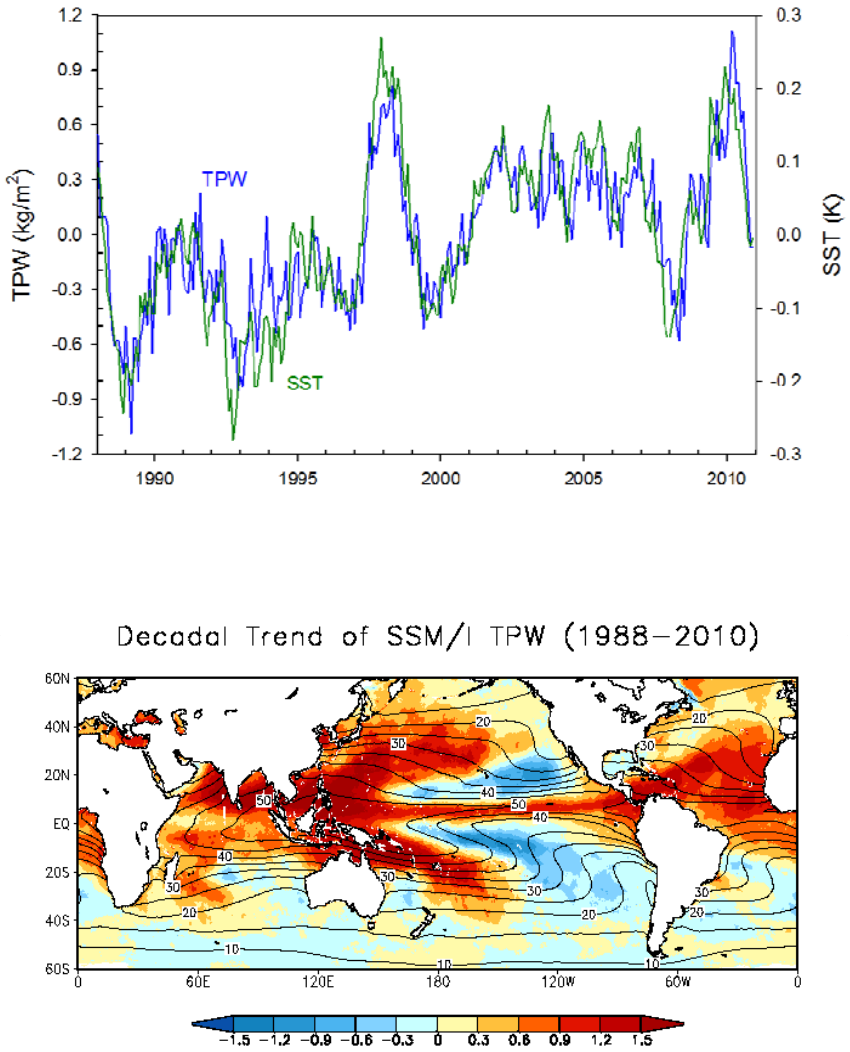

Figure 2.19: Top**:** Time series of anomalies in total precipitable water vapour (TPW, blue) and sea surface temperature (SST, green) averaged over ocean surfaces from 60°N–60°S. Bottom: The linear trend in TPW in (kg m^{-2} per decade, shaded) and time-mean TPW (kg m^{-2}, contours) from Special Sensor Microwave Imager (SSM/I, Wentz et al., 2007) for the period 1988–2010.

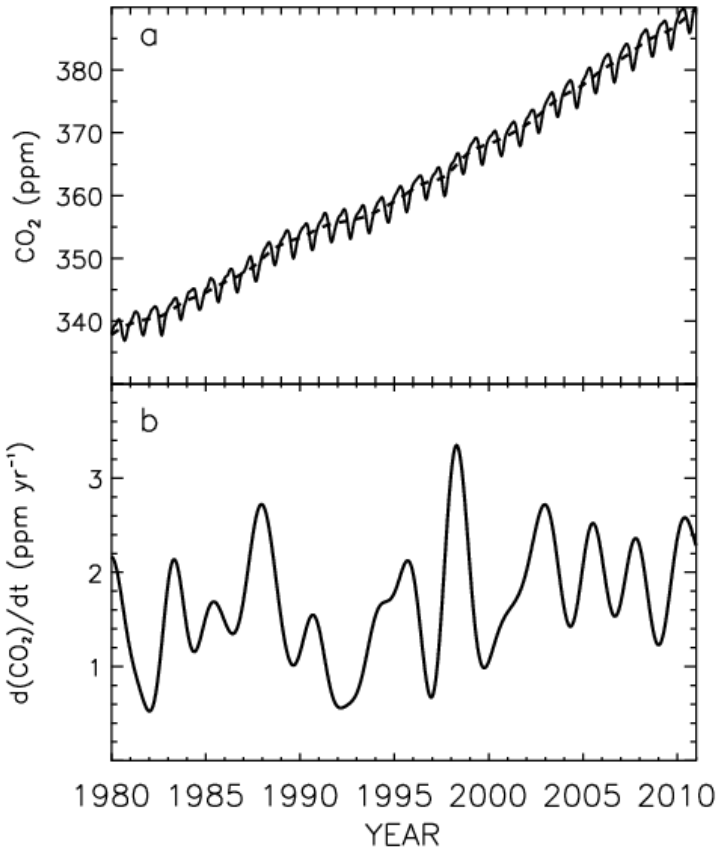

Figure 2.20: a) Solid line shows globally averaged CO_2 dry air moles fractions; dashed line is a deseasonalized trend curve fitted to the global averages. b) Instantaneous growth rate for globally averaged atmospheric CO_2. The growth rate is the time-derivative of the dashed line in a).

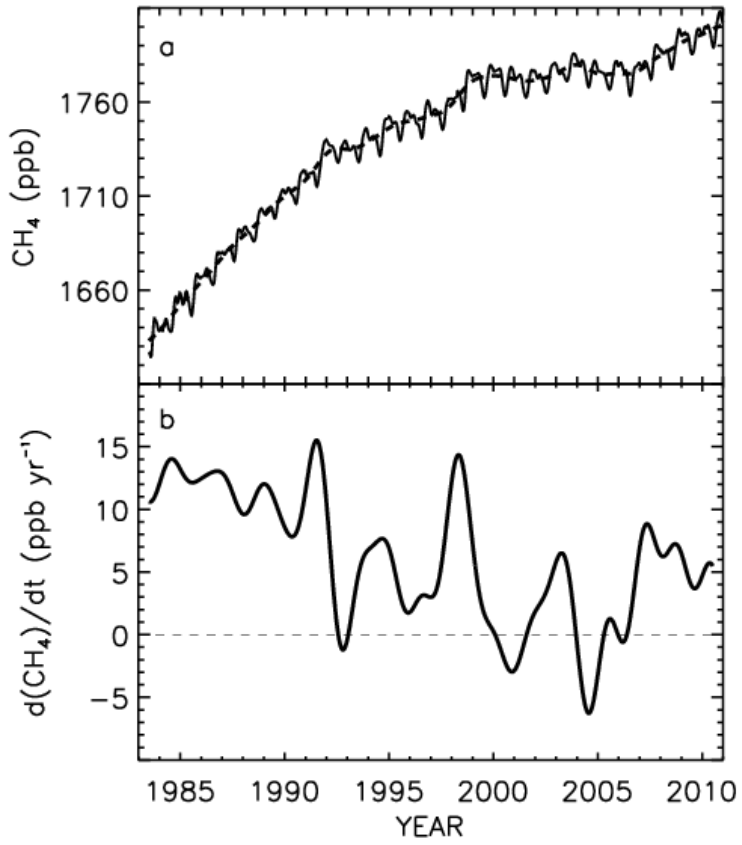

Figure 2.21: a) Solid line shows globally averaged CH_4 dry air moles fractions; dashed line is a deseasonalized trend curve fitted to the global averages. b) Instantaneous growth rate for globally averaged atmospheric CH_4. The growth rate is the time-derivative of the dashed line in a).

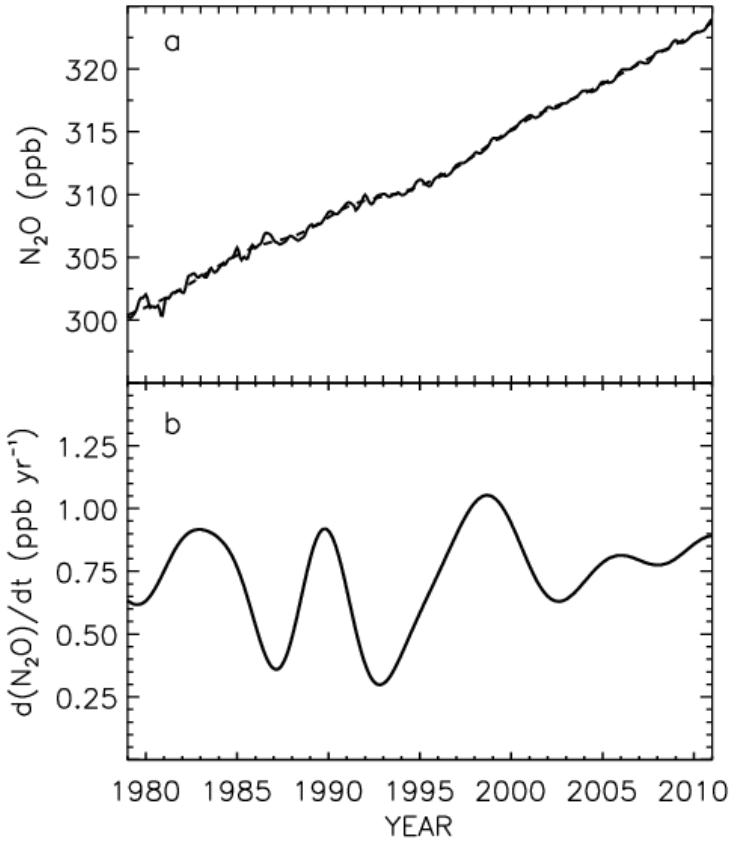

Figure 2.22: a) Solid line shows globally averaged N_2O dry air moles fractions; dashed line is a deseasonalized trend curve fitted to the global averages. b) Instantaneous growth rate for globally averaged atmospheric N_2O. The growth rate is the time-derivative of the dashed line in a).

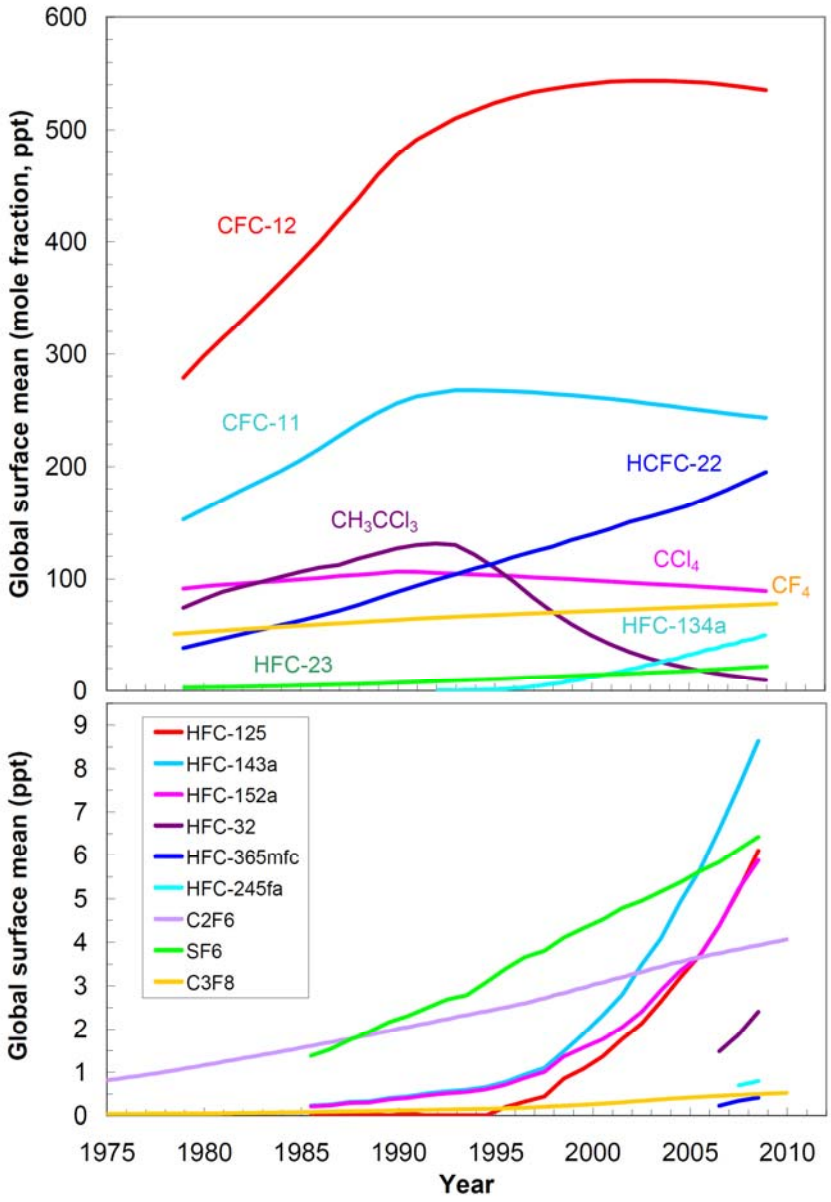

Figure 2.23: Temporal evolution of the global average dry-air mole fractions (ppt) at Earth's surface of the major halogen-containing LLGHGs. These are derived mainly using monthly mean measurements from the AGAGE and NOAA/GMD networks. For clarity, only the most abundant chemicals are shown in different compound classes and results from different networks have been combined when both are available. While differences exist, different network measurements agree reasonably well (except for CCl_4 (differences of 2–4% between networks) and HCFC-142b (differences of 3–6% between networks)) (see also WMO, 2011, Chapter 1).

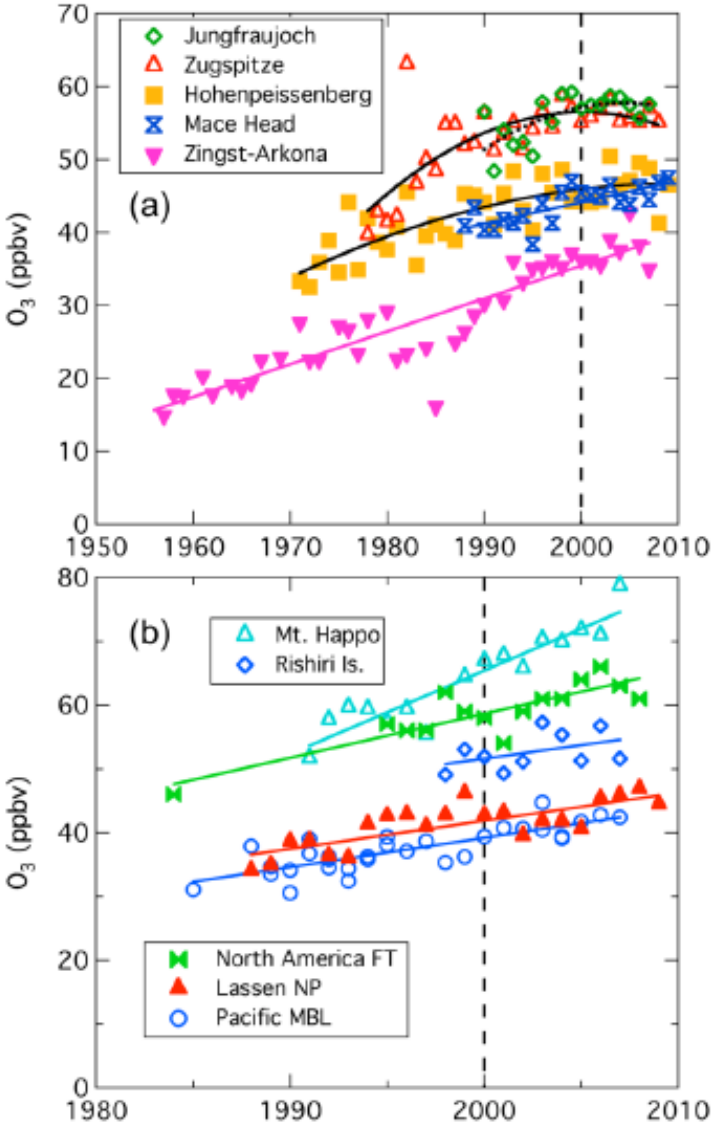

Figure 2.24: Springtime trends in surface O_3 mixing ratios measured in a) Europe and b) western North America and Japan. The lines (in color) are linear regressions fitted to the data, and the curves (in black) indicate quadratic polynomial fits to the three central European sites over the time span of the lines. Arkona and Zingst are close to the Baltic Sea. Mace Head is at the west coast of Ireland. Hohenpiessenberg (1.0 km asl) and Zugspitze (3.0 km asl) are in southern Germany, and Jungfraujoch (3.6 km asl) is in Switzerland. The North American data are from several sea level Pacific coastal sites and Lassen Volcanic National Park (1.8 km asl) near the west coast, and from the free troposphere over the western part of the continent. The Japanese data are from Mt. Happo (1.9 km asl) on the Japanese mainland and Rishiri, a northern (45°N) sea level island site (HTAP, 2010).

(a)

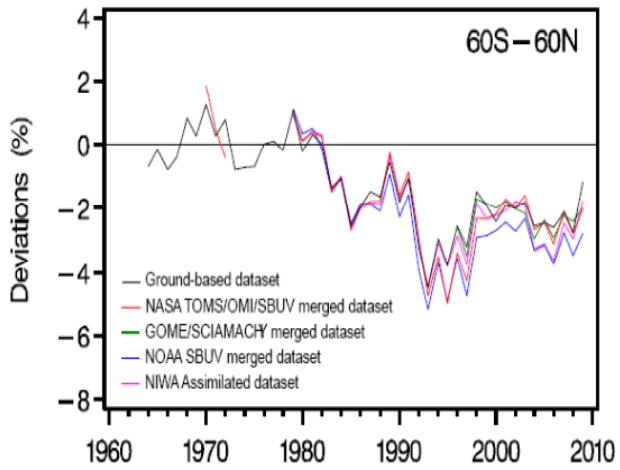

(b)

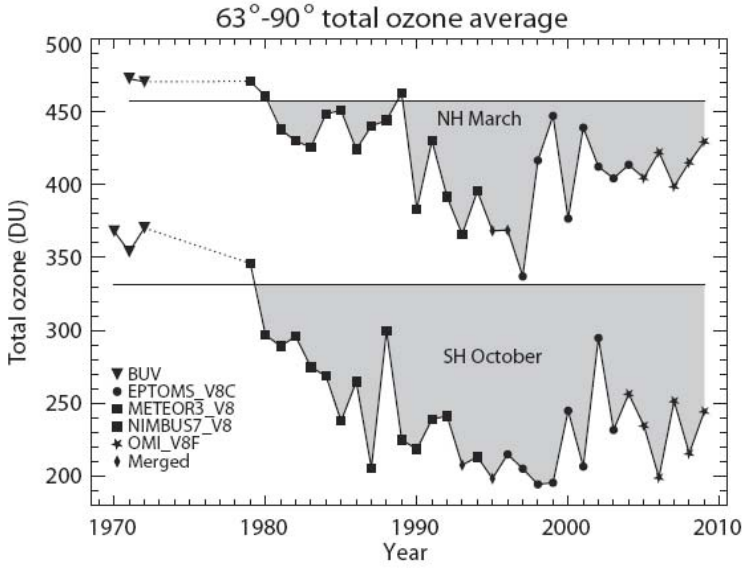

Figure 2.25: Trends in midlatitude (a) and polar (b) stratospheric ozone. Total ozone average of 63°–90° latitude in March (NH) and October (SH). Symbols indicate the satellite data that have been used in different years. The horizontal grey lines represent the average total ozone for the years prior to 1983 in March for the NH and in October in the SH.

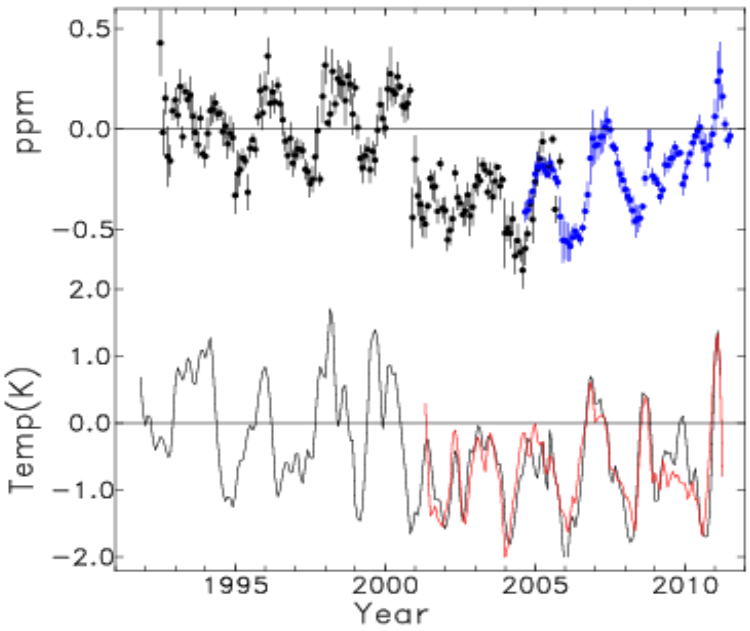

Figure 2.26: Top) Deseasonalized stratospheric water 155apour anomalies from HALOE (black) and MLS (blue). Bottom) Temperature anomalies over the time span as the top panel from near-equatorial radiosonde stations (black), and a shorter record (after 2001) based on GPS radio occultation (red).

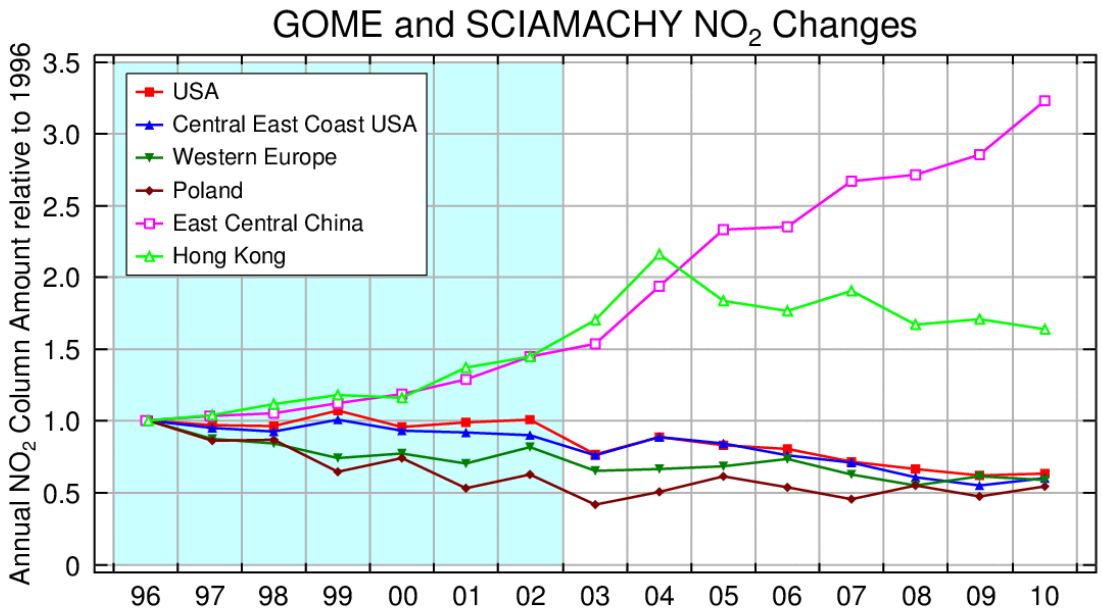

Figure 2.27: Relative changes in tropospheric NO_2 columns, normalized for 1996, derived from two instruments, the Global Ozone Monitoring Experiment (GOME) until the end of 2002 and the Scanning Imaging Spectrometer for Atmospheric Chartography (SCIAMACHY) until 2010. Updated from Richter et al. (2005)

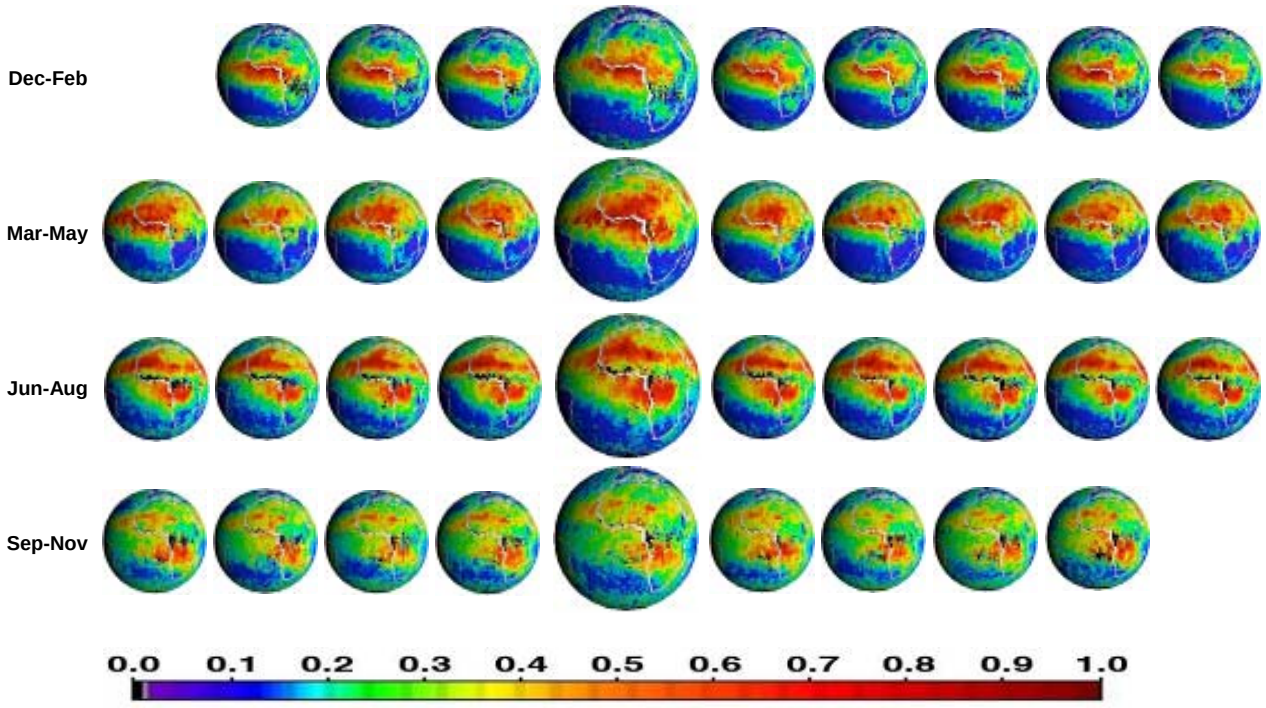

Figure 2.28: Mid-visible seasonal AOD data from 2000 to 2009 data over Africa and the Atlantic as detected by MISR samples. Updated from Kahn et al. (2010), courtesy MISR Team, Jet Propulsion Lab/Caltech and NASA Goddard Space Flight Center

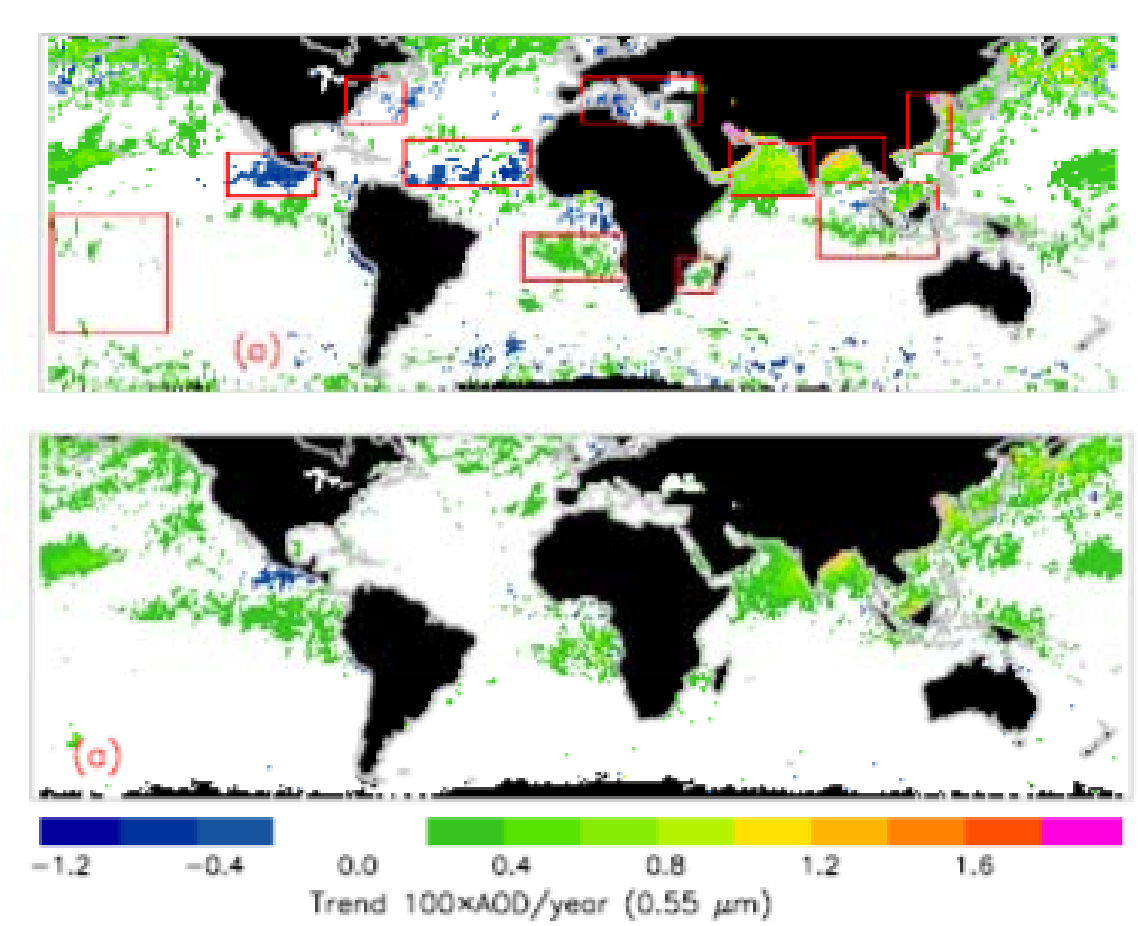

Figure 2.29: Spatial distribution of ten year trends for the mid-visible total AOD (upper panel) and the derived anthropogenic AOD (lower panel) over oceans based on MODIS data trends (Zhang and Reid, 2010). Red boxes indicate regions with statistically significant trends.

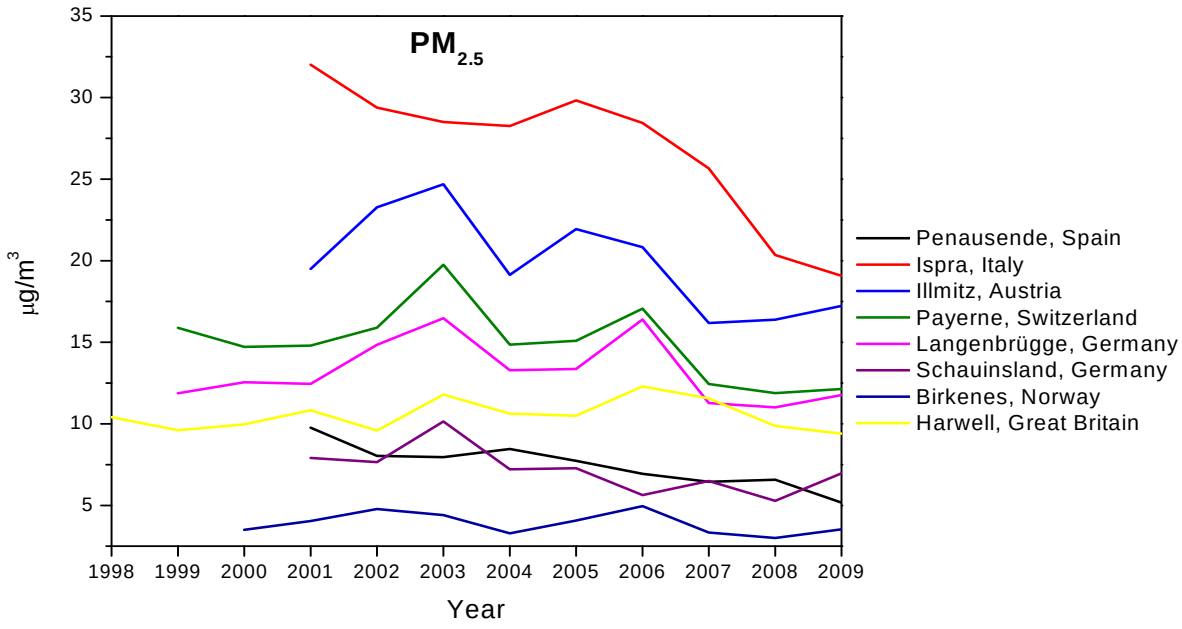

Figure 2.30: Time series of annual average PM2.5 (ug m^{-3}) in Europe; updated from (EMEP, 2010)

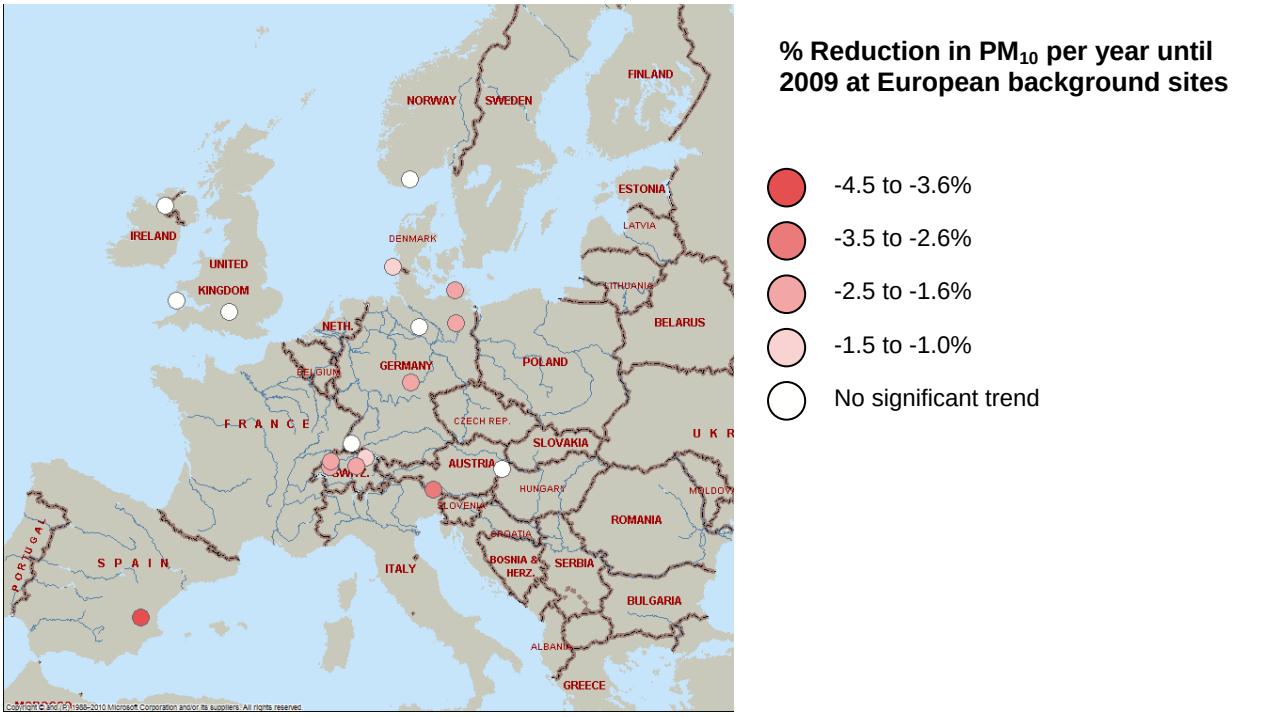

Figure 2.31: Reduction of PM10 at European rural background sites. Adapted from (EMEP, 2010).

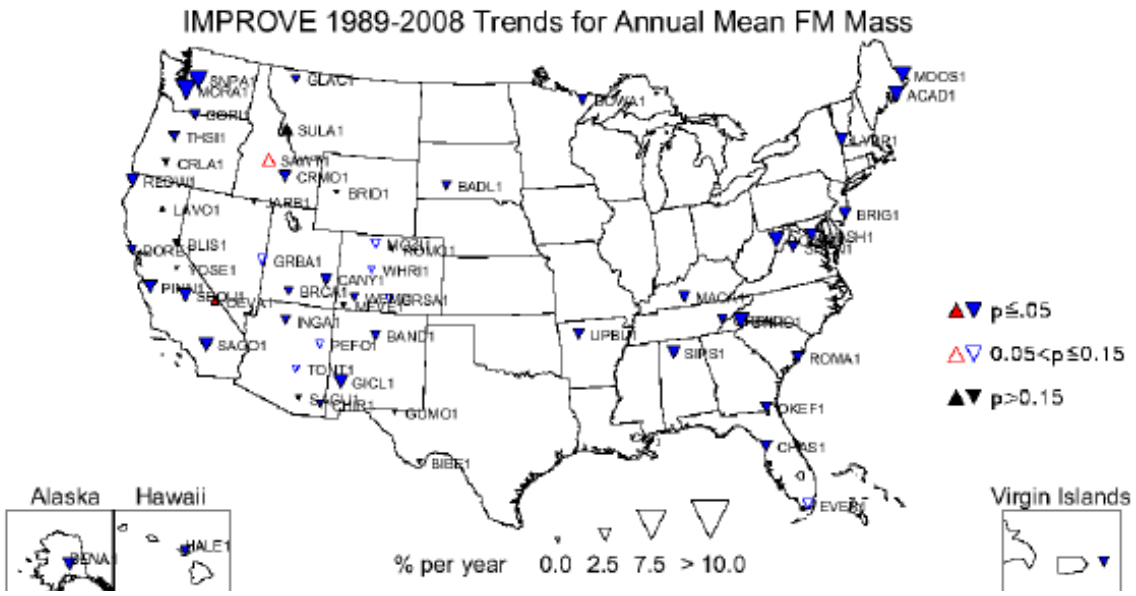

Figure 2.32: IMPROVE (Hand et al., 2011) trends and significance of fine particulate matter levels in the USA.

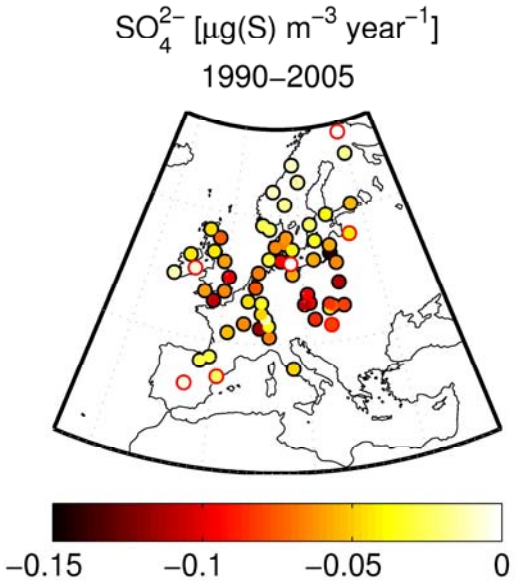

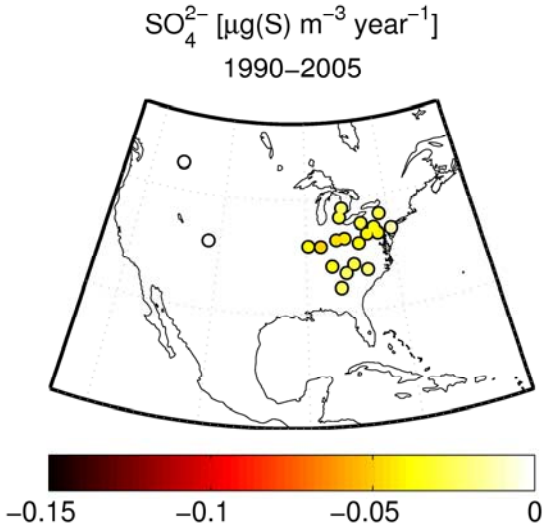

Figure 2.33: Observed SO_4 trends 1990–2005 (ug S m^{-3} yr^{-1}) in Europe and the US. Non-significant trends are denoted with red circle adapted from (Pozzoli et al., 2011).

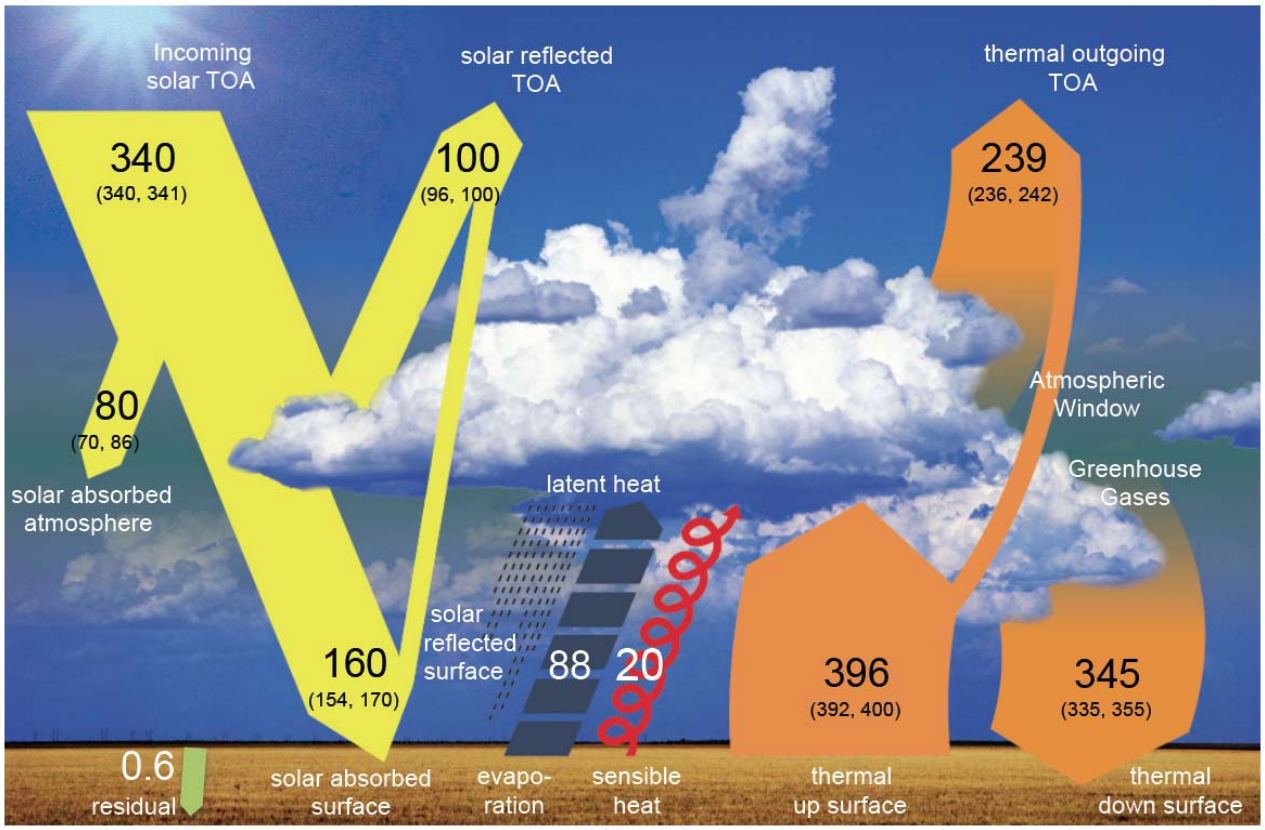

Figure 2.34: The global mean energy budget. Numbers state magnitudes of the individual energy flows in W m^{-2}, adjusted within their uncertainty ranges to close the energy budgets. Numbers in parentheses attached to the radiative fluxes cover the range of values in line with observational constraints.

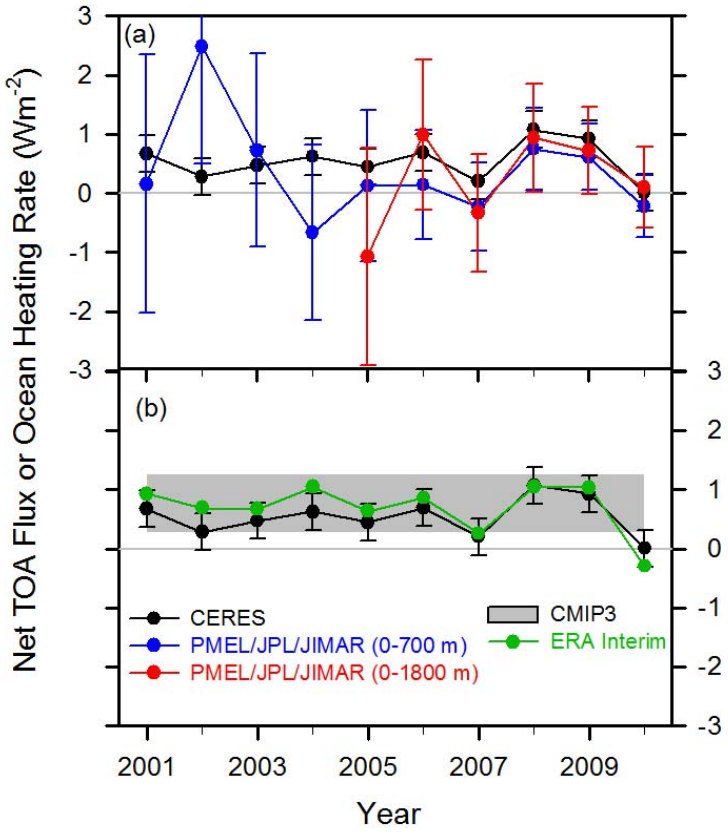

Figure 2.35: Comparison of net TOA flux and upper ocean heating rates. (a) Global annual average net TOA flux from CERES observations (based upon the EBAFTOA_ Ed2.6 product) and (b) ERA Interim reanalysis are anchored to an estimate of Earth's heating rate for 2006–2010. The Pacific Marine Environmental Laboratory/Jet Propulsion Laboratory/Joint Institute for Marine and Atmospheric Research (PMEL/JPL/JIMAR) ocean heating rate estimates (a) use data from Argo and World Ocean Database 2009; The gray bar (b) corresponds to one standard deviation about the 2001–2010 average net TOA flux of 15 CMIP3 models. From Loeb et al. (2011).

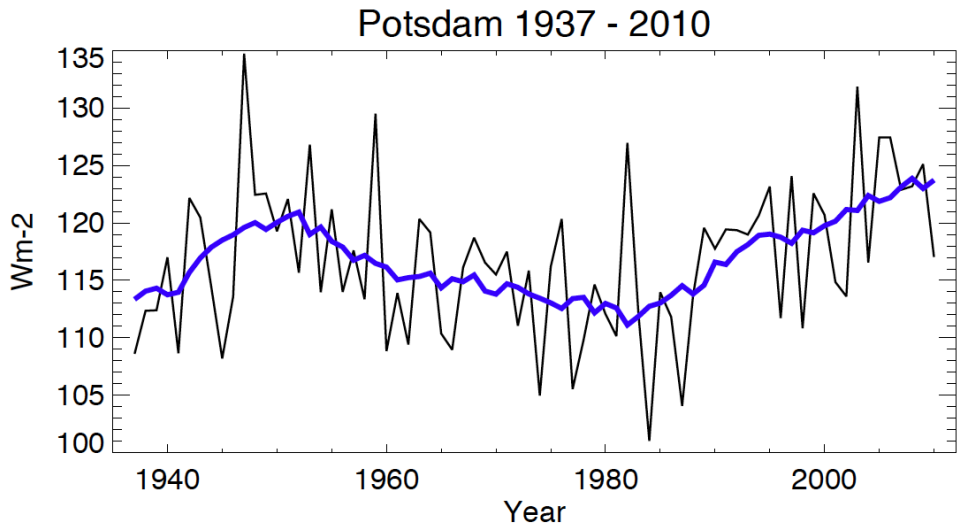

Figure 2.36: Annual mean surface solar radiation (in W m^{-2}) as observed at Potsdam, Germany, from 1937 to 2010. Five year moving average in blue. Extended phases of declines (1950s–1980s, "dimming") and increases (since 1980s, "brightening) can be seen, a characteristics found in many of the long term solar radiation records. There are also indications for an increase before the 1950s ("early brightening"). Updated from Wild (2009) and Ohmura (2009).

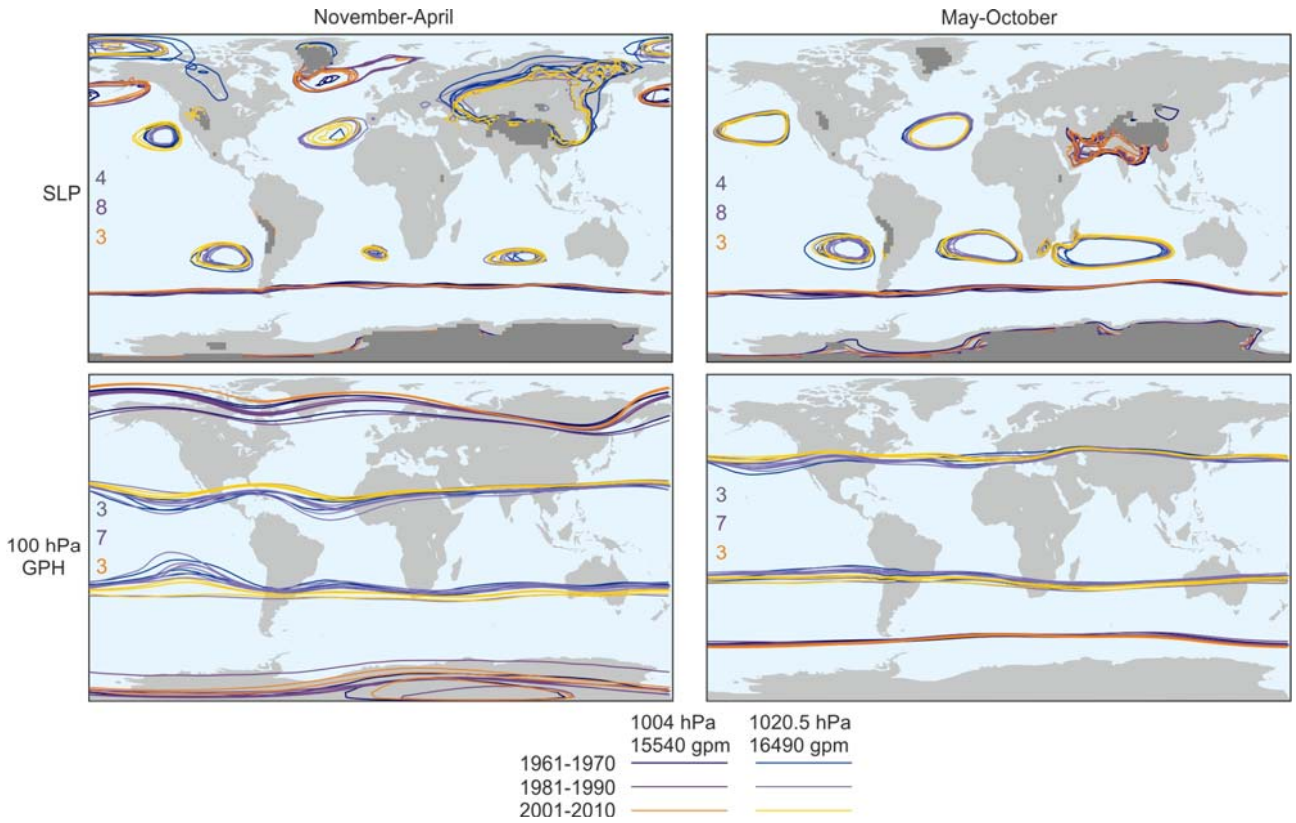

Figure 2.37: Decadal averages for the 1960s, 1980s and 2000s of SLP (top) and 100 hPa GPH (bottom) for November to March (left) and May to October (right) shown by two selected contour lines. Each line represents a data set (listed in Box 2.3, Table 1, plus HadSLP2 for SLP; CFSR was only available up to 2009 and is not shown for the last period), the number of data sets is indicated with the coloured numbers. Topography above 2 km asl (as depicted in the Twentieth Century Reanalysis) is shaded in dark grey for the case of SLP.

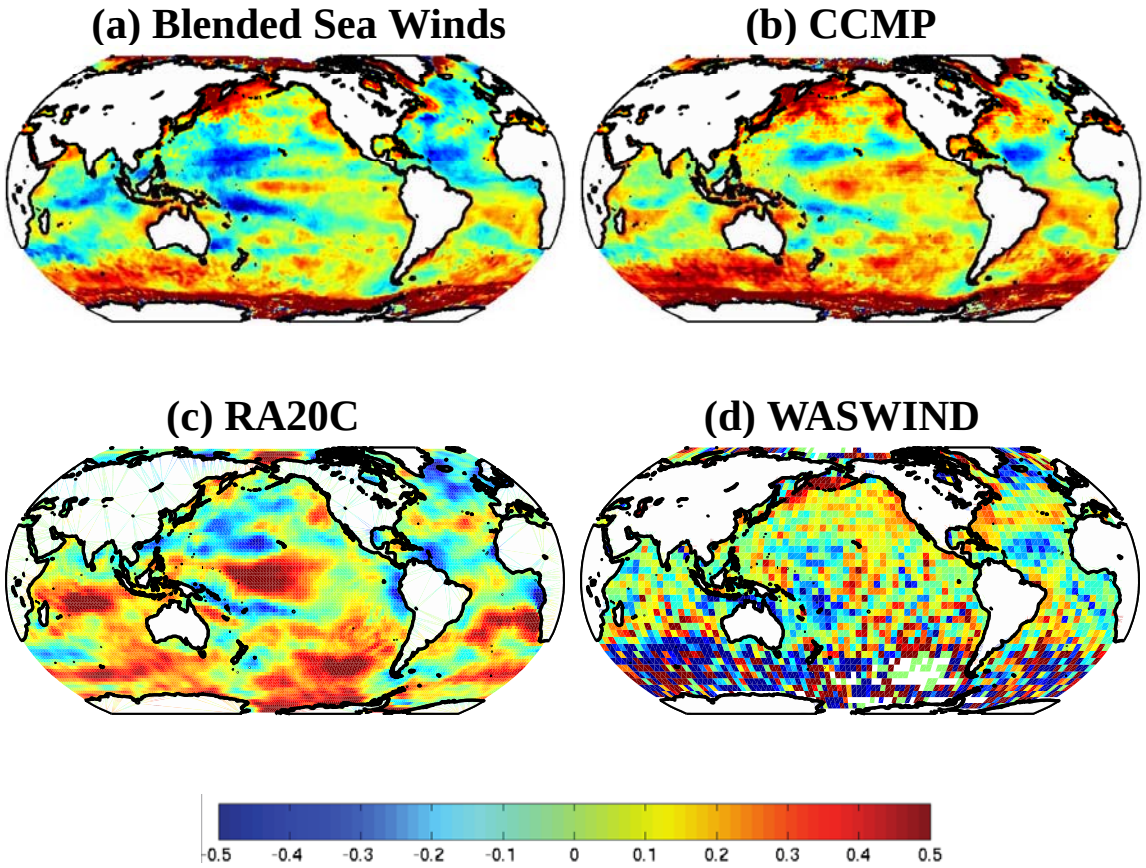

Figure 2.38: Surface 10m windspeed trends for the period July 1986 to August 2006. A) Blended Sea Winds (Zhang et al., 2006), b) CCMP (Atlas et al., 2011), c) 20th Century Reanalysis (Compo et al., 2011), and d) WASWind (Tokinaga and Xie, 2011a).

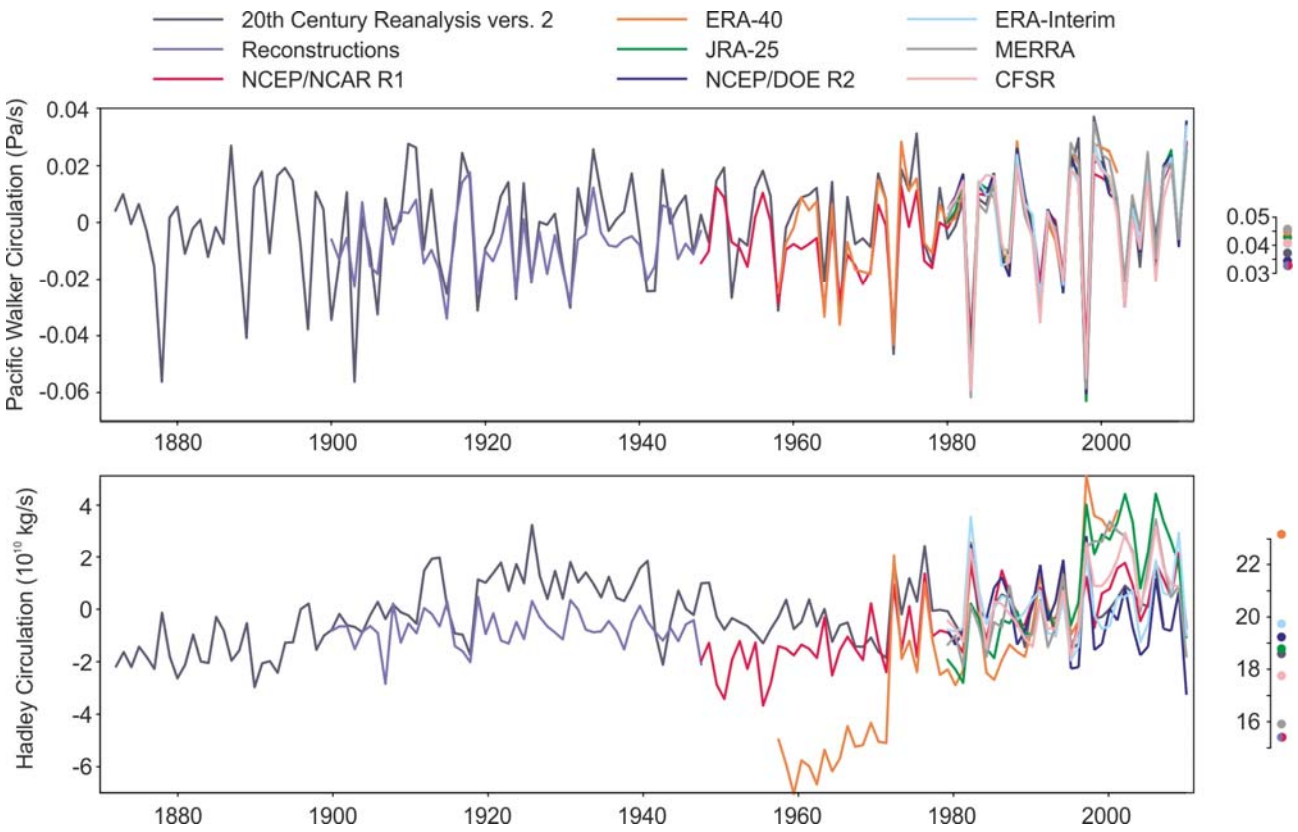

Figure 2.39: The strengths of the Pacific Walker circulation in September to January (top) and of the northern Hadley circulation in December to March (bottom) in different data sets. Monthly values of Hadley and Walker circulation strengths were defined similar as in Oort and Yienger (1996) as the maximum of the meridional mass stream function at 500 hPa between the equator and 40° N and the difference in the vertical velocity between [10°S to 10°N, 180°W to 100°W] and [10°S to 10°N, 100°E to 150°E], respectively. Time series show anomalies from the 1979/1980 to 2001/2002 mean values of each series (dots on the right). Reconstructions are based on historical upper-air and surface observations and extend NCEP/NCAR back in time (updated from Broennimann et al. (2009), and Compo et al. (2011)).

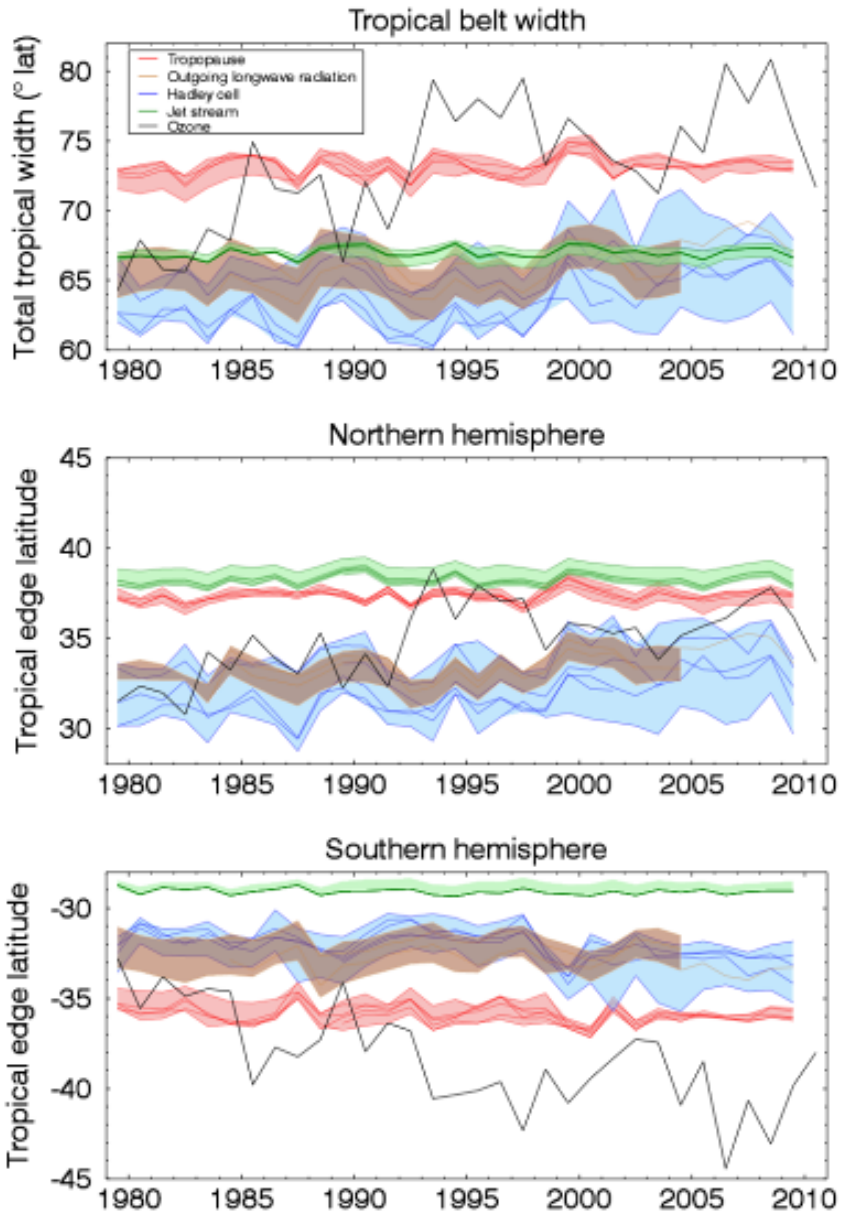

Figure 2.40: Variations in annual mean tropical belt width (top) and tropical edge latitudes in each hemisphere (middle and bottom) during 1979–2009. The tropopause, Hadley cell, and jet stream metrics are based on reanalyses; outgoing longwave radiation and ozone metrics are based on satellite measurements. Adapted and updated from Seidel et al. (2008) using data presented in Davis and Rosenlof (2011). Where multiple datasets are available for a particular metric, all are shown as light solid lines, with shading showing their range and a heavy solid line showing their median.

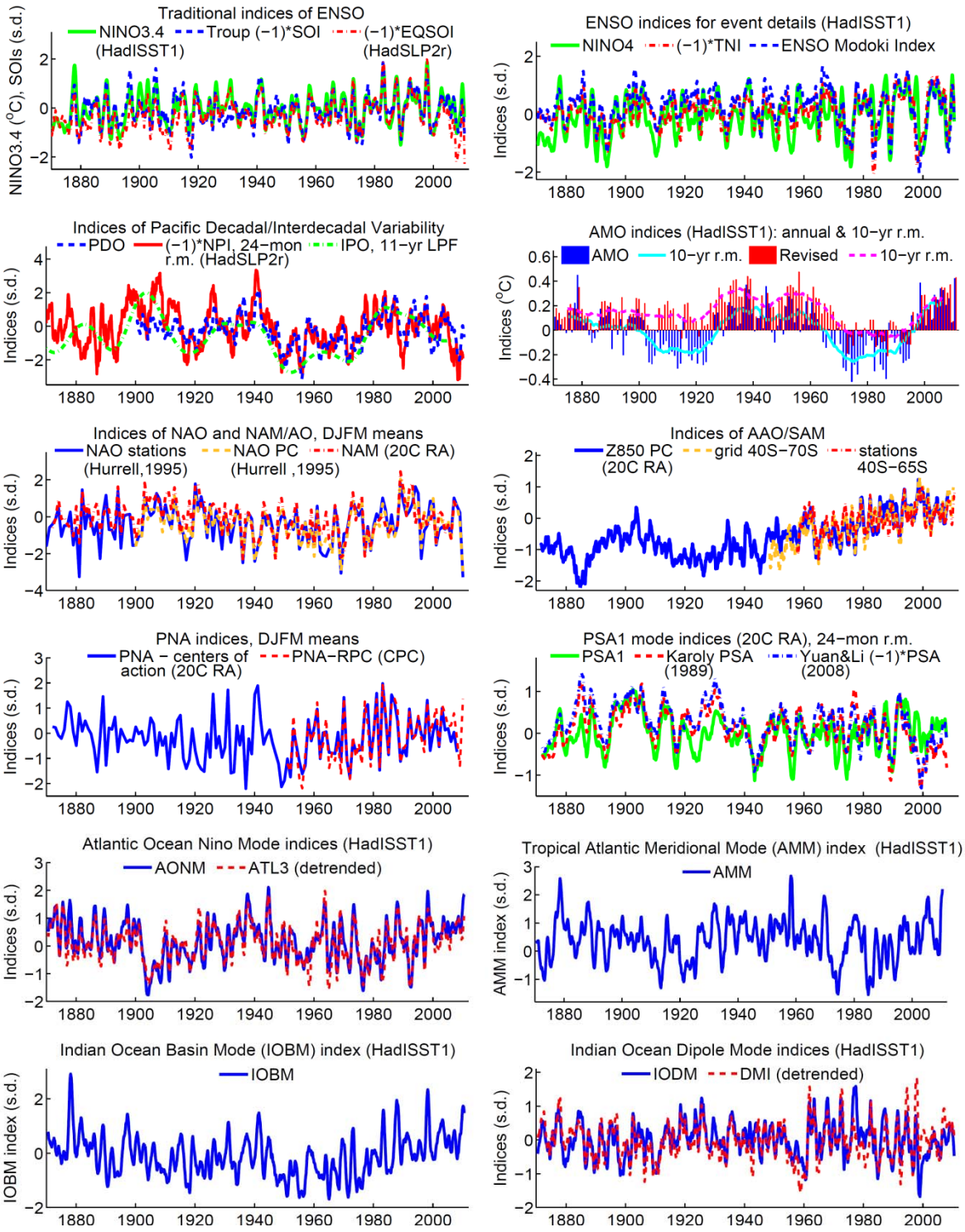

Box 2.4, Figure 1: Some indices of climate variability, as defined in Table 1. Where "HadISST1", "HadSLP2r", or "20C RA" are indicated, the indices were computed from the SST or MSLP values of the former two data sets or from 500 or 850 hPa geopotential height fields from the 20th Century Reanalysis, version 2. A data set reference given in the title of each panel applies to all indices shown in that panel. "CPC" indicated an index timeseries publicly available from the NOAA Climate Prediction Center. Where no data set is specified, a publicly available regularly updated version of an index from the authors of a primary reference given in Table 1 was used. (Citations are given in panel legends only when needed for unambiguous identification of a particular index definition from Table 1; their presence or absence does not mean on its own that the index values obtained from the authors were or were not used here). All indices are shown as 12-month running means (r.m.) except when their resolution (e.g., "DJFM" for December-to-March averages) or smoothing level (e.g., 11-year LPF for a low-pass filter with half-power at 11 years) are explicitly indicated.

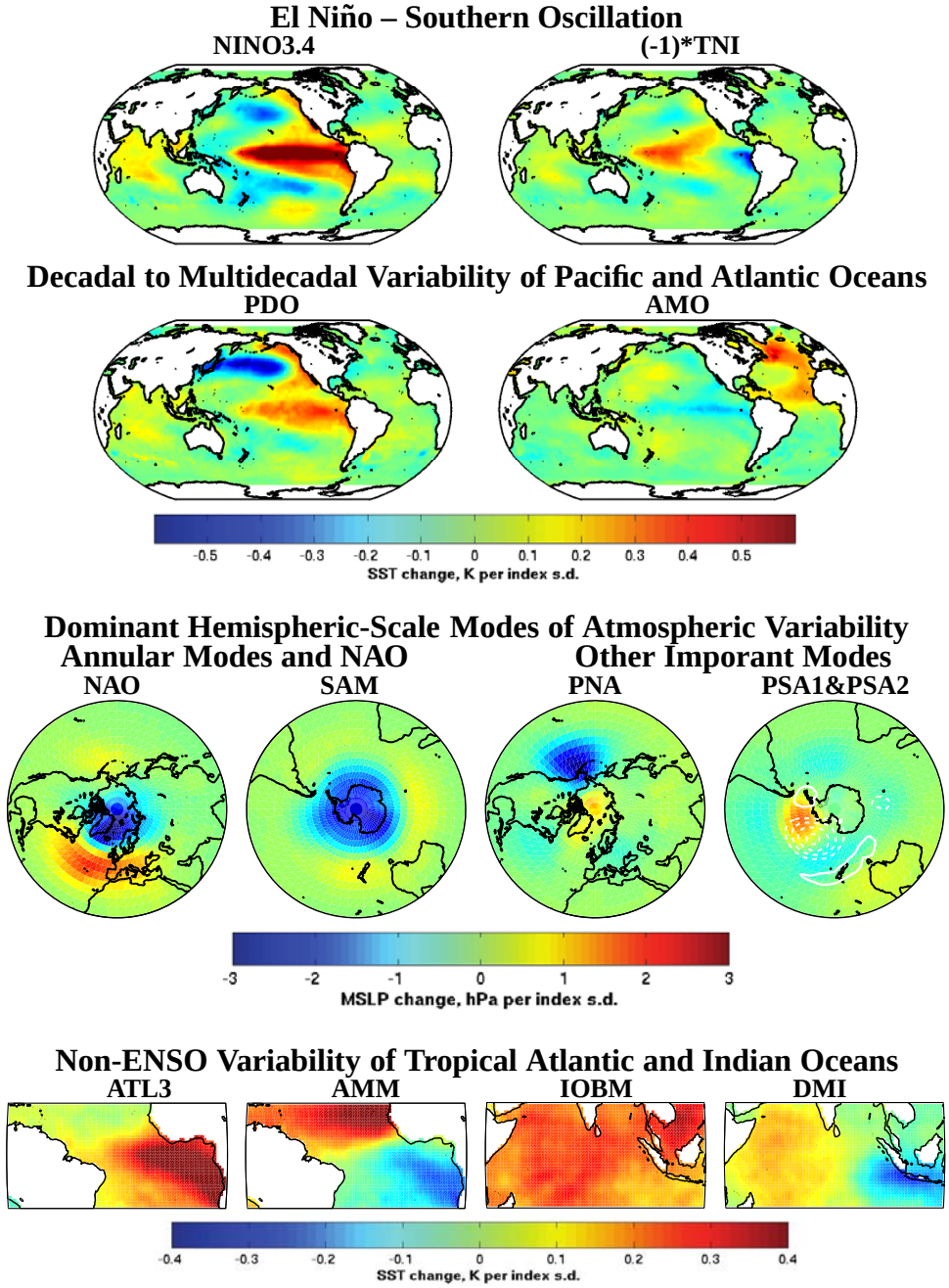

Box 2.4, Figure 2: Spatial patterns of climate modes listed in Table 1. The patterns shown here are obtained by regression of either SST or MSLP fields on the standardized indices climate modes. For each climate mode one of the indices shown in Figure 1 was used. SST and MSLP fields are from HadISST1 and HadSLP2r data sets (interpolated gridded products based on data sets of historical observations). All SST-based patterns are results of monthly regressions for the 1870–2010 period except for the PDO regression pattern, which was computed for 1900–2010. The MSLP-based patterns of NAO and PNA are regression coefficients of the DJFM means; PSA1 and PSA2 patterns are regressions of seasonal means; SAM pattern is from a monthly regression. For each pattern the data was linearly de-trended over the regression interval. All patterns are shown by color plots, except for PSA2, which is shown by white contours over the PSA1 color plot (contour steps are 0.5 hPa, zero contour is skipped, negative values are indicated by dash).

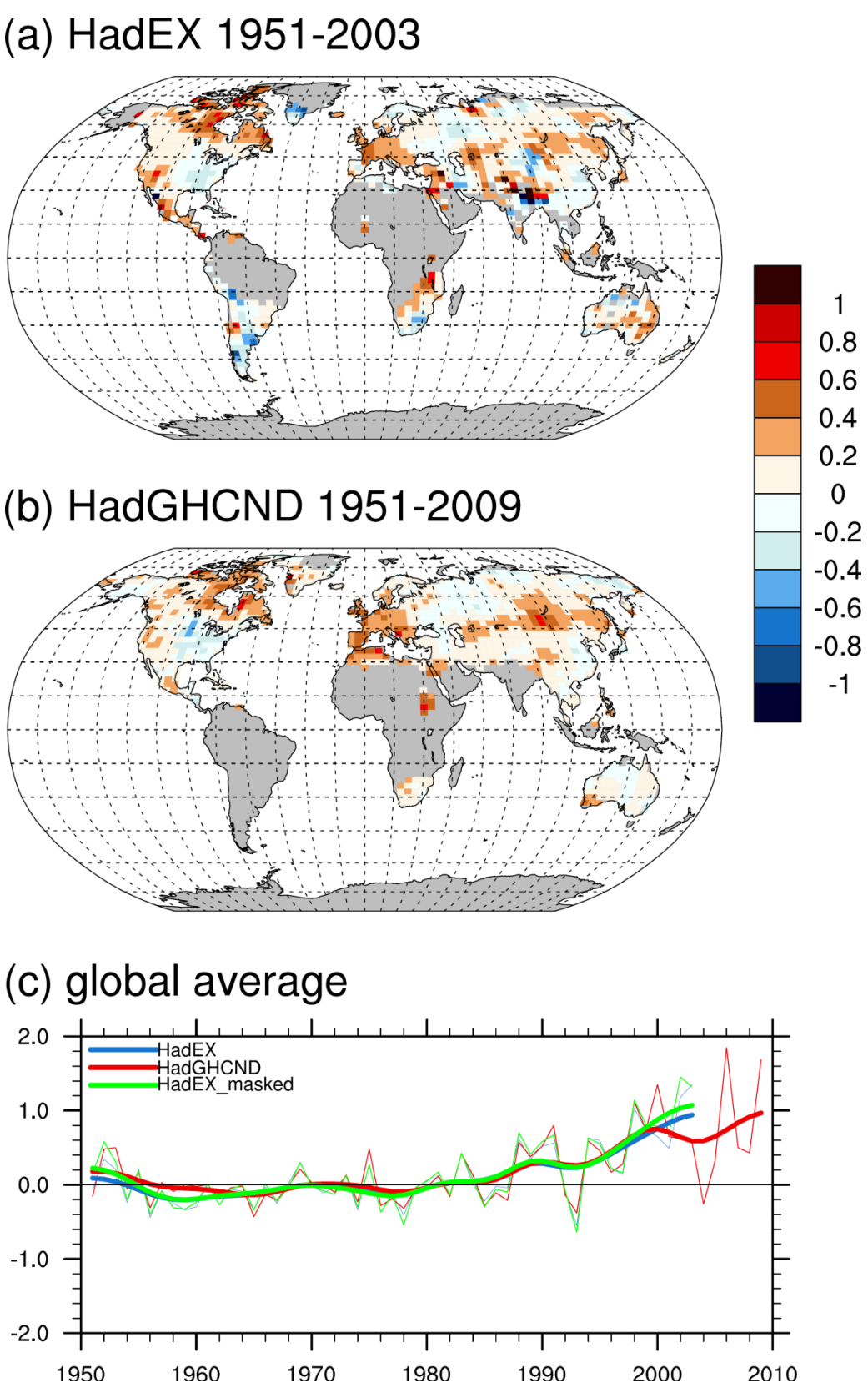

Box 2.5, Figure 1: Trends (°C/decade) in the warmest day of the year using different datasets for the periods indicated. The datasets are (a) HadEX (Alexander et al., 2006), (b) HadGHCND (Caesar et al., 2006) using data updated to 2009) and (c) global average timeseries plots (thin solid lines) for each dataset with associated decadal variations (thick solid lines). Also shown is the globally averaged timeseries for HadEX masked to the gridboxes where HadGHCND data are available.

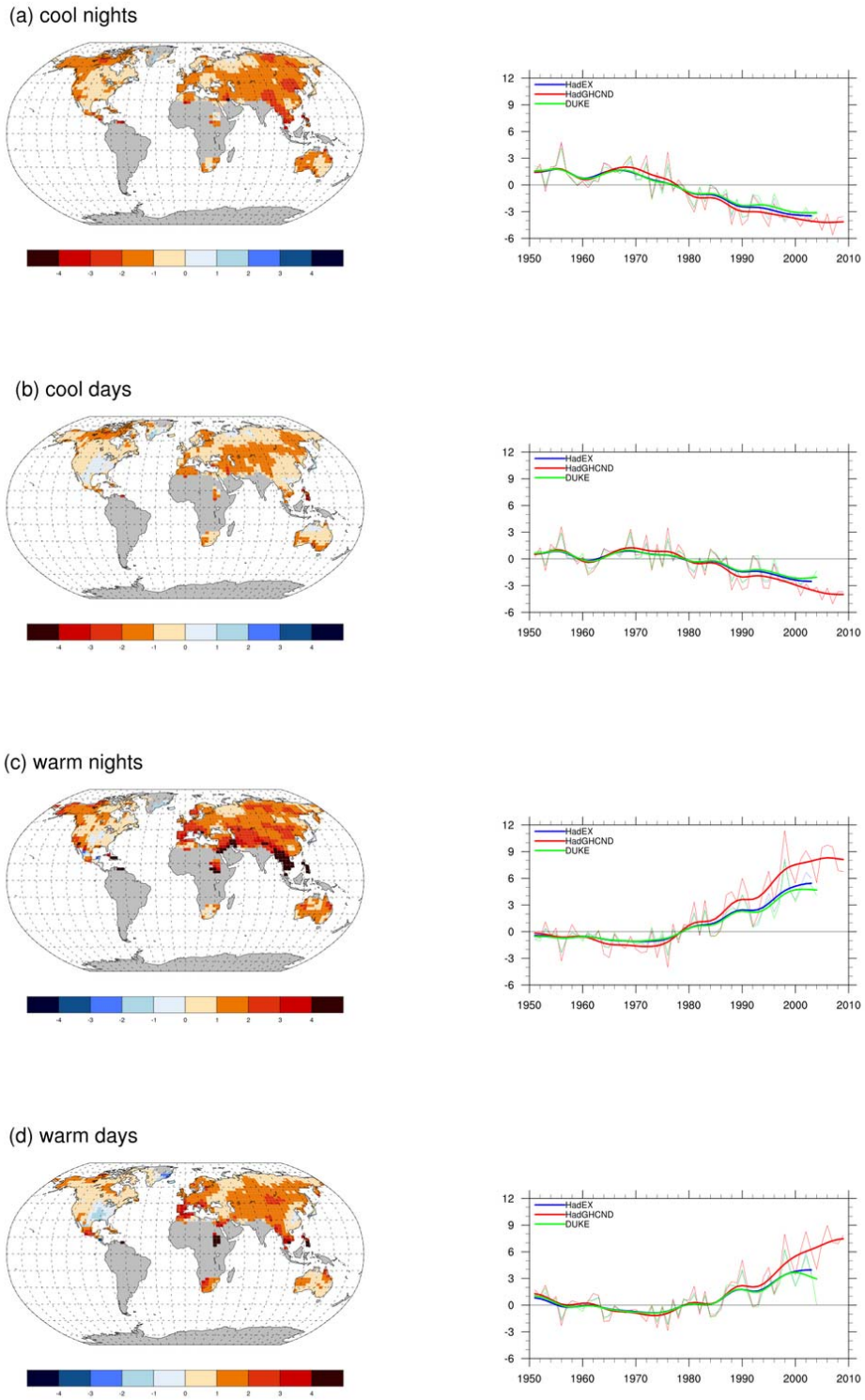

Figure 2.41: Maps show observed trends (% per decade) in the frequency of extreme temperatures, over the period 1951 to 2009, for: (a) cool nights (10th percentile), (b) cool days (10th percentile), (c) warm nights (90th percentile) and (d) warm days (90th percentile). Trends were calculated only for grid boxes that had at least 30 years of data during this period. The data source for trend maps is HadGHCND (Caesar et al., 2006). Beside each map are the global annual time series of anomalies with respect to 1961 to 1990 (thin solid lines) along with decadal variations (thick solid lines) for three global datasets: HadEX (Alexander et al., 2006), HadGHCND (Caesar et al., 2006) and Duke (Morak et al., 2011). Trends are significant at the 5% level for all the global indices shown.

(a)

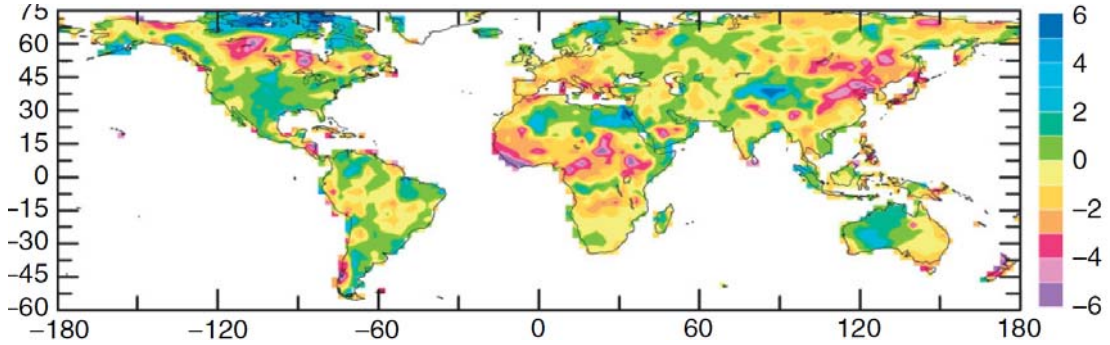

(b)

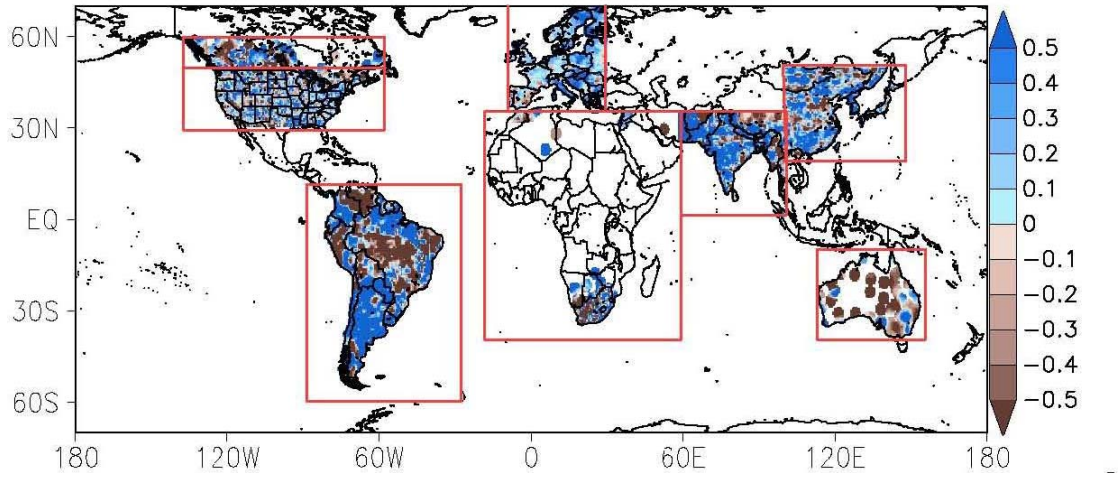

Figure 2.42: Spatial trends in (a) an annual drought index using the self-calibrated PDSI (change per 50 years) with the Penman-Monteith potential evaporation calculated over the period 1950 to 2008 (red indicates drying – from Dai, 2011b) and (b) hydroclimatic intensity (HY-INT: a multiplicative measure of length of dry spell and precipitation intensity) over the period 1976 to 2000 (from Giorgi et al. (2011)). An increase (decrease) in HY-INT reflects an increase (decrease) in the length of drought and /or extreme precipitation events.

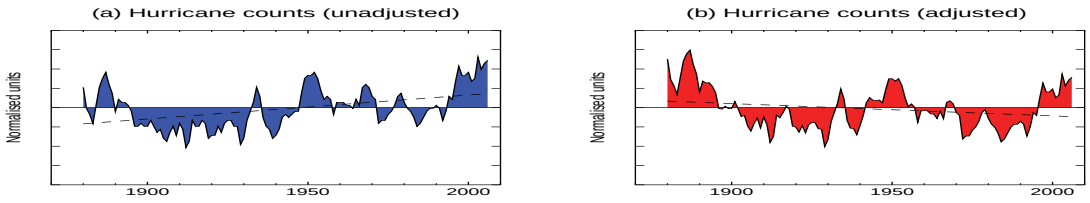

Figure 2.43: Atlantic hurricane frequency changes using raw and adjusted data. Filled lines indicate the normalized 5-year running means, during 1878–2008, with straight dashed lines indicating the linear least squares trends. The blue-shaded curve represent unadjusted hurricane counts (HURDAT; (Landsea et al., 2008). The red curve includes time dependent adjustments for missing storms based on ship track density (Landsea et al., 2010; Vecchi and Knutson, 2008) and for the adjusted hurricane count record from Vecchi and Knutson (2011). Vertical axis ticks represent one standard deviation, with all series normalized to unit standard deviation after a 5-year running mean was applied (Vecchi and Knutson, 2011).

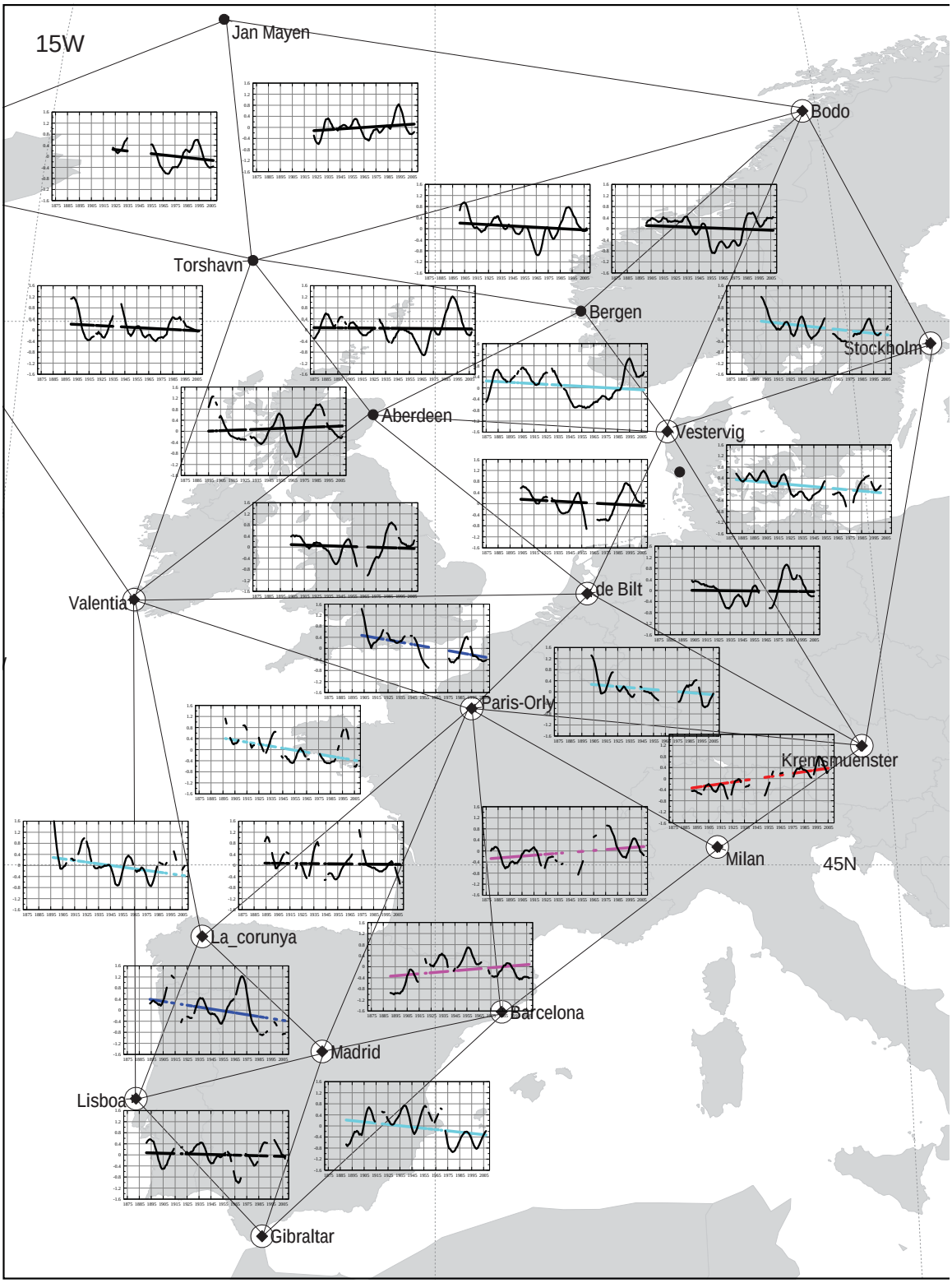

Figure 2.44: Triangles show regions where geostrophic wind speeds have been calculated from in situ surface pressure observations. Within each pressure triangle, Gaussian low-pass filtered curves and estimated linear trends of the 99th percentile of these geostrophic wind speeds for winter are shown. The ticks of the time (horizontal) axis range from 1875 to 2005, with an interval of 10 years. Disconnections in lines show periods of missing data. Red and magenta (blue and cyan) trend lines indicate upward (downward) trends of at least 5 and 20% significance, respectively. From Wang et al. (2011).

(a)

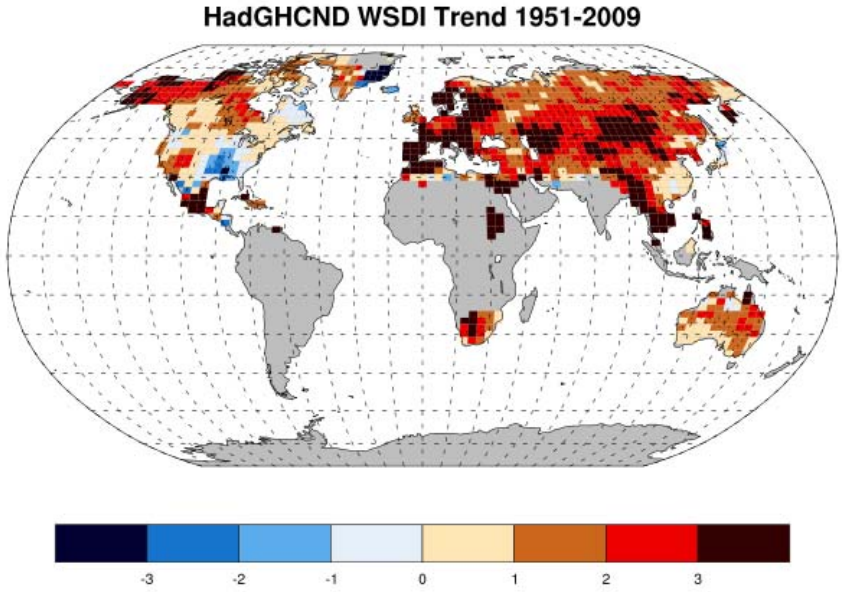

(b)

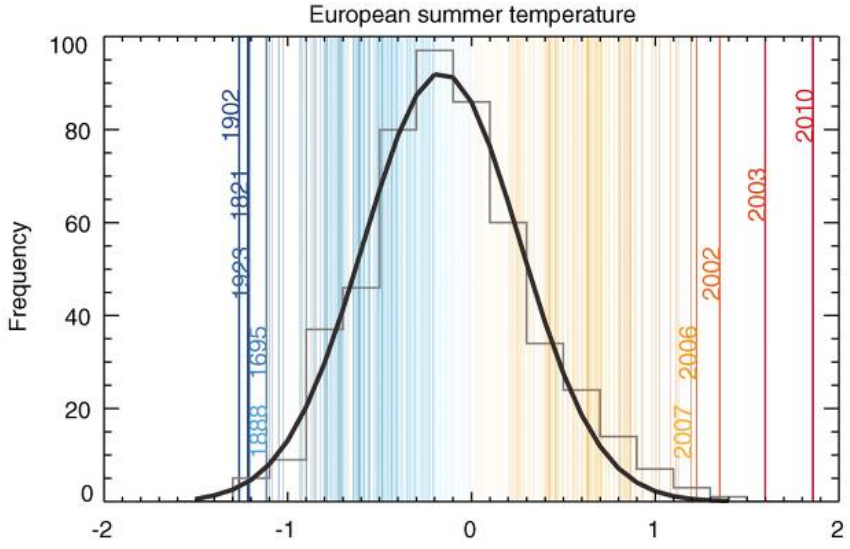

FAQ 2.2, Figure 1: (a) Trends (days/decade) in a heatwave duration measure (WSDI - see Zhang et al., 2011a), over the period 1951 to 2009 (using updated HadGHCND data from Caesar et al. (2006)). Stippling indicates where trends are significant at 5% level. (b) European summer temperatures for the period 1500 to 2010 represented by a statistical frequency distribution of best-guess reconstructed and instrument based European ([35°N, 70°N], [25°W, 40°E]) summer land temperature anomalies (°C, relative to the 1970 to 1999 period). The five warmest and coldest summers are highlighted. Gray bars represent the distribution for the 1500–2002 period, with a Gaussian fit in black (Barriopedro et al., 2011).

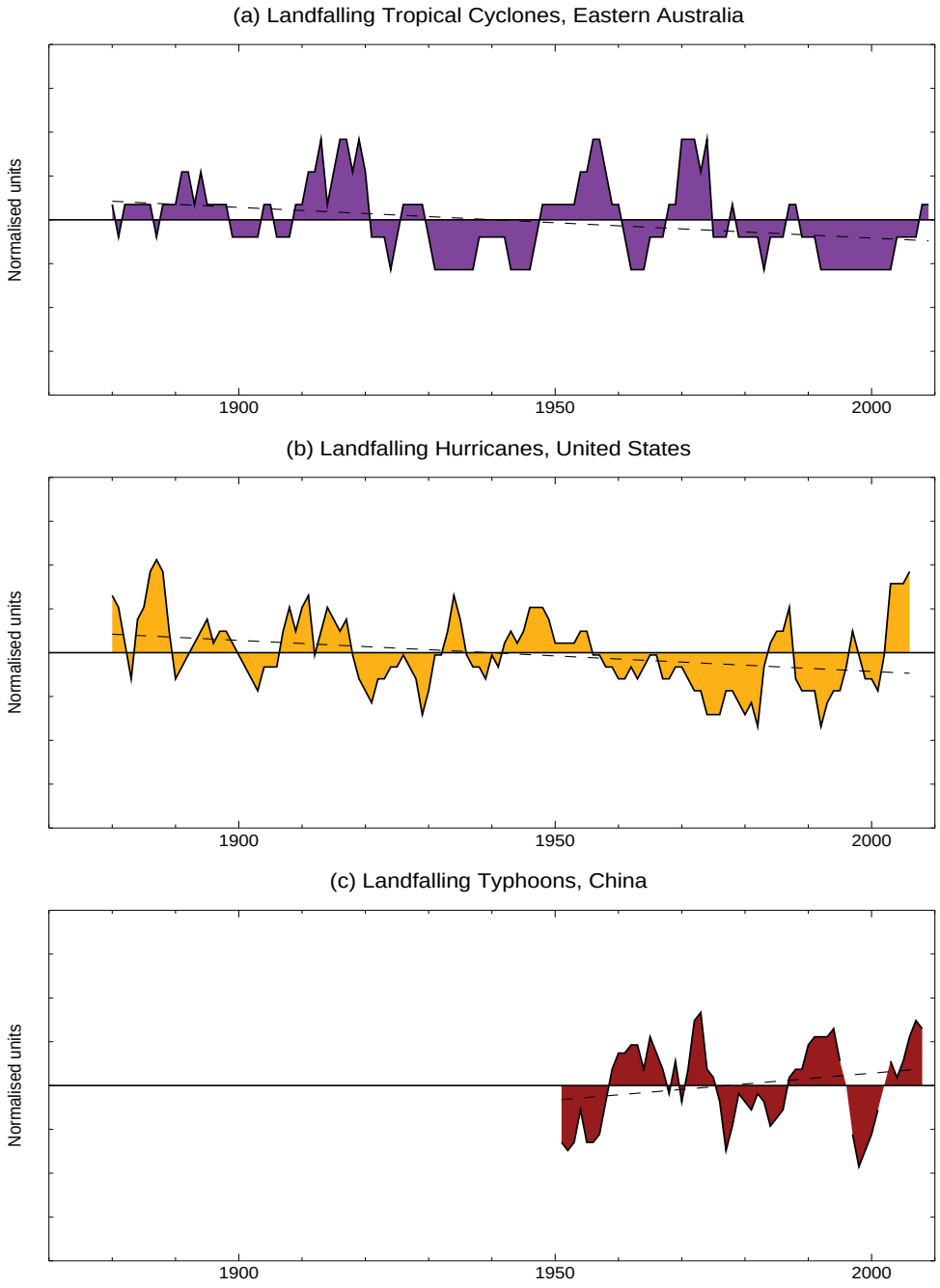

FAQ 2.2, Figure 2: Filled lines indicate the normalized 5-yr running means of the number of (a) land falling eastern Australian cyclones tropical cyclones, 1872/1873 to 2010/2011 (adapted from Callaghan and Power (2011) and updated to include 2010/2011 season) and (b) land falling U.S. hurricanes (adjusted to account for under-reporting in early part of record), 1878 to 2008 (adapted from Vecchi and Knutson, 2011) and (c) land falling Chinese typhoons, 1948 to 2010 (adapted from (CMA, 2007). Vertical axis major ticks represent one standard deviation, with all series normalized to unit standard deviation after a 5-year running mean was applied. The dashed lines are trends calculated using ordinary least squares regression.